

For New Technology Network

**NTN**®

# TECHNICAL REVIEW

No.  
**76**

**Special Issue;**  
**Elemental technologies**  
**October 2008**



**NTN's Elemental Technological Research & Development Center will be commissioned in January 2009 to enhance development functions for elemental technologies and bearings for industrial machinery.**

To enhance NTN's R&D framework in the Kuwana area, our "Elemental Technological Research & Development Center" is now under construction in the Kuwana Business Research Park. This facility will be commissioned in January 2009.

Situated in the Kuwana Business Research Park at Hidamari-no-oka, Kuwana-shi, Mie Prefecture, the R&D center boasts a total floor area of 12,000 m<sup>2</sup> consisting of two buildings : a five-story seismically isolated main research building and a separate single-story laboratory building. Incorporating a seismically isolating structure comprising a unique sliding bearing (SSB<sup>\*1</sup>) system from NTN Engineering Plastics Corp., the main building not only can withstand a big earthquake as intense as the notorious Hanshin-Awaji Great Earthquake but also will function as NTN's disaster relief center in NTN's Kuwana area of operation such that it is capable of emergency control in the event of disaster. The Main Research Building incorporates solar power generation panels, a wind power generator and a rooftop garden to realize both energy savings and eco-friendliness. Also, striving for harmony with nature, this building has a unique arrangement to prevent the adverse effect of lighting toward the east because a local volunteer group is cultivating fireflies in the green space conservation park No. 2 situated directly east of the building.

To Elemental Technological Research & Development Center, Element Technology Laboratory currently situated in present NTN Kuwana R&D Center (it will be renamed Industrial Machinery Engineering Development Center) and a portion of experiment functions from Industrial Machinery Product Headquarters will be transferred. Through improved R&D environments, elemental technologies, which are the very source of NTN's competitiveness, will be more sophisticated. These improvements include development of eco-friendly heat treatment technique and materials, research into higher mechanical strength of materials through nano-level research and surface generation, development of next-generation lubricants, and more strenuous cultivation of analysis technique which can help accelerate development work. Additionally, in cooperation with the current Kuwana Research & Development Center, the Elemental Technological R&D Center will enhance NTN's capability in assessment tests for large and extra-large bearings for wind power generators, large building construction machines, medical equipment, railway rolling stocks and aircraft in order for NTN to strengthen its R&D functions and ability to satisfy customer needs in the industrial machinery product segment which will grow significantly in the near future.

[ \*1 : Super Sliding Bearing]



**[Features of the Elemental Technological Research & Development Center]**

- Site address : 5-105 Hidamari-no-oka, Kuwana-shi, Mie Prefecture, Japan (in Kuwana Business Research Park): approximately 30,000 m<sup>2</sup>
- Total floor area : Five-story Main Building, single-story Laboratory Building: total floor area approximately 12,000 m<sup>2</sup>
- Structure : Seismically isolated building (Main Building) incorporating "elastic sliding bearing" from NTN Engineering Plastics Corp.
- Equipment : Solar power generation, wind power generation, rooftop garden, eco-friendly air-conditioning with cool pit



# TECHNICAL REVIEW

**No.76**

**Special Issue:**  
**Elemental technologies**

# NTN TECHNICAL REVIEW No.76

## CONTENTS

### Preface

Kenji OKADA 1

### Contribution

#### Industry-University Partnerships in R&D of Machine Elements

Yoshitsugu KIMURA Professor Emeritus The University of Tokyo and Kagawa University

2

### ● Elemental Technology

Trends in Materials and Heat Treatments for Rolling Bearings Hirokazu NAKASHIMA	10
Improvement of Carburized Steel Wear Resistance by Heat Treatment Nobuyuki MOURI and Kazuhiko TAGUCHI	18
Deep Nitrided 32CrMoV13 Steel for Aerospace Bearings Applications Daniel GIRODIN	24
Test Design and Result Interpretation Methods for Evaluating Rolling Contact Fatigue Life to Maintain Both Efficiency and Reliability Takumi FUJITA	32
Research on the Lubrication Mechanism of Grease for High Speed Bearings Takayuki KAWAMURA	40
Friction Properties of Polymer Gel with High Mechanical Strength Eiichirou SHIMAZU, Masaki EGAMI, Takayuki KUROKAWA and Jian Ping Gong	46
Study on the Effect of Physical Properties on Wear Resistances of TiN Films Coated by Arc-plasma Ion Plating Hideyuki TSUTSUI	52
Development of an Antenna Material Based on Rubber that has Flexibility and High Impact Resistance Kouya OOHIRA	58
Development of Sensing System for Cerebral Aneurysm Treatment Yoshitaka NAGANO and Hideo FUJIMOTO	64
Development of a Method for Monitoring Lubricant Deterioration Kentaro NISHIKAWA and Tomomi ISHIKAWA	69
Heat Transfer Analysis of Machine Tool Main Spindles Yoshimitsu HIRASAWA and Yukimitsu YAMAMOTO	75
Development of High-Speed Cylindrical Roller Bearings for Machine Tools Masatsugu MORI and Takuji KOBAYASHI	82

### ● Products for Industrial Machinery

Angular Contact Ball Bearings that Require a Minimum Quantity of Grease Supply for Lubrication Sun-Woo LEE and Tadaaki MAEDA	90
Minimum Quantity and Cooling Jet Lubrication Single-row Cylindrical Roller Bearings Futoshi KOSUGI and Susumu NOJIMA	96
Introduction of 3D Electronic Catalog for Precision Machine Tool Bearings Takehiko UMEMOTO	101
ULTAGE Series Large, Long-lasting Double-row Cylindrical Roller Bearings for the Main Spindles of Large Turning Machines Naota YAMAMOTO	109
Technical Trends in Wind Turbine Bearings Souichi YAGI and Nobuyuki NINOYU	113
NTN Sensor Units for Construction Machinery Shoji ITOMI and Hiroyoshi ITO	121
Duplexing Gear Unit for Office Equipment Tsutomu MAIWA	129

### ● Precision Apparatus Products

Large Gantry Table for the 10th Generation LCD Substrates Katsuyoshi SUZUKI and Naoshi SUZUKI	134
Development of a Linear Changer with a Built-in Pasting Unit for a Flat Panel Defect Repair System Akihiro YAMANAKA and Akira MATSUSHIMA	138

### ● Our Line of Award Winning Products

<b>2007 JSPE Technology Award</b> Development and Practical Application of MQCJ-Lubricated Angular Contact Ball Bearings for Machine Tool Main Spindles Masatsugu MORI, Yoshinobu AKAMATSU, Mineo KOYAMA, Futoshi KOSUGI, and Hiroshi TAKIUCHI	144
--	-----

### Our Line of New Products

146



– Introduction to this Special Feature Issue –

*To the new issue featuring  
elemental technologies*

**Kenji OKADA**  
Executive Director

Global warming, currently occurring on this 4.6 billion years old earth, is a very critical issue to be addressed by the modern society that has been enjoying economical growth thanks to the consumption of fossil energies. Since the Industrial Revolution in Great Britain, much carbon dioxide (CO<sub>2</sub>) has been emitted as a result of the combustion of petroleum and coal. In the past 200 years, the carbon dioxide concentration in the atmosphere has increased by as much as 25%, and now the entire earth is, so to speak, situated in a greenhouse.

In this situation, NTN has remained committed to global environment conservation as its most important challenge not only in its production activities but also in its R&D activities. In the industrial machinery field, we are committed to the development of bearing technologies for natural energy utilizing equipment such as wind power generation plants and for next-generation transportation equipment while “modal shift” is in progress. We are promoting product development activities to help realize low fuel consumption and electrification in the car industry. We are attempting to more strenuously cultivate and expand “elemental technologies” that constitute the basis for these technologies. More specifically, we are committed to new R&D efforts that include use of bioplastic materials, use of novel materials which can reduce use of rare metals, eco-friendly heat treatment techniques, research into nano-structure level metal materials, surface generation for higher mechanical strength and lower friction, and use of higher-polymer gel (a next-generation material) for decreased friction, as well as development of more sophisticated analysis techniques.

For distribution at JIMTOF 2008 (24th Japan International Machine Tool Fair) held October 30 to November 4, 2008, we published the Japanese language version of NTN TECHNICAL REVIEW No.76 (2008) featuring topics about NTN’s latest elemental technologies that support engineering aspects of eco-friendly products boasting compact size, light weight, lower running torque (lower friction) and longer service life. This issue begins with a contribution titled “Industry-University Partnerships in R&D of Machine Elements” written by Yoshitsugu KIMURA, Professor Emeritus, The University of Tokyo and Kagawa University, a world’s authority in the field of tribology. This topic is followed by presentations of our recent new technologies and developments for new products such as elemental technologies including those for improving wear resistance by surface generation and advanced sensor technologies applied in the medical field; industrial machinery products and precision equipment products such as wind power generator bearings; and “Development and Commercialization of Minimum Quantity and Cooling Jet (MQCJ) Lubrication Angular Ball Bearings for Machine Tool Spindles” which won the 2007 Engineering Award from The Japan Society for Precision Engineering.

Since the beginning of its research and manufacturing of ball bearings in 1918 at the then Kuwana-cho, Kuwana-gun (present-day Kuwana City, Mie Prefecture, Japan), NTN has been attempting for 90 years to develop new products always aiming at “realization of quality that can satisfy customers’ needs”. Strictly adhering to our philosophy “For New Technology Network - We contribute to the international society through creation of new technologies and development of new products”, we will further remain committed to promote, based on the achievements obtained through more strenuous cultivation of our elemental technologies, our R&D activities to satisfy requirements for the ecology, safety and comfort from a global standpoint, thereby we will contribute to society.

**FOR NEW TECHNOLOGY NETWORK**

## Industry-University Partnerships in R&D of Machine Elements



**Yoshitsugu KIMURA**

Professor Emeritus The University of Tokyo and Kagawa University

Significance of matured technology, is discussed, exemplified by the technology of machine elements. Discussed are the roles of universities in handing down technologies between generations and in clearing the hurdles facing class leaders, along with potential ways to develop fruitful partnerships between industry and universities.

### 1. Introduction

After changing trains at Nagoya from the Shinkansen line to the Kintetsu or JR Kansai line and crossing bridges over the Kiso, Nagara and Ibi Rivers, one finds Kuwana City. It is said that in 1918, the founder of NTN started researching and manufacturing ball bearings in the town of Kuwana in Kuwana County. Thus, the firm reached the 90th anniversary of its foundation this year. As a person who has been given opportunities to be involved with the company, I would first like to express my sincere feelings of congratulations.

With a history of 90 years, younger readers will surely feel the foundation of NTN is an event long ago. Having lived for 80% of that period, however, I have different feelings. For this reason, I would like to begin this article with my personal recollections.

Having finished a postgraduate course in 1966, when the term "tribology" was made known to the world, I was employed as an assistant by Professor Norimune Soda's laboratory at the Institute of Space and Aeronautical Science University of Tokyo. From then on, I have been destined to follow a career as a tribologist. In 1997, I retired from the University of Tokyo and moved to Kagawa University to help create its Faculty of Engineering. Though the period that I worked for the Faculty of Engineering was short, I became involved in the management of that university. Here I was given the opportunity to look at tribology, a field in which I had been engaged for a long time, from a somewhat different perspective.

From such a standpoint, I would like to talk about machine elements and how cooperation between industry and academia contributes to the development of machine element technology.

### 2. What is meant by advanced technology?

As a toothed gear is used as the symbol of the Japan Society of Mechanical Engineers, which recently celebrated the 110th anniversary of its foundation, machine elements are symbols of engineering.

There was an era in which smoke from factory smokestacks, seen only as a cause of air pollution at present, was included in school songs as a symbol of industrial development. Perceptions are often changed as time passes, and there is probably no one now who sees machine elements as products of frontier or high technologies. Tribology is no exception. Someone wrote sarcastically, "Is tribology high technology, low technology, or no technology?"

What does frontier technology mean anyway? This is a term that has come to be used without being clearly defined, but I prefer the definition<sup>2)</sup> given by Mr. Hiroyuki Yoshikawa, a former president of the University of Tokyo, some 20 years ago.

In the first place, all technologies are destined to continue evolving and in that sense, must be regarded

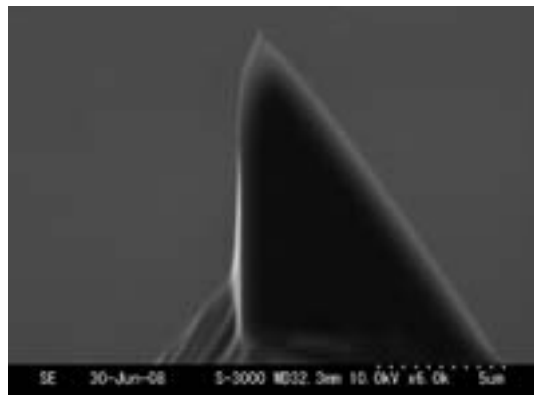


**Fig. 1** Example of "high-technology" : AFM probe <sup>1)</sup>

as being at the outset. Why, then, is the “frontier technology” designation limited to certain technologies? Mr. Yoshikawa started with this question. What is the concept that is opposite that of frontier technologies? Is the opposite of the frontier completed? No. Mr. Yoshikawa says that they are mature technologies. He took up water-related technologies as an example for this. The market for brand-name water has now grown large as we are entering an age in which water shortages have become a global issue.

What Mr. Yoshikawa wanted to say is that the production of water, for example, has its own sophisticated technology, but it has been involved deeply in conditions of human society and, thus, reached a stage of maturity. This makes groundbreaking changes inconceivable. Let us define such technologies as mature ones for the time being. Moreover, as a result of the increase in the number of such mature technologies and in the importance of their influence, the degree that a technology has advanced has become relative, with the notion of a frontier technology being created as a result, says Mr. Yoshikawa.

Mr. Yoshikawa points out that mature technologies are indispensable for supporting society, and therefore should be considered to be very important technologies. However, it may be inevitable that the attention of society in general is attracted to frontier technologies because the nature of journalism is to intentionally focus on “groundbreaking changes.”

### 3. If we only chase after frontiers

Is it good for us to chase after only frontier technologies? I know one person who has raised this question.<sup>3)</sup> Carl Becker, a professor at the University of Kyoto who hails from the University of Hawaii, has a very interesting opinion related to this subject.

For example, one object of frontier technology that Japan has prioritized is large liquid crystal (LCD) television sets. With sales opportunities like the Beijing Olympics held this year and the switch to terrestrial digital broadcasting only a few years ahead, it is natural that manufacturers place high priority on LCD TVs.

Mr. Becker says, however, “If you consider the world’s needs, you will find that there are few countries that desire large LCD TVs.”

Basically, countries for which terrestrial digital broadcasting is more advantageous are limited to those, like Japan, with limited territories and particularly high population densities. When you receive satellite broadcasting in China or in the United States, signals deteriorate significantly before they arrive at television sets. Therefore, even if you use a large, 50-inch screen, you will not have images that are as beautiful as you would have in Japan. These countries do not need the clarity that is one of the major features of large LCD televisions. For this reason, even if they are successful inside Japan, they

will not become exports that support Japan’s future economy.

More importantly than this, according to Mr. Becker, you have technologies indispensable to the world in the near future, such as technologies to handle natural energy sources including the sun, geothermal heat, wind and the sea, as well as organic agriculture, recycling, and the afore mentioned drinking water.

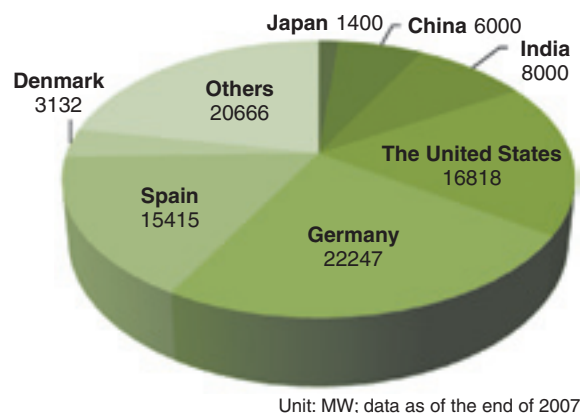
For example, try to determine who is the leader in the field of natural energy technology, and you will find that Germany leads solar energy utilization technology, with Australia in second place and Japan just managing to be within a group of competitors. In the field of geothermal power generation, Iceland stands first with Italy following. In the field of wind power generation, Denmark stands first, while in the field of ocean thermal energy conversion, the state of Hawaii is ahead of Japan.

The capacity of wind power generation is shown in Fig. 2.<sup>4)</sup> This figure shows that Germany is first, but Denmark dominates in terms of per-capita capacity. Either way, the fact remains unchanged that Japan is lagging behind.

Mr. Becker places his expectations on Japan, saying, “If only Japan had the desire, it would never lose to Australia in the field of solar thermal power generation.” He criticizes Japan severely, saying, “Japan took the wrong end of the stick in giving priority only to large-size digital screens and neglecting the needs of the world in the near future.”

Of course, he does not say that it is wrong to pursue frontier technologies. It is not wrong, but pursuing only frontier technologies casts a shadow on the future of Japan in the world. “For example, a country capable of stably supplying solar energy at a substantially reduced price for export will experience a second growth stage. There is no reason for not focusing on this with the concerted efforts of the nation,” insists Mr. Becker.

However, one may guess that, regardless of whether we take on natural energy, organic agriculture, drinking water, or recycling, we can handle all of them through the application of the mature technologies on which they are founded. Moreover, I



Unit: MW; data as of the end of 2007

Fig. 2 Capacity of aerogeneration<sup>4)</sup>

am certain that many of the readers would think that the application of technologies is a field at which Japan, proud of its skillfulness, is good. Unfortunately, however, it is not that simple.

#### 4. Why did the Kiku VI engineering test satellite fail?

Fourteen years ago there was an incident in which an engineering test satellite named “Kiku VI” was not successfully put into orbit.<sup>5)</sup> It left an impression in my mind because I joined in the investigation.

Kiku VI was a two-ton class satellite, shown in **Fig. 3**,<sup>6)</sup> that was launched from Tanegashima Island on August 28, 1994 and put in an elliptical orbit with the earth set as one focus. Everything went well concerning this. The next step in the launch program was to change orbits through the use of a small rocket, called an apogee engine, at the apogee in order to put the satellite into geostationary orbit. Things started going wrong when a command to start the apogee engine was sent two days after the launch. The pressure in the combustion chamber did not rise beyond one-tenth of the planned value. As many measures as possible were taken in vain, but the satellite remained orbiting in the original elliptical orbit.

Although it was impossible to investigate the cause or recover the actual satellite for examination, a variety of analysis suggested a problem with the coiled springs as the most probable cause.

The engine was provided with a mechanism that controlled the hydrazine, the fuel, and an  $N_2O_4$  oxidant with a two-propellant valve to feed it into the combustion chamber. The return spring of this valve was thought to have shifted in a lateral direction by the vibration produced by the launch, and was caught in a gap between the valve piston and casing. This would cause the valve shaft to become bent, thereby making the planned control impossible.

Needless to say, preliminary vibration tests had been performed. The ex post facto analysis, however, revealed that such a shift occurs only in a few of the



**Fig. 3** Engineering test satellite-Ⅵ “KIKU No.6”<sup>6)</sup>

many springs manufactured with the same method, and, moreover, that such a shift occurs only at a certain level of vibration that is about the same level as that of actual flight conditions. If you only look at a drawing, you will overlook this detail: the coiled spring is neither axis-symmetric nor plane-symmetric. For this reason, the asymmetric motion of “shifting” in a direction is a phenomenon that can occur.

What was made clear in the course of analyzing potential causes was the fact that experts on coiled springs, which are very common machine elements, could not be found, at least not in Japan. As a result, nobody was able to foresee the possibility that the destiny of an engineering test satellite costing several tens of billion yen could be determined by the capricious behavior of a spring.

This coiled spring is one example, but have we not ignored the transmission of expertise related to commonplace machine elements that seem remote from frontier technologies?

#### 5. Elemental technologies in wind power generation

Another example Mr. Becker mentioned is wind power generation.

Wind power generation is one topic that is currently attracting public attention.<sup>7,8)</sup> Among so-called new energy sources, wind power generation exhibits a worldwide growth rate of 15 to 20% because of its cost-effectiveness, efficiency<sup>1</sup> and environmental-friendliness, as well as the low ratio of construction cost to power generation cost. Each year sees larger and larger wind power generators, and it is said that a 6-MW unit was tested in 2007.

Among other things, the huge rotors used in wind power generation are impressive. The energy that can be extracted is proportional to the square of the rotor diameter, while the weight is proportional to the cube of the diameter. It is impossible, therefore, to say simply that “the larger a rotor is, the better it is,” and technologies for increasing generator efficiency and reducing generator weight are sought.

As shown in the example in **Fig. 4**,<sup>7)</sup> various mechanisms are packed in the nacelle. The casing contains the bearing for the rotor shaft a generator, and a gearbox that increases the 10-to-30-rpm rotation of the rotor to a speed of 1500 to 2000 rpm. These are the essential pieces of equipment, to which components specific to a windmill are added such as a pitch drive mechanism that changes the blade pitch, a swivel ring that changes the orientation of the rotor in response to the wind direction, a yaw drive mechanism, and a lubrication device. In comparison, the casing of an electric fan contains only a motor. In all, the number of bearings per nacelle is upwards of 100, which can be compared to about 150 bearings per automobile. Even this fact alone could convince us that wind turbines are quite amazing.

Operating conditions for wind turbines are also particularly severe. To support a rotor that is several

tens of meters in diameter, the bearing of the main shaft sometimes exceeds three meters in outside diameter, and it must withstand randomly occurring high loads caused by wind gusts. In addition, the bearings of the pitch drive mechanism and swivel rings face the demanding condition of intermittent swing. Furthermore, installing a wind turbine on the top of a tower as high as 100 meters makes measures against lightning crucial, with measures against salt damage and low temperatures also necessary depending on the location of installation. Combine all this with the high reliability that is required to provide a stable electricity supply.

Even simply enumerating the requirements for wind power generation should have convinced us that it is not something that can be realized by merely extending conventional basic technologies. In fact, a survey of the actual circumstances<sup>9)</sup> in Hokkaido, which has 192 wind turbines and accounts for 24% of the total wind-generated electric energy in Japan, revealed a total of 240 problems that have occurred in a total of 270 units at 44 power stations during the two-year period from 2004 to 2005. Under these circumstances, control devices caused problems most frequently, 67 times, followed by drive devices, 63 times, combining for 26% of the total number of problems.

Such being the case, the difficulties with wind power generation are that the wind does not blow as planned, that wind turbines do not exhibit expected performance, and that they are shut down frequently because of problems. These problems are mentioned as challenges to wind power generation. What matters then is the fact that 92% of the 192 wind turbines, 176 units, are foreign-made. As a result, obtaining parts takes a long time, which in turn lengthens the down time.

As is seen in this case, the technologies of machine elements are crucial in the “technologies that will be indispensable for the world in the near future” that Mr. Becker mentions. The fact that Japan is falling behind in this crucial area has already become apparent.

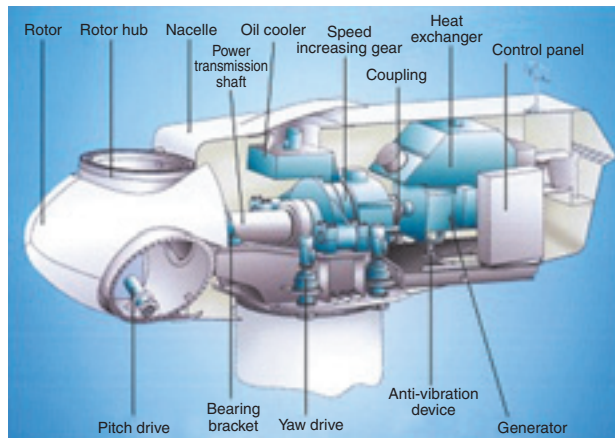


Fig. 4 Example of aerogenerator<sup>7)</sup>

## 6. Two aspects of the year 2007 problem

I have explained that chasing after only frontier technologies invites an interruption in the transmission of elemental technologies, which will be both crucial and indispensable in the near future.

I expect that, based on what I have written, many readers will think that the crisis in handing down technologies is not limited to elemental technologies. In Japan, people talk much about the “year 2007 problem.” The year 2007 problem is defined as when all the baby-boomers retire from working life at the same time, taking with them all their expertise. How can the expertise they possess and have accumulated be transmitted to their successors without problems? This problem will linger far beyond 2007, and the aspects of “quantity” and “quality” cannot be ignored.<sup>10)</sup>

Our country’s age distribution is no longer a pyramid. Estimates provided by the National Institute of Population and Social Security Research<sup>11)</sup> give us pictures of Japan’s five-year-interval population pyramids for 2030 and 2055. In the former, the population peak moves into the 55-to-59-year-old bracket, while in the latter the peak shifts to the 80-to-84-year-old bracket, with the shape changing from a pyramid to something like a bucket. The quantity aspect of the problem becomes that if you want to transmit expertise, you no longer can find younger people to whom you can pass on your skills.

People of the first generation, namely people older than those of the baby-boomer generation, went through their lives almost in step with the high economic growth of Japan. They are people of a hard-working generation who built Japan into a major manufacturing country, starting with the introduction of foreign technologies. They put their experience into the form of manuals and created systems in which any person could work.

The second generation followed in the latter half of the 1970s when Japan had ended the age of high growth and had established such systems.

As a logical consequence, they carried out their activities according to the manuals they inherited from their predecessors, and, in this sense, the transfer of skills can be said to have been smooth. However, it was difficult for the second generation of people to perceive the thought that the previous generation had poured into the manuals, and it is said that the background of thought was difficult to transmit.

The problem lies in the days after the first generation had retired. Needless to say, social needs changed as time passed from the era of high economic growth to the bubble economy to its collapse, while technologies progressed and people’s senses of values also changed. As a logical consequence, the age changed into one in which traditional manuals could no longer be used without modifications. This leads to the quality aspect of the problem; how would the second generation modify manuals to hand them down to the next generation if the background hadn’t been transmitted successfully?

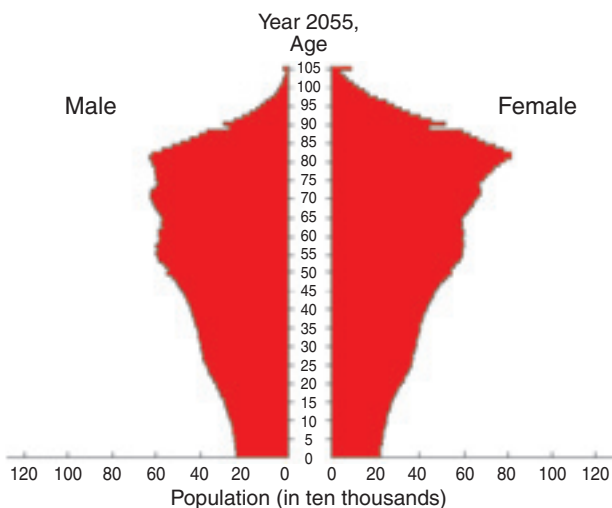


Fig. 5 Population "bucket" in 2055 <sup>11)</sup>

## 7. Role of academia in transmitting expertise

The author thinks that one of the roles to be borne by academia should be the transmission of technologies, which has become difficult for the reasons described above. The author believes this for a couple of reasons.

The first reason is the change in the management policies of Japanese enterprises. <sup>12)</sup> It has been said that, in the past, the enterprises of Japan conducted long-term-oriented management and were eager to cultivate manpower, while the management of US enterprises was short-term-oriented and treated human resources as disposable. For the past 10 years, however, the shareholders' voice has become stronger, and the managements of companies with listed stock have tended to prioritize policies that achieve results in a short period to create favorable effects on stock prices. As a result, a number of enterprises have come to follow a policy of pushing ahead with the reduction of labor costs, tending to prefer to meet labor demand by employing manpower trained by other enterprises, part-timers, and contract workers rather than spend time, money and effort to cultivate their own people.

In this sense, Japanese enterprises have become similar to American ones. We must say that it has become extremely difficult to transmit expertise from one generation to the next in such an environment.

There is another reason why transferring expertise is one of the key roles of academia. Education is not merely the transmission of skills, this is too simple a viewpoint.

Regarding researchers in academia, there is a theory of "1/3-1/3-1/3" which means there are three equally sized groups of researchers. As an example, if we consider a somewhat large group of researchers such as a university faculty or laboratory, one third of them should be those who "enjoy good sales." In our context, this means that one third of them are working

on the leading edge of high technologies. However, the point is that one third is enough for this task, and not more.

The next third according to this theory are researchers that should be "jealous" of the first third that is "enjoying good sales," because they believe that they are doing comparable research work. The vicissitudes of the world dictate that one field of research will not always continue to enjoy good sales. Then, the "jealous" third will be in the spotlight instead of the first third.

What is the remaining third doing? They are those who regard their "sales" as irrelevant and are dedicated to the retention and evolution of systems of learning. This theory insists that these people, one third of all researchers, are necessary. They are directly involved in the transmission of knowledge, and, in the field of engineering, this is the transmission of expertise and skill. If technological expertise is positioned somewhere in the system of learning, it will be transferred more efficiently. Mach reputedly once said, "Science is the economy of thought." I think that the role of academia also includes the transmission of expertise and that this is a reason why hopes are placed on the results of cooperation between industry and academia.

## 8. Cooperation between industry and academia as viewed by the ministry of economy, trade and industry

I have repeatedly used the expression "one of the roles" in the previous section because the roles of academia in cooperation with industry involve much more. Transmitting knowledge is the transfer of skill and expertise that already exist. This is the starting point, of course, with much more beyond it.

Now, let us change our focus. The Ministry of Economy, Trade, and Industry have high hopes for the cooperation between industry and academia.

Four years ago, a lecture meeting titled "Research Integration and Cooperation between Industry and Academia" was held at the Institute of Industrial Science in the University of Tokyo, where I had worked for some time. At the lecture meeting, Mr. Kubota, Chief of the Research and Development Section of the Industrial Science and Technology Policy and Environment Bureau, made a speech with the title of "Critical Challenges in Industrial Technology Development and Expectations Placed on the Academia." <sup>13)</sup>

In this speech, Mr. Kubota mentioned the following three points as increasingly prominent trends observed among enterprises. First are the strong demands of investors, who are asserting themselves with increasingly louder voices, due to the globalization of value standards. As a result of this, enterprises are forced to compress fundamental and infrastructural research. Second in this environment is the thought that buying technologies from other enterprises is simpler and quicker than carrying out

research and development work independently. These two observations lead no doubt to the first reason that I presented in the previous section. The third point is the concern of having reached a place from which one can see the “hurdle” to be surmounted, as a result of having become a technological front-runner.

Under these circumstances, what should industry expect of academia? There are two types of expectations, says Mr. Kubota. The first of them is from the viewpoint of breaking through limits. One finds seeds of academic research in industrial technologies and pushes ahead with solid academic research in order to provide solutions to performance or structural limits backed by scientific knowledge and theories. This is the “progressive research.” The second is from the viewpoint of carrying out new development. One extracts seeds from academic research from which industrial technologies will grow in order to start up university-launched ventures, for example, that take future business development into consideration. This is the “developmental research.”

For elemental technologies, I think the significance of the “progressive research” is predominant. Regarding this, Mr. Kubota made a special request of universities. He states that universities should have a firm grip on what industrial technology is, follow its trends, see where its limits are, and respond to this seriously. If a university loses sight of this duty, the meaning of its existence will be questioned. He points out that the enterprise side would trouble them, though, if they were to “bring individual themes and seek their solutions,” instead of presenting major trends that can guide research activities and transmitting industrial strategies and visions properly. He is very severe in saying, “Before being critical of present-day universities, saying that they are not useful to industry at all or that they know nothing of industry, please think carefully how much information you provide them.”

To borrow the words of Mr. Kubota, elemental technologies are the very fields in which “the hurdles are visible,” and it will be extremely difficult for industry to overcome those hurdles without external assistance. I think that his remarks are very valuable in supporting the significance of cooperation between industry and academia.

## 9. Current state of universities

Cooperation between industry and academia takes various forms. The results<sup>14)</sup> of a survey conducted by the Ministry of Education, Culture, Sports, Science and Technology on the state of joint research with industry and academia and contract research activities shows that both the number of cases and the amount of money increase at a pace of over one percent a year. The number of cases in 2006 was 32,000 with an amount reaching 180 billion yen. Since national universities, the Inter-University Research Institute Corporation and national colleges of technology account for 70% of the cases and 79% of the money, I

will discuss the current state of national universities.

“Eagle eats no carrion.” Being as proud as eagle, national universities did not disclose their internal affairs. Under these circumstances, Mr. Akito Arima, a former president of the University of Tokyo, started publicizing the poverty of Japanese national universities. A dedicated physicist, he disclosed, in a brutally blunt manner, the miserable state of university research facilities, particularly in science and engineering faculties, by citing actual examples close to us.<sup>15)</sup> Thanks to his enlightening activities, I think that society’s recognition of this issue has been improved considerably, but how has subsequent follow-up been conducted? The state is somewhat similar to Japan’s recent business situation.

For example, let me cite the example of how the Grant-in-Aid for Scientific Research funds, which are competitive funds provided by the Ministry of Education, Culture, Sports, Science and Technology, exceeded 50 billion yen in fiscal 1989, 100 billion yen in fiscal 1996, and reached 191.3 billion yen in fiscal 2008. Proud of this great increase, this Ministry holds its head high.<sup>16)</sup>

True, the expenditure as a whole has increased, but as with the business trend, there is a gap here, too. Nearly 90% of the Grant-in-Aid for Scientific Research is distributed to universities, but among over 700 universities 40% or more of the total is distributed to former Imperial Universities. Universities naturally differ in their scale from one another, and the funds are said to be concentrated investments, but there are a number of weaker universities that cannot conduct research properly and are on the brink of death. In fact, if managed improperly, incorporation brings the possibility of collapse to national universities.

I think that the incorporation of Japanese public universities was a change difficult to understand.

For example, the University of Tokyo is still a national university whose basic expenditures are paid as operational grants by the government. What, then, has been changed?

National universities under the former system were national organizations established by the Ministry of Education, Culture, Sports, Science and Technology and this Ministry was accountable for explaining the meaning of their existence collectively. In contrast, a separate corporation was created for each national university and, in turn, each corporation reestablished its associated national university. For example, the University of Tokyo has been reestablished by the National University Corporation, the University of Tokyo. The true character of incorporation is that each university must bear the accountability for its own existence. The system has changed to allow a university that loses purpose for its existence to perish as it will. In fact, a one percent reduction per year is applied to operational grants as an efficiency promotion factor, accelerating the difficulty in running universities.

Now, recall the amount of research expenditures I

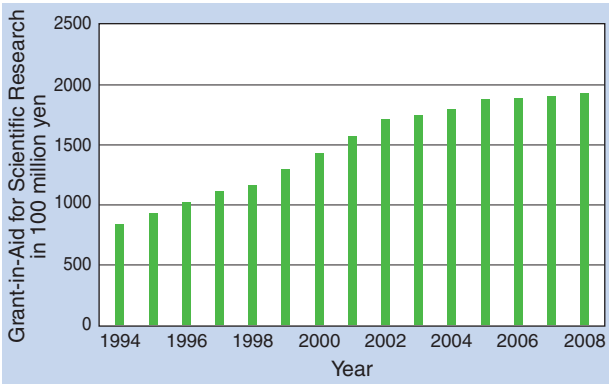


Fig. 6 Increase in Grants-in-Aid for Scientific Research <sup>16)</sup>

mentioned above. The amount of expenditures provided by “industry” for joint research and entrusted research efforts nearly equals the Grant-in-Aid for Scientific Research amount, which are research funds from the government. I think that university staff members, in their hearts, are crying out for research funds through cooperation with industry.

### 10. Cooperation between industry and academia for science

There are, no doubt, problems with the research funds mentioned above, but cooperation between industry and academia has a more essential significance to academia.

A common view is that research can be divided into basic, application, and development research. Pursuing basic research gives birth to application research, which in turn leads linearly to development research, thereby propelling technology.

About 10 years ago, the Science Council of Japan raised a question about this way of seeing research, and proposed “the concept of model research.” <sup>17)</sup>

A survey that the author made on examples of various innovations in science and technology showed that greater progress in the field of applications is made when research is first done on an actual problem then basic phenomena associated with this problem are addressed. On the basis of this finding, I propose that instead of classifying research into the basic, application and development phases, we should classify it as “creative model research,” “extension model research” and “unified model research.” This method of classification follows the motion of researchers’ minds as research advances. “Creative model research” is proposing and verifying a hypothesis, that is, a subjective phase in which one comes to know and find something new. “Extension model research” that follows is standardization and learning, which is the phase of objective conception and creation. One of the most easily understandable examples of this is generalization by means of mathematical equations. Finally, “unified model research” is the phase of harmonization with actual

society, and the keywords for this are social value, humanity and rationality.

At the first glance, one may take these as substitutes for the three models of basic, application and development research, but this is not so. The concept of classification is different. For example, research that does not aim at practical applications and would rank as basic in the traditional classification can be classified as an extension model if its concept and methodology are conventional and it is characterized by precise verification testing. On the contrary, research that does not aim at practical applications may be classified into a creative model if it proposes a new method with no prior example.

And as is shown in Fig. 7, <sup>17)</sup> there is certainly a course of evolution from the creative model to the extension model to the unified model, but evolution is not limited to that course. Unified model research gives birth to creative model research, and extension model research gives birth to creative model research. Through repeated cycling between these three models of research, truth is approached and creativity of academic research is enhanced.

If you look for examples in the field of engineering, you will find a number of them in which an encounter with a technological problem raised a question about an existing theory and this lead to the expansion of the theory. Machine elements provide a good example. In these cases, it will be the role of industry to provide triggers and the role of academia to extend new theories. We see there the possibility of cooperation between industry and academia bringing about essential developments in science.

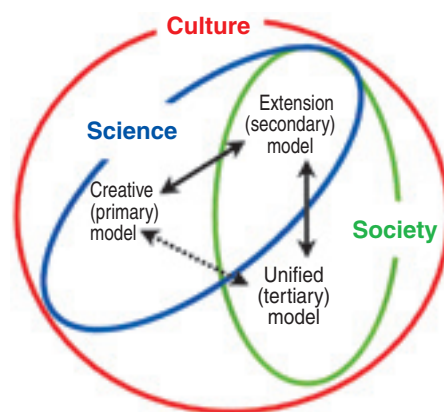


Fig. 7 Concept of “Model research” <sup>17)</sup>

## 11. Concluding remarks

Ten years ago, I was given the honor of contributing a congratulatory article on the occasion of the 80th anniversary of NTN's foundation. I wrote, "The maturation of technology and advances in international standardization are probably the reasons why roller bearings have become highly reliable and widespread. However, I should say something to the effect that, therefore, the roller bearing field seems to have lost technological frontiers," and "the way out of this impasse is to be found in the exploration of technologies by which NTN can create products no other firm can imitate." This belief remains unchanged, and I place great expectations on fruitful partnerships between industry and academia for the technologies that support society, as well as for the future of Japanese universities.

## References

- 1) According to Nobuo Ohmae (2008)
- 2) H. Yoshikawa, Recent Technology and People, Sekai, No.509, P19-34 (1988)
- 3) Carl Becker, What Can Japanese Do about Threats to Life? Gakushikai Magazine, No.864, P24-37 (2007)
- 4) According to data in the NEDO Overseas Report, No.1021 (2008)
- 5) Y. Kimura, About the Defects that Occurred in the Engineering Test Satellite Kiku VI, Journal of Japanese Society of Tribologists, Vol.40, No.11, P889-892
- 6) JAXA, Engineering Test Satellite VI "Kiku 6 (ETS-VI)," [www.jaxa.jp/projects/sat/ets6/index\\_j.html](http://www.jaxa.jp/projects/sat/ets6/index_j.html)
- 7) K. Kobayashi, Bearings and Bearing Steels for Wind Turbines, Sanyo Technical Report, Vol.13, No.1, P73-76 (2006)
- 8) H. Imai, Windmill Tribology, Japan Society of Tribologists 19th Conference Proceedings, P31-34 (2008)
- 9) Hokkaido Bureau of Economy, Trade and Industry, Status and issues related to wind power generation in Hokkaido, [www.hkd.meti.go.jp/hokns/wp\\_enquete/wp\\_text.pdf](http://www.hkd.meti.go.jp/hokns/wp_enquete/wp_text.pdf) (2005)
- 10) Y. Kimura et al., The Study of Maintenance for Management, Japan Institute of Plant Management, P14-16 (2006)
- 11) National Institute of Population and Social Security Research, Collection of Population Statistics Documentation 2008, [www.ipss.go.jp/syoushika/tohkei/Popular/Popular2008.asp?chap=0](http://www.ipss.go.jp/syoushika/tohkei/Popular/Popular2008.asp?chap=0) (2008)
- 12) H. Fujimura, Personnel in Japanese Enterprises [1], Tokyo Shimbun, June 24 edition (2008)
- 13) A. Kubota, Important Issues in the Development of Industrial Technology and Expectations for Learning, Monthly Journal of the Institute of Industrial Science, Vol.56, No.4, P328-335 (2004)
- 14) Ministry of Education, Culture, Sports, Science and Technology, About the Status of Cooperation between Industry and Universities and other Academic Institutions in 2006, [www.mext.go.jp/a\\_menu/shinkou/sangaku/sangakub/07083106.htm](http://www.mext.go.jp/a_menu/shinkou/sangaku/sangakub/07083106.htm) (2008)
- 15) For example, A. Arima, Story of University Poverty, University of Tokyo Press (1996)
- 16) Japan Society for the Promotion of Science, Research conducted with scientific research grants-in-aid, Overview, [www.jsps.go.jp/j-grantsinaid/01\\_seido/01\\_shumoku/index.html#suii](http://www.jsps.go.jp/j-grantsinaid/01_seido/01_shumoku/index.html#suii) (2008)
- 17) Science Council of Japan 3rd Standing Committee, Seeking Renewed Research Concepts, [www.scj.go.jp/ja/info/kohyo/17htm/1708z.html](http://www.scj.go.jp/ja/info/kohyo/17htm/1708z.html) (1999)

### Introduction of the author

#### Yoshitsugu KIMURA

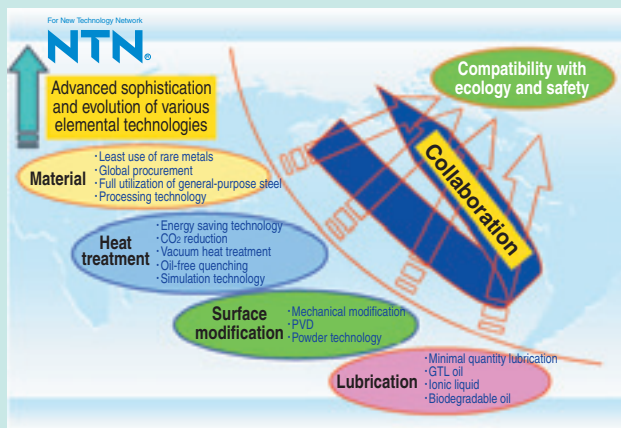
Professor Emeritus, the University of Tokyo, Kagawa University (Doctor of Engineering)  
 1959: Graduated from the Mechanical Engineering Department, Faculty of Engineering, the University of Tokyo  
 1966: Finished the doctorate course, the Graduate School of Engineering, the University of Tokyo  
 1971: Assistant Professor, the University of Tokyo  
 1979: Professor, the University of Tokyo  
 1997: Retired from the University of Tokyo; appointed: Professor, Kagawa University  
 2002: Retired from Kagawa University  
 2003: President, Kagawa University  
 2003-2005: Member, the Science Council of Japan  
 2005: Retired as President of Kagawa University

### Awards

Fiscal 1984: Best Paper Award, the Japanese Society of Tribologist  
 Fiscal 1991: Best Paper Award, the Japan Society of Mechanical Engineers  
 Fiscal 1991: Achievement Award, the Japan Society of Mechanical Engineers Machine Design & Tribology Division  
 Fiscal 2003: The 2003 Tribology Gold Medal

## Trends in Materials and Heat Treatments for Rolling Bearings

Hirokazu NAKASHIMA\*



The focus of this paper is the review of past, current, and future trends regarding steel used for rolling bearings, steel making, and heat treatment technologies. The improvement of steel purity and the development of new steels have been conducted mainly with steel manufacturers so far.

Considering the issues related to globalization, the environment, raw materials such as rare metals, and safety, the future focus will be on surface modification technologies and the coordination of each elemental technology.

### 1. Introduction

Rolling element bearings are used in various industrial machines and equipment with operating conditions which are increasingly more demanding for the bearing. In addition to the more demanding conditions, end users continue to desire longer life and lower operating torque. Steel is the most common material used in rolling element bearings, but other materials such as non-ferrous metal materials including copper alloys as well as resin and ceramic materials are also used. The focus of this paper is limited to steel materials that are typically used for the inner rings, outer rings and rolling elements of NTN's rolling bearings.

Any rolling bearing is a machine element that must be able to roll smoothly while its small contact surface carries a large load. Therefore, the material of every rolling bearing is essentially required to satisfy high degrees of fatigue strength (rolling contact fatigue life), wear resistance, dimensional stability, etc.

The most typical material for rolling bearings is 1% Cr-1.5% Cr high carbon chromium bearing steel. This steel, developed as early as in 1905<sup>1)</sup>, has been used for more than one century without modification to its major components. This paper briefly summarizes the history having taking place during this period about bearing materials and heat treatment techniques for them. Then, based on this knowledge, the author wants to determine the challenges NTN should to address.

### 2. Past trend in life-extending techniques through improvement in materials

#### 2.1 Cleaner -steel technology

The history of evolution of high carbon chromium bearing steel is not presented in this paper as it is described in detail in a paper within the library<sup>1)</sup> of The Iron and Steel Institute of Japan. This history may be defined as a series of attempts to eliminate inclusions in bearing steel. It is known that oxygen and hard oxide inclusions (alumina) adversely affects the rolling contact fatigue life of bearings. In order to reduce the amount of oxide-type inclusions, various steel making techniques have been developed which include vacuum degassing process, ladle furnace process, and continuous casting process.

In Fig. 1<sup>2)</sup>, the trend of oxygen content in bearing steel is plotted. Since 1964 when vacuum degassing process was introduced in Japan (in this year, the world's first high-speed railway system, shinkansen, began operation in Japan), oxygen content in steel has been dramatically decreased as compared with steel materials melted in atmosphere. In the 1980's, ladle furnace process and continuous casting process were established, and as a result, the oxygen content in steel was further reduced. The oxygen content continued to decrease and is now as low as 5 ppm. The effect of these technologies will be apparent from the result of rolling contact fatigue test with specimens plotted in Fig. 2 which shows correlation between the years of steel manufacture and rolling contact fatigue

\*Former General Manager, Elemental Technological R&D Center

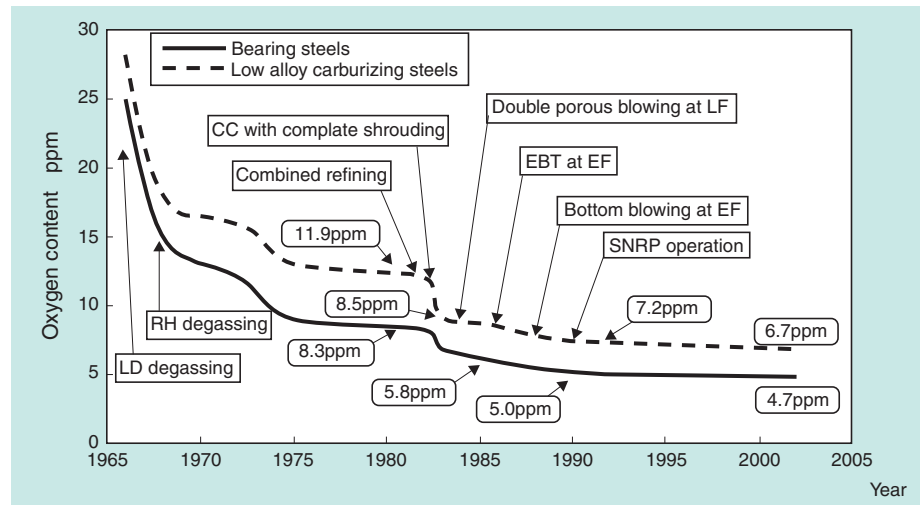


Fig. 1 The trend of oxygen content in steel<sup>2)</sup>

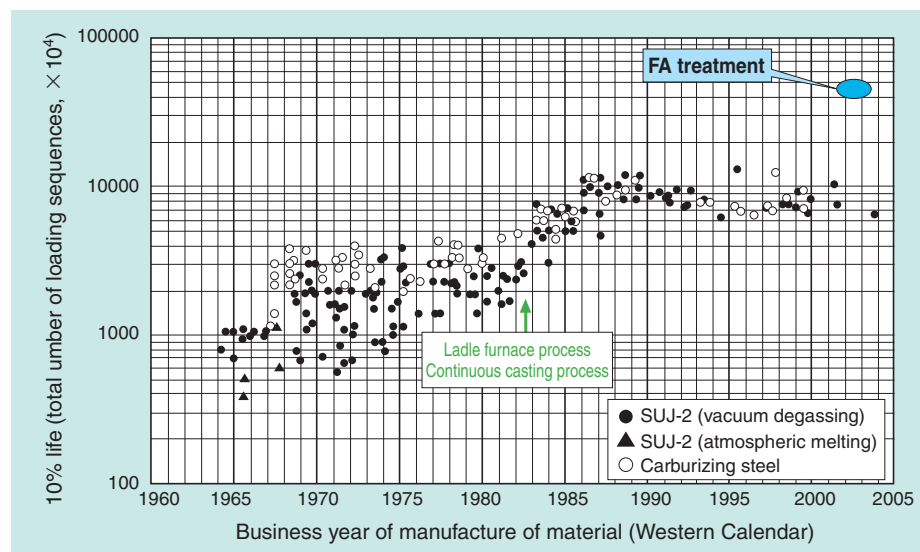


Fig. 2 The trend of rolling contact fatigue life of 12mm in diameter specimen

lives of test steel specimens.

The lives of the present-day specimens are more than 10 times longer than those from 1964. However, no significantly novel steel-making technologies have been introduced since 2000, and the increase in rolling contact fatigue life of bearings has already leveled out. Incidentally, in 1964, the rolling contact fatigue life of carburizing steel (SCr420) was about twice as long as that of bearing steel (SUJ2). The fatigue life difference continued to decrease and by 1990 the carburizing grade material no longer had an advantage for fatigue life.

## 2.2 Advance in assessment technologies for effects of non-metallic inclusions

As mentioned above, the history of bearing steel has been a history of efforts for decreasing inclusions, and as a result, technologies for making highly clean

steels have shown significant improvements. Now, let us think of assessment technologies for evaluating effects of non-metallic inclusions. The most common assessment techniques for non-metallic inclusions among conventional methods are the point count method per JIS (Japanese Industrial Standards) and ASTM-A method for indicating worst visual field.

However, owing to dramatic advance in steel making technologies, these assessment techniques are no longer capable of accurately differentiating between steel materials. Since the latter half of the 1980's, new assessment techniques have been considered which focus into the numbers, sizes and distributions of inclusions. Typical examples of such techniques include extreme value statistics<sup>3)</sup>, electron beam melting process<sup>4)</sup>, ultrasonic method<sup>5)</sup>, and a method where material is electrolyzed, resultant solution is subjected to filtration and the filtration

residue is analyzed<sup>6)</sup>. Despite these efforts, we are still not able to estimate the rolling contact fatigue life of a given steel material based on an assessment of the inclusions contained in it.

Utilizing its unique knowledge about image analysis, NTN has successfully developed a unique system that automatically determines the sizes and types of all the inclusions in a given steel material. By using this system, NTN has been developing technologies for quantifying the physical properties of inclusions contained in a given rolling bearing material and estimating the rolling contact fatigue life of this material<sup>7) 8)</sup>.

Typical examples of the interrelation between rolling contact fatigue lives estimated based on measured inclusion ratings and actual rolling contact fatigue lives is graphically plotted in Fig. 3. Thanks to these new assessment techniques, it is now possible to adopt a simplified rolling contact life test for a steel material and promptly assess the quality of the material in question.

Furthermore, there is a recent attempt<sup>9)</sup> to analyze inclusions occurring on the fish-eye fracture appearance on specimens undergone test using an ultrasonic fatigue tester that is capable of high speed at 20 kHz (fatigue test is completed in a very short test run as short as about 10 minutes) in order to assess the quality of specimens. It is said that the volume of specimen possibly treated with this technique can be larger compared with that with microscopic examination and this technique is capable of examining much larger inclusions. However, owing to variation in the state of bonding between inclusions and the base surface, the inclusions detected with this technique somewhat differs from specimen to specimen. Also, for this technique, correlation

between inclusions and rolling contact fatigue life of steel material will need to be clarified in the future.

### 2.3 Rolling contact fatigue life and chemical components

Various researches<sup>10) 11)</sup> are so far available as to the effects of alloy elements onto rolling contact fatigue lives of steels. Efforts for these studies were very active in a period from the latter half of the 1980's to 1990's. This is because during this period it became possible to further clarify the effects of alloy elements in highly clean steels. At the same time, various manufacturers strenuously developed bearing materials each optimized for a particular application while bearing operating conditions were becoming more demanding.

The alloy elements possibly affecting rolling contact life of bearing include Si, Mn, Ni, Cr, Mo and V. However, for convenience, discussion here is made taking Si as an example because this elemental additive is relatively cheap and is very effective.

As summarized in Table 1, the rolling contact fatigue life is longer with a greater Si content. This is because addition of Si improves the resistance to temper softening for the steel material. Using this

**Table 1** Relationship between rolling contact fatigue life and Si content

Steel	Chemical component (%)				10% life
	C	Si	Mn	Cr	
SUJ 2	0.97	0.31	0.45	1.46	6570
A	1.02	1.01	0.41	1.43	6990
B	0.96	1.30	0.40	1.45	10800
C	1.00	1.42	0.40	1.41	12600

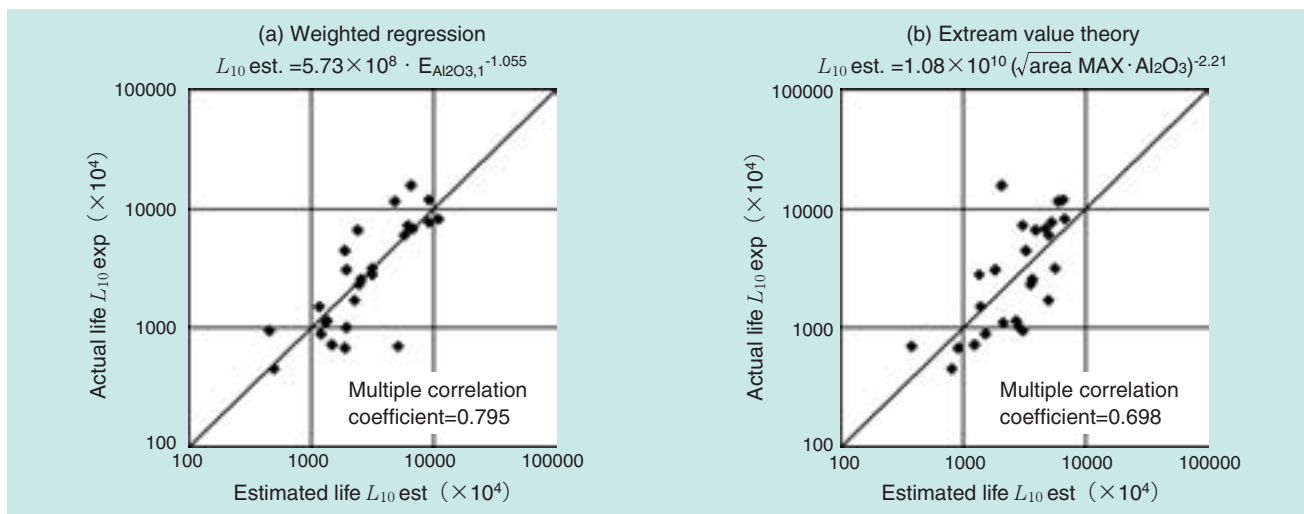


**Fig. 3** The comparison of rolling contact fatigue life and estimated life based on inclusion rating

advantage of Si, NTJ2 material<sup>12)</sup> as semi-high temperature material and STJ2<sup>13)</sup> were developed. Other bearing manufacturers developed similar steel materials<sup>14) 15)</sup> having a higher Si content; however, these materials have Mo additive which is an expensive alloy element.

Novel longer life application specific bearing materials have been developed. At the same time, novel materials featuring optimal machinability have also been developed. Consequently, NTN has successfully commercialized NKJ65 material<sup>16)</sup> based on medium carbon steel and utilizing the above-mentioned advantage of utilizing Si.

Global demand for raw materials has been accelerating since the beginning of the 21<sup>st</sup> century resulting in skyrocketing prices and reduced availability of resources including coke and rare metals.

### 3. Life-extending efforts through improvement in heat-treatment techniques

The basic requirements for bearing materials are longer lives, good wear resistance and higher dimensional stability. Various heat-treatment techniques have been developed to obtain bearing materials that satisfy these requirements.

#### 3.1 Effects of retained austenite

A quenched high-carbon chromium bearing steel contains retained austenite in a range of several % to 15%, though this percentage can vary depending on the heating temperature before quenching. Because retained austenite is essentially a soft, unstable structure, it has been believed that too much retained austenite in a bearing steel material will cause the material to be less hard and more wear-prone as well

as lead to greater deformation from aging (in other words, poorer dimensional stability). Therefore, people believed that a lower retained austenite content is favorable.

In contrast, ever since it was learned that retained austenite can help extend rolling contact fatigue lives of bearing steel materials<sup>17) 18)</sup>, heat-treatment techniques positively utilizing retained austenite have been adopted in applications aiming at longer bearing life, in particular, applications intended to extend bearing lives in a contaminated oil-lubrication environment, thereby NTN has developed the TMB bearing products<sup>19)</sup> by utilizing these techniques.

As discussed earlier, the rolling contact fatigue life with highly inclusion-free carburizing steel is roughly equivalent to that with highly inclusion-free bearing steel (Fig. 2), and, therefore, the effect of retained austenite is less apparent. Nevertheless, if bearings are used under contaminated oil lubrication, the effect of retained austenite is still apparent as shown in Fig. 4<sup>20)</sup>. To summarize, retained austenite is an important material factor for longer bearing life.

#### 3.2 Carbonitriding process

In carbonitriding process, propane or butane is fired to generate reformed carburizing gas into which 5-15% of ammonia gas is added, thereby in the so-formed atmosphere, C and N are allowed to simultaneously enter and get diffused in a bearing steel material.

Nitrogen diffused in the surface layer stabilizes retained austenite. Consequently, the amount of retained austenite is greater after quenching, and, at the same time, the solution of nitrogen helps enhance resistance to temper softening, thereby the rolling contact fatigue life of bearing steel is extended. This process is identical to the multi-stressing process<sup>21)</sup>

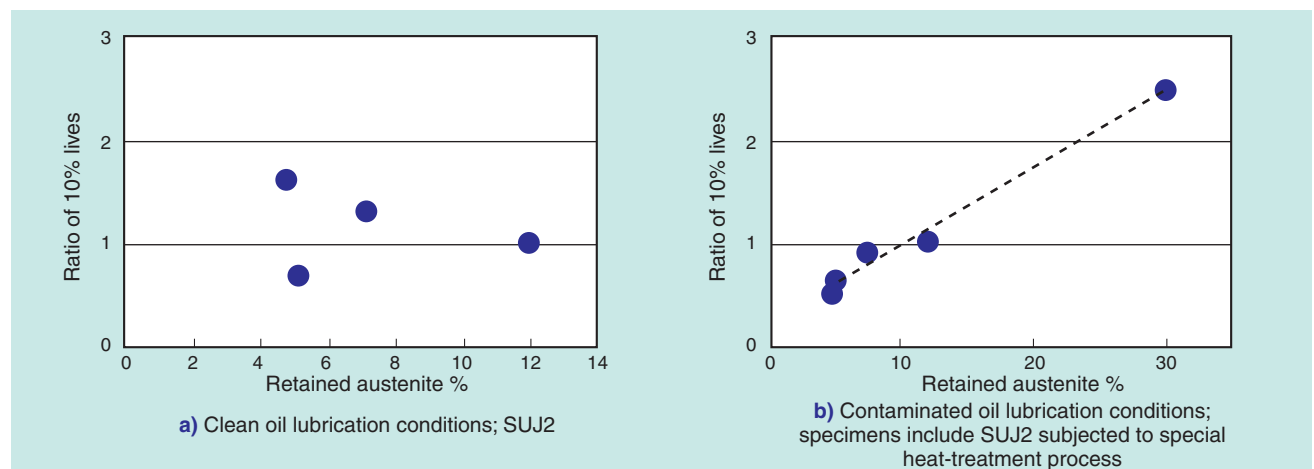


Fig. 4 Relationship between retained austenite and rolling contact fatigue life

disclosed in USA in 1964, and has been positively employed as a special heat treatment technique by various Japanese bearing manufacturers since the beginning of the 1990's.

In Fig. 5<sup>22)</sup>, rolling contact fatigue lives of various bearing materials, to which this process was applied, are graphically plotted, wherein each steel species exhibits extended life owing to carbonitriding process. NTN calls this process the AS (Austenite Strengthening) treatment, and has been adopted for long-life bearings<sup>23) 24)</sup>. NTN believes that a carbonitriding process will remain used to extend bearing life.

### 3.3 Crystal grain refinement process

As described above, the technologies for longer bearing life so far attempted use effects of either retained austenite or nitrogen-derived enhanced resistance to temper softening. In addition to these

longer bearing life-endowing material factors, a new technology has been developed since the year 2000, wherein the new technology features adoption of a novel longer bearing life-endowing factor that is based on crystal grain refining technique. This new technique is the NTN's unique FA treatment (Fine AS treatment)<sup>25)</sup>. Though researches for obtaining higher-strength structural steel materials through enhanced crystal grain refinement were encouraged by the Japan's national super steel material research project<sup>26)</sup>, NTN is the very first bearing manufacturer who positively adopted increased crystal grain refinement for bearings that are highly hard mechanical members. This FA treatment is a complex heat-treatment technique comprising grain refinement featuring crystal grain size less than 1/2 (see Fig. 6) compared with that obtained from conventional quenching technique as well as a carbonitriding process.

By combining two techniques, NTN has attempted

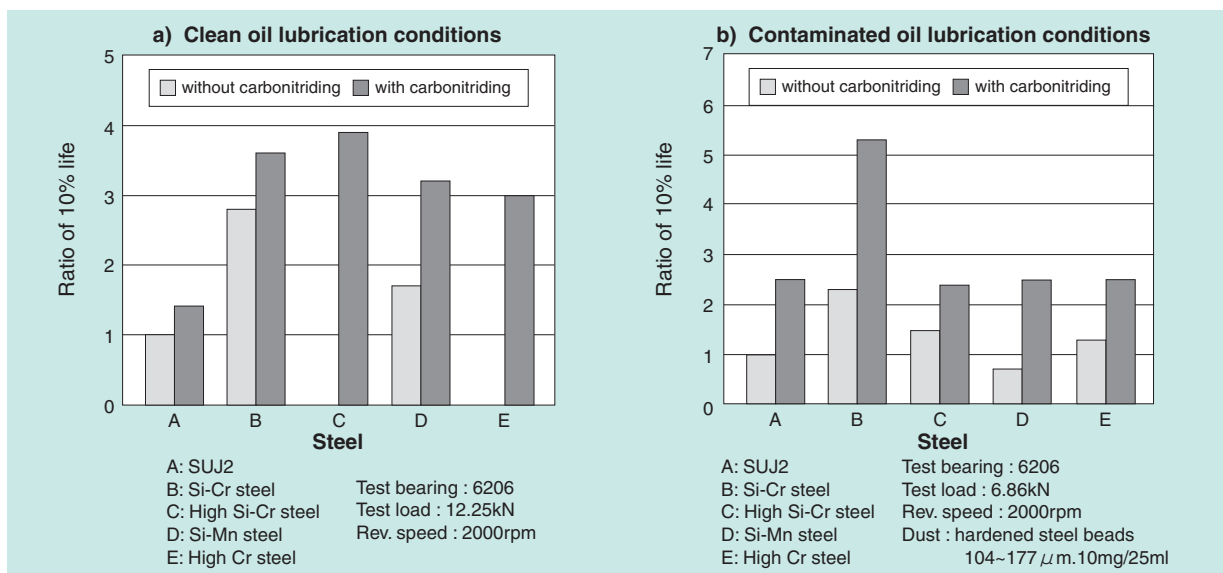


Fig. 5 Improvement of rolling contact fatigue life of various steels with special heat treatment

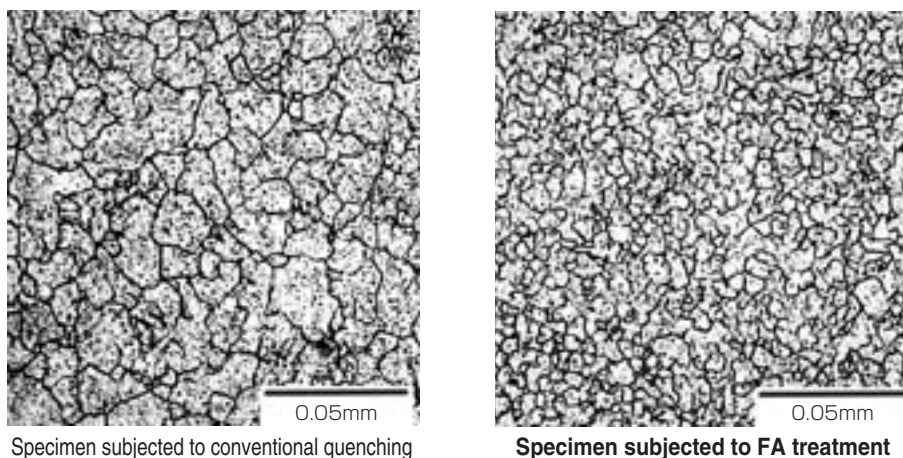


Fig. 6 The comparison of prior austenite grain size between conventional heat treatment and FA treatment

to further extend rolling contact fatigue life of its bearing (see Fig. 2). This heat-treatment technique is suitable for attaining longer rolling contact fatigue life with general-purpose bearing steel. Such a heat-treatment technique will be more commonly used.

## 4. Future challenges

### 4.1 Development of novel materials

As a material assessing technique develops, the performance of subject materials will further improve. This is also true in the field of bearing technology. Much progress has been made in the various assessment and analysis techniques related to bearings. Typical examples of such techniques include microspace assessment technology, surface analysis technology, analysis technique, and simulation technique. NTN expects that these novel tools help us attain new knowledge and technologies such that we can now view nano-structures where in the past the minimum-possible were micro-structures. In the field of steel-making, the oxygen content in steel has already reached lowest practical level, and further bearing life extension in this aspect seems to be virtually impossible.

Despite this, we hope that further improvement in bearing life is realized through researches into bonding between inclusions and base surface and into techniques to turn inclusions harmless by modification of inclusions.

In the aspect of bearing material development, there will remain two long-lasting approaches: one approach is an attempt to seek highly functional materials and the other approach is placement of heaviest importance onto cost-performance. NTN believes that the latter approach in particular requires more strenuous utilization of surface modification technology. More specifically, in an extreme case, it is important with a rolling bearing to modify the surface area in a depth of 1 to 2 mm (can vary depending on the bearing size) where Hertzian contact pressure is applied, and it is not necessary to enhance the hole bulk of the bearing.

Though details are not presented in this report owing to space limitation, flaking (brittle flaking) accompanying a white etching structure such as one shown in Fig. 7 can still occur in limited situations. Previously this brittle flaking was explained by the stress field theory<sup>27)</sup>, hydrogen embrittlement theory<sup>28)</sup><sup>29)</sup> or vibration theory<sup>30)</sup>. However, recently, the most widely accepted explanation is tribochemical reaction-derived hydrogen embrittlement. These flaking modes previously occurred only under operating conditions associated with severe lubricating conditions such as

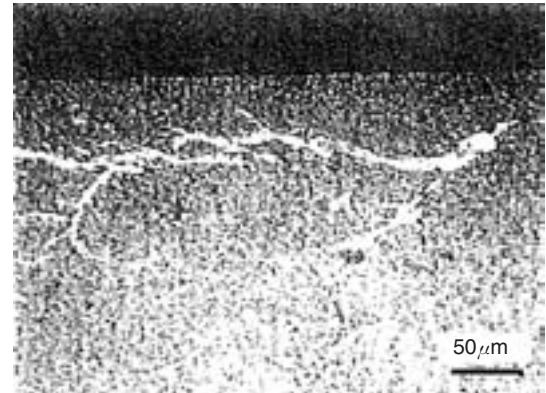


Fig. 7 Cross sectional view of the flaking

those in alternator bearing applications. Bearing operating conditions are becoming increasingly severe, and at the same time, the requirements for lubrication become more demanding. There are also now examples of brittle flaking occurring in less demanding applications where low viscosity oils are used for reduced torque.

Therefore, though attempts have been so far made to prevent this problem by using improved lubricants, we will implement comprehensive countermeasures against this problem, and such countermeasures will include improvements in heat-treatment technique, surface modification technique and bearing design.

### 4.2 About heat-treatment technologies

Commonly applied heat-treatment technologies for bearing steel are atmospheric heat hardening, gas carburizing hardening and induction hardening. Recently, the price of crude oil has been soaring and, at the same time, environmental issues (such as reduction in CO<sub>2</sub> emission to help prevent global warming) as well as problems associated with work environment and labor safety have been increasingly highlighted. These issues are important challenges closely related with heat-treatment process.

In this context, we expect particular carburizing process will be more commonly utilized. Examples of such process include carburizing process based on nitrogen gas, where reforming gas generated from propane or butane and used for atmospheric heating and carburizing is not used; vacuum carburizing process; plasma carbonitriding; high-temperature carburizing for reducing process time. Table 2, presented for providing additional information, summarizes features of various carburizing processes.

Incidentally, use of quenching oil (coolant) is disadvantageous in terms of safety and work environment of hardening operation. NTN believes that a positive attempt will be made to supersede oil

**Table. 2** The comparison of various carburizing process

Item		Plasma carburizing	Vacuum carburizing	Gas carburizing
Quality	Presence/absence of abnormal layer	Absent	Absent	Present
	Cleanliness of surface	High	High	Low
	Surface hardness	High	High	Medium
	Carburizing on porous area	Good	Good	Difficult
Environment	Operating environment	Excellent	Excellent	Medium
	Working energy	Low	Low	High
	Amount of gas consumed	Low	Low	High
	Maintenance cost	Low	Medium	High

Excellent

Moderate

Inferior

hardening, which is currently employed, with air hardening, cooling with pressurized gas or water-soluble coolant.

Induction heating technique is said to be advantageous in reducing CO<sub>2</sub> emission, and an ultra-rapid short-time induction hardening technique<sup>31)</sup> has been sometimes used on a commercial basis in manufacturing gears. Induction hardening techniques are very often used in manufacturing automotive bearing components, and this trend will be more common. Simulation techniques for induction hardening have shown much progress. In addition, a unique control technique for induction hardening process, known as feedback control-based induction hardening technique<sup>32)</sup> has been developed.

According to this technique, a product is heated while its temperature is being monitored; the austenitic state of the material in quenching is calculated, thereby the quenching timing as well as the tempering hardness are calculated, estimated and controlled by the computer. These new techniques will be eventually adopted.

Furthermore, dramatic advancements in sensor technologies, analysis techniques and simulation techniques<sup>33) 34)</sup> applicable to heat-treatment process have recently developed. NTN believes that a heat-treatment process, more positively utilizing these techniques and capable of more active control, will show much more advance.

## 5. Conclusion

The achievements so far attained in the field of materials for rolling bearing and associated heat-treatment techniques have been described above. These achievements are primarily contributable to developments in material engineering and material assessment techniques supported by steel manufacturers. Typical results of the efforts by steel manufacturers include development of highly clean steel materials containing minimal non-metallic inclusions as well as development of special steel material with varying alloy components. The future challenges in our research and development efforts will fall in two fields: development of ultimate material and research R&D efforts thoroughly centered onto cost-performance. In particular, in the cost-performance aspect, material engineers at any bearing manufacturer will need to fulfill required bearing functions even when using a general-purpose material. To this end, it will be increasingly more important, not only to develop more sophisticated elemental technologies including materials, heat-treatment techniques, surface modification techniques (by heat treatment as well as by processing, powder technology and surface coating) and lubrication techniques but also to attempt to realize integration and collaboration with individual technologies.

## References

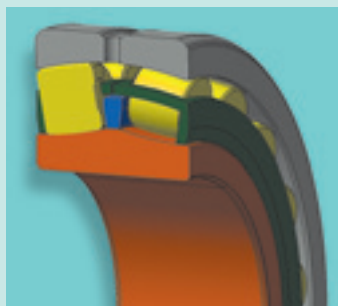
- 1) K. Seto: The Flow of Steel Technologies Series Vol.9: Steel for Bearings, The Iron and Steel Institute of Japan
- 2) K. Kawakami: Sanyo Technical Report, Vol.14, 1 (2007) 22
- 3) Y. Murakami: Metal Fatigue: Effects of Small Defects and Nonmetallic Inclusions, Yokendo (1993)
- 4) Y. Nuri, S. Umezawa: Tetsu-to-Hagane, 75 (1989) 1897
- 5) N. Ishikawa, T. Fujimori: Tetsu-to-Hagane, 71 (1985) 893
- 6) Y. Nuri, S. Kitano: patent publication 2001-159627 (2001)
- 7) H. Murakami: NTN Technical Review No.68 (2000) 58
- 8) K. Yagita, T. Fujita, CAMP-ISIJ, Vol.20 (2007) 1353
- 9) Y. Furuya, S. Matsuoka, T. Abe: Tetsu-to-Hagane, Vol.88, 10 (2002) 643
- 10) T. Yamamoto: Journal of The Japan Institute of Metals 11 (1972) 419
- 11) N. Tsushima: J. Japan Inst. Metals 23 (1984) 50
- 12) K. Maeda, H. Nakashima: NTN Technical Review No.63 (1994) 83
- 13) H. Tanaka, Y. Fujii and K. Maeda: NTN Technical Review No.68 (2000) 51
- 14) T. Hoshino, K. Amano, Y. Yamamoto, A. Ohta and M. Goto: Materia Japan Vol.37, 6 (1998) 516
- 15) M. Imajo: Special Steel Association of Japan, Vol.41, 3 (1992) 19
- 16) K. Maeda, H. Kashimura and K. Sahashi: NTN Technical Review, No.65 (1996) 23
- 17) H. Muro, Y. Sadaoka, S. Ito and N. Tsushima: Proc. 12th Japan Congress on Materials Research- Metallic Materials, 3 (1969) 74
- 18) E. Yajima, T. Miyazaki, T. Sugiyama, H. Terashima: Journal of The Japan Institute of Metals, 36 (1972) 711
- 19) N. Tsushima: Bearing Engineer 47 (1980) 33
- 20) K. Maeda: Mechanical Design, Vol.39, No.13 (1995) 48
- 21) D. P. Koistinen: Trans. ASM, 57 (1964) 581
- 22) K. Maeda, H. Nakashima and N. Tsushima: ITC YOKOHAMA (1995) 1387
- 23) H. Nakashima, K. Maeda and H. Kashimura: NTN Technical Review No.63 (1994) 13
- 24) K. Maeda, H. Nakashima, and H. Kashimura: NTN Technical Review No.65 (1994) 17
- 25) C. Ohki, K. Maeda and H. Nakashima: NTN Technical Review No.71 (2003) 2
- 26) A. Sato: Materia, Vol.37, 10 (1998) 888
- 27) Y. Murakami, H. Takemura, M. Naka, T. Ogawa, T. Momono, A. Iwamoto, S. Ishihara: NSK Technical Journal, 656 (1993) 1
- 28) K. Tamada and H. Tanaka: Wear, 199 (1996) 245
- 29) N. Kino, K. Otani: CAMP-ISIJ, Vol.15 (2002) 1016
- 30) M. Shibata, M. Goto, N. Oguma, T. Mikami: Koyo Engineering Journal, 150 (1996) 16
- 31) K. Kawasaki: Ferrum, Vol.10, 7 (2005) 27
- 32) T. Fujita, N. Suzuki: The Japan Society for Heat Treatment Conference Proceedings (2005) 21
- 33) C. Ohki: NTN Technical Review, No.69 (2001) 61
- 34) C. Ohki: Tetsu-to-Hagane, Vol.93, 3 (2007) 20

Photo of author



Hirokazu NAKASHIMA  
Former General Manager,  
Elemental Technological  
R&D Center

# Improvement of Carburized Steel Wear Resistance by Heat Treatment



Nobuyuki MOURI\*  
Kazuhiko TAGUCHI\*

The bearings for the guide rolls of continuous casting machines used in steel manufacturing have wear on the outer ring because the bearings are used at low rotational speeds and high loads. Therefore, it is necessary that the outer rings of guide roll bearings have high wear resistance. Carbonitriding is known as a common and effective treatment for improving wear resistance. In fact, carbonitrided bearings are used widely for the guide rolls of continuous casting machines. In addition, it is possible to improve wear resistance more by using special steel that includes Cr and

V as elements that form nitrides. However, the use of special steel has problems that include the difficulty of acquisition and high material costs. The purpose of this study is to define a method to improve the wear resistance of standard carburized steel. We have performed an investigation to quantitatively confirm that the wear resistance of bearing materials is improved with increased nitrogen concentration at the wear surface. In addition, we believe that carbonitrided bearing steels transition from severe to mild wear quickly, such that the overall wear resistance is improved.

## 1. Foreword

A typical bearing application that requires excellent wear resistance is guide roll bearings for continuous casting machines in steel-making plants. Because this type of bearing is used at an extremely low speed with inner ring rotation and very high loads, problems including difficulty in oil film formation and deviated wear on the outer ring raceway surface often occur. One measure known to improve the wear resistance of bearing components is nitriding <sup>1)</sup>. Currently many bearings for continuous casting machines are carbonitrided <sup>2)</sup>. Furthermore, by using a special steel which contains large amounts of nitride forming elements such as Chromium and Vanadium, the bearing can feature much improved wear resistance <sup>3)</sup>. However, use of high alloy steel is not desirable because of soaring prices and depletion of scarce resources for alloying elements. In the present research, we have studied heat-treatment techniques for improving the wear resistance of common carburizing steels (SCM420, SNCM420) and attempted to determine the reasons for excellent wear resistance in nitrided steels.

## 2. Carbonitriding conditions for realizing excellent wear resistance

Measures to improve wear resistance of a steel material are increased surface hardness and increased quantities of precipitants with high hardness. However, these two measures do not always hold as reasons for why carbonitrided carburizing steels excel in wear resistance (refer to Section <sup>4)</sup>). In the present research, we have attempted to quantitatively determine the relationship between surface nitrogen concentration and wear-resistance in steel materials, focusing specifically on the quantity of nitrogen in the form of solid solution, with the goal of finding a heat treatment process that provides a material with excellent wear resistance.

It is known that the quantity of interstitial nitrogen in a steel material as a result of a carbonitriding process is dependent on the concentration of undecomposed  $\text{NH}_3$  gas present in the furnace atmosphere <sup>4)</sup>. In other words, in order to increase the nitrogen concentration on the surface of a given product, it is necessary to control the atmosphere in the furnace such that the concentration of undecomposed  $\text{NH}_3$  gas in the furnace is sufficiently high. Incidentally, when the temperature inside the furnace is increased, a higher proportion of  $\text{NH}_3$  gas will be decomposed into  $\text{N}_2$  gas and  $\text{H}_2$  gas immediately after addition into the furnace.

\*Elemental Technological R&D Center

In an attempt to achieve higher carbon penetration velocity, a carbonitriding process is often performed at a higher temperature, and in this situation, it is difficult to increase surface nitrogen concentration.

**Fig. 1** presents examples of interrelation between NH<sub>3</sub> gas addition percent and undecomposed NH<sub>3</sub> concentration percent at 940°C and 850°C in a 120L capacity batch furnace. A temperature of 940°C is assumed to be an appropriate carbonitriding temperature for carburizing steel, and a temperature of 850°C is assumed to be an appropriate carbonitriding temperature for SUJ2. The “NH<sub>3</sub> gas addition percent” is the proportion of NH<sub>3</sub> gas to the total gas addition including the generated endothermic gas required for carburizing. **Fig. 1** shows a result obtained by setting the flow rate of generated endothermic gas at a constant level and varying the flow rate of NH<sub>3</sub> gas. The concentration of undecomposed NH<sub>3</sub> gas in the batch furnace was measured using gas chromatography.

From **Fig. 1**, it is apparent that at the same NH<sub>3</sub> gas addition percent, the concentration of undecomposed NH<sub>3</sub> gas in the furnace is lower at the furnace temperature of 940°C than that at 850°C. In other words, to obtain a particular concentration of undecomposed NH<sub>3</sub>, carbonitriding processes at higher temperatures require a greater NH<sub>3</sub> flow rate. If a carbonitriding process is executed while a higher undecomposed NH<sub>3</sub> concentration is maintained in the furnace, the quantity of penetrated nitrogen will increase and surface nitrogen concentration will be higher even with SCM420 and SNCM420, each containing only negligible quantities of elements which feature good nitrogen reactivity (such elements include V, Cr, Al and Ti). Therefore, we have executed a carbonitriding process with the undecomposed NH<sub>3</sub> concentration regulated at a higher level in order to increase the surface nitrogen concentration, and we

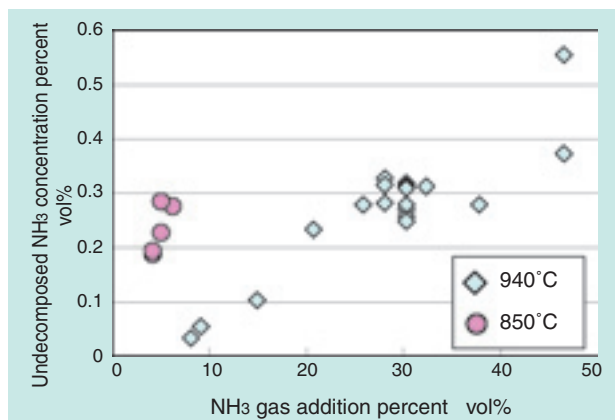


**Fig. 1** Relationship between addition rate of NH<sub>3</sub> gas and undecomposed NH<sub>3</sub> gas

have checked that this technique will improve the wear resistance of the material specimens.

### 3. Carbonitriding process with steel specimens

The specimens representing carburizing steel for this study were SCM420 and SNCM420, while the behavior of SUJ2 was evaluated for comparison purposes. The composition of each steel species is summarized in **Table 1**. The heat patterns applied to these steel species for carbonitriding are shown in **Figs. 2** and **3**. The shape of the specimens used is a ring ( $\phi 50 \times \phi 64 \times 18$ ).

The carburizing steel specimens (SCM420, SNCM420) were subjected to carbonitriding at 940°C, and the specimens of SUJ2 were subjected to carbonitriding at 850°C. The flow rate of NH<sub>3</sub> was varied during the process to control the surface nitrogen concentration on each steel specimen. Also, the atmosphere in the furnace was regulated to maintain constant CP (carbon potential) in the furnace so that the carbon concentration distribution is consistent for all of the carburizing steel specimens.

Examples of carbon-nitrogen concentration distribution for SCM420, SNCM420, and SUJ2 are presented in **Figs. 4**, **5**, and **6** respectively. This carbon-nitrogen distribution data has been obtained from steel specimens carbonitrided in an atmosphere

**Table 1** Component table of test sample mass %

Steel species	C	Si	Mn	Ni	Cr	Mo	Cu
SCM420	0.22	0.32	0.83	0.09	1.18	0.15	0.13
SNCM420	0.20	0.25	0.61	1.62	0.47	0.20	0.14
SUJ2	1.00	0.17	0.39	0.08	1.40	0.03	0.10

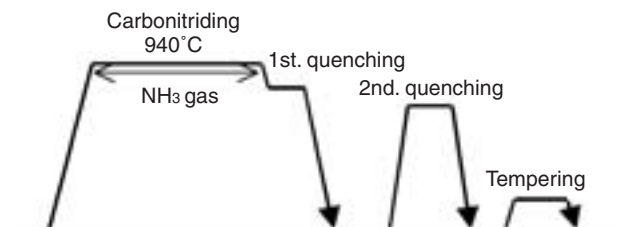


**Fig. 2** Heat pattern of SCM420 and SNCM420

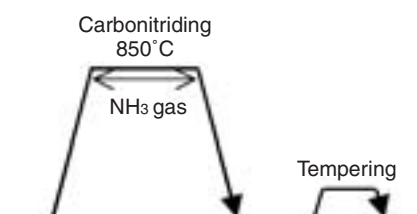


**Fig. 3** Heat pattern of SUJ2

where undecomposed NH<sub>3</sub> concentration was regulated to about 0.2 vol%. It should be understood that a higher nitrogen concentration may be achieved even in a standard carburizing steel by regulating the undecomposed NH<sub>3</sub> concentration in the furnace atmosphere at a higher level. When specimens of SCM420 and SNCM420 were subjected to a carbonitriding process in the same batch, the surface nitrogen concentration on the SCM420 specimens was found to be higher than that on the SNCM420

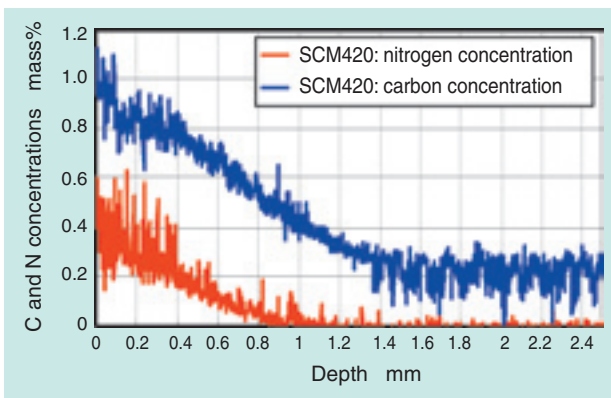


Fig. 4 Distribution of carbon and nitrogen concentration in SCM420

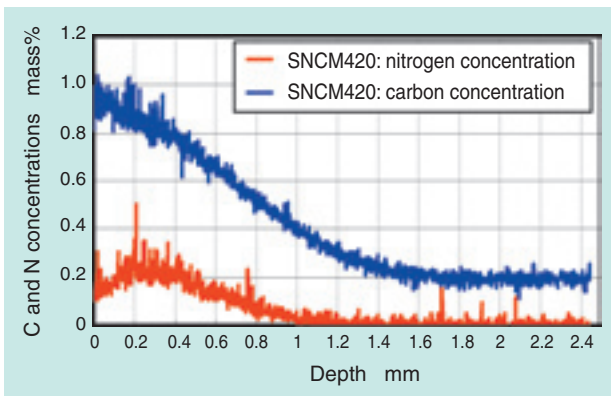


Fig. 5 Distribution of carbon and nitrogen concentration in SNCM420

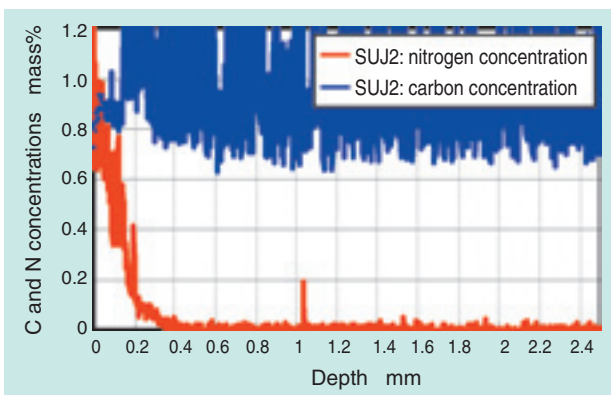


Fig. 6 Distribution of carbon and nitrogen concentration in SUJ2

specimens.

The reason for this seems to be the higher Cr content in SCM420 steel material. In contrast, the nitrogen concentration on the surface layer is higher with SUJ2 as shown in Fig. 6 though the nitriding depth is shallower when compared with the examples in Figs. 4 and 5. The reason for this seems to be that the heat-treatment temperature is relatively low and the nitrogen penetration velocity is low with SUJ2. Incidentally, In order to realize a higher nitrogen concentration on the surface of the final bearing product, it is important to increase the nitrogen concentration at the depth of the grinding allowance.

#### 4. Wear test under oil lubrication

To be able to quantitatively verify wear the inhibition effects of nitrogen in the form of solid solution in steel material, we have executed a test that determines the interrelation between surface nitrogen concentration and wear resistance of various steel species. For assessment of wear resistance, a Savin wear test rig was used. The test rig is schematically illustrated in Fig. 7, and the test conditions are summarized in Table 2.

By running the counterpart at a lower speed and using low viscosity lubricant, wear resistance of steel material under lubricating conditions involving metal-to-metal contact can be evaluated. Wear resistance of a given test piece is evaluated by measuring the minor axis width (parallel with running direction) on the wear mark (oval shape) occurring on the test piece and then calculating the wear volume.

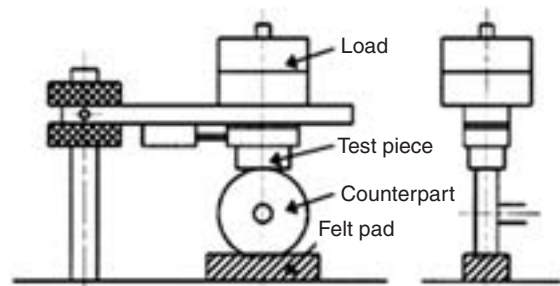


Fig. 7 Schematic of wear test rig

Table 2 Test condition of wear test

Counterpart	Material: SUJ2, through-hardened (60HRC) Size: diameter of rotary member; $\phi 40$ , curvature; R60 Surface roughness: $0.01 \mu\text{mRa}$
Load	50 N (contact pressure $P_{\text{max}}=0.49 \text{ GPa}$ )
Velocity	$0.05\text{m/s}$ ( $24\text{min}^{-1}$ )
Duration	60 min. (sliding distance; approx. 180 m)
Lubrication system	Oil lubrication (lubrication via felt pad, VG2)

Test results of surface nitrogen concentrations and wear resistance (specific wear amount) of the steel species being evaluated are plotted in Fig. 8.

The “specific wear amount” presented along the vertical axis of the graph is a unit for representing the wear volume per unit load and unit distance. The specific wear amount is obtained from dividing the volume of wear by the applied load multiplied by the sliding distance. To determine the surface nitrogen concentration on each test piece, the nitrogen concentration distribution on the ring cross section was analyzed in advance, and then the surface nitrogen concentration of that test piece was read at its grinding allowance region.

From the results of this test, it has been learned that wear resistance significantly improves increases in surface nitrogen concentration, virtually independent of steel species. In other words, while factors including high surface hardness and increased quantities of precipitants with high hardness have contributed to improved wear resistance, increases in surface nitrogen concentration have been shown to exhibit an even greater effect. To provide supporting evidence, Table 3 summarizes the hardness and precipitation area percent information for sample ①, ② and ③, and Figs. 9, 10 and 11 show SEM photos of precipitants for samples ①, ② and ③.

Sample ③ is through-hardened SUJ2 and its surface hardness is higher compared with sample ① (carbonitrided SCM420) and sample ② (carbonitrided SNCM420). It should be understood from these

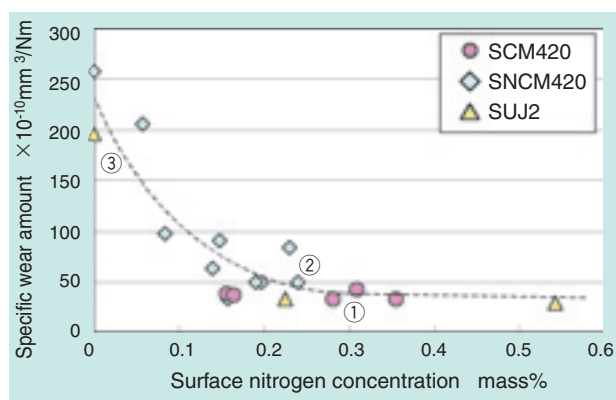


Fig. 8 Relationship between nitrogen concentration of surface and specific wear amount under oil lubrication

Table 3 Hardness and Area rate of precipitates

Sample	Surface hardness HV	Precipitation area percent Area %
①SCM420	710	6.3
②SNCM420	710	2.7
③SUJ2	740	6.7

microstructural photos that the quantity of precipitants is larger in sample ③ than in sample ②. Even so, the carbonitrided samples ① and ② boast better wear resistance. We believe that this is due to nitrogen in the form of solid solution in steel material greatly contributing to improvements in the wear resistance of the steel material. Additionally, with SNCM420 and SCM420, excellent wear resistance has been achieved by increasing the surface nitrogen concentration.

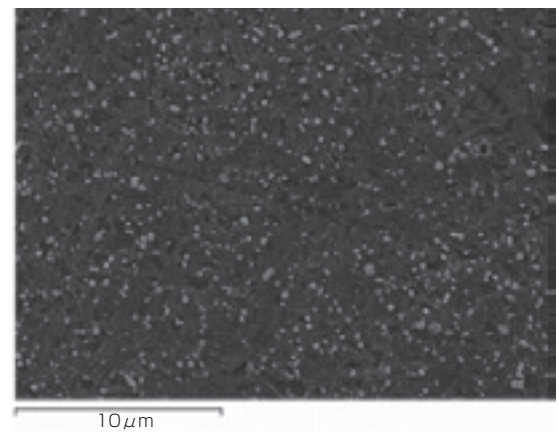


Fig. 9 ① Microstructure of Carbonitrided SCM420 (SEM)

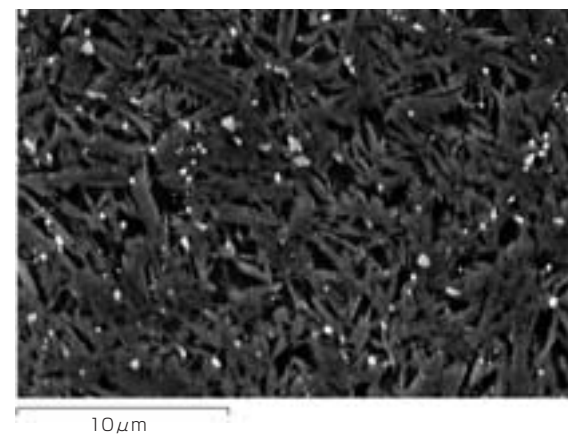


Fig. 10 ② Microstructure of Carbonitrided SNCM420 (SEM)

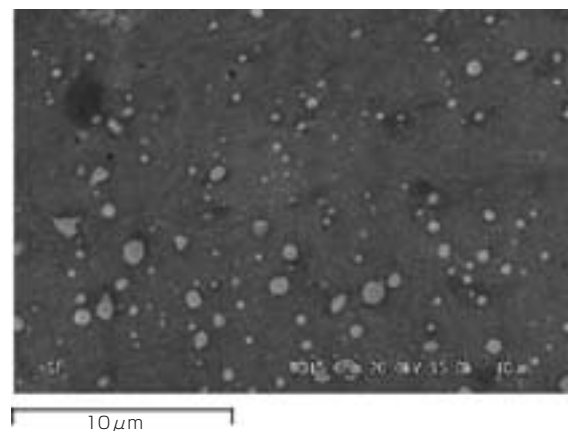


Fig. 11 ③ Microstructure of SUJ2 (SEM)

## 5. Wear test under water lubrication

In a continuous casting line in a steel making plant, a large quantity of water is sprayed onto hot steel material, and not only dust but also water and steam can enter the bearings. The ingress of water into a bearing will accelerate wear of the bearing.

We have assessed wear resistance of specimens under a water lubrication environment using the Sabin wear resistance test rig that is identical to the one used in the wear resistance test under oil lubrication environment. However, because oil and water are not readily mixed homogeneously, we have executed the wear test using pure water in order to simulate a lubrication system contaminated with water. For lubrication, a felt pad moistened with pure water was used, while other test conditions were kept the same as those summarized in [Table 2](#).

[Fig. 12](#) summarizes the interrelation between surface nitrogen concentration and specific wear amount with specimens subjected to wear test under water lubrication. Compared with the test results in [Fig. 8](#) obtained from oil lubrication, the wear amounts with water lubrication are much greater; nevertheless, the trend of increasing wear resistance with higher nitrogen concentration remains same. The wear amount of carbonitrided SNCM420 tends to be greater than that of carbonitrided SCM420. As can be understood from [Figs. 9](#) and [10](#), the quantity of precipitants in the surface layer of carbonitrided SNCM420 is smaller compared with carbonitrided SCM420, though the surface nitrogen concentration is roughly same with both materials. The above-mentioned difference in the quantities of precipitants in the surface layer of the SNCM420 and SCM420 samples seems to lead to the difference in wear resistance. The wear mode under water lubrication appears to be severe wear. The wear amount is much greater when compared with oil lubrication. The reason for the excellent wear resistance of

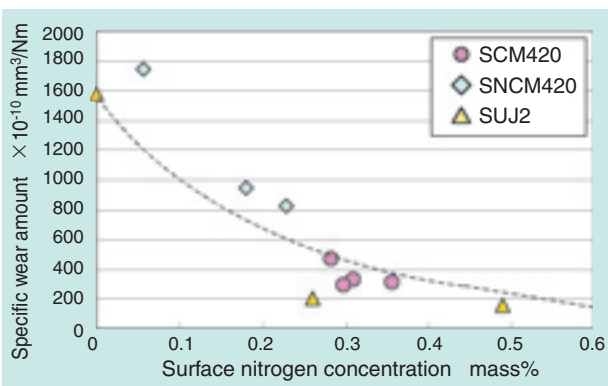


**Fig. 12** Relationship between nitrogen concentration and specific wear amount under water lubrication

carbonitrided SCM420 specimens appears to be inhibition of wear by synergy between an increased quantity of nitrogen in the form of solid solution and an increased quantity of precipitants with high hardness.

## 6. Reasons for why carbonitrided steel materials boast excellent wear resistance

We have considered why carbonitrided SUJ2, which is not a carburizing steel, boasts excellent wear resistance. [Fig. 13](#) illustrates change in wear amount over time of through hardened SUJ2 and carburized SCM420 as well as that of carbonitrided SUJ2 and SCM420, with each test piece being tested on the Sabin wear test rig. The test conditions applied are same as those summarized in [Table 2](#). Wear progresses with through-hardened SUJ2 and carburized SCM420 in proportion with time elapsed until about 90 minutes after start of the test, and then progress in wear decelerates. In contrast, progress in wear with both carbonitrided steel species decelerates in a short time span, after elapse of 15 to 30 minutes. It may seem possible that with the Sabin wear test rig, the contact area increases as wear progresses, and, as a result, the contact pressure decreases and the wear amount over a given time frame also decreases. However, since the progression of wear decelerates at an early stage with nitrided specimens that feature a smaller wear amount and a negligible decrease in contact pressure, decelerated wear progression with these specimens must not result from increased contact area. In other words, it is estimated that the carbonitrided specimens are capable of a “severe-to-mild wear mode transition”<sup>5)</sup>, from severe wear mode where wear occurs rapidly to mild wear mode where limited wear occurs, and that this transition takes place at an earlier stage with these specimens. We consider that the main reason for excellent wear resistance with the carbonitrided specimens in this test is earlier occurrence of “severe-to-mild wear mode transition”,

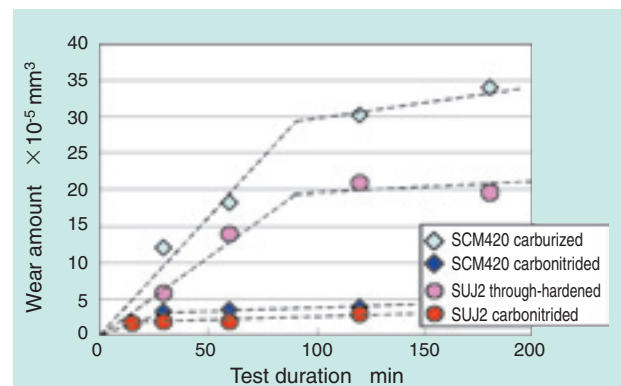


**Fig. 13** Change with time of wear amount under oil lubrication

and believe that the carbonitriding process improves the wear resistance of these specimens in an environment where transition to mild wear mode can occur.

In a similar manner, we have investigated the wear progress with specimens under water lubrication. For this purpose, we have subjected carbonitrided SCM420 specimens and through-hardened SUJ2 specimens to testing on a Savin wear test rig; therefore, one group of specimens has been subjected to testing under oil lubrication while the other group has been subjected to testing under water lubrication. Fig. 14 exhibits the resulting time-dependent wear behavior of these specimens. Though capable of quick transition to mild wear mode under oil lubrication, wear amounts seen in the carbonitrided SCM420 specimens under water lubrication are greater per unit time, and we have not detected a transition point to mild wear mode.

Likewise, through-hardened SUJ2 has not exhibited transition to mild wear mode. When wear progress in through-hardened SUJ2 under water lubrication is compared with that in carbonitrided SCM420 under water lubrication, it becomes apparent that the carbonitrided steel features excellent wear resistance. In a situation where transition to mild wear mode does not take place, such as in the case of the water lubrication wear test, the amount severe wear that occurs as time elapses greatly affects the wear resistance of a steel sample. By increasing the surface nitrogen concentration of a steel material, the wear resistance of the material in severe wear mode is improved.

From the above-mentioned findings, it seems that improvement in wear resistance of carbonitrided products is contributable the following two major reasons:

- ① **Transition from severe to mild wear mode is accelerated.**
- ② **Wear resistance in severe wear mode is enhanced.**

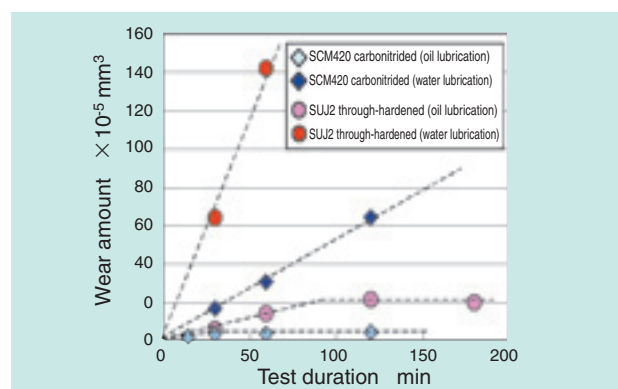


Fig. 14 Change with time of wear amount under oil and water lubrication

Reason ① "accelerated transition to mild wear mode" appears to be an effect of nitrogen in the form of solid solution. As to reason ②, we believe that higher nitrogen concentration is combined with increased quantities of hard precipitants and synergy from these factors helps improve wear resistance of associated steel materials.

## 7. Conclusion

We have quantitatively assessed the interrelation between surface nitrogen concentration and wear resistance with various steel species, focusing on carbonitriding technique as a method for improving wear resistance of ordinary carburizing steel. As a result, we have verified that by maintaining a furnace atmosphere with a higher concentration of undecomposed  $\text{NH}_3$  gas in order to increase the surface nitrogen concentration of a steel product, the performance of that product in situations requiring high wear resistance is much improved. Also, we have studied reasons for improved wear resistance of carbonitrided steel species, and have determined that transition from severe wear mode to mild wear mode occurs more quickly with carbonitrided steel materials, and that carbonitrided steel materials boast good wear resistance even in severe wear mode under water lubrication.

We will further clarify the wear resistance improvement mechanism found through continued testing, and this new knowledge will be reflected in new NTN bearing products.

## References

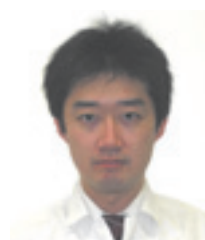
- 1) Iron and Steel Materials Handbook, Bulletin of The Iron and Steel Institute of Japan, 177
- 2) S. Nasu: Applications of AS Series Bearings for Steel and General Industry, NTN Technical Review, No.67, 65 (1998)
- 3) For example, K. Yamamura, M. Oohori: Development of High Wear Resistant "SWR™ Bearing," NSK Technical Journal, No.671, 30 (2001)
- 4) C. Ooki: Effect of Carbon Activity and Base Gas Compositions for Carbonitriding of SUJ2 Steel, Tetsu-to-Hagane, Vol.93 No.1, 44 (2007)
- 5) T. Sasada: Wear (8), Science of Machine, Vol.57, No.8 (2005)

## Photos of authors



Nobuyuki MOURI

Elemental Technological  
R&D Center

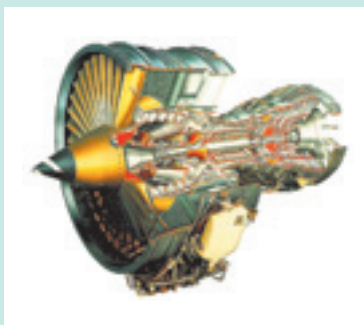


Kazuhiko TAGUCHI

Elemental Technological  
R&D Center

# Deep Nitrided 32CrMoV13 Steel for Aerospace Bearings Applications

Daniel GIRODIN\*



Bearings for aerospace applications such as main shafts of jet engines need to be extremely reliable in order to reduce the In Flight Shut Down (IFSD) ratio and extend the frequency of maintenance operations.

These functional and economic issues require for the material the implementation of appropriate and reliable metallurgical solutions.

This report describes the developments of the nitriding 32CrMoV13 steel (AMS 6481) to optimize its properties in order to overcome the limits of classical steels used for aeronautical applications, such as resistance to surface damage and toughness. The deep nitriding provides a case deeper than 600  $\mu\text{m}$ , a high surface hardness in the diffusion zone due to a semi-coherent precipitation of nano-metric chromium nitrides. This precipitation also generate compressive

residual stresses, while maintaining a notably high tough core. These properties offer considerable advantages in extending both the surface resistance to contamination and the ability to design bearings with integrated design and thin sections that consequently reduce the weight of components.

## 1. Introduction

Bearings for aerospace applications operate under severe service conditions and have been a continuous challenge from the material point of view over the years. Bearings for aircraft turbine engines are required to operate at high speed and temperature, while bearings for helicopter transmission gearboxes require high load capacity. These conditions are combined with a demanding operating environment such as contamination, deformation and vibration of the surrounding structure.

In the meantime, the demand for safety is increased, asking for extended fatigue life and reliability. Modern bearings are also asked to be lighter and cheaper both for supply and maintenance.

These requirements induce bearing designed with thin sections, with integrated functions such as flanges, squirrel cages, or integrated bearing raceways.

The economic aspects require a process with the minimum amount of distortion and grinding and the maintenance costs require raceways more tolerant to surface damages.

To offset the deficiencies of through hardened and carburised steels with regard to surface resistance

and toughness mainly, the nitriding of the 32CrMoV13 steel grade has been optimized.

## 2. Material requirements of aerospace bearings

The history of aircraft turbine engine bearings shows great improvements in reliability and performance due to the simultaneous progress in steels both in composition and quality to sustain the development of new engines<sup>1)</sup>. The through hardened M50 steel (80MoCrV42-16) developed during the late 50's to fulfill the increase in operating temperature shows, as other through-hardened steels, limited high speed capabilities. Indeed, the high tensile hoop stresses resulting from ring centrifugal stresses at high rotational speed and press fit of the bearing ring, are liable to cause the following problems :

- added to the rolling contact stresses, they increase the overall stressing and may reduce the bearing fatigue life.
- over approximately 2.4 millions  $d_n$  (bearing bore in mm  $\times$  shaft speed in  $\text{min}^{-1}$ ), they increase the stress intensity so that fatigue spalling which may arise can lead to fracture of rings<sup>2)</sup>.

High temperature case hardening steels such as

\*SNR Elemental Bearing Technology

M50 NiL (13MoCrNi42-16-14) and X20WCr10 used later on, brought improvements, not only in relation with their tough core but also due to the achievement of compressive residual stresses in the case<sup>3)</sup>. The residual stresses influence the equivalent stress distribution and consequently the initiation and propagation of cracks, thus retarding the fatigue process.

Nevertheless, the fracture toughness of these steels remains poor. They are also subjected to the common disadvantage of carburizing steels regarding the important distortion induced by oil quenching during the heat treatment process that requires expensive grinding and impacts manufacturing costs.

Moreover, under high speed conditions, the lubrication is not permanently fully flooded (EHD) but may be mixed or starved (at least during the transient periods) so that surface fatigue is experienced<sup>4-5)</sup>. In these conditions, both through hardened steels and carburized steels show limitations.

### 3. The development of nitriding 32CrMoV13 steel

The operating conditions, design and manufacturing aspects of the aeronautical bearings previously described require a hard surface and a tough core, ie a surface hardened steel.

Surface modification processes such as nitriding have an advantage over carburising because they usually provide higher hardness, impart higher compressive residual stresses in the subsurface, both properties known to improve indentation damage and sliding wear resistance. The alloy elements (Cr, Mo, V, Mn and Al) added in nitriding steel to improve the solubility in ferrite conditions and to promote fine precipitation that strengthen the diffusion layer, are also favorable for fracture toughness.

Contrary to carburising, the nitriding treatment performed at relatively low temperature (500 - 550° C), on pre-treated material, without subsequent quenching, leads to low distortions, while maintaining a structural and mechanical stability during temperature holding.

According to these features, nitriding of 32CrMoV13 grade, already used for other mechanical applications, offers a good solution to the complex and numerous problems of modern bearings, provided the depth of the case will be deep enough to be compatible with Hertzian stresses. This particular point implies the development of a deep nitriding treatment.

### 3.1 The base steel

The chemical composition of the 32CrMoV13 Steel grade, that has been standardized as AMS 6481 is given in **Table 1**.

**Table 1** Chemical composition of 32CrMoV13 as per AMS6481

	Eléments (%)					
	C	Cr	Mo	V	Mn	Si
32CrMoV13 AMS 6481	0.29~ 0.36	2.80~ 3.30	0.70~ 1.20	0.15~ 0.35	0.40~ 0.70	0.10~ 0.40
M50NiL	0.11~ 0.15	4.00~ 4.25	4.00~ 4.50	1.13~ 1.33	0.15~ 0.35	0.10~ 0.25

NOTE: Other than the components listed above, M50NiL contains 3.20 to 3.60% of Ni.

A VIM + VAR (Vacuum Induction Melting + Vacuum Arc Remelting) melting process is performed, in order to achieve a good level of micro-inclusion cleanliness required to obtain both high and reliable rolling contact fatigue properties and structural fatigue resistance.

The case hardness after a nitriding treatment depends on the hardness of the base metal (measured conventionally at the depth = Hv core hardness + 100 Hv), determined by the heat treatment, and on the composition of the steel, particularly the amount of elements promoting nitride precipitates (Cr, Mo, V, Al).

The 32CrMoV13 steel is a good compromise, in order to achieve surface hardness higher than that of carburized steels, with a rather good diffusivity of nitrogen for acceptable nitriding duration (deep case  $\geq$  0.6 mm in 100h max). It should be made without Al for a better nitrided layer toughness, without Ni and with a close control of residual elements such as P (avoid temper embrittlement) for a higher core toughness.

### 3.2 Nitriding treatment

#### Prior heat treatment<sup>6)</sup>

Nitriding process is performed on parts, after prior heat treatment, in a more advanced stage of machining. Although distortion during nitriding is smaller than for carburized and quenched parts, it is necessary to induce a distortion as low as possible and to control it.

One major cause of part distortion during nitriding is the softening of the base metal, due to complementary tempering effects.

The effect of different nitriding treatments (from 25 h to 100 h at 555°C) on the softening of the base metal for different initial hardness values (from 400 to 480 Hv) is shown in **Fig. 1**<sup>7)</sup>.

In order to restrict distortion after a treatment as long as 100 h, needed to obtain the required case depth, the initial hardness should be close to 380 -

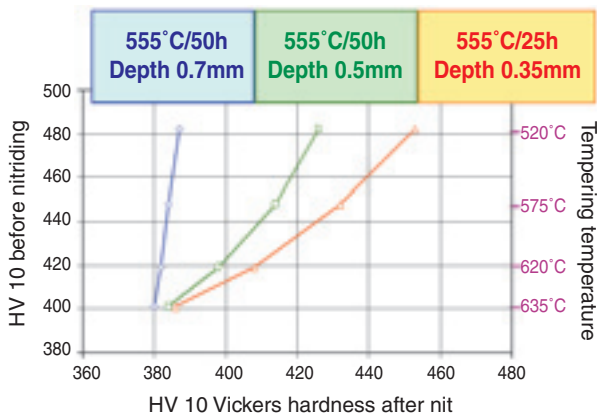


**Fig. 1** Hardness of 32CrMoV13 base metal, before and after different nitriding treatments

420 HV, which corresponds to a tempering temperature in the range 625 - 650°C.

The typical mechanical properties obtained after prior heat treatment compared to AMS 6481 requirements are given in **Table 2**.

A comparison between fracture toughness and rotative bending endurance limit of 32CrMoV13 and M50NiL carburizing steel is given **Table 3**. The better toughness of 32CrMoV13 can be explained by both a slightly lower strength, along with a composition and a microstructure less sensitive to temper embrittlement. The fatigue limit is comparable or higher than that of M50NiL. It may be due to the detrimental effect of the coarser grain size of M50NiL.

**The deep nitriding process**

The basic principle of the process, is to build up, right from the beginning of the cycle, on the outermost

**Table 2** Mechanical properties of 32 CrMoV13 compared to the requirements of AMS 6481

	Hardness (Brinell)	U.T.S (MPa)	Yield Rp 0.2 (MPa)	A (%)	Z (%)	KV Impact strength (J)	K <sub>1</sub> C Toughness (MPa√m)
AMS 6481	352~388	≥ 1137	>951	≥ 13		≥ 68	
Typical values	370~380	1250	1060	16.5	70	133	154

**Table 3** Comparison of main mechanical properties of 32CrMoV13 and M50NiL carburizing steel

	UTS Rm (MPa)	Yield Rp0.2 (MPa)	A (%)	K <sub>1</sub> C 20°C (MPa√m)	Endurance Limit (10 <sup>7</sup> cycles) (MPa)
32CrMoV13	951	1137	13	130	770
M50NiL	1060	1250	16.5	55	750

surface of the parts, a uniform white layer made of nitrides  $\gamma'$  (Fe<sub>4</sub>N) and  $\epsilon$  (Fe<sub>2-3</sub>N), by setting the nitriding potential of the atmosphere to a high value<sup>8)</sup>. A stable white layer, guarantees a permanent source of nitrogen to the diffusion layer, thus avoiding any nitriding defects (de-nitriding or heterogeneous nitriding) of the surface.

The nitriding depth is controlled by solid state diffusion and precipitation, mainly depending on the amount of nitrogen introduced in the subsurface and on the time-temperature cycle. The conventional depth of the diffusion layer, as a function of time and temperature, was measured on samples nitrided in an industrial equipment (**Fig. 2**).

In order to obtain a depth of more than 0.6 mm required by applications, in less than 100 h, nitriding should be performed in the range 525 - 550°C. The temperature (class 5 vertical furnace) and the furnace atmosphere are controlled in order to maintain a stable thickness for the white layer that guarantee an homogeneous treatment.

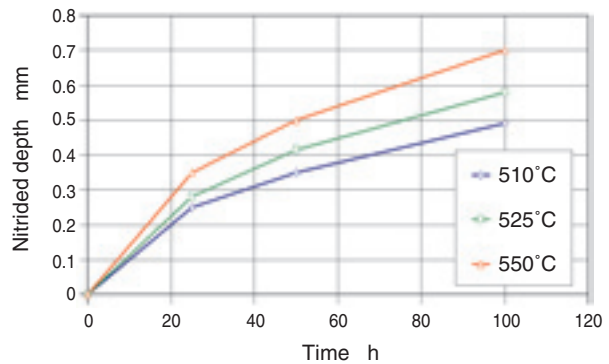


**Fig. 2** Conventional depth of nitriding vs nitriding time for various temperatures

**4. Properties of the deep nitrided layer**

**4.1 Microstructural characterization**

**Structure after prior heat treatment**

Before nitriding, the steel is quenched and tempered at 625-650°C corresponding to the 3rd stage of martensite tempering. The ferrite structure have retained the size of the early martensite laths that ranges between about 0.1 and 1 μm, while tempering carbides precipitate at the lath boundaries and inside the laths. The intragranular carbides are rodlike shaped, about 100 nm in length and arranged in two families oriented 65 degrees from each other (**Fig 3**). These carbides have been identified as cementite Fe<sub>3</sub>C.



**Fig. 3** T.E.M micrograph of the structure after prior heat treatment

**Structure after nitriding**

Nitrogen and carbon concentration profiles have been made through the diffusion layer using an electron microprobe (Fig. 5b). The amount of nitrogen introduced into the surface in the ferrite condition is above 1% Wt in the main part of the diffusion layer and decreases rapidly beyond 500μm in depth. In the meantime, the carbon content is well beneath the content of the base material, then increases to reach a maximum at about a depth of 600 - 700 μm that coincides with the maximum of the diffusion front of nitrogen. Some local carbon peaks reveal the presence of carbide precipitates.

It could be noticed that the hardness profile varies accordingly to the nitrogen profile.

The white layer (compound layer), less than 30 μm deep, combine porous Fe<sub>2-3</sub>N- ε nitride on the outer side with compact Fe<sub>4</sub>N- γ ' nitride on the inner side. Some branchings may grow along grain boundaries (Fig. 4). The white layer is systematically removed by grinding, on the rolling races and working surfaces (typically 70-80 mm).

- The diffusion layer is divided in 2 zones (Fig. 5a):
- A zone, beneath the white layer, about 100 μm deep, relatively depleted in precipitates.
  - A zone, toward the core, where "angel hair" precipitates are present, along the grain boundaries, in the direction parallel to the surface. These precipitates have been identified as cementite carbides.

The lack of carbide precipitation in the first zone could be explained by the dissolution of carbides and the precipitation of more stable nitrides. It results that the carbon is pushed inward by the nitrogen diffusion, leading to the precipitation of "angel hair" carbides.

After the nitriding process, the microstructure of the diffusion layer retains the tempered martensite morphology as observed after prior heat treatment. Inter and intragranular carbides are still observed, except in the sub-surface zone where most of them have disappeared being replaced by smaller nitride or carbonitride precipitates.

A fine nano-metric precipitation of disk-shaped nitrides also occurs inside the needles in the whole diffusion zone. Diffraction and high resolution T.E.M pictures (Fig. 6a and Fig. 6b) of these semi-coherent precipitates show they are of CrN type, only a few interatomic distances wide, while their diameter is about 10 nm<sup>8)</sup>.

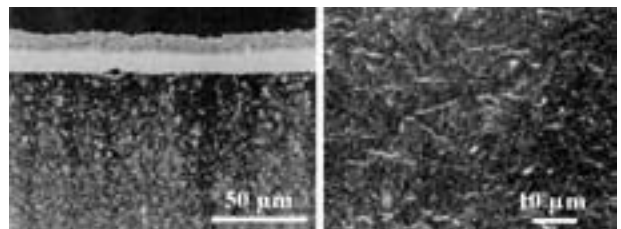


**Fig. 4** Microstructure of the nitrided case (optical)

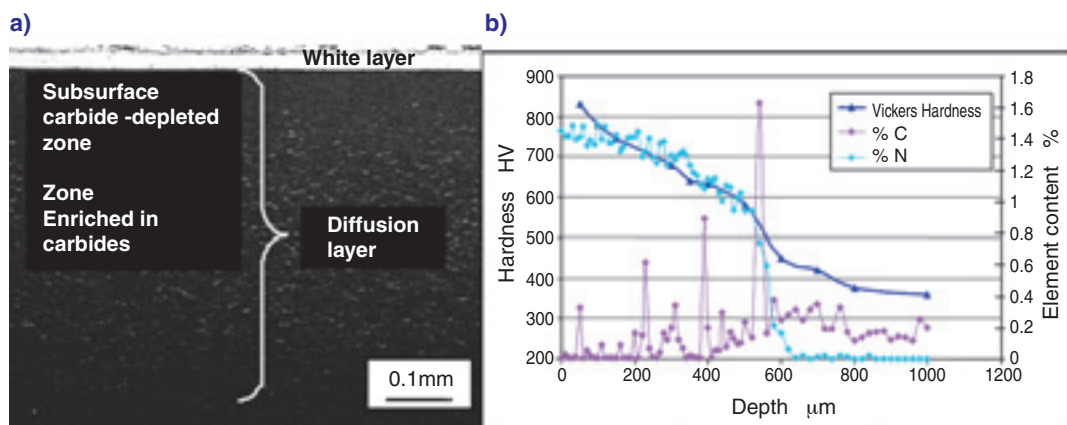


**Fig. 5 a)** Optical micrograph of the nitrided case (nital etching)  
**b)** Vickers micro-hardness, weight %C, weight %N profiles of the nitrided layer

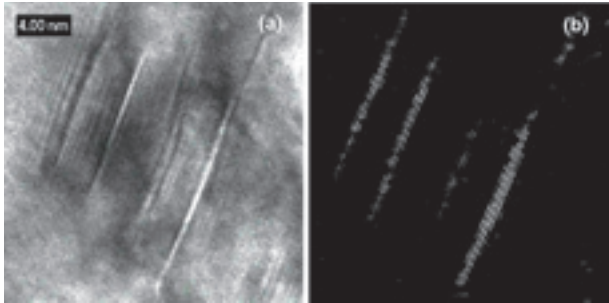


**Fig. 6 a)** High resolution image of semi-coherent precipitates. **b)** Inverse Fourier Transform showing the very thin width (≈3-4 atomic planes)

Two other types of precipitates have been observed :

- Large (Fe,Cr)<sub>3</sub>C carbides, probably residual carbides in which small globular precipitates are formed. These precipitates are chromium nitrides, partially substituted with vanadium and molybdenium
- Intergranular precipitates, probably resulting from former intergranular carbides : A few isolated globular precipitates (about 100 nm in depth), identified as vanadium carbonitrides with partial substitution in chromium and molybdenium and other precipitates, smaller than 50 nm which are chromium nitrides partially substituted with vanadium and molybdenium.

The structure of the core does not evolve significantly after nitriding, only the mechanical properties slightly decrease (Table 4).

**4.2 Mechanical properties**

The nitriding process induces metallurgical transformations that result in changes of the macroscopic mechanical characteristics :

**- A significant hardening of the surface layer.**

The surface hardness of the parts ranges between 730 and 830 HV30 with a case depth between 0.55 and 0.75 mm. This value is achieved after removal of

**Table 4** Modification of mechanical properties after ageing

Condition	Surface	Case	Core				
	Vickers hardness HV10	Nitriding depth mm	Vickers hardness HV50	UTS MPa	Y.S MPa	EL %	Charpy impact J/cm <sup>2</sup>
As treated	375	-	375	1245	1050	15	140
Nitrided	815	0.65	373	1200	995	15.5	125
After ageing	450°C/100H 550°C/100H	0.70 0.80	373 356	1195 1150	985 945	16 16	145 155

the "white layer" (75 µm removed in average by grinding). A typical hardness profile is shown Fig.7 in comparison with carburised M50NiL. The surface hardness of the nitrided 32CrMoV13 steel is higher than that of the carburized M50NiL steel, but the case depth is shallow.

The hardness and other mechanical properties are maintained after 100h ageing at 450° C for both nitrided case and core (Table 4). On the other hand, the hot hardness of the nitrided layer (surface hardness) is comparable to that of M50 steel (Fig. 5).

**- Compressive residual stresses.**

The formation of nano-metric nitrides induce an expansion of the ferrite matrix which, according to the principle of the mechanical balance, builds up the observed stresses (Fig. 8). The residual stresses were measured using X-ray diffraction in the circumferential direction on a ball bearing race ground and polished. The high level of compressive stresses observed in the first 10 µm is due to the work hardening produced by the grinding process, while the rise between the depth of 100 µm and 200 µm is probably linked to the growth of precipitates in this zone.

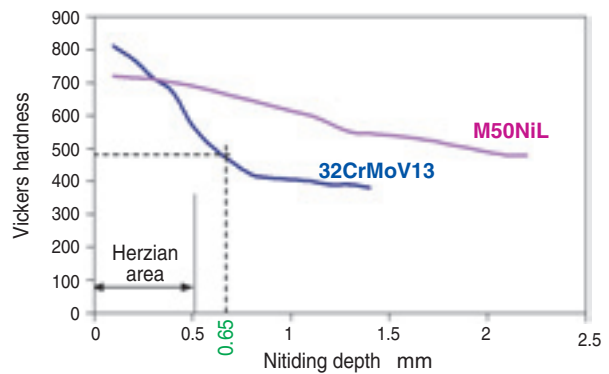


**Fig. 7** Hardness profile of the nitrided layer

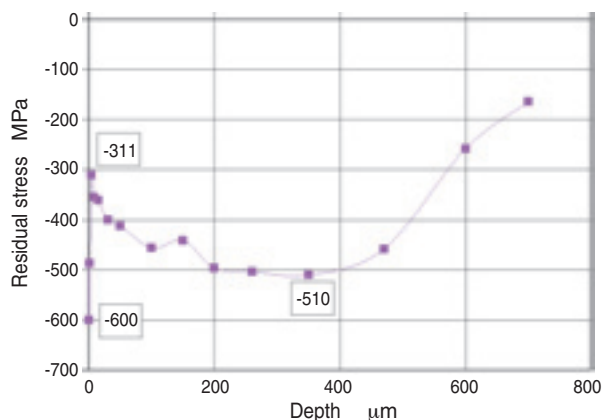


**Fig. 8** Residual stress profile

With a maximum peak value of about -550 Mpa, the compressive residual stresses are much higher than that of case hardened M50NiL ( $\approx$  -200 Mpa), and of course higher than that of through hardened steels (no residual stresses except the grinding one).

### 4.3 Rolling contact fatigue properties)

The ability to resist rolling bearing fatigue is a prime requirement for bearing steels, both concerning subsurface initiated fatigue and surface initiated fatigue.

Subsurface fatigue, experienced under EHD lubrication conditions is linked to the micro-inclusion cleanliness but is not assumed to be the critical damaging process for remelted steels.

According to the Hertzian theory, rolling contact under EHD lubrication conditions is characterized by a sub-surface stress field whose maximum is located at a depth related to the contact loading. The case depth of nitrided parts (as well as for carburised one) has to be fitted to the Hertzian stress profile in such a way that the profile of micro-yield stress limit  $\tau_f(z)$  is above the equivalent stress curve  $\tau_d(z)$  related to the loading conditions.

In this way, a method for determining the profile of compressive micro-yield stress in the nitrided case, based on nano-indentation measurements, has been developed<sup>10-11)</sup>. The comparison of the evolution of the micro-limit profile with the loading stresses can then provide an evaluation of the potential risk of subsurface damage.

Fig. 9 shows the local equivalent stress profile representative of the loading conditions (Hertzian stress = 3100MPa) for NJ212 cylindrical roller bearings compared to the micro-yield shear stress limit of M50 and nitrided steel (the local micro-yield stress is taken at  $20 \times 10^{-6}$  plastic strain).

The middle curve represents the maximum shear stress for the M50 steel without any stress raiser (such as for example oxide inclusions, carbides...). The

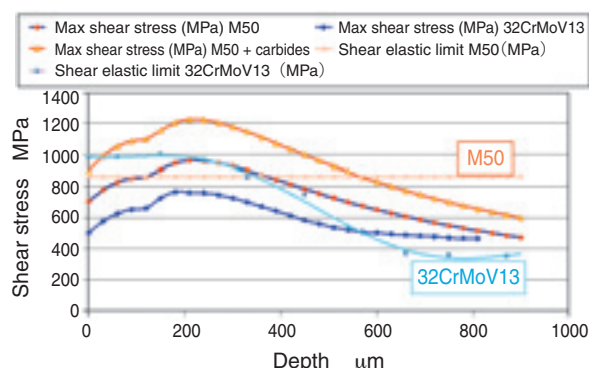


Fig. 9 Comparison of local maximum shear stress for NJ212 bearings (PHz=3100MPa)

upper curve is the local maximum shear stress taking into account the local stress concentration due to carbides. The lower curve is representative of the nitrided steel, including the compressive residual stresses that reduce the local value of the maximum shear stress.

Therefore, the M50 steel may develop fatigue subsurface cracks up to 600 µm in depth contrary to the nitrided steel which is theoretically free from local structural modifications in the area of maximum Hertzian shear stress and thus not subjected to damage except for depth over 550 µm, where the stress is relatively low and the risk unlikely to happen.

Several types of rolling contact fatigue tests were performed, under various lubrication and operating conditions, in order to qualify the behavior of the nitrided case.

### Fatigue life under EHD lubrication conditions

Rolling contact fatigue tests under fully flooded oil lubrication were performed for different type of contacts (testing conditions and results are given Table 5):

- flat washer (trust bearing) on the SNR FB2 test machine
- 6309 deep groove ball bearing on SNR standard "S" machine
- NJ212 roller bearing on SNR "FC" bench

For all these tests, the rolling elements were made from through hardened steel.

Both for point and linear contacts, the endurance tests show a fatigue life better for the deep nitrided 32CrMoV13 steel than for trough hardened or carburized steels. On deep groove ball bearings and tapered roller bearings, the life is about 2 to 3 times the life of M50 steel.

Table 5 Comparison of rolling contact fatigue of test samples and actual bearings

	Bearing type	Flat washer	6309	NJ212
Test conditions	Axial load (daN)	1075	530	300
	Radial load (daN)	—	1600	1200
	Hertzian stress (MPa)	4200	3200	3100
	Speed (min <sup>-1</sup> )	1500	2200	1200
	Lubrication	ISO 46 oil	ISO 46 oil	ISO 46 oil
	Temperature (°C)	40	Room Temp.	Room Temp.
L <sub>10</sub> Life (h)	32CrMoV13	≥ 1300	3863	1240
	M50	≥ 1300	942	560
	M50 Nil	850	—	980
	X20WCr10	990	—	—

### Fatigue life under boundary lubrication

Tests have been made on FB2 machine using NATO 0156 oil at room temperature under a 2500 MPa contact stress. In these conditions, the lubricant oil film parameter  $\lambda = \text{oil film thickness} / (\text{Ra}^2_{\text{raceway}} + \text{Ra}^2_{\text{ball}})^{1/2} \approx 1.5$ . Comparative results for M50NiL, M50 and 32CrMoV 13 are given in **table 6**.

Considering the experimental results, the behavior of the deep nitrided 32CrMoV13 steel that experienced no failures is much better than carburised M50NiL that shows peeling damage.

**Table 6** Rolling contact fatigue under boundary lubrication and of dented raceways (flat washer)

		M50NiL	M50	32CrMoV13 DN
Boundary lubrication	$L_{10}$ (h)	218	>900	>900
Dented raceways	$L_{10}$ (h)	123	503	>900

### Simulation of contaminated lubrication

Under contaminated lubrication conditions, the life of bearings decreases and surface initiated spalling occurs on dents produced by foreign particles going through the contact. The effect of the shape and size of artificial dents on the bearing life provides useful information with regard to the fatigue life under contaminated lubrication.

For this purpose, tests have been performed on the SNR FB2 machine. Four Vickers dents, 280  $\mu\text{m}$  in diagonal, had been printed on the race before testing. Rings were run under a 2500 MPa Hertzian stress using NATO 0156 oil lubrication.

Deep nitrided 32CrMoV13 steel shows a longer life compared to M50 and M50NiL steels (**Table 6**). Tests were interrupted after 900 hours without any failure having been observed, contrary to M50 and particularly M50NiL that experience early failure.

This favorable behavior could be explain by the combined effects of large surface hardness and high compressive residual stresses.

## 5. Industrial statistics and products

When the nitriding conditions described previously are applied, after proper prior heat treatment for hardness 380 - 420 Hv, the statistical results for hardness, conventional depth and distortion measured on more than 70 batches of a 150 mm outer ring, are given in the **table 7**. These results confirm the great reproducibility of the process.

Bearings with different shapes and sizes are manufactured by SNR Roulements using deep nitrided 32CrMoV13. It concerns deep groove ball bearing, roller bearing with thin sections and/or complex integrated shapes such as bearing for main shaft of aircraft turbine engines or rotor mast of helicopters (**Fig. 10**).

**Table 7** Metallurgical and dimensional properties of deep nitrided parts

	Specification	Average value	Range
As nitrided depth (mm)	0.63~0.75	0.67	0.62~0.72
Depth on finish parts (mm)	$\geq 0.55$	0.60	0.55~0.65
White layer ( $\mu\text{m}$ )	$\leq 35$	25	20~30
Surface Hardness (HV0.5)	750~850	795	760~830
Core surface (HV0.5)	360~420	400	380~420
Diameter expansion ratio ( $\mu\text{m}/\text{mm}$ )	—	0.8	0.7~0.9
Out of roundness ( $\mu\text{m}$ )	—	25	10~40



**Fig. 10** Example of aerospace bearings

## 6. Conclusion

The deep nitriding process applied to 32CrMoV13 steel (AMS 6481) solves in a convenient way the difficult compromise concerning the incompatible properties required for aerospace bearings.

Indeed, these bearings may operate under severe conditions such as high-speed, high temperature, starved or contaminated lubrication. Furthermore, their design may be complex, integrating multiple functions, and requires thin sections for weight reduction.

The Deep Nitriding of 32CrMV13 steel offers a better compromise than classical high temperature bearing steels (through hardened or carburized) to meet these requirements.

The core material has excellent toughness for structural functions and high rotational speeds. Due to the semi-coherent precipitation of nano-metric nitrides, the nitrided layer features high hardness, high compressive residual stresses and superior rolling contact properties.

The nitriding technology makes easier the production of parts with complex shapes, with a limited amount of finish grinding because of the limited distortions resulting from low temperature cycle. The manufacturing process is under control and properties show small dispersion.

All these features make the deep nitrided 32CrMoV13 an excellent solution for high reliability and safety aerospace components.

**Acknowledgment** : *Author would like to thank the Aubert & Duval Company and the Mateis laboratory of Lyon INSA for their collaboration to this work.*

## References

- 1) Pearson, P.K., "The history and future of aircraft turbine engine bearings, Bearing steels: Into the 21<sup>st</sup> century", J.J.C. Hoo Ed, ASTM STP 1327, p335-353, 1998.
- 2) Spitzer, R. "New case-hardening steel provides greater fracture toughness", Ball Bearing J., SKF, 234, 6-11, 1989.
- 3) Böhmer, H.J., "Residual stresses and material behavior of M50NiL and RBD", Bearing Steels, J.J.C. Hoo Ed, ASTM STP 1195, p34-48, 1993.
- 4) Averbach, B.L. and Bamberger, E.N., "Analysis of bearing incidents in aircraft gas turbine mainshaft bearings", Tribology Transaction, 34 ; 2, pp 241-247, 1991.
- 5) Averbach, B.L, Van Pelt, S.G., Pearson, P.K. and Bamberger, E.N., "Surface initiated spalling fatigue in M50 and M50 NiL bearings", Lubrication engineering, vol.47,10, pp 837-843, 1991.
- 6) Joly, P. and Daniel Girodin. "Deep Nitriding of the 32CrMoV13 Steel (AMS 6481 0.32% C-3% Cr-1% Mo-0.2% V) and its Application for Aerospace Bearings," Toronto, May 2005.
- 7) Joly, P., FREY, J. and LARREUR, B., "Développements récents dans les aciers de nitruration et le contrôle des cycles de nitruration pour l'obtention de couches nitrurées très profondes, "NITRURATION, Journées franco-allemandes", J. Grosch et E.J. Mittermeijer, April 2002
- 8) Dulcy, J., Torchane, L., Gantois, M., "Mécanismes de formation et cinétique de croissance des couches nitrurées, "NITRURATION, Journées franco-allemandes", J. Grosch et E.J. Mittermeijer , April 2002.
- 9) M. Sennour, PhD Thesis, Lyon INSA, 2002
- 10) El Ghazal, H., " Study of microstructural and mechanical properties of case hardened 16NiCrMo13 and nitrided 32CrMoV13 steels – Application to the estimation of the rolling fatigue life", PhD Thesis, Lyon INSA, 1999.
- 11) Vincent, A., Elghazal, H., Lormand, G., Hamel, A., Girodin, D., "Local elasto-plastic properties of bearings determined by nano-indentation measurements", Bearing steel technology–Advances and state of the art in bearing steel quality assurance, J. M. Beswick Ed, ASTM STP 1419, p427-442, 2002

Photo of author

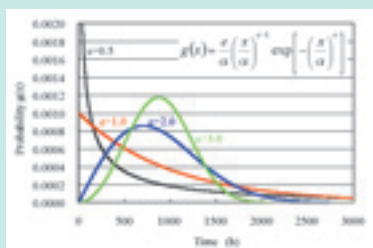


**Daniel GIRODIN**

SNR Elemental  
Bearing Technology

# Test Design and Result Interpretation Methods for Evaluating Rolling Contact Fatigue Life to Maintain Both Efficiency and Reliability

Takumi FUJITA\*



In this report, several methods for rolling contact fatigue (RCF) life test design and result interpretation are introduced. These methods generate results using random numbers following a Weibull distribution. The first method illustrates the relationship between the minimum number of test pieces and the suspension time in a fixed time test required at  $L_{10}$  and  $L_{50}$  life with an arbitrary reliability. This relationship is useful to maintain qualitative reliability and avoid excessive quantitative testing. The second method can clarify the relationship between a given number of test pieces and a resultant significant difference in  $L_{10}$  and  $L_{50}$  life in accelerated testing with an arbitrary reliability. This relationship is also useful to

estimate the necessary number of test pieces based on statistical logic. Of note, applying calculations allows estimation of the test results. The third method enables the calculation of a range of  $L_{10}$  and  $L_{50}$  lives with significant reliability even if the number of test pieces is too small to estimate  $L_{10}$  or  $L_{50}$  lives employing Weibull plots. The fourth method can determine the significant difference of  $L_{10}$  and  $L_{50}$  life between two lots and allow the quantitative estimation of the minimum difference between their lives from data obtained experimentally.

These methods provide techniques that are easier to understand compared to recent mathematical models, and they show enough flexibility to apply to almost all types of testing. These new systems will therefore eliminate the need for special experience in statistical design and result interpretation for RCF life tests.

## 1. Introduction

Rolling contact fatigue life testing is one of the tests that must be performed to assess bearing performance. Generally, the rolling contact fatigue life of a given bearing is compatible with Weibull distribution<sup>1,2)</sup>, and variation in estimated rolling contact fatigue life is significantly large. Therefore, it is an important practice in rolling contact fatigue life testing of bearings to assess the bearing life in a conservative manner using high reliability in order to avoid problems in the market with the bearing product in question. Rolling contact fatigue life of a bearing can be roughly categorized into a test to be performed under conditions that simulate the operating conditions of a bearing installed onto machinery, and another test to be performed in relatively severe conditions. In the former test scheme, we may judge that the bearing in question has sufficient life if the test successfully continues to a target timing without bearing failure on the bearing (hereinafter this type of test is referred to as "fixed time test").

With the latter test practice, a test piece develops failure in a relatively short run, and we can estimate

the life of a bearing based on Weibull plots and we can evaluate the bearing performance based on the resultant estimated life (hereinafter this type of test is referred to as "accelerated test").

With a fixed time test, guaranteed bearing life is in theory longer when a large number of test pieces of the bearing in question do not develop a failure in a longer time span: however, it has been difficult to select the necessary number of test pieces (herein after referred to "test pieces") and suspension time for a fixed time test based on statistical data. Attempting to solve this issue, there have been proposed techniques intended to solve bearing life based on the relation between test pieces and suspension time<sup>3)-5)</sup>.

However, because these methods are mathematical approaches, there have been difficulties in handling mathematical expressions to cope with situations and interpreting the resultant solutions.

Incidentally, in accelerated testing, the difference in life between lots can be more reliably determined if a more test pieces are tested and a greater difference in life is attained: however, it has been difficult to set up the difference in life that allows positive judgment of a particular number of test pieces and significant

\*Elemental Technological R&D Center

difference. To address this issue, Johnson<sup>6)</sup> has developed a plotting method that helps the user to approximate the relationship between test pieces and difference in  $L_{10}$  lives for determining significant difference. This technique, however, has been less often used because it does not offer a graphical plotting arrangement that can be used under an arbitrary set of conditions.

Thus, conventional rolling contact fatigue life testing has several drawbacks as to design of test and test result interpretation. This report presents a novel method for objectively and quantitatively designing rolling contact fatigue life tests and interpreting test results. The author's method is a technique that utilizes calculation based on Weibull random numbers.

**2. Items calculable with the present method and technique for generating Weibull random numbers used in calculation**

By using Weibull random numbers, the author's method can solve all the problems in **Table 1**. Though a variety of contents are presented in **Table 1**, only one common calculation approach exists there. That is, "Weibull random numbers are generated and then a rolling contact fatigue life test is simulated, and the obtained result is applied to design for rolling contact fatigue life test and interpretation for test result".

To be able to generate Weibull random numbers, it is necessary to define three parameters of Weibull distribution. Probability density function of Weibull distribution is give below:

$$g(x) = \frac{e}{\alpha} \left( \frac{x-\gamma}{\alpha} \right)^{e-1} \exp \left[ - \left( \frac{x-\gamma}{\alpha} \right)^e \right] \dots \dots \dots (1)$$

$e$  : shape parameter,  $\alpha$  : scale parameter,  
 $\gamma$  : location parameter

Because Weibull distribution involves three parameters, three conditions about these parameters need to be defined, wherein the author's method utilizes three sets of conditions for defining Weibull distribution, and they are ① a relation<sup>11)</sup> between  $L_{10}$  life and location parameter determined from the past vast accumulation of test results<sup>7)-10)</sup>, ② life values that are governed by the purpose of calculation ( $L_{10}$  lives,  $L_{50}$  lives, etc.) and ③ shape parameter assumed from past test performances (a group of shape parameters is hereinafter referred to as "Weibull slope"). Incidentally, the condition set ① is represented by the following expression<sup>11)</sup>:

$$\gamma = 0.05 \cdot L_{10} \dots \dots \dots (2)$$

$L_{10}$  :  $L_{10}$  life

Now, let us assume that the  $L_{10}$  life among Weibull random numbers to be generated is 100 for convenience of calculation and that the Weibull slope is 10/9 which is an ordinary value of life distribution of bearing<sup>1), 2), 12)</sup>. Then, in conjunction with relation in expression (2), the Weibull distribution can be defined as follows:

$$g(x) = \frac{10/9}{720} \left( \frac{x-5}{720} \right)^{1/9} \exp \left[ - \left( \frac{x-5}{720} \right)^{10/9} \right] \dots (3)$$

**Table 1** Applicable contents of this method

Type of test	Classification	Contents (problem)	Item
Fixed time test	Design ①	How many test pieces are needed to be able to complete the fixed time test before the deadline (delivery date)?	3. 1
	Design ②	If the number of test pieces or test rigs is fixed, how many hours should be selected as the suspension time prior to failure?	—
	Design ③	If a failure prematurely occurs in an apparently short time span, then how many hours the test piece in question has run at maximum without developing failure so that we are able to judge that the bearing in question does not fulfill the targeted bearing life (what are the criteria for judging that the test run may be suspended)?	—
	Design ④	If a failure occurs before the fixed time has not yet been reached, then how many hours must be selected to set suspension time with the other test pieces?	—
	Interpretation ①	How many hours are at least assured a bearing life that is based on the data from 100% non-failed test pieces?	3. 2
	Interpretation ②	When several bearing products have failed, how wide is the range of life with bearing products in question that can be judged from non-failed test pieces data and failed test pieces data?	—
Accelerated test	Design ①	How many test pieces are necessary to realize a bearing life with a particular degree of reliability? Or, if the number of test pieces used has been predetermined, then how great difference is needed between lots so that we are able to judge that there is significant difference between the lots?	4. 1
	Interpretation ①	Is there true significant difference between two lives?	4. 2
	Interpretation ②	If there is significant difference between two lives, then how many times long is the longer life compared with the shorter life?	4. 2

Incidentally, the scale parameter was calculated with the relation given below. This relation is obtained by substituting expression (2) for expression (5) which is a cumulative distribution function of Weibull distribution, and by solving the resultant expression about:

$$\alpha (L_{10}) = \frac{0.95 \cdot L_{10}}{\{\ln (10/9)\}^{1/e}} \dots\dots\dots(4)$$

$$G(x) = 1 - \exp\left[-\left(\frac{x-\gamma}{\alpha}\right)^e\right] \dots\dots\dots(5)$$

According to the author's method, the three parameters of Weibull distribution are determined by the above-mentioned technique, thereby Weibull random numbers are generated. Generation of Weibull random numbers can be executed by applying either rejection method or inverse function method to uniform random numbers. Either of these random number generation techniques can generate Weibull random numbers: however, it is necessary to use quality random numbers for uniform random numbers. Therefore, the author's method has adopted the Mersenne twister method<sup>13)</sup> as a technique for generating uniform random numbers. Incidentally, since calculation with an infinite number of random numbers is impossible even with the author's method, we should remain aware that there can be maximum probable error of about 5% with the result of the author's method.

Of course, all the contents in Table 1 can be calculated. However, the present report only describes the underlined contents in Table 1 which are the most basic contents.

### 3. Fixed time test

#### 3.1 Settings for number of test pieces and suspension time for a fixed time test

Fig. 1 provides the author's design flowchart for determining the number of test pieces for a fixed time test. For simplification of explanation below, a concrete example is now provided. Suppose that the lead time before delivery (deadline) of a particular bearing product type is 3 months (about 2100 hours), and a test needs to be executed to guarantee that the  $L_{10}$  life of the product is longer than 500 hours (targeted quality). For calculation, a Weibull slope (hereinafter "e") for determining the shape of life distribution needs to be assumed: let us assume the value of this Weibull slope to be 10/9 which is an ordinary value for bearing life distribution<sup>1, 2, 12)</sup>. Supposing that the appropriate test number is six (that is, six test pieces are tested), let us calculate the

suspending time for a test intended to guarantee that the  $L_{10}$  lives of these test pieces are at least 500 hours.

Fig. 2 provides an example Weibull probability distribution for  $e=10/9$  where  $L_{10}$  life is 500 hours. First, six Weibull random numbers satisfying Fig. 2 are generated; this stands for a practice for obtaining bearing life data where six test pieces are sampled from bearing products that are characterized by life distribution of  $e=10/9$  and  $L_{10}=500$ .

Next, the time group (classified by how many hours elapsed) all the so-obtained six random numbers belonged to was determined, and this step was repeated 1000 times, thereby the case (how many hours elapsed) which provides higher probability was determined through an effort to develop the cumulative probability distribution shown in Fig. 3. When the cumulative probability is 0.9, the time elapsed coincides with 1499 h point, and it should be understood that certain numbers among the six Weibull random numbers are not longer than 1499 hours at 90% probability. In other words, when the data for suspension time longer than 1499 hours for

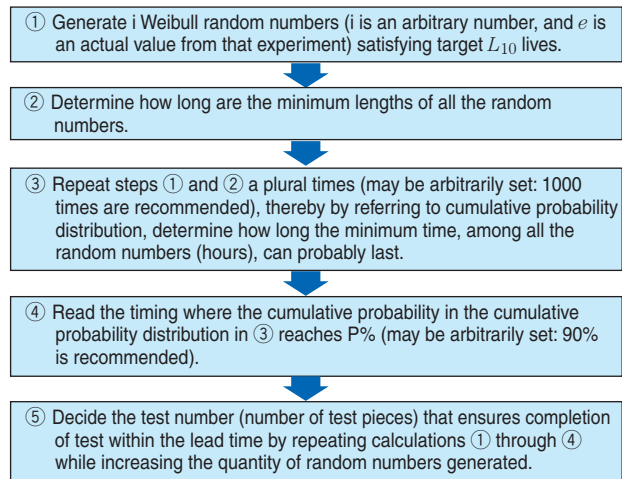


Fig. 1 Flowchart to design test number in fixed time test

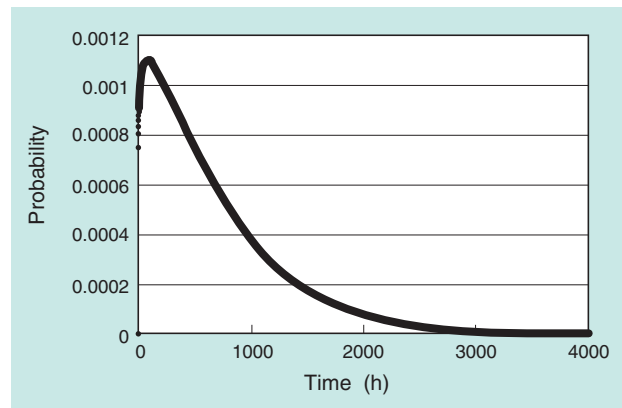
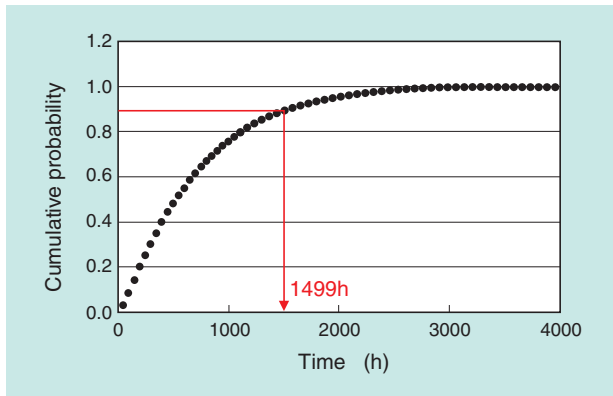


Fig. 2 Weibull probability density distribution for  $L_{10}=500h$  and  $e=10/9$



**Fig. 3** Cumulative probability distribution to estimate suspending time prior to failure (Required  $L_{10}$  life=500h,  $e=10/9$ , Test number=6)

suspending the test prior to failure has been obtained, the  $L_{10}$  life of that bearing product is 500 hours or longer at 90% probability, and 1499 hours marks the suspending time for 100% non-failed test pieces under this situation. Because the lead time before delivery is as long as 2100 hours, the suspending time at the 1499 hours point does not pose a problem in terms of delivery of bearing product in question, and the test number can be six pieces. If the suspending time for suspending test prior to failure comes after the completion of lead time, it is necessary to find a condition according to which the quantity of random numbers generated (number of test pieces) is increased so that the suspending time for suspending test prior to failure arrives earlier than the completion of lead time (delivery date). The target quality for the present calculation has been set in terms of the  $L_{10}$  lives: however, the author's method is capable of setting all the items in **Table 1** relative to an arbitrary failure probability.

### 3.2 Estimation of life judging from result of test suspended prior to failure

**Fig. 4** provides a flowchart for estimating  $L_{10}$  life from a result of test suspended prior to failure. For simplicity of explanation, a concrete example is presented below. Let us think of a situation where a test is being performed to guarantee  $L_{10}$  life of 500 hours given in Sec. 3.1. In this test, all the six test pieces did not develop failure during a time span of 1499 hours, and then the test was further continued. As a result, all the test pieces did not failed during a time span of 3000 hours. The  $L_{10}$  life estimated from this situation is hereunder calculated.

First, six random numbers are generated from the Weibull distribution whose  $L_{10}$  lives (1/10 the suspension time for 100% non-failed test pieces is recommended) are shorter than 3000 hours which is

shorter than the suspension time for 100% non-failed test pieces, thereby whether or not the so-obtained six random numbers are longer than 3000 hours is determined. This process is repeated 1000 times, thereby how many times among 1000 times the six test pieces withstand more than 3000 operating hours is determined. This procedure corresponds with the previous investigation work where the lives of six test pieces whose Weibull slope was 10/9 and  $L_{10}$  life was 300 hours were tested to determine the probability at which all the six test pieces remained non-failed for 3000 hours. Furthermore, this investigation was repeated for Weibull distributions whose  $L_{10}$  lives were gradually extended, thereby **Fig. 5** was developed, wherein the axis of abscissa represents the  $L_{10}$  lives and the axis of ordinate stands for the probabilities at

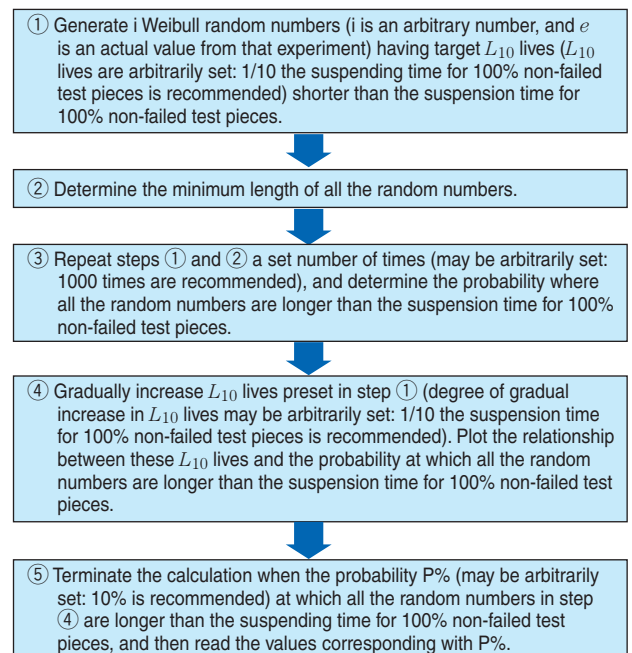


**Fig. 4** Flowchart to estimate  $L_{10}$  life from suspending time prior to failure

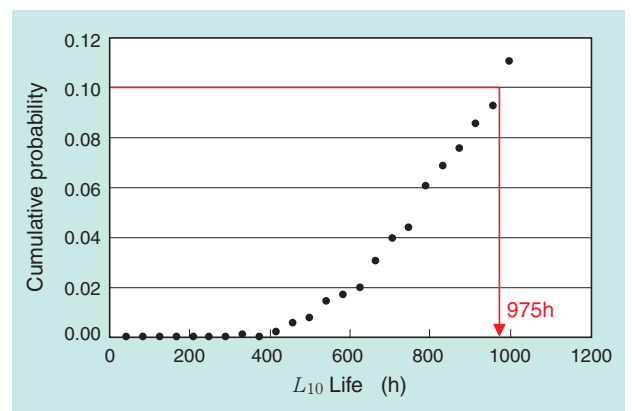


**Fig. 5** Cumulative probability distribution to estimate  $L_{10}$  life from the suspending time prior to failure ( $e=10/9$ , Test number=6)

which all the test pieces remain non-failed for 3000 hours (to improve precision of calculation result, the probabilities at which all the test pieces remain non-failed for 3000 hours are indicated in Fig. 5 for  $L_{10}$  lives for every 50 hours rather than every 300 hours). The life distributions whose  $L_{10}$  life is 975 hours provide the data about 100% non-failed test pieces (not failed for 3000 hours or longer) only at 10% probability. Accordingly, if data is available which shows all the test pieces which remain non-failed for 3000 hours, the test pieces in question highly probably have  $L_{10}$  lives of 975 hours or longer.

#### 4. Accelerated test

##### 4.1 Settings for number of test pieces for accelerated test

Fig. 6 provides a flowchart for designing the test number for accelerated test. For simplicity of explanation, a concrete example is presented below. In most accelerated tests, several lots of test pieces are subjected to life test, and the result of a given lot is compared with that of another lot. Suppose that two lots, each lot consisting of three test pieces, are compared with each other, and let us think of how much difference in life is necessary to constitute significant difference between the lives of the two lots. Now let us assume that  $e$  of life distribution is 10/9 (refer to the probability density distribution in Fig. 2).

Three random numbers were generated from Weibull distribution having a given  $L_{10}$  life, and from data of these three random numbers, the  $L_{10}$  life was estimated by Weibull plotting. The methods used to estimate the  $L_{10}$  life were the Jonson's method<sup>5)</sup> for calculating the median rank and a correlation function

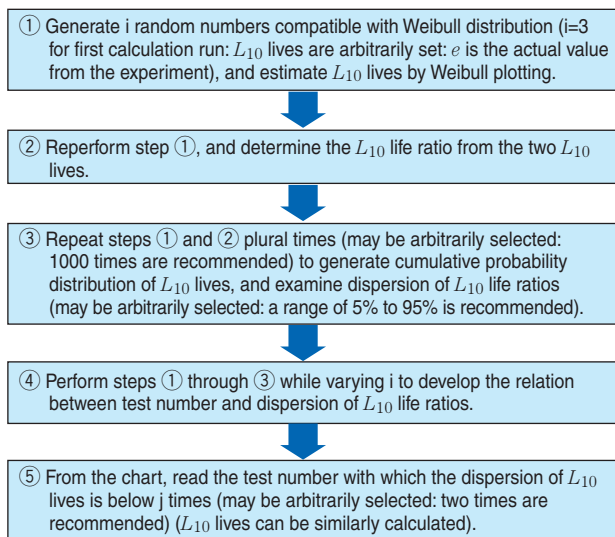


Fig. 6 Flowchart to determine test numbers on accelerated test

method<sup>14)</sup> for determining the regression linear line per Weibull plotting. Next, three random numbers compatible with Weibull distributions having a same  $L_{10}$  life were generated, and from the data of these random numbers, the  $L_{10}$  lives were estimated based on Weibull plotting, and from  $L_{10}$  lives of both members, the  $L_{10}$  life ration was determined. This process was repeated 1000 times, thereby the cumulative probability distribution for 1000 sets of  $L_{10}$  life ratio in Fig. 7 was generated. From this chart, it should be understood that even though test pieces were sampled from a same lot, the life ratios were not always 1 and dispersed in a range of 0.042 to 21.8 times (values in a range of 5% and 95% of cumulative probability distribution).

This means that with a quantity of test pieces as small as three (even though belonging to same lot), difference in life in a range of 0.042 to 21.8 times can occur at 90% probability. In other words, if only three test pieces are available, it is possible to judge that there is significant difference between the lives of two

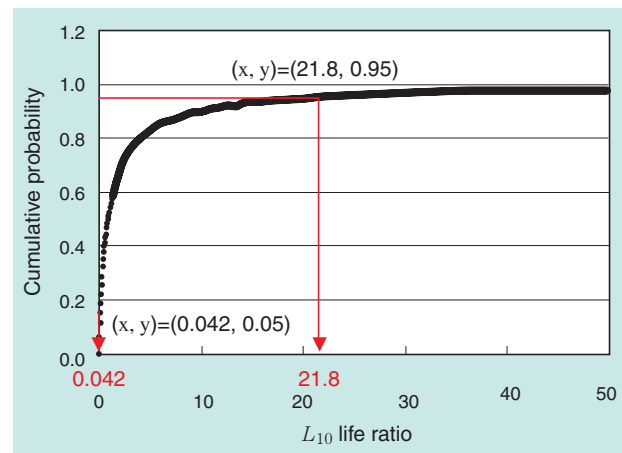


Fig. 7 Cumulative probability distribution of  $L_{10}$  life ratio ( $e=10/9$ , Test number=3)

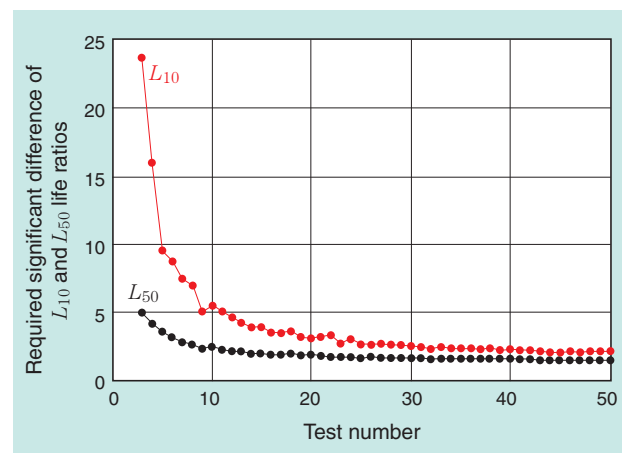


Fig. 8 Relationship between test number and required significant difference of  $L_{10}$  and  $L_{50}$  life ratios ( $e=10/9$ )

lots only when the difference in life is greater than 21.8 times or smaller than 0.042 times.

Next, the quantity of random numbers (test number) was increased, the dispersion of life ratios was calculated in a manner as described above, and the relation between test numbers and life ratios was plotted as shown in Fig. 8. When judging the significant difference in lives between lots, based on the difference in lives of more than two times, the quantity of necessary test pieces in a test where  $e$  is 10/9 is 45 in the case of evaluation in terms of  $L_{10}$  lives and 15 in the case of evaluation in terms of  $L_{50}$  lives.

#### 4.2 Estimation of difference in lives from result of accelerated test

Verification of significant difference for the result of an accelerated test can be achieved from the result presented in Fig. 8 in Sec. 4.1. For example, when ten test pieces are available, and if a difference of five times is present in  $L_{10}$  lives, it can be judged that there is significant difference. However, it is not possible with this chart to determine how much difference in lives is guaranteed based on the magnitude in significant difference. In this section, the calculation method for difference in lives when there is significant difference is described.

Fig. 9 presents a flowchart for estimating difference in lives from result of accelerated test. For simplification of explanation below, a concrete example is now provided. Suppose that life comparison has been attempted with ten test pieces and difference in lives of ten times was obtained in terms of  $L_{10}$  lives. As is apparent from Fig. 8, it can be judged that there is significant difference between lives of these two lots. Difference in lives under this situation is hereunder calculated.

The earlier part of the procedure is identical to that up to generation of Fig. 7 in Sec. 4.1 except in that ten random numbers are generated. Fig. 10 provides cumulative probability distribution of  $L_{10}$  life ratio with ten test pieces. From Fig. 10, it should be understood that the magnitude of dispersion in  $L_{10}$  life ratio is smaller as compared with that in Fig. 7 because the plotting in Fig. 10 involves a greater number of test pieces. Next, in conjunction with Weibull distribution having a different  $L_{10}$  life, plotting similar to one in Fig. 10 is generated. More specifically, distributions of  $L_{10}$  life ratios are plotted wherein the differences in  $L_{10}$  life in combinations of distributions are 1.1 times, 1.2 times ... 3 times.

As an example, Fig. 11 shows cumulative probability distribution of  $L_{10}$  life ratio calculated from combinations of distributions that involve difference of 2.1 times in  $L_{10}$  lives. From this chart, it should be

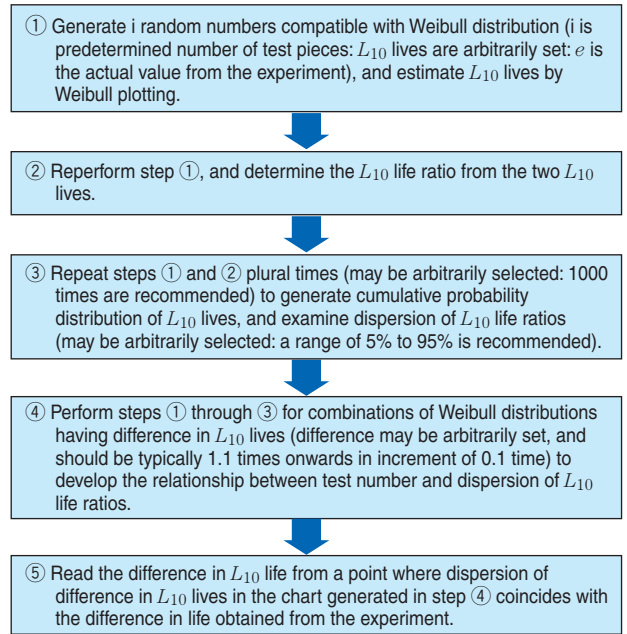


Fig. 9 Flowchart to estimate the minimum life difference with respect to accelerated test results of 2 lots

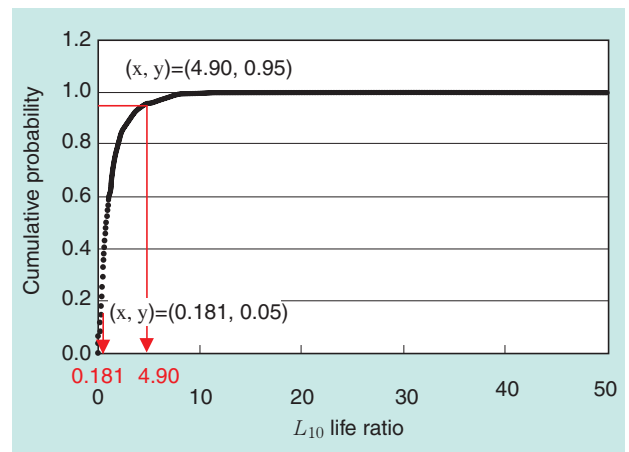


Fig. 10 Cumulative probability distribution of  $L_{10}$  life ratio ( $e=10/9$ , Test number=10)

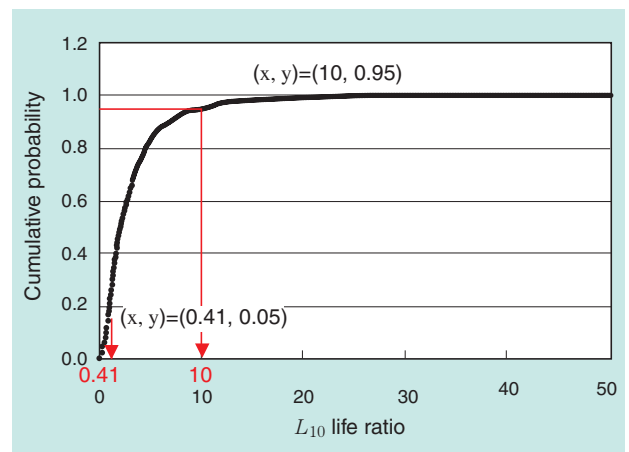


Fig. 11 Cumulative probability distribution of  $L_{10}$  life ratio ( $e=10/9$ , Test number=10, Difference of  $L_{10}$  life=2.1)

understood that a difference in life of ten times at maximum (at a point coinciding with 95% cumulative probability) is present with which the difference in  $L_{10}$  lives is 2.1 times as large. Finally, dispersion in  $L_{10}$  life ratios relative to these differences in  $L_{10}$  lives has been determined, thereby a diagram such as that shown in Fig. 12 has been developed. The plotted diagram in Fig. 12 means that if the data for ten test pieces are sampled from the lots between which there is difference in lives along the axis of ordinate, then the probability where the difference in lives falls in a range of values along the axis of abscissa is 90%. Consequently, from Fig. 12, it should be understood that difference in  $L_{10}$  lives of ten times can occur only between lots between which difference in  $L_{10}$  lives is 2.1 times or greater and rarely occurs in other cases. Accordingly, the difference in  $L_{10}$  lives conservatively estimated under this situation is 2.1 times.

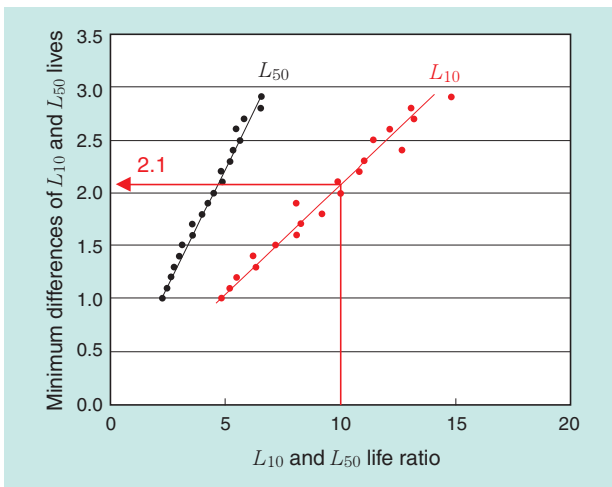


Fig. 12 Diagram to estimate the minimum differences of  $L_{10}$  and  $L_{50}$  lives with respect to accelerated test results of 2 lots ( $e=10/9$ , Test number=10)

### 5. Discussion (method for determining assumed $e$ from result of experiment)

According to the author's method, the result greatly varies depending on the magnitude of  $e$ : therefore, it is very important whether or not the assumed  $e$  is correct. The considerations for determining an appropriate value for  $e$  from an experiment are described below.

Generally,  $e$  is regarded as a parameter that is dependent on change in the state of contact stress on the rolling surface as well as variation in the fracture mode<sup>12)</sup>, and is considered to vary depending on the test conditions. To provide one example, Fig. 13 provides a result of rolling contact fatigue life test

under high contact pressure (point contact,  $P_{max}=5.88$  GPa).  $e$  in this test was 2.88 and is greater than 10/9 or 9/8, each often used in ordinary rolling contact fatigue tests<sup>1), 2) 12)</sup>. Thus,  $e$  can greatly vary depending on test conditions: therefore, an assumed  $e$  needs to be correctly determined for each set of test conditions in question. Fig. 14 presents relationship between test numbers and dispersion of  $e$  (possible values in a range between the lower limit (5%) and the upper limit (95%) in the cumulative density distribution). This result has been obtained by generating Weibull random numbers from life distribution where  $e$  is 10/9 and repeating this process 1000 times. It should be understood that the dispersion in  $e$  approaches 10/9 in either the upper limit region or lower limit region as the test number (number of test pieces) increases. Also, it should be apparent that the variation in dispersion is significantly great in a segment of plotting up to test number ten.

Fig. 15 provides a result derived from the lower limit and upper limit in Fig. 14, wherein the lower and upper limit values have been differentiated with the

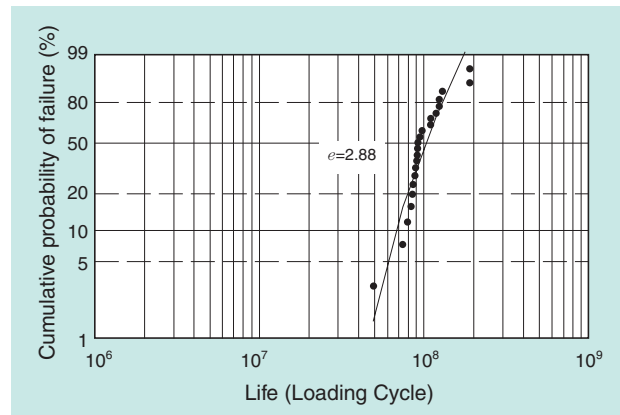


Fig. 13 Example of RCF life test result (Point contact,  $P_{max}=5.88$  GPa)

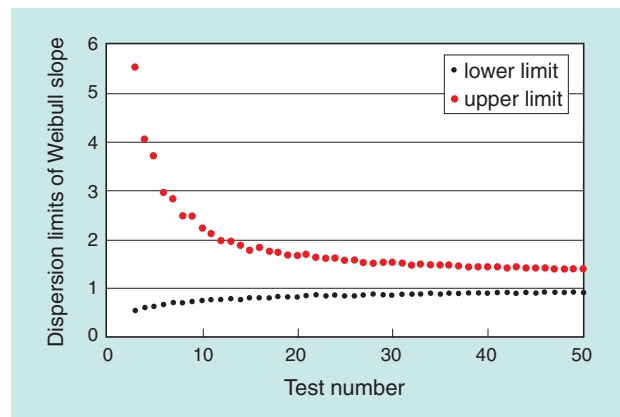


Fig. 14 Relationship between test number and dispersion of Weibull slope (The result is conducted as  $e=10/9$  of life distribution)

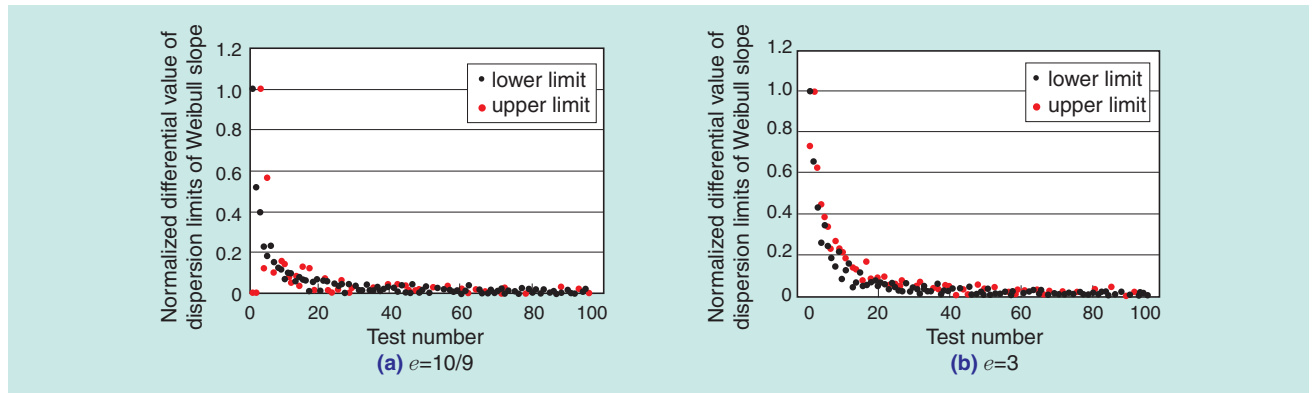


Fig. 15 Normalized differential value of dispersion limits of Weibull slope depending on test number ( $e=10/9$  and  $3$ )

test number and the resultant values have been normalized with the maximum differential. Regardless of  $e$ , the differential drops to 0.2 when the test number is ten and approximately 0.1 when the test number is 20. To sum up, in order to be able to estimate an appropriate  $e$  from an experiment, the minimum recommended number of test pieces is ten, and the preferable number of test pieces is 20.

## 6. Conclusion

This report has described a design method for realizing both reliability and speediness of rolling contact fatigue life test and a method for interpreting a result from rolling contact fatigue life test. The author's method is capable of intuitive understanding, compared with techniques using mathematical models, and is a flexible technique capable of most situations experienced in rolling contact fatigue life test. By following the author's method, a person, even not experienced in rolling contact fatigue life test, will be able to attempt to design a test and reliably interpret the test result while realizing reliability and speediness in executing a series of tests.

## References

- 1) G. Lundberg and A. Palmgren: IVA Handlinger, (1947) 196
- 2) G. Lundberg and A. Palmgren: IVA Handlinger, (1952) 210
- 3) R.B. Abernethy: The New Weibull Handbook 5th edition, (2006) chapter 6
- 4) Reliability Engineering Association of Japan: Reliability Handbook, Nihon Giren Publishing, (1997) 209
- 5) S.N. Luko: SAE Technical Paper Series, No.012859, (1999)
- 6) L.G. Johnson: The Statistical Treatment of Fatigue Experiments, Elsevier, (1964) 16
- 7) T.E. Tallian: ASLE Trans., 5 (1962) 183
- 8) B. Snare: The Ball Bearing Journal (SKF), (1970) 162
- 9) M. Kuroda: Lubrication, 17, 9 (1972) 569
- 10) J. Okamoto, T. Yoshioka, T. Fujiwara, K. Fujita, T. Kitahara, S. Koizumi: Lubrication, 22, 5 (1976) 307
- 11) ISO/TS16281 (2006)
- 12) S. Shimizu: Introduction to Reliability Design for Machinery, Suurikougakusha, (2006) 36
- 13) M. Matsumoto and T. Nishimura: ACM Trans. on Modeling and Computer Simulation, 6 (1996) 99
- 14) T. Hoshide, T. Sakai, A. Sakata: Science of Machine, 41-2 (1989) 320

Photo of author



Takumi FUJITA

Elemental Technological  
R&D Center

# Research on the Lubrication Mechanism of Grease for High Speed Bearings

Takayuki KAWAMURA\*



Machine tools bearings are operated at high speeds and temperatures. They are widely used with oil lubrication, but also with grease lubrication.

In the case of grease lubrication, it is necessary to lubricate for tens of thousands of hours without supplying new grease. However, excellent anti-oxidation grease does not necessarily lubricate for a longer time.

This report investigates used grease from operation at high speed and temperature. It was found that the ability to supply oil to the rolling contact area was more important than oxidation stability.

Moreover, it was also found that grease with easy oil separation and stable thickener structure had longer life.

## 1. Foreword

To help shorten processing time and improve machining precision, machine tools bearings require higher rigidity, higher running speed and limited heat rise. Also, to mitigate environmental impacts, reduced lubricant consumption and more common adoption of grease lubrication have been increasingly needed. In particular, the most wanted technology in the bearing market is adoption of a grease lubrication system that is eco-friendly and is easy to handle and maintain. A grease lubricated bearing system is required to withstand operation of 20,000 hours without relubrication; therefore, grease boasting long lasting durability is much needed.

Generally, durability of a given grease is considered to be greatly affected by its heat resistance feature (resistance against oxidation-deterioration<sup>1)-6</sup>). Accordingly, NTN's grease-lubricated bearings have been subjected to continuous test at a high temperature in excess of 150°C to check their durability<sup>7)-9</sup>). However, on machine tool bearings that are used under ordinary-temperature high-speed environment, it has been known from experience that greases with high-temperature durability do not always achieve longer life. Therefore, greases for actual machine tool bearings have been evaluated and selected through durability tests lasting for tens of thousands of hours<sup>10)-13</sup>).

Consequently, in order for machine tools bearings to efficiently achieve longer life under grease

lubrication, we had to (a) define the mechanism that controls grease life under an ordinary-temperature high-speed environment and (b) develop a long-life bearing based on the resultant finding.

This technical paper clarifies the characteristics needed for long-life grease in machine tool bearings, and presents the information about "SE-1" grease that is used on NTN sealed angular contact ball bearings that can operated with  $d_{min}=1.7$  million.

## 2. Grease life under ordinary-temperature high-speed environment

Three different grease types, Greases A, B and SE-1, each having unique composition, have been subjected to ordinary-temperature high-speed durability test (test I) and high-temperature durability test (Test II). **Table 1** summarizes grease compositions, **Table 2** provides test conditions and **Figs. 1** and **2** illustrate the test results obtained. The grease lives are indicated relative to the life of Grease A that is taken as 1. In the high-temperature durability test (Test II), Grease B boasts a longest life, while in the ordinary-temperature high-speed test (Test I), SE-1 exhibits a longest life.

From these results, it should be understood that all the greases excelling in high-temperature durability are not always excellent in durability under an ordinary-temperature high-speed environment.

To determine whether this variation is attributed to temperature or running speed, ordinary-temperature

\*Elemental Technological R&D Center

durability test (Test III) was performed. Test III was executed using a test rig identical to that used in Test II. However, the temperature conditions were varied (amount of prefilled grease was also varied). The obtained result is graphically plotted in Fig. 3. In Test II, the grease life was longer in the order of Grease A < SE-1 < Grease B. In Test III, the grease life was longer in the order of Grease A < Grease B < SE-1, and this trend was the same as that with Test I, which also performed at room temperature. In other words, it has become apparent that grease that boasts a longest life can vary depending on the bearing operating temperature.

**Table 1** Tested greases

Grease	Grease A	Grease B	SE-1
Thickener	Metal soap	Urea	Urea
Base oil	Synthetic oil	Synthetic oil	Ester
Kinematic viscosity mm <sup>2</sup> /s (40°C)	23	40	22
Consistency	280	230	280

**Table 2** Test conditions

Test	Test I	Test II	Test III
	Ordinary-temperature high-speed durability	High-speed durability	Ordinary-temperature durability
Bearing	7020	6204	6204
Temperature	Room temperature	150°C	Room temperature
Running speed min <sup>-1</sup>	7500	10000	10000
d <sub>mn</sub>	1 million	1 million	0.34 million
Contact surface pressure GPa	1.62	1.54	1.54

### 3. Observation of lubrication state on rolling contact surface

Using an infrared microscope spectroscope, the author inspected the state of residual grease on the outer ring rolling contact surface and circumferential areas on the bearing specimens lubricated with Grease A, Grease B and SE-1, each specimen having undergone Test III. The resultant findings are shown in Figs. 4 through 6 and summarized in Table 3.

In the case of Grease A whose life was shortest, although a sufficient amount of oil was present in the vicinity of rolling contact surface (Fig. 4-②) and the periphery of rolling contact surface (Fig. 4-③), virtually no grease was present on the rolling contact surface itself (Fig. 4-①). This means that virtually no thickener is present on the rolling surface and supply of oil from grease is insufficient in the vicinity of the rolling contact surface to the rolling contact surface.

**Table 3** Grease distribution in tested bearings

Grease	① Rolling contact surface	② Vicinity of rolling contact surface	③ Periphery
Grease A	×	⊙	⊙
Grease B	○	×	⊙
SE-1	○	○	⊙

⊙: Sufficiently present, ○: present, ×: depleted

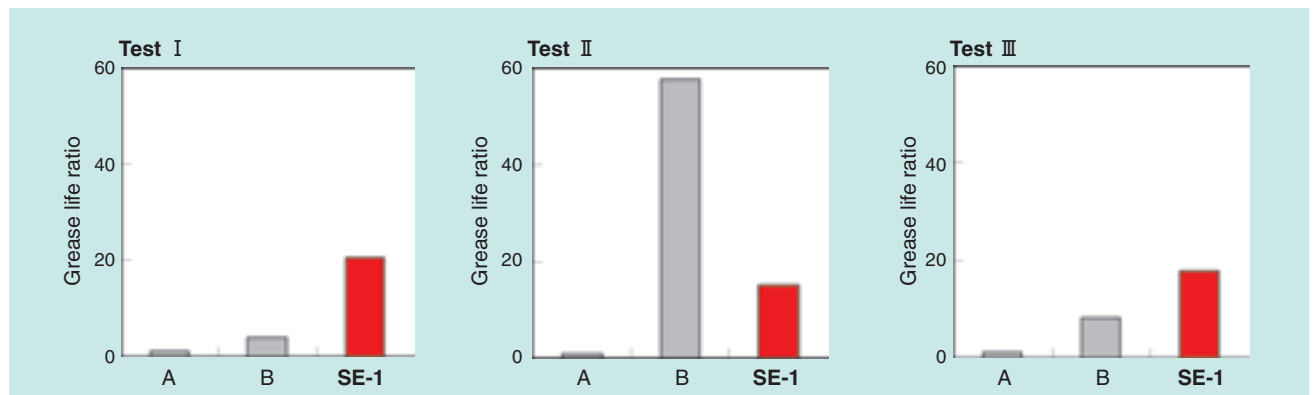
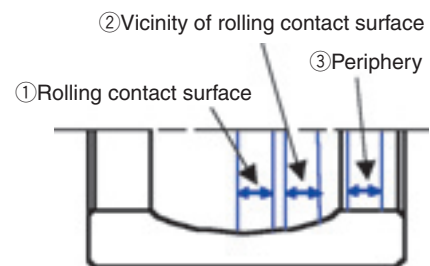


**Fig. 1** Grease life at high speed and room temperature

**Fig. 2** Grease life at high temperature

**Fig. 3** Grease life at room temperature

It has been found that, in the case of Grease B whose life was second shortest next to Grease B, though the grease in the vicinity of rolling contact surface has been depleted (Fig. 5-②), the rolling contact surface (Fig. 5-①) still holds grease and a sufficient amount of oil was present in the grease in the periphery (Fig. 5-③). More specifically, it is apparent that though the oil in the grease the vicinity of rolling contact surface is supplied to the rolling contact surface, the amount of oil transferred from the grease in the periphery to the vicinity of rolling contact surface is insufficient.

In the case of SE-1, which boasts the longest life, it has been verified that a sufficient amount of oil is present in the grease in the periphery (Fig. 6-③) and at the same time grease is present in the vicinity of

rolling contact surface (Fig. 6-②) and on the rolling contact surface itself (Fig. 6-①).

To sum up, grease is positively present on the rolling contact surface and the oil in grease in the periphery is supplied to the rolling contact surface.

As can be understood from Table 3, the mode of oil supply to the rolling contact surface varies from grease to grease. The capability for supplying oil to the rolling contact surface is the highest with SE-1, followed by Grease B and Grease A. In an ordinary-temperature high-speed environment, oil supply to the rolling contact surface is the most important consideration, and it is believed that even grease excelling in heat resistance, such as Grease B, will be deteriorated in a short run if its ability to supply oil to the rolling contact surface is inferior.

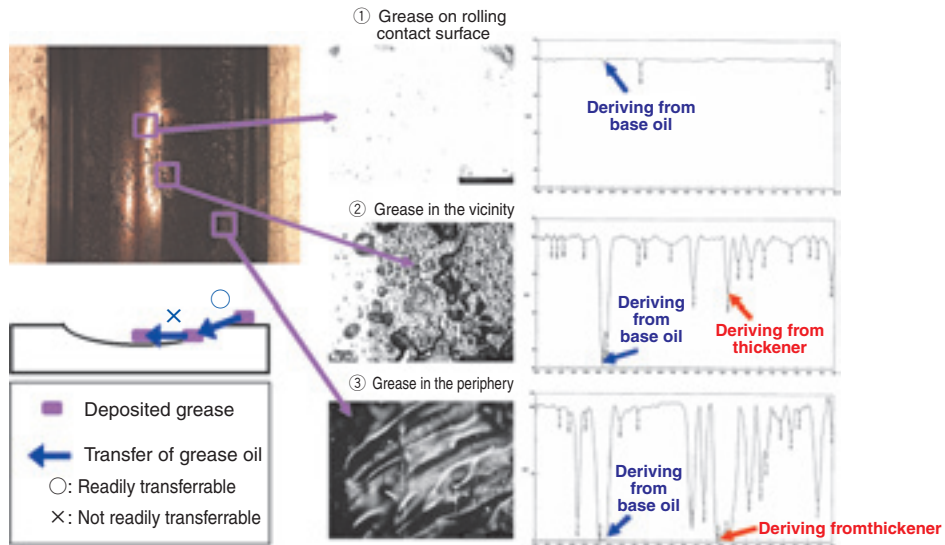


Fig. 4 Distribution of tested grease A in a bearing

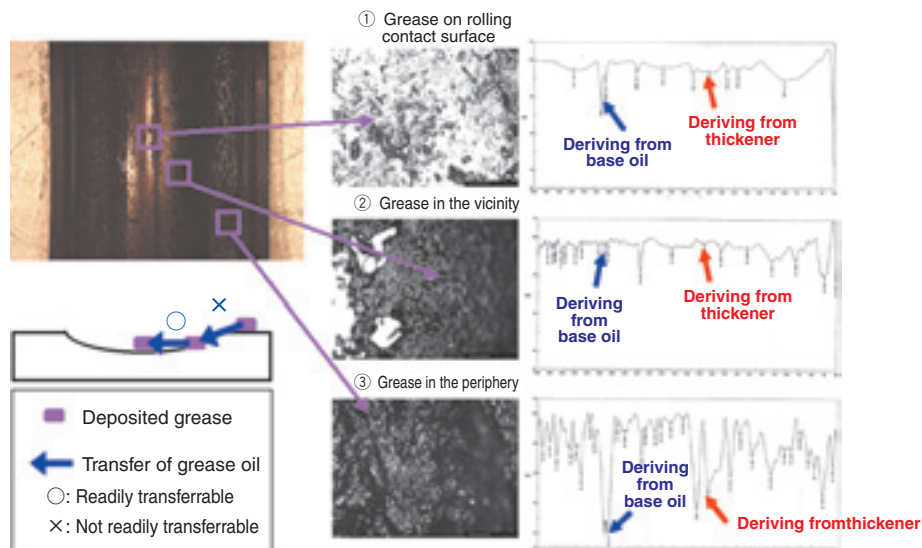


Fig. 5 Distribution of tested grease B in a bearing

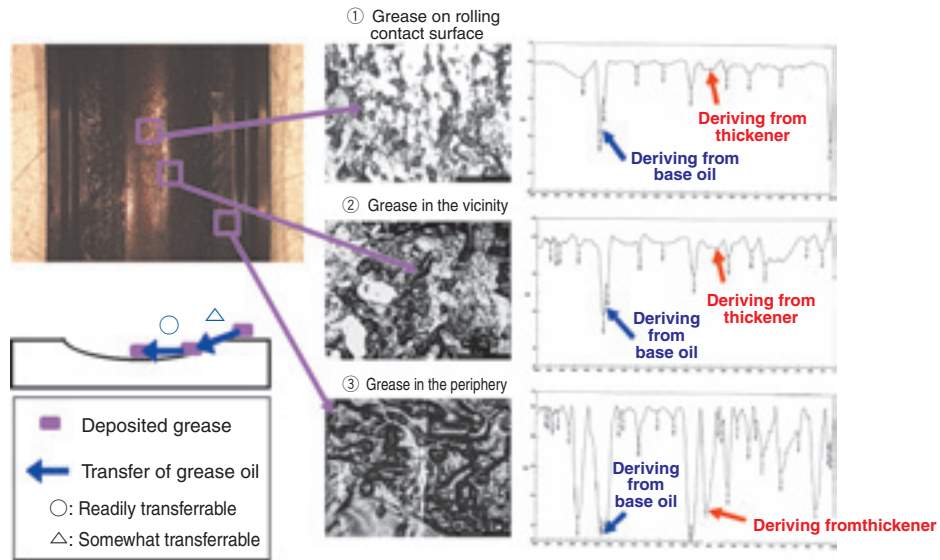


Fig. 6 Distribution of tested SE-1 in a bearing

#### 4. Experiment for oil transferability with simulation model

To be able to verify that SE-1 excels Greases A and B in terms of oil supply performance, a basic experiment was performed with a model that was intended to simulate transfer of the oil from the grease deposited on the shoulder of bearing outer ring bore to the rolling contact surface (Fig. 7). The reason for why the author has attempted to develop a model of grease deposited on the bore surface of bearing outer ring is because the author believes that, on a bearing running at a higher speed, a lump of grease accumulates on the bore surface of bearing outer ring due to centrifugal force.

In this experiment, transferability of oil from the grease to a strip of paraffin paper has been evaluated, wherein the amount of oil from the grease on a level plane to the strip of paraffin paper situated in a sloped plane was measured as the amount of oil transferred. Under a standard set of conditions, a thin layer of grease was intentionally formed between the strip of paraffin paper and the sloped plane (provision of grease film). For Grease A only, the specimen was

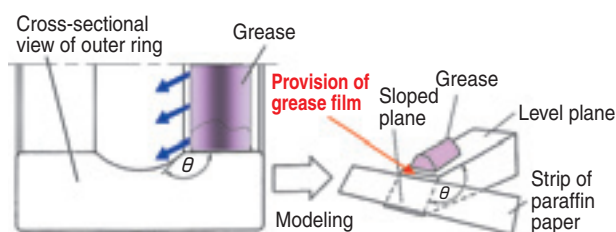


Fig. 7 Oil flow model on a raceway of bearing outer ring

also tested in a situation where thin film of base oil alone was formed between the paraffin paper and the sloped plane surface (provision of base oil film).

##### 4.1 Oil transferability modeling the situation where grease is present on rolling contact surface

Test pieces have been provided with thin grease film. The results of test with these test pieces are graphically plotted in Fig. 8. The degree of positive oil transferability to the sloped plane is in the order of Grease B < SE-1 < Grease A. Grease A boasts best oil transferability while Grease B lacks in good transferability. From these findings, it is considered that with Grease B, the amount of oil supplied from the vicinity of rolling contact surface to the rolling contact surface itself is limited, and Grease B exhibited shorter life in Tests I and II because of poor lubrication ability.

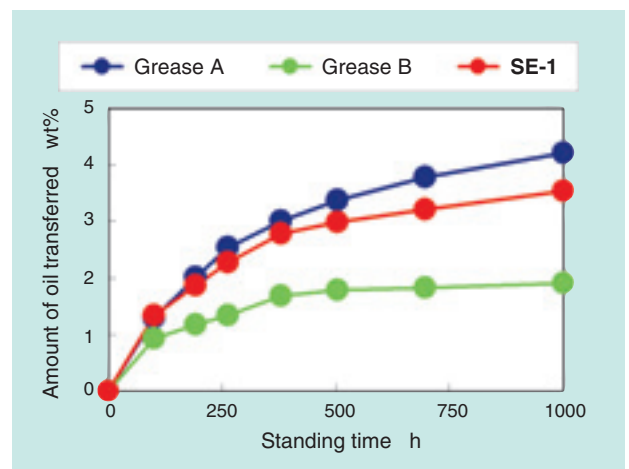


Fig. 8 Oil flow with grease film treatment on a slope plane

#### 4.2 Oil transferability modeling the situation where grease is not present on rolling contact surface

When grease was present on the sloped surface, the oil transferability was better in the order of SE-1 < Grease A. Since no grease (thickener) was observed on the rolling contact surface lubricated with Grease A (short life) after the grease durability test, it was expected that presence/absence of a thickener in grease can affect transferability of oil in the grease in question. Therefore, the author has assessed the oil transferability of Grease A in a state where the thickener was not present on the slope plane. It has been learned that in a model experiment (treatment to form film of base oil) (Fig. 9), where absence of grease on the rolling contact surface was assumed, the oil supply capability of Grease A was significantly jeopardized and the amount of supplied oil was insufficient as compared to the oil supply with Grease B and SE-1 described in Sec. 4.1.

A thickener in grease forms a fibrous structure and oil is held among the fibers. Accordingly, the gaps in the fibrous structure in thickener functions as capillaries that allow base oil of grease to be transferred.

In the case of Grease A, it appears that shearing

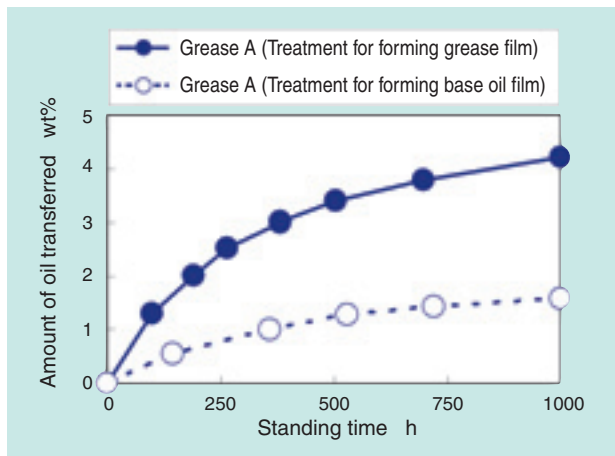


Fig. 9 Oil flow with oil film treatment on a slope plane

associated with grease on a bearing running at higher speed causes the thickener to be destroyed or eliminated from the rolling contact surface of the bearing. As a result, the oil from grease in the periphery of rolling contact surface is not supplied to the rolling contact surface any more, and the grease has exhibited shorter life (see Fig. 10).

### 5. Conclusion

From the findings in the series of experiments, it has been learned that to be able to achieve longer grease life under an ordinary-temperature high-speed environment, the oil in grease in the periphery of rolling contact surface needs to be quickly supplied to the rolling contact surface by the capillary phenomenon unique to a thickener. The important considerations are ① use of thickener with high resistance to shearing and ② use of grease whose oil component is readily separated (see Fig. 11).

Being an excellent bearing grease that has resilient

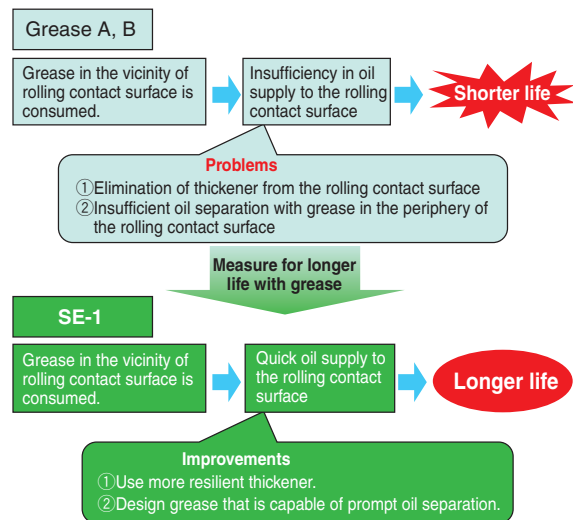


Fig. 11 Improvement of grease endurance ability for high speed bearing at room temperature

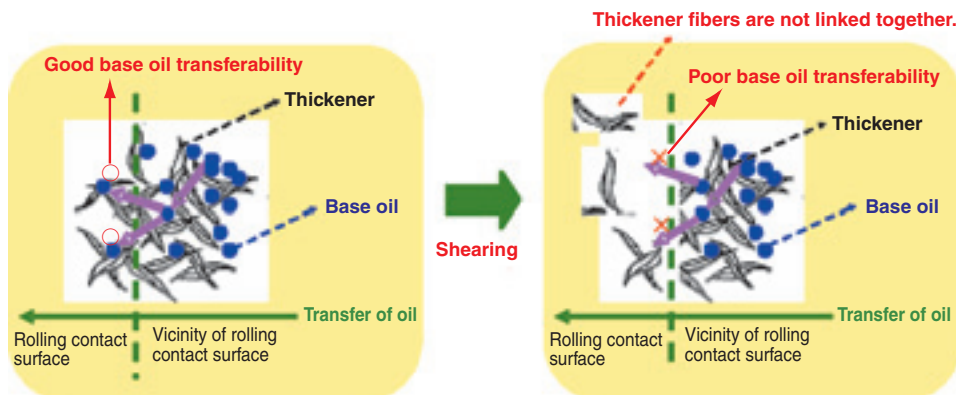


Fig. 10 Effect of grease thickener to oil flow toward a rolling contact area

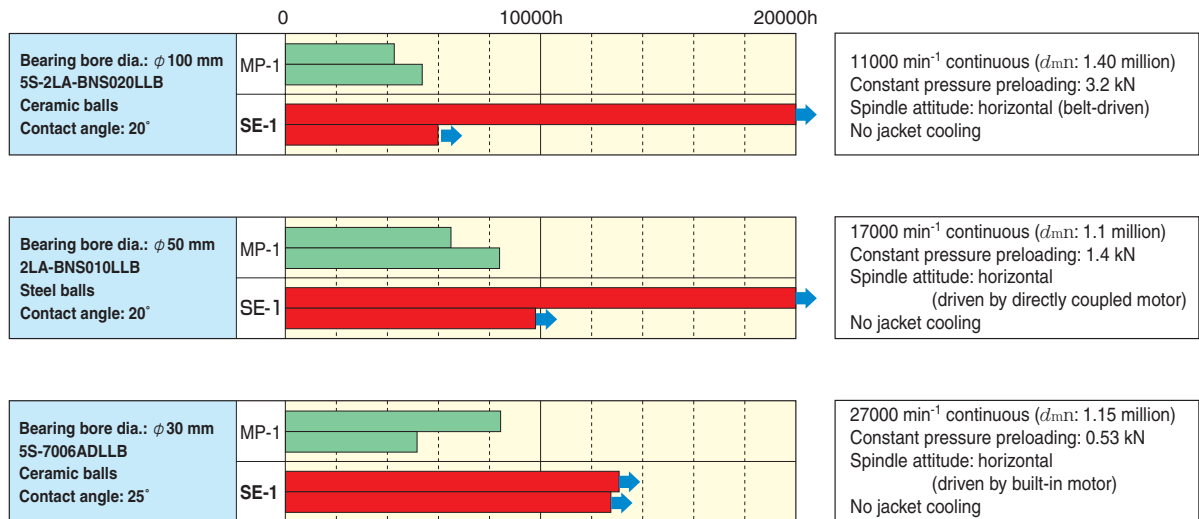


Fig. 12 Endurance ability of SE-1 grease with machine tools bearings

thickener and boasts good oil supply capability, SE-1 Grease appears to exhibit excellent grease durability when used on machine tools bearings operated in an ordinary-temperature high-speed environment (see Fig. 12<sup>13)</sup>). Much higher speed will be needed for machine tools bearings, and we will need to develop grease that boasts better oil supply capability. In this context, NTN will remain committed to development of grease that boasts much longer life.

## References

- 1) E.R. Booser (1974), "Grease Life Forecast for Ball Bearings," Lubrication Engineering, 30, P536-541
- 2) E.R. Booser and A.E. Baker (1976), "Evaporation-A Factor in Ball Bearing Grease Life," NLGI Spokesman, 40, P60-65
- 3) W.W. Bailey and S. Pratt (1982), "Dynamic Oxidation Stability of Lubricating Greases," NLGI Spokesman, 46, P15-18
- 4) T. Kawamura, M. Minami and M. Hirata (2001), "Grease Life Predication for Sealed Ball Bearings," Tribology Transactions, 44, 2, P256-262
- 5) T. Kawamura, M. Minami and M. Hirata: "Grease Life Predication for Sealed Ball Bearings," NTN Technical Review No.69 (2001) 76-81
- 6) H. Mikami: "Latest Trends in Lifespan Prediction for Lubrication Grease and Grease," Hydraulics & Pneumatics (Japan) 576, Vol.46, No.11, (2007) P42-46
- 7) H. Mikami: "Development of Long Life Grease for High-Speed Application "ME-1" Grease for Motor

- 8) M. Egami, M. Asao and T. Goto: "Hybrid Grease NA204F for Automotive Electrical Instruments and Auxiliary Device," NTN Technical Review No.73 (2005) 66-71
- 9) T. Kawamura and H. Hikami: Development of Long Life Grease NA103A for Automotive Components, NTN Technical Review No.75 (2007) 116-123
- 10) H. Takiuchi: "Environmental Response Technologies for Roller Bearings in the Machine Tools Field," The Tribology, No.174, 2 (2002) P24-25
- 11) K. Ueda: "Technology Trends in Bearings for Machine Tools: Environmental Response Technologies," The Tribology, No.188, 4 (2003) P19-21
- 12) F. Kosugi: "ULTAGE" Series Precision Bearings for Machine Tools, NTN Technical Review No.74 (2003) 26-29
- 13) F. Kosugi:  $d_{mN}$  170 × 10<sup>4</sup> Sealed High-Speed Angular Contact Bearing "New BNS Type," NTN Technical Review No.74 (2006) 28-33

Photo of author



Takayuki KAWAMURA

Elemental Technological  
R&D Center

# Friction Properties of Polymer Gel with High Mechanical Strength



Eiichirou SHIMAZU\*  
Masaki EGAMI\*  
Takayuki KUROKAWA\*\*  
Jian Ping Gong\*\*

A polymer gel is composed of a three-dimensional network polymer and a large amount of liquid. There is the potential to apply it as a low friction material because it has large amount of liquid internally, compared with the oil-impregnated resin currently used as a sliding material. In this paper, we report on the friction properties of high strength polymer gel, called double network gel, when used in conjunction with a steel under various conditions.

## 1. Introduction

Polymer gels each comprise a polymer skeleton of chemically bonded three-dimensional network structure and a significant liquid component (solvent). Compared with other polymer materials such as plastic and rubber, conventional polymer gels have often been brittle materials featuring lower mechanical strength and lower elastic modulus. This may be readily understood when considering examples of familiar polymer gels such as jelly and tofu soy bean curd.

The swelling degree of a polymer gel will vary, owing to external stimuli such as temperature, pressure, hydrogen ion index (pH value), light, and electric field, whereby the volume of polymer gel is altered. Focusing on this feature, applications of polymer gels as functional and intelligent materials have been researched and commercially adopted for sensors and actuators.

Recent developments regarding polymer gels include high-strength gel types known as double network gels<sup>1)</sup> and nano-composite gels<sup>2)</sup> as well as high-tenacity gel called topological gel<sup>3)</sup>, whereby brittleness-induced quality issues with polymer gels resulting from poor handling have been much alleviated. Consequently, the scope of utilization of polymer gels in industrial applications seems to expand.

Incidentally, though being solid matter, polymer gels consist primarily of liquid: as such it is known that they

feature significantly low friction coefficients and unique friction behavior. Their unique friction mechanism<sup>4)</sup> has been increasingly elucidated. However, many examples thus far reported on friction properties of polymer gels have been associated with combinations of water-solvent polymer gels and smooth-surfaced glass plates.

Now, let us consider utilizing the excellent low-friction features of polymer gels in order to reduce friction loss that occurs between machine components. In this case, the solvent for gel is needed, for example, not to corrode nearby metal parts, solidify, evaporate, or boil in a wider temperature range.

In this technical paper, we hereafter report the friction properties of water solvent-free double network gel (refer to **Fig. 1**; hereinafter referred to as DN gel)<sup>1)</sup> used in conjunction with a steel (bearing steel: SUJ2) under various conditions.

## 2. Overview of the DN gel

A polymer constituting a skeletal component in a polymer gel has a three-dimensional network structure when situated in a solvent. A polymer gel in which the bonds of polymer chains forming the network (that is, cross-links) are covalent is known as chemical gel; if the bonds are not covalent bonds, the polymer gel is called physical gel.

Because cross-links in a chemical gel are formed by covalent bonds, the network structure once formed is

\*Elemental Technological R&D Center

\*\*Hokkaido University, Faculty of Science

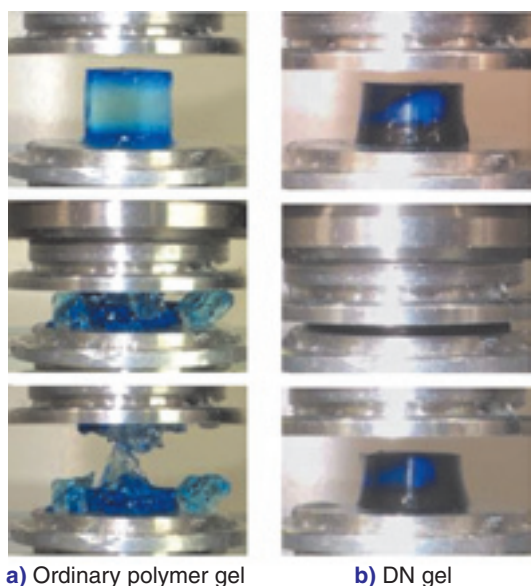


**Fig. 1** Compression property of DN gel <sup>1)</sup>  
 J. P. Gong, Y. Katsuyama, T. Kurokawa, Y. Osada,  
 "Double Network Hydrogels with Extremely High  
 Mechanical Strength", *Advanced Materials*, (2003),  
 15(14), 1155-1158.  
 Copyright Wiley-VCH Verlag GmbH & Co. KGaA.  
 Reproduced with permission.

very stable, being insoluble and infusible. In contrast, a physical gel is characterized in that its cross-links are liberated by external factors including temperature, thereby reversibly changing from liquid to solid or vice versa. Our DN gel is a type of polymer gel that belongs to a chemical gel category.

For a given chemical gel, a uniform cross-linking reaction is difficult to achieve, and as a result, a certain degree of nonuniformity in density with cross-links occurs in a process of cross-linking reaction (see **Fig. 2**, red circles represent higher density cross-links).

A network structure involving nonuniform density with cross-links will exhibit differences in the degree of "elongation (tensile force)" on the individual polymer chains across cross-links. Also, there will be difference in degree of transformation (elastic modulus) between the higher cross-linking density area and the lower cross-linking density area. Because of these reasons, when an external force is applied to a gel having nonuniformity in density of cross-links, the force is not evenly exerted onto the polymer links, and fracture will occur at a particular polymer link where a greatest tension takes place.

Any gel material consists primarily of liquid, and contains only a small amount of skeleton component that is responsible for mechanical strength, and accordingly, it is essentially a low-strength material. In addition, while an external force is being applied to a

chemical gel, such fracture of polymer chains continuously occurs, and, consequently, chemical gel is a very brittle, low-strength material.

It is estimated that the DN gel has a unique structure such as a one shown in **Fig. 3**, known as the sea-island structure. Incidentally, **Fig. 3** provides a schematic diagram, and actual DN gel possesses nonuniformity in density of cross-links.

The sea phase, which is a matrix, consists of a mixed phase comprising a fine network (high cross-linking density) and a coarse network (low cross-linking density), while the island phase virtually comprises soft gel alone. The most outstanding feature of DN gel is a ratio of hard gel to soft gel: more specifically, the composition of DN gel is designed such that the volume of soft gel is about 20 times as great as that of hard gel.

Having such a unique structure, the DN gel has compressive strength in a range of 10 to 50 MPa. This strength is 10 to 100 times as great as that of each gel constituting the DN gel <sup>1)</sup>. Furthermore, as shown in **Fig. 1**, even when compressed by about 90%, the DN gel does not fail: when the load is removed, it restores its original shape like a rubber material.

The high strength mechanism of the DN gel cannot be explained by using a conventional fracture model that can reflect elasticity alone: this mechanism seems

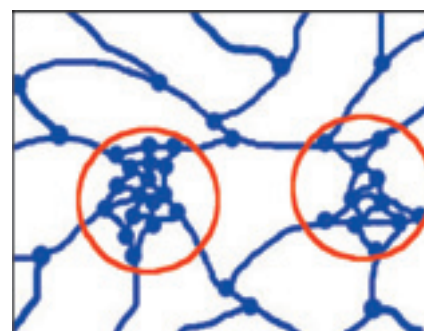


**Fig. 2** Schematic drawing of polymer structure of chemical gel

Sea phase: mixed phase consisting of hard gel and soft gel

Island phase: phase primarily consisting of soft gel

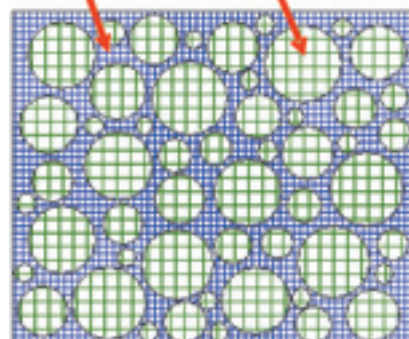


**Fig. 3** Schematic drawing of DN gel

to derive from the unique structure of the DN gel comprising both hard gel and soft gel rather than from mechanical properties of each material<sup>5)</sup>.

### 3. DN gel specimen

As previously mentioned, the DN gel comprises two polymer gel types, each having a polymer network structure independent of the other: since much of the soft gel exists in a mixed phase comprising hard gel and soft gel, the DN gel boasts greater mechanical strength.

The specimen used is the DN gel whose hard gel is poly (2-acrylamido-2-methylpropanesulfonate) gel (hereafter simply referred to as PAMPS gel) and whose soft gel is polyacryl amide gel (hereafter simply referred to as PAAm gel), wherein the cross-linking agent used is methylene bis-acryl amide (hereafter simply referred to as MBAAm).

Having such composition, the DN gel is hydrophilic and the solvent usually used is water. For this technical paper, ethylene glycol was used as the solvent that features a solidifying point lower than that

**Table 1** Composition of DN gel

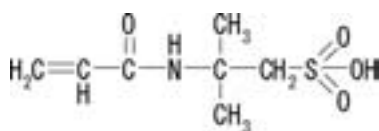
		Polymer composition ratio	wt %
Hard gel	PAMPS gel	1	Approx. 10
Soft gel	PAAm gel	20	
Solvent	Ethylene glycol		Approx. 90

※Boiling point of ethylene glycol: 198°C, solidifying point: -13°C

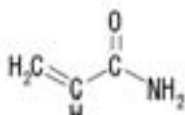
**Table 1** Compression property of DN gel

Compressive strength	MPa	20
Compressive modulus of elasticity	MPa	0.5
Compression failure skew	%	95

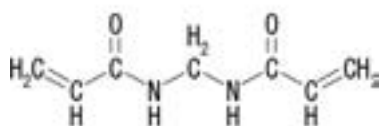
※Test piece dimensions: □10 mm×t5 mm



a) Main monomer of PAMPS gel



b) Main monomer of PAAm gel



c) Crosslinking agent

**Fig. 4** Chemical structures of the materials

of water and a boiling point higher than that of water.

**Table 1** summarizes the composition of the DN gel specimen used, and **Fig. 4** shows the chemical structures of the raw materials used.

The compression properties of the DN gel specimen using ethylene glycol solvent are provided in **Table 2**.

### 4. Friction properties of DN gel

#### 4.1 Test conditions

The test rig adopted for the sliding test is schematically illustrated in **Fig. 5**. The block portion in this diagram represents the DN gel test piece, and the disk portion stands for a metal mating material. The substance of the metal mating material used is SUJ2.

The load was applied onto the test piece, and the mating material was turned, thereby the sliding test was performed. The friction coefficient was calculated by dividing the friction force detected with a load cell by the test load.

The test conditions applied are summarized in **Table 3**, which gives the parameters about friction properties for the DN gel and SUJ2 material. The parameters include the load, sliding velocity, surface roughness of the mating material, and test temperatures. This technical report hereafter describes the effects of these parameters.

**Table 3** Test condition

Test piece dimensions	mm	5×5×t5.6
Gel solvent		Ethylene glycol (viscosity at 25°C: 19 mPa-s)
Load	N	2.0, 4.9, 9.8, 24.5
Sliding velocity	m/min	0.5, 1.0, 1.4, 3, 4, 6, 7, 9, 10
Mating material		SUJ2 (0.005 μmRa, 0.05 μmRa, 0.4 μmRa)
Sliding track dia.	mm	φ23
Time	min	5-30 (per time setting)
Temperature	°C	25, 50, 80
Atmosphere		Ethylene glycol is applied, as necessary, to the mating material in air.

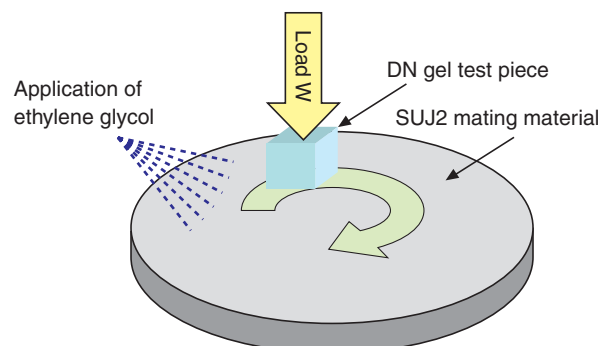


**Fig. 5** Sliding test method

4.2 Test result (part 1)

-Effects of surface roughness of mating material, load, and velocity-

Fig. 6 shows the effects of surface roughness of mating material, load, and velocity on the friction behavior of the DN gel having ethylene glycol solvent (temperature 25°C).

For the test, several mating material types, each having a unique degree of surface roughness were used, whereby the surface roughness ranged from a

very smooth surface equivalent to that of a rolling contact bearing raceway surface to the mating material surface of a sliding bearing.

In any case, the kinetic friction coefficient  $\mu_k$  is less than about 0.01, and under the test conditions, the DN boasts very low friction coefficient. However, when the surface roughness of mating material is as high as 0.4  $\mu\text{mRa}$ , the kinetic friction coefficient of the DN gel is somewhat higher.

When an ordinary plastic material is allowed to slide

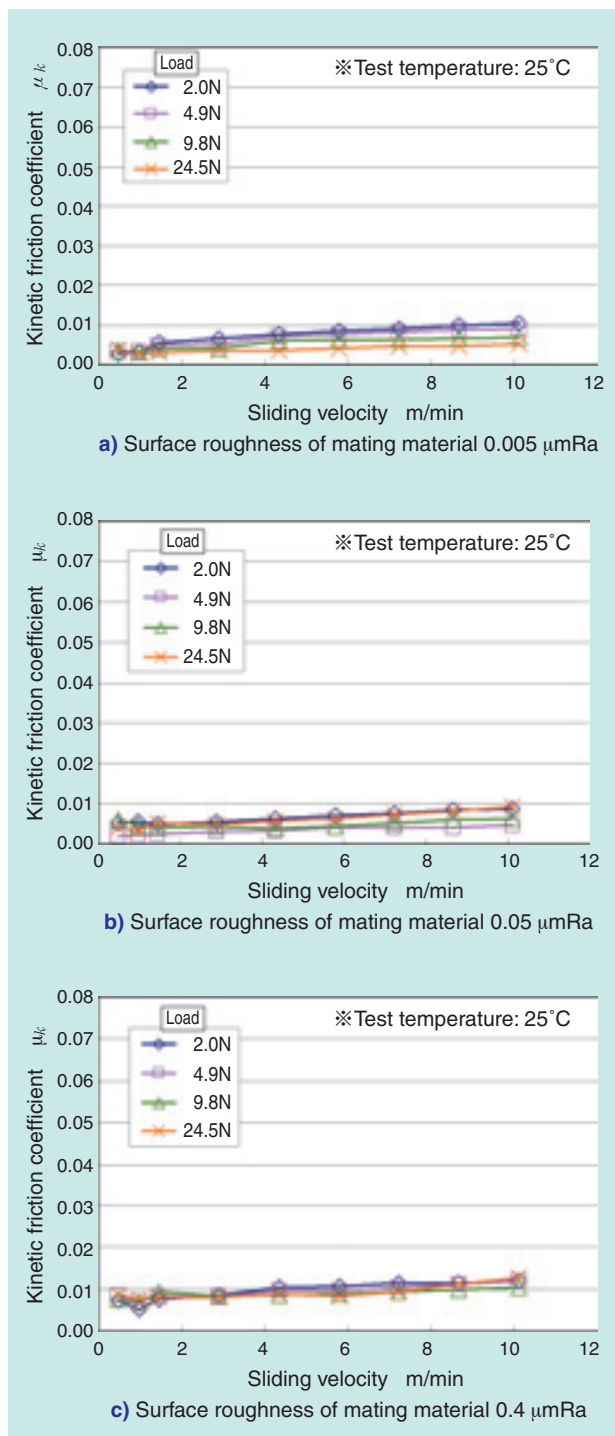


Fig. 6 Friction properties of DN gel(Part.1)

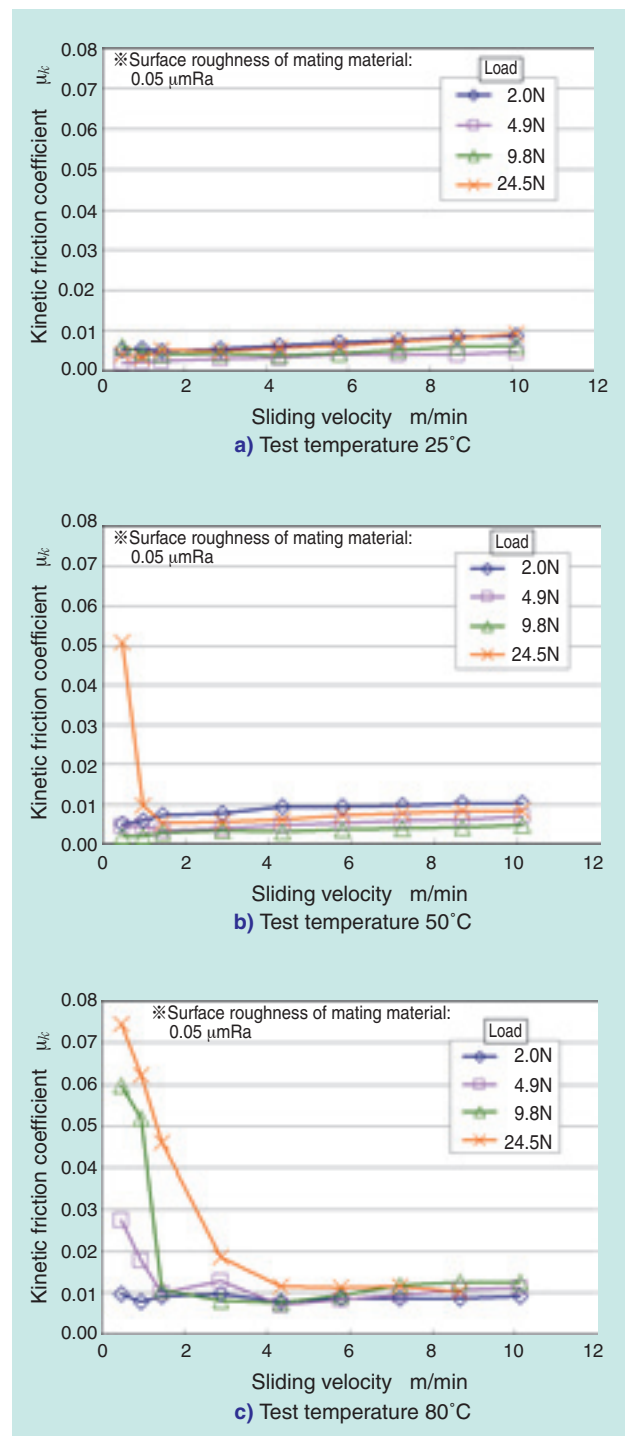


Fig. 7 Friction properties of DN gel (Part. 2)

relative to SUJ2 under similar conditions, a lubrication state known as boundary lubrication usually occurs and the resultant kinetic friction coefficient  $\mu_k$  is approximately 0.1. From this fact, it should be understood that the DN gel having ethylene glycol solvent features unconventional low friction properties when sliding relative to SUJ2.

Incidentally, the DN gel having ethylene glycol solvent exhibits unique friction behavior, that is, slow increase in kinetic friction coefficient  $\mu_k$ . Usually, this trend is experienced in the hydrodynamic lubrication state.

**4.3 Test result (part 2)**

**-Effects of temperature, load, and velocity-**

**Fig. 7** illustrates the effects of load and sliding velocity onto the friction behavior of the DN gel having ethylene glycol solvent with several atmospheric temperature settings (25°C, 50°C and 80°C) (surface roughness of mating material: 0.05  $\mu\text{mRa}$ ).

At 25°C, the DN gel exhibits excellent friction coefficients, that is, kinetic friction coefficient  $\mu_k$  as low as 0.01 or smaller in a very wide range of load and sliding velocity. However, at the higher temperature range, the kinetic friction coefficient  $\mu_k$  of the DN gel tends to significantly increase at low-speed, high-load condition settings.

Though the kinetic friction coefficient of the DN gel,  $\mu_k$ , is high at a limited region in low sliding velocity range, the  $\mu_k$  slowly increases as the sliding velocity increases. Under any test temperature setting in the regions where the kinetic friction coefficient of the DN gel,  $\mu_k$ , increases, the DN gel boasts excellent low friction quality, that is, a kinetic friction coefficient  $\mu_k$  of 0.01 or smaller.

**5. Discussion**

The DN gel having ethylene glycol solvent was allowed to slide against a mating material (SUJ2), and the kinetic friction coefficient,  $\mu_k$ , was thereby determined. At the same time, with a similar test rig, a variety of polymer materials including conventionally used plastic materials were tested to determine their kinetic friction coefficients. Consequently, it has been learned that the kinetic friction coefficient,  $\mu_k$ , of the DN gel is very low; about 1/10 as low as that of the other examined polymer materials. Beginning with this finding, we have attempted to estimate a possible lubrication state that can occur with the DN gel having ethylene glycol solvent under the test conditions adopted for the present research. The method for estimation is described below.

Let us assume that under the test conditions

mentioned above, the DN gel takes a hydrodynamic lubrication state by the so-called wedge effect and that the DN gel in this state can be expressed with the model in **Fig. 8**.

With this model, the DN gel test piece is assumed to be a fixed piece and the mating material (SUJ2) is assumed to move to the right in the model shown in this page at a sliding velocity  $U$ . A liquid film of ethylene glycol is assumed to be present between the DN gel test piece and the mating material (SUJ2), whereby the thickness of the liquid film at the inlet side is taken as  $h_1$  and that at the outlet side as  $h_2$  ( $h_1 > h_2 > 0$ ).

The pressure  $P$  working on the DN gel test piece in this model (the so-called bearing load capacity) can be expressed by expression ① derived from the Reynolds equation. Where,  $\eta$  is the viscosity of ethylene glycol, and  $\alpha$  is a coefficient determined by the bearing surface length  $B$  and  $h_1$  and  $h_2$ :

$$P = \frac{\eta U \alpha}{h_2^2} \dots\dots\dots \text{①}$$

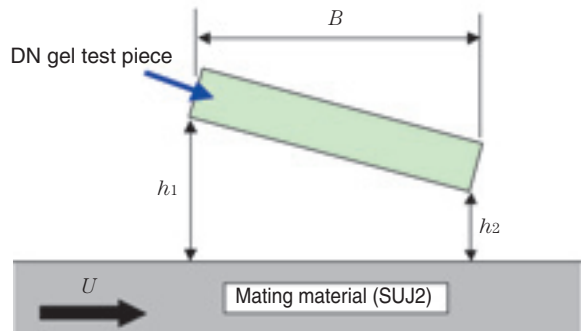


**Fig. 8** Hydrodynamic lubrication model of DN gel

At the same time, the friction force  $F$  working on the DN gel test piece can be defined by expression ②, where  $A$  is the area of the sliding surface of the DN gel test piece,  $\beta$  is a coefficient determined by the bearing surface length  $B$ ,  $h_1$ , and  $h_2$ :

$$F = \frac{\eta UA}{h_2} \beta \dots\dots\dots \text{②}$$

When the test load is  $W$ , the contact surface pressure  $P=W/A$ , and kinetic friction coefficient,  $\mu_k=F/W$ , then from expressions ① and ②, the kinetic friction coefficient  $\mu_k$  can be expressed by expression ③, where  $\gamma$  is a coefficient determined by  $h_1$  and  $h_2$ :

$$\mu_k = \left( \frac{\eta U}{P} \right)^{\frac{1}{2}} \gamma \dots\dots\dots \text{③}$$

Consequently, from expression ③, it appears that the kinetic friction coefficient  $\mu_k$  in the case of fluid lubrication state is proportional to  $\eta UIP$  to the 1/2 power.

The results of Figs. 6 and 7 have been reorganized, taking  $\eta UIP$  along the X axis. The result of reorganization is plotted in Fig. 9. Incidentally, for comparison purpose, this diagram also includes the plotting of friction coefficient values obtained from a series of measurements that used polyether etherketone (PEEK) resin (a super-engineering plastic) in place of the DN gel.

In this diagram, two broken lines having inclination of the 1/2 power are indicated. In a region where  $hUP$  is greater than about  $1 \times 10^{-9}$  [m], the inclination of  $\eta UIP$  is nearly proportional to the "1/2 power" broken lines: in this situation, the test pieces are under a lubrication state equivalent to fluid lubrication. Incidentally, a fluid lubrication state never occurs with a conventional material under such load-velocity conditions: this finding is supported by the friction

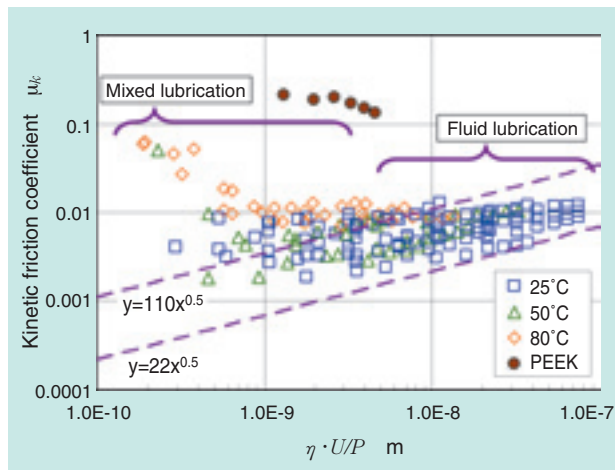


Fig. 9 Presumption of sliding condition

behavior of PEEK resin test pieces that were subjected to test conditions identical to those for our DN gel test pieces. In summary, we believe that our DN gel is a very unique material that is capable of low-friction sliding in a fluid lubrication state, beginning at an unconventionally low  $\eta UIP$  region, whereby this gel material boasts a high degree of physical strength which conventional gel materials lack.

## 6. Conclusion

We have proven that our DN gel, having ethylene glycol solvent, exhibits extremely low friction coefficients under various conditions when used in conjunction with a steel species which is commonly used as a mating material for a sliding member.

In addition, it has been suggested that, compared with other polymer materials, the DN gel enables easy achievement of fluid lubrication state by controlling contact surface pressure, sliding velocity and solvent viscosity.

We wish to utilize this technology to help further reduce friction loss occurring on machine components.

## References

- 1) J. P. Gong, Y. Katsuyama, T. Kurokawa, Y. Osada, *Advanced Materials*, 15(14), 1155 (2003).
- 2) K. Haraguchi, T. Takehisa, *Advanced Materials*, 14, 1120(2002).
- 3) Y. Okumura, K. Ito, *Advanced Materials*, 13, 485 (2001).
- 4) J. P. Gong, G. Kagata, Y. Iwasaki, Y. Osada, *Wear*, 251, 1183(2001).
- 5) M. Huang, H. Furukawa, Y. Tanaka, T. Nakajima, Y. Osada, J. P. Gong, *Macromolecules*, 40(18), 6658(2007).

Photo of authors



Eiichirou SHIMAZU

Elemental Technological  
R&D Center



Masaki EGAMI

Elemental Technological  
R&D Center



Takayuki KUROKAWA

Hokkaido University,  
Faculty of Science



Jian Ping Gong

Hokkaido University,  
Faculty of Science

# Study on the Effect of Physical Properties on Wear Resistances of TiN Films Coated by Arc-plasma Ion Plating



Hideyuki TSUTSUI\*

Relationships between the physical properties and wear resistance of TiN films coated by Arc-plasma Ion Plating in different conditions were studied. From the result of multiple regression analysis of these properties, it was clarified that the orientation of the crystal face is a dominant factor in the wear resistance of TiN films. TiN films that have high orientation of the (111) crystal face and low orientation of the (220) crystal face show good wear resistance.

## 1. Introduction

Nitride based hard films, including TiN films, feature a higher degree of wear resistance compared with that of steels. Such hard nitride films are commonly applied to machine components that must satisfy higher level of requirements for wear resistance. Examples of such machine components include cutting tools and dies. Nitride based hard films can have a significant variation in physical properties, even if composed of the same material, depending on the coating technique and coating conditions. Therefore, these techniques and conditions need to be carefully selected. Present research studies the effects of varying physical properties of TiN films formed with varying coating conditions on wear resistance. This paper reports the resultant findings.

## 2. Coating conditions and test pieces used

The test pieces were prepared with an arc-plasma ion plating (AIP) apparatus.

The operating principle of the AIP apparatus used is schematically illustrated in Fig. 1. Compared with a hollow cathode ion plating system or sputtering system, the AIP apparatus is advantageous in that it provides a higher ionization rate and is capable of quickly forming a high-density film with good adhesion.

When a TiN film is formed with an AIP apparatus, nitrogen atoms are converted into plasma by arc within a vacuum chamber. The energy of the resultant

plasma causes the solid pure titanium target to evaporate. The evaporated titanium ion and the nitrogen atom in plasma state chemically react with each other to form titanium nitride (TiN). By negative voltage (bias) applied to a base material, TiN coating particles are attracted to and accumulate on the base material to form a film.

For the present study, eight types of test pieces were prepared by varying the coating parameters, that is, coating pressure, arc current and bias voltage. The thickness of the resultant films fall in a range of 2 to 3  $\mu\text{m}$ .

Each test piece (base material) is a disk measuring 48 mm in outside diameter and 7 mm in thickness. The material used was SUS440C hardened stainless steel with a surface roughness of 0.005  $\mu\text{m}$  Ra on the flat area where the TiN film was formed.

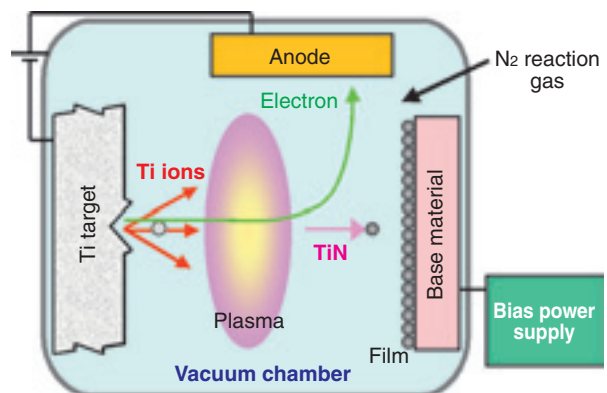


Fig. 1 Principle of Arc-plasma Ion Plating apparatus

\*Elemental Technological R&D Center

**Table 1** Conditions of TiN film coating

Test piece description	Coating pressure Pa	Arc current A	Bias voltage V
TiN-standard	4	150	30
TiN-2Pa	2	150	30
TiN-6Pa	6	150	30
TiN-100A	4	100	30
TiN-200A	4	200	30
TiN-10V	4	150	10
TiN-100V	4	150	100
TiN-300V	4	150	300

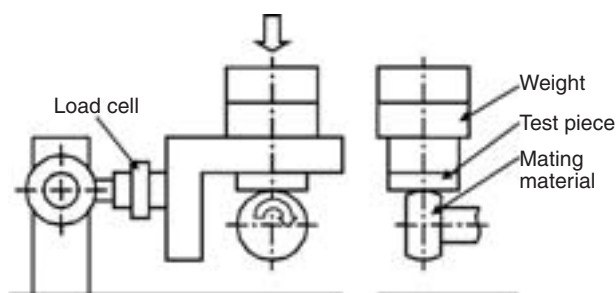
### 3. Evaluation of wear resistance

#### 3.1 Evaluation method

The NTN Savin type wear test rig was used to evaluate the wear resistance of the test pieces. The test rig is schematically illustrated in Fig. 2, and the applied test conditions are summarized in Table 2.

On the test rig, the flat surface of the test piece (where the TiN film being evaluated is formed) slides on the circumferential surface of the disk-shaped mating piece. The mating piece is made from quenched-tempered SUJ2 material with a hardness of HV784. The mating section has a curvature of R60 mm and a surface roughness of 0.01  $\mu\text{m Ra}$ .

The NTN Savin type wear test rig is identical to the standard Savin type wear test rig except for the mating piece. In a standard Savin type wear test rig the outer circumferential surface of the mating piece is


**Fig. 2** Schematic drawing of NTN Savin type wear test rig

**Table 2** Conditions of Savin wear test

Mating material	Quenched-tempered SUJ2, curvature R60 mm hardness Hv784, surface roughness 0.01 $\mu\text{mRa}$
Load	50 N (max. contact surface pressure 0.5 GPa))
Velocity	0.05m/s
Time	3 min. (sliding distance 9 m)
Atmosphere	Blowing of dry air, humidity 0-20%RH
N number	2

flat—the load is applied at an edge and greater variation in test result can occur. In contrast, the NTN's wear test rig employs a uniquely shaped mating piece whose outer circumferential surface has a curvature to avoid possible partial contact. Therefore, the NTN test rig has a higher evaluation accuracy.

In order to determine wear resistance of the TiN films, the test duration was set so that the TiN film wear does not reach the base material of the test piece. Furthermore, a base material was selected whose surface roughness value is small so that an adhesion wear configuration is established.

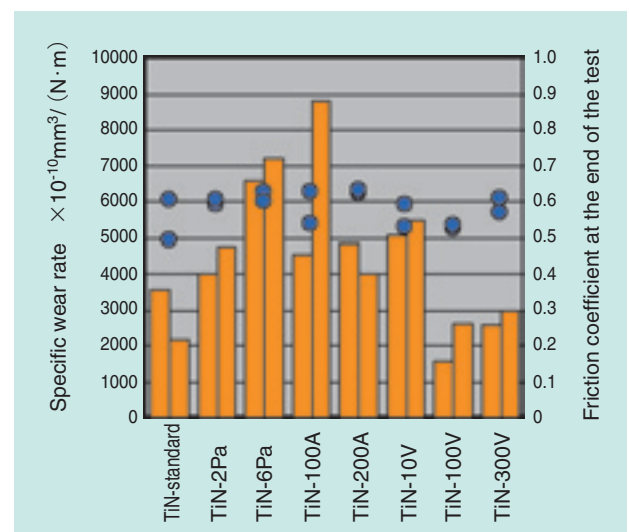
The specific wear rates were determined by first measuring the widths of wear marks after the end of test run and then subjecting the measurements to a calculation method. Additionally, friction coefficients were calculated from friction force measurements obtained with a load cell.

#### 3.2 Evaluation result

The specific wear rates and friction coefficients obtained with the NTN Savin type wear test rig are shown in Fig. 3.

It is apparent that specific wear rates with TiN films can vary depending on the coating conditions. The maximum specific wear rate can be about five times as great as the minimum specific wear rate.

The friction coefficients of the TiN films at the end of the test fall in a range of roughly 0.5 to 0.6 with no clear-cut variation between test pieces.


**Fig. 3** Specific wear rates and friction of TiN films

#### 4. Relationship between hardness and wear resistance

Generally, the hardness of a TiN film is associated with its wear resistance. Therefore, the effects of hardness of the TiN film were investigated. To determine the hardness, a nano-indenter was used to obtain indentation hardness values using a continuous rigidity measurement technique <sup>1)</sup>.

The relationship between the indentation hardness values and specific wear rates is shown in Fig 4. The diagram includes data for contribution factors.

Note that the contribution factor of indentation hardness relative to specific wear rate is low; this means that indentation hardness is least associated with specific wear rate.

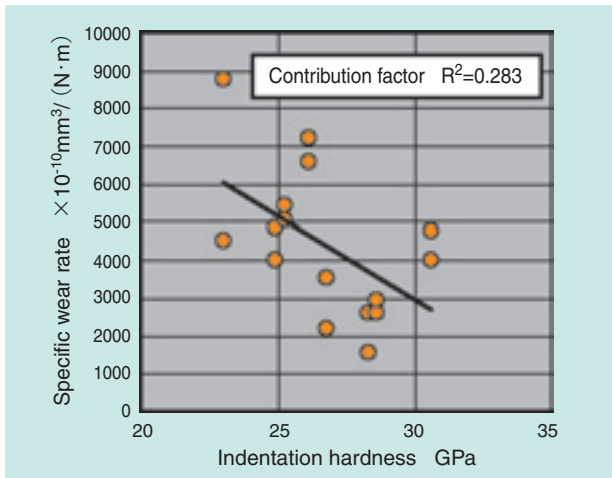


Fig. 4 Relationship between hardness and specific wear rate

#### 5. Relationship between orientation of TiN crystals and wear resistance of TiN film

Some recent research reports conclude that the wear resistance properties of nitride-based hard films such as TiN films are affected by the orientation of the nitride crystals <sup>2)-5)</sup>.

X-ray diffraction analysis was used to determine the crystal orientation state of the test pieces used in our study. As a result, the pattern in Fig. 5 was obtained. This pattern shows there is a significant variation in the state of crystal orientation between test pieces.

Because of this, the relation between TiN crystal orientation and wear resistance about the main peaks of TiN films was studied, where main peaks means the (111) crystal face peak and (200) crystal face peak. Fig. 6 shows the relationship between the peak strength and wear resistance about the (111) crystal face. Fig. 7 provides the relationship between the

peak strength and wear resistance about the (200) crystal face.

These possible factors, the peak strength of (111)

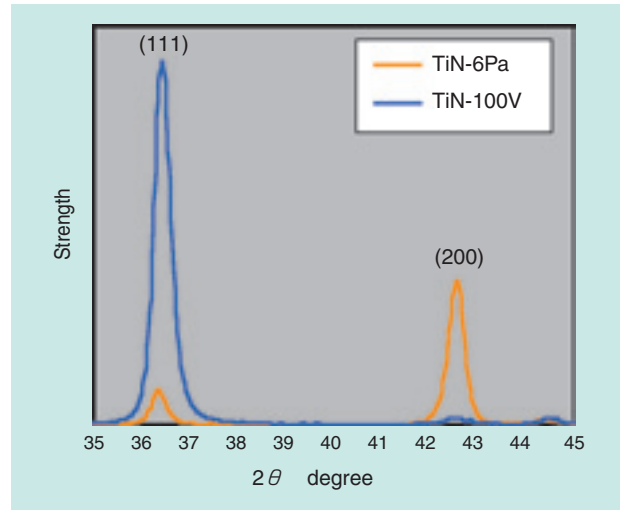


Fig. 5 X-ray diffraction (XRD) patterns of TiN films

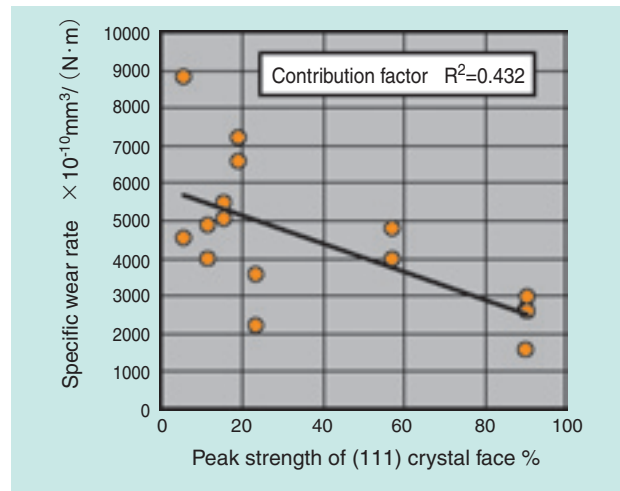


Fig. 6 Relationship between peak strength of (111) crystal face in XRD pattern and specific wear rate of TiN film

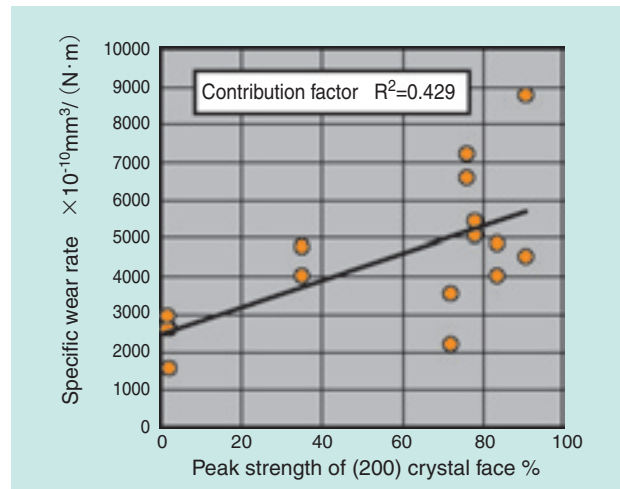


Fig. 7 Relationship between peak strength of (200) crystal face in XRD pattern and specific wear rate of TiN film

crystal face (contribution factor of 0.432) and peak strength of (200) crystal face (contribution factor of 0.429), do not provide enough information for explaining the specific wear rates for the test pieces used. However, the values from contribution factors are relatively high. This shows that wear resistance of TiN films is more strongly affected by their specific wear rates than their indentation hardness values.

## 6. Relationship between various TiN film physical properties and wear resistance

As mentioned in Section 5, it has been learned that crystal orientation states are relatively closely related to wear resistance. Therefore, in order to verify this relationship more precisely, the effects of all the film physical properties that can affect wear resistance of TiN films were evaluated. This was done using a multiple linear regression analysis technique. The film physical properties evaluated are summarized in **Table 3**.

Compared with other hard coating techniques, our AIP technique involves a relatively large proportion of particles known as droplets (the particles ejected from the target to undergo chemical reaction and get deposited on the base material; see **Fig. 1**) that are significantly larger than ordinary coating particles. **Fig. 8** provides a SEM photo of a TiN film. The droplets appear as foreign matter on the film surface and measure several microns in size. These droplets are present not only on the film surface but also in the film itself. Therefore, to be able to determine the effect of the coating particle size, we have attempted to analyze the surface roughness of TiN film.

To determine the crystal orientation state, all the peak strength ratios in the X-ray diffraction patterns obtained from the TiN film were used (seemingly

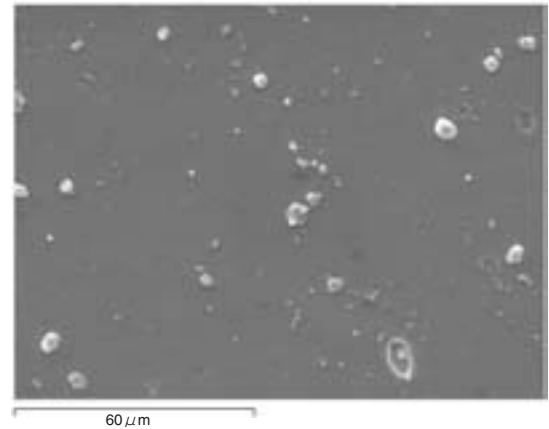


**Fig. 8** SEM image of TiN film surface

equivalent crystal faces which include (111) crystal face and (200) crystal face have also been incorporated).

The crystal sizes (maximum sizes of those regarded as single crystals) were determined by the Scherrer method, using the values for the (111) crystal faces and (200) crystal faces which correspond with the main peaks.

By the multiple linear regression analysis method, the specific wear rates were used as target variables in combination with the film physical properties as explanatory variables. In the field of multiple linear regression analysis, variables subjected to investigation into the relation with target variables are called explanatory variables. The combinations that exhibited strongest relation with the target variables were evaluated.

As a result of multiple linear regression analysis, it was determined that the TiN film physical properties that are most closely related with the wear resistance of TiN film are the peak strength of (111) crystal face and peak strength of (220) crystal face. Like the result of single linear regression analysis, the effects of hardness are also small in the multiple linear regression analysis (see Section 4). The standard deviation regression coefficients of the explanatory variables selected are summarized in **Table 4**. These coefficients are parameters that represent the magnitude of the effect of the explanatory variables on the target variables; the larger the absolute value, the greater the effect. A positive or negative sign indicates the direction of effect. The relation between estimated specific wear rates derived from the multiple regression analysis and actual measurements of specific wear rates is graphically shown in **Fig. 9**.

From the result of multiple linear regression analysis, it is apparent that the wear resistance of TiN film is greater with a higher peak strength of (111)

**Table 3** Physical properties of TiN film investigated in multiple regression analysis

Film physical properties	Unit	Measuring instrument
Surface roughness Ra	μm	Surface roughness measuring instrument
Surface roughness Rz	μm	Surface roughness measuring instrument
Indentation hardness	GPa	Nano-indenter
Indentation hardness elastic modulus	GPa	Nano-indenter
Peak strength of (111) crystal face	%	X-ray diffraction analyzer
Peak strength of (200) crystal face	%	X-ray diffraction analyzer
Peak strength of (220) crystal face	%	X-ray diffraction analyzer
Peak strength of (311) crystal face	%	X-ray diffraction analyzer
Peak strength of (222) crystal face	%	X-ray diffraction analyzer
Peak strength of (400) crystal face	%	X-ray diffraction analyzer
(111) crystal face crystallite size	nm	X-ray diffraction analyzer
(200) crystal face crystallite size	nm	X-ray diffraction analyzer

**Table 4** Dominant physical properties on wear resistance of TiN film in multiple regression analysis

Explanatory variable	Standard deviation regression coefficient
Peak strength of (111) crystal face	-0.703
Peak strength of (200) crystal face	+0.479

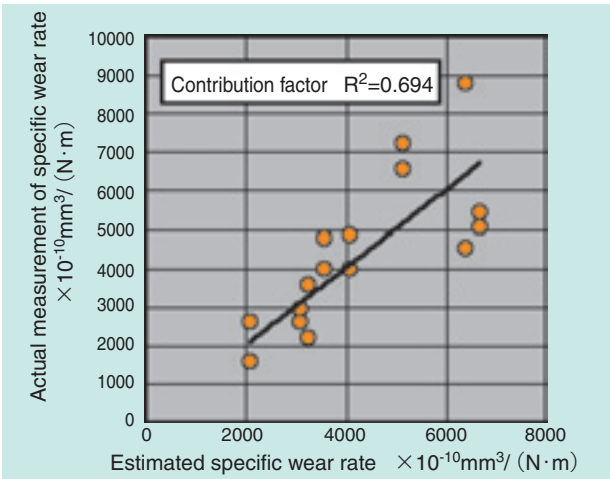


**Fig. 9** Relationship between estimated data by multiple linear regression and experimental data of specific wear rate of TiN film

crystal face and a smaller peak strength of (220) crystal face. Furthermore, the peak strength of (111) crystal face significantly affects the wear resistance of TiN film.

### 7. Relation between coating conditions and wear resistance

To determine whether or not the wear resistance of TiN films can be controlled by adjusting the coating conditions, multiple linear regression analysis was performed by taking specific wear rates as target variables and coating conditions as explanatory variables. The coating conditions investigated are summarized in **Table 5**.

As a result of the multiple linear regression analysis, it has been learned that because the highest contribution factor is as low as 0.411, coating conditions do not completely explain the degree of wear resistance of TiN film.

Therefore, the coating conditions were studied using a multiple linear regression analysis technique

**Table 5** Parameters in coating conditions of TiN film investigated in multiple regression analysis

Coating conditions	Unit
Coating pressure	Pa
Arc current	A
Bias voltage	V

by taking the peak strength of (111) crystal face that is known to most greatly (though indirectly) affect the wear resistance of TiN film as target variables.

The standard deviation regression coefficients of selected explanatory variables are summarized in **Table 6**. The relation between estimated values and actual measurements is graphically plotted in **Fig. 10**.

As a result of the multiple linear analysis, a multiple linear regression equation of relatively high reliability (contribution factor = 0.668) was generated. According to this multiple linear regression equation, it was learned that the peak strength of (111) crystal face of TiN film tends to be greater with a lower coating pressure and higher arc current and bias voltage with bias voltage being the predominant factor.

**Table 6** Dominant parameters of coating conditions on peak strength of (111) crystal face in XRD pattern of TiN film

Explanatory variable	Standard deviation regression coefficient
Coating pressure	-0.341
Arc current	+0.281
Bias voltage	+0.692

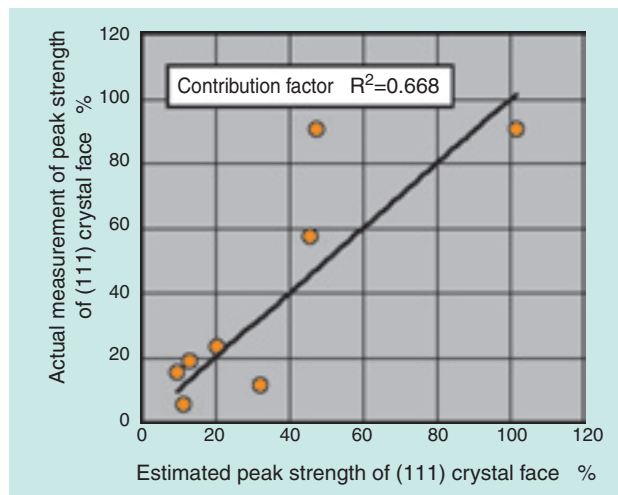


**Fig. 10** Relationship between estimated data by multiple linear regression and experimental data of peak strength of (111) crystal face in XRD pattern of TiN film

### 8. Relationship between coating conditions and hardness

It was learned that in a wear resistance test where an adhesive wear mode is the predominant mode, an indentation hardness technique does not explain the wear resistance of TiN film. However, if an aggressive wear mode is valid for some reason, such as presence of hard foreign matters on the sliding surface, then the indentation hardness becomes a

predominant factor.

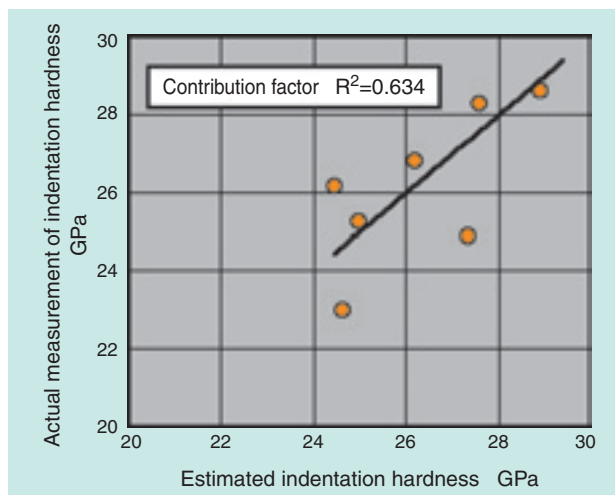
Accordingly, in order to determine the coating conditions that can control the indentation hardness of TiN film, multiple linear regressive analysis was performed taking indentation hardness as the target variable (the explanation variables studied are same as those summarized in Table 5).

Table 7 summarizes the explanatory variables and the standard deviation regression variables used for the present multiple linear regression analysis. The relationship between the estimated values and actual measurements obtained from the present multiple linear regression analysis operation is graphically plotted in Fig. 11.

From this multiple linear regression equation, it was found that the coating conditions that help establish a harder TiN film have a tendency similar to that with peak strength of (111) crystal face (see Section 7). However, in contrast with peak strength of (111) crystal face, the magnitude of the effect of the coating pressure is roughly equivalent to that of the bias voltage.

**Table 7** Dominant parameters of coating conditions on hardness of TiN film

Explanatory variable	Standard deviation regression coefficient
Coating pressure	-0.560
Arc current	+0.316
Bias voltage	+0.480



**Fig. 11** Relationship between estimated data by multiple linear regression and experimental data of hardness of TiN film

## 9. Conclusion

Multiple linear regression analysis was used to investigate the effects of various TiN film physical properties on the wear resistance of various TiN films each featuring a unique set of coating conditions. The resultant findings are summarized below:

- 1) Crystal orientation state is a significant factor for wear resistance of the TiN film, and the wear resistance is higher with a greater peak strength of (111) crystal face and a lower peak strength of (220) crystal face. In addition, the effect of peak strength of (111) crystal face on wear resistance is significantly higher.**
- 2) Coating conditions alone cannot explain the wear resistance of the TiN film. However, the adjustment of coating conditions can control the peak strength of (111) crystal face, which affects the wear resistance of TiN film most significantly.**
- 3) The hardness of TiN film can be controlled through the adjustment of coating conditions.**

We will attempt to explain the reason why higher peak strength of (111) crystal faces leads to greater wear resistance of TiN film and remain committed to the development of high performance hard films.

## References

- 1) W.C. Oliver and G.M. Pharr: An improved technique for determining hardness and elastic modules using load and displacement sensing indentation experiments, J. Mater. Res., Vol.7 No.6, 64, 1992
- 2) Azushima et al.: Proceedings of the 2006 Japan Society of Mechanical Engineers Annual Conference Proceedings, No.06-1 (2006) 417
- 3) Tanno et al.: Wear characteristics under drying conditions of Ti-B-N hard capsules that have crystal orientation control through AIP, Tribology Conference Proceedings, Saga (2007-9) 147
- 4) Tanno et al.: Wear mechanism under drying conditions of TiN hard capsules that have orientation control through AIP, Tribology Conference Proceedings, Tokyo (2008-5) 187
- 5) Ishii et al.: Improvement of capsule characteristics in titanium nitride compound surface reform, Tribology Conference Proceedings, Tokyo (2008-5) 219

Photo of author

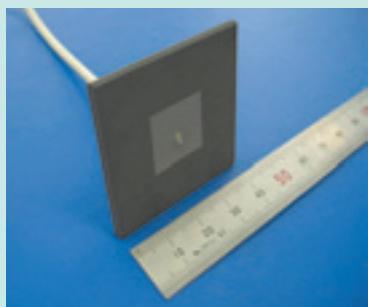


Hideyuki TSUTSUI

Elemental Technological  
R&D Center

# Development of an Antenna Material Based on Rubber that has Flexibility and High Impact Resistance

Kouya OOHIRA\*



NTN has developed an antenna material based on rubber that displays superior flexibility and high impact resistance compared to ceramic and polymer antenna materials. The developed material also has fire retardancy. The developed material is suitable for dielectric antennas that are used for wireless LAN, radio frequency identification, ultra wide band and other applications. This report introduces the characteristics of the developed material and test results.

## 1. Introduction

Recently, the markets have been dramatically expanding in the field of equipment for high-frequency wireless LAN, RFID (radio frequency identification), UWB, GPS, terrestrial digital broadcasting and home network, etc. In this context, a diversity of dielectric antennas are currently used. A material of dielectric antenna used for these applications is preferably needed to feature a higher dielectric constant and a lower dielectric loss tangent. By using a highly dielectric material for an antenna, a compact antenna can be designed thanks to frequency shortening effect of wave that is transmitted in the dielectric material. Incidentally, use of a material of low dielectric loss tangent will help suppress heat generation-induced energy loss and can improve antenna performance.

Conventional antennas have often been consisted of a ceramic material, and the relative dielectric constant for a ceramic material cannot be arbitrarily selected. Consequently, degree of freedom in designing antenna is low. As an antenna material capable of arbitrary selection of relative dielectric constant, resin type <sup>1)</sup> (composite material containing ceramic powder) is available. However, these materials have involved drawbacks that include ① surface treatment is needed to improve adhesiveness for electrode strips, and ② injection-forming with a high dielectric material having a larger portion of ceramic powder is difficult. Furthermore, these conventional antenna materials are hard and brittle,

lack in flexibility and are vulnerable to impact.

To address these challenges, NTN has newly developed "rubber-based antenna materials" <sup>2)-5)</sup>. Consisting of a rubber (EPDM) base material, this series of rubber materials is capable of arbitrary setup of relative dielectric constant by appropriately adjusting the content of highly dielectric ceramic powder. Being flexible, the NTN's newly developed rubber material boasts excellent shock resistance and can be attached to a curved surface: furthermore, since being formed by a heat-compression technique, the rubber material can be formed into a cylinder or prism, or even into a large-sized sheet that is not formed with a ceramic or resin material. This feature is an outstanding advantage of this material. Conventional rubber materials have a drawback of inferior flame retardance. In contrast, the NTN's new rubber material boasts excellent flame retardance equivalent to UL94 V0 by adoption of optimally blended flame retarding agent.

## 2. Advantages of new rubber antenna material

The typical features of the NTN's new rubber antenna material are summarized as follows:

### ① Advantages in functionality

- Relative dielectric constant can be arbitrarily selected (4-20).
- Low dielectric loss tangent (0.01 or lower)
- High degree of flexibility

\*Elemental Technological R&D Center

- High degree of shock resistance
  - Flame retardance (HB, V1, V0)
  - Easy machining works including cutting and grinding
- ② **Advantage in forming (molding)**
- Forming into cylinder or prism is possible.
  - Forming into a larger sized sheet is possible.
- Sheet dimensions: 150 mm×150 mm to 230 mm×230 mm  
Sheet thickness: 1 to 3 mm

**Fig. 1** shows an RFID patch antenna consisting of the NTN's new rubber material (100 mm×100 mm×t6 mm), **Fig. 2** provides a view of the new rubber material attached to a curved surface, and **Fig. 3** presents a view of cylindrical moldings of the new rubber material.

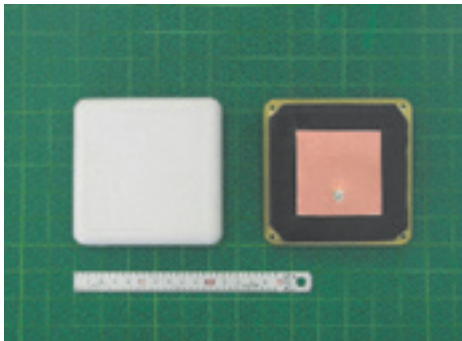


**Fig. 1** Patch antenna of developed material for RFID

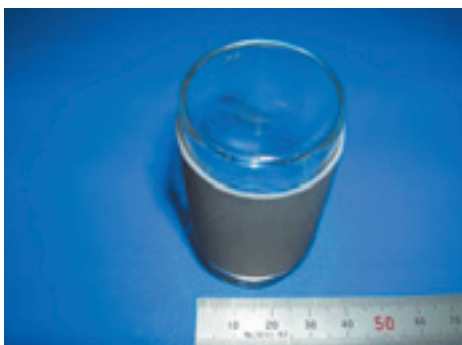


**Fig. 2** The developed material stuck on curved surface

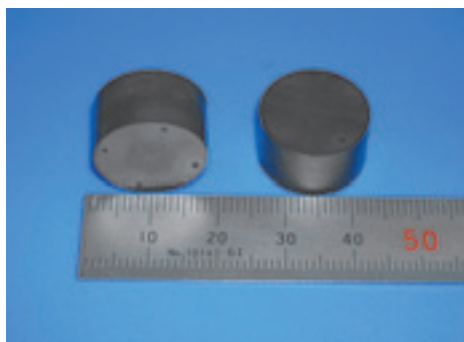


**Fig. 3** Example of cylinder molding of the developed material

The prototype antenna shown in **Fig. 1** comprises a sheet of NTN's new rubber antenna material: to each of its faces, a piece of copper foil electrode is attached, and this electrode is designed to the wavelength of intended radio frequency wave being transmitted and received. **Fig. 2** shows a situation where a piece of the new rubber antenna material is attached to a curved surface. Since the base material of the new material is flexible rubber, such a piece can be readily attached to a curved surface. A conventional ceramic antenna or a resin antenna containing ceramic powder cannot be readily glued to a curved surface such as a one shown in **Fig. 2**.

**Fig. 3** provides a view of cylindrical moldings formed by heating-compression technique using a 4-gate press die. As necessary, the new material is capable of insert molding with electrodes embedded.

### 3. Dielectric properties

#### 3.1 Amounts of ceramic powder and corresponding dielectric properties

EPDM has been used as a base material, and the amount of ceramic powder was varied in a range of 0 to 1200 weight parts (amount of ceramic powder has been varied relative to 100 weight parts of EPDM), thereby rubber sheets (each measuring 150 mm×150 mm×t2 mm) have been prepared. Each test piece of a specified shape has been cut from each rubber sheet, thereby the relative dielectric constant and dielectric loss tangent with each test piece have been measured with cavity resonance method. The test conditions used are summarized in **Table 1**, and the test results are graphically plotted in **Figs. 4** and **5**.

With a greater ceramic powder content, the relative dielectric constant is greater and the dielectric loss tangent is smaller. With a higher test frequency, both the relative dielectric constant and dielectric loss tangent tend to be greater.

With NTN's new rubber antenna material, it is possible to obtain a desired relative dielectric constant by arbitrarily adjusting the ceramic powder content in it. Because NTN's new material is capable of arbitrarily setting a relative dielectric constant, the antenna can be more freely designed: thus, the material is advantageous as an antenna material.

**Table 1** Test conditions

	Contents
Measuring method	Cavity resonance method
Test piece shape	Cylinder (1.5mm×1.5mm×70mm)
Frequency MHz	1000, 3000
Temperature °C	25

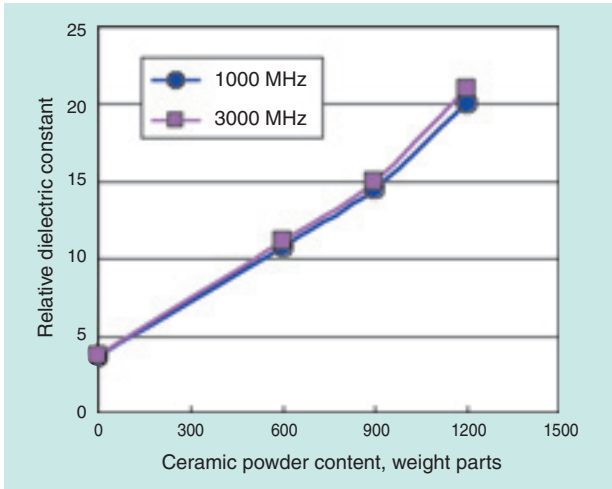


Fig. 4 Relationship between content of ceramic powder and dielectric constant

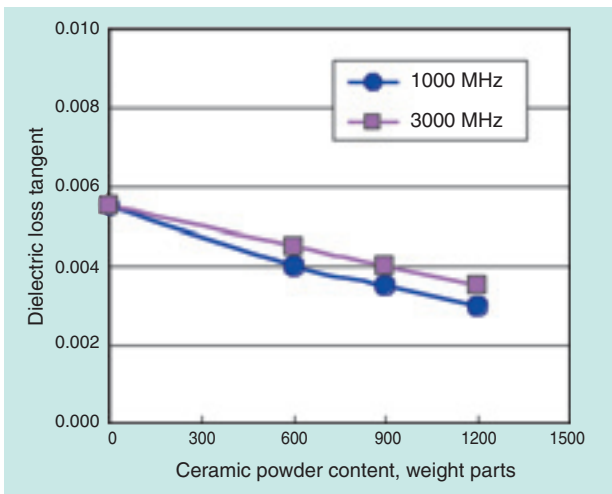


Fig. 5 Relationship between content of ceramic powder and tan δ

### 3.2 Temperature-dependency of relative dielectric constant

A rubber sheet was prepared which was blended so that its relative dielectric constant at a room temperature (25°C) is 16.5, and then its relative dielectric constant at various temperatures was measured by capacitor method. The test conditions are summarized in Table 2, and the test result is plotted in Fig. 6.

The relative dielectric constant of a rubber sheet alone decreases as the temperature increases. Greater variation in relative dielectric constant is not preferable because the resonance frequency can deviate depending on the temperature. In particular, when the rubber sheet alone is used at a higher frequency band, the deviation in resonant frequency can pose greater adverse effects.

In order to limit temperature-dependency of relative dielectric constant, trial and error were repeated in

designing better rubber sheet. As a result, it has been found that a composite rubber sheet comprising a plurality of rubber sheets each featuring a different material can provide a solution to this problem.

Fig. 6 also includes information about the temperature-dependency of the so-obtained hybrid sheet. Featuring relative dielectric constant less dependent on temperature, the hybrid sheet exhibits the relative dielectric constant nearly constant in a temperature range from -40°C to +120°C, thereby this material can be used in a wider temperature range.

Table 2 Test conditions

Contents	
Measuring method	Capacitor method
Test piece shape	Plate (30mm×30mm×t1mm)
Frequency MHz	400
Temperature °C	-40, -10, 30, 70, 100, 120

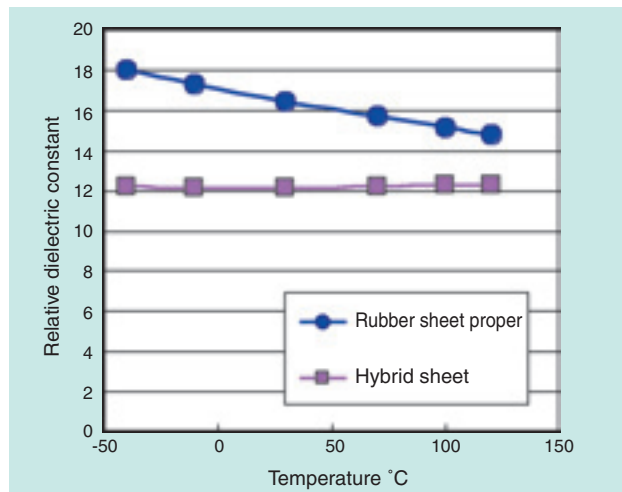


Fig. 6 Relationship between temperature and dielectric constant

### 3.3 Long-term aging quality

Test pieces (relative dielectric constant: 18, measured at 25°C) were obtained from the rubber sheet made of NTN's new rubber antenna material, and long-term aging quality of their relative dielectric constant has been evaluated. The aging conditions are summarized in Table 3, the measuring conditions for post-aging dielectric constant are listed in Table 4, and the test result is graphically plotted in Fig. 7.

From Fig. 7, it should be understood that the relative dielectric constants of the test pieces, each allowed to stand for 1000 hours at -40°C, +80°C or +120°C, remained virtually unchanged, and that NTN's newly developed rubber antenna material is satisfactorily stable.

**Table 3** Condition of aging test

	Contents
Test piece shape	Plate (30mm×30mm×t2mm)
Temperature °C	-40, 80, 120
Process time h	0, 250, 500, 1000

**Table 4** Test conditions

	Contents
Measuring method	Capacitor method
Test piece shape	Plate (30mm×30mm×t2mm)
Frequency MHz	400
Temperature °C	25

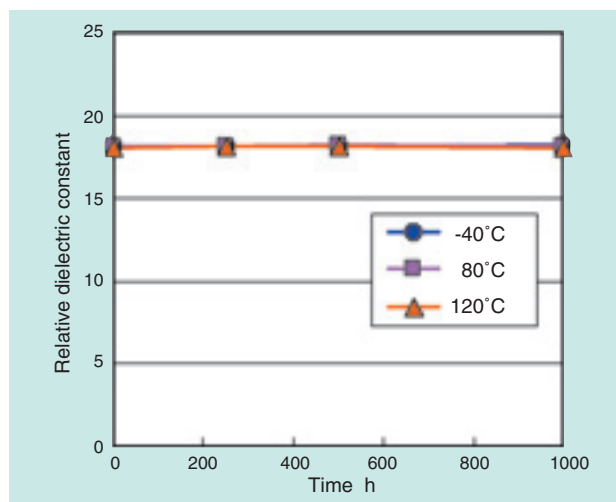


**Fig. 7** Relationship between aging time and dielectric constant

## 4. General physical properties

### 4.1 Mechanical properties

Ceramic powder contents and mechanical properties of the test pieces are summarized in **Table 5**. With a greater ceramic powder content, the specific gravity, tensile strength and hardness increase and elongation decreases. Note that no problem will occur with a specimen having 1200 weight parts of ceramic powder.

**Table 5** Mechanical properties of test specimen

Ceramic powder content, weight parts	Specific gravity	Tensile strength MPa	Elongation %	Hardness JIS-A
	JIS K6268	JIS K6251	JIS K6251	JIS K6253
0	1.0	4.5	290	47
600	2.8	6.1	150	90
900	3.2	6.5	110	92
1200	3.6	7.8	75	94

### 4.2 Immunity against molten solder

When used in a commercial application, the new rubber antenna material is needed to withstand the heat of molten solder because the power lines between power feed points and electrodes and the connector mounts are subjected to heat of molten solder. This is always a case with dielectric antennas.

**Table 6** summarizes the result of solder bath immersion test for NTN's newly developed rubber antenna material (per JIS C6471: test pieces are placed on the surface of solder bath kept at a specified temperature; they are removed after elapse of a specified time, and their appearance is inspected). At each solder bath temperature, the surface of each test piece did not exhibit a blister or crack. This fact means that NTN's new rubber antenna material boasts good heat resistance, positively withstanding the temperature of solder bath.

In reality, when fabricating a prototype rubber antenna for evaluation, NTN used molten solder for attaching the connector and grounding electrode and soldering the power feed point, and found that the material does not pose a practical problem.

**Table 6** Result of dipping test in melted solder

	Test duration s	
	5	10
260°C	No irregularity	No irregularity
280°C	↑	↑

## 5. Antenna characteristics

### 5.1 Resonant frequency, voltage standing wave ratio (VSWR) and gain

From a material featuring relative dielectric constant of 18 (25°C), two 2450 MHz patch antenna pieces (40 mm×40 mm×t2 mm) were obtained. The initial characteristics of both antennas are summarized in **Table 7**. It is apparent that both antenna pieces are performing well as antenna in terms of both VSWR (Voltage Standing Wave Ratio: a ratio of maximum value to a minimum value of waves that occur from superposing of incoming wave and reflected wave) and gain (ratio of the received power with the antenna

**Table 7** Antenna characteristics

No.	Resonance frequency MHz	VSWR	Gain dBi
1	2475	1.23	2.1
2	2446	1.19	2.1
Target value	2450±50	2 or less	1.5 or higher

being tested to that with the reference antenna, wherein the received power is measured when both antennas are directed in their maximum electric field while a same level of electricity is applied to both antennas).

**5.2 Heat cycle test**

The antenna prototypes were subjected to heat cycle test under the test condition shown in Fig. 8. Various antenna characteristics values (resonance frequency, VSWR, gain) with the antennas before and after the heat cycle test are summarized in Tables 8 through 10.

The test pieces having undergone the heat cycle test do not exhibit loosening of electrodes or blistering. At the same time, the variations in resonance frequency, VSWR and gain are very small (below target limits) and apparently do not pose problems in practical use of the antenna.

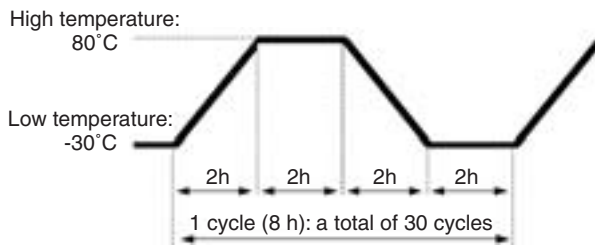


Fig. 8 Condition of heat cycle test

Table 8 Changing rate of resonate frequency

	Resonance frequency MHz		Variation %
	Before test	After test	
1	2475	2465	-0.4
2	2446	2434	-0.5
Target value	—	—	±2.0

Table 9 Changing rate of VSWR

	VSWR		Variation %
	Before test	After test	
1	1.23	1.31	6.1
2	1.19	1.26	5.6
Target value	—	—	±10

Table 10 Changing rate of gain

	Gain dBi		Variation %
	Before test	After test	
1	2.1	2.1	0
2	2.1	2.1	0
Target value	—	—	±10

**6. Flame retardance grade**

**6.1 Dielectric characteristics**

EPDM used for rubber antenna is readily combustible. However, antenna materials used on home electronic equipment are sometimes needed to be flame-retardant.

Rubber sheet samples were prepared by blending specific amounts of metal hydroxide (capable of retarding flame) and bromine-based flame retarding agent (outside the scope of RoHS directive), and by varying the content of ceramic powder. Test pieces of a particular shape were cut out from each rubber sheet sample, and the relative dielectric constant and dielectric loss tangent of each test piece have been measured. The test conditions are summarized in Table 11, the test conditions are graphically plotted in Figs. 9 and 10.

With increase in the ceramic powder content, the relative dielectric constant increases. The dielectric loss tangent of test pieces having the flame retarding agent is as high as 0.005 while that of test pieces lacking the flame retardant is as low as 0.003; this means an increase of about 0.002 (Fig. 10). Currently, it is expected that NTN will soon be able to establish a technique to limit the increase in the dielectric loss

Table 11 Test conditions

	Contents
Measuring method	Capacitor method
Test piece shape	Plate (20mm×20mm×t2mm)
Frequency MHz	400
Temperature °C	25

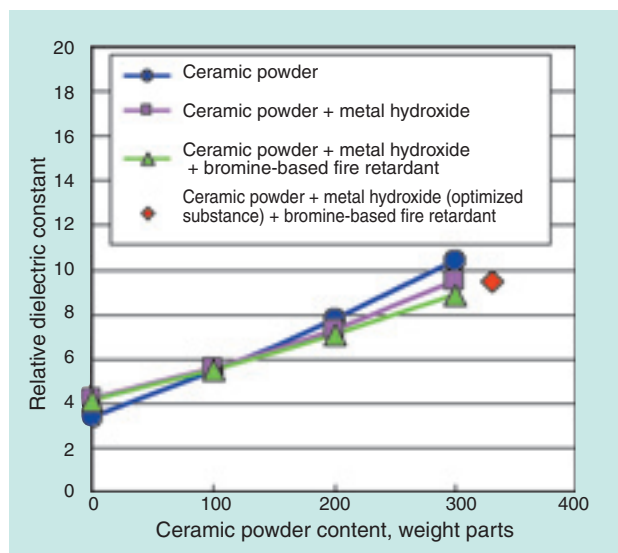


Fig. 9 Relationship between content of ceramic powder and dielectric constant

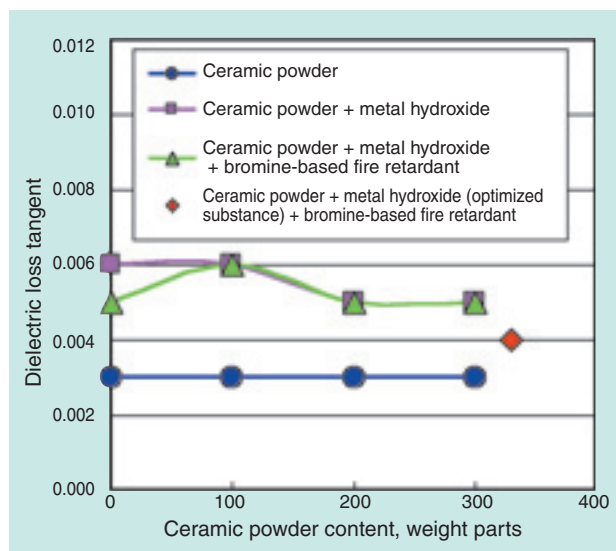


Fig. 10 Relationship between content of ceramic powder and  $\tan \delta$

tangent to approximately 0.001 through optimization of the metal hydroxide added. As reference, the dielectric characteristics data for a rubber sheet that contains 330 weight parts of ceramic powder are provided in Figs. 9 and 10.

## 6.2 Flame retardance

The flame retardance of each test piece has been evaluated through the flammability test per UL94 standard, and the result is summarized in Table 12. A test piece with low ceramic powder content burns violently. Test pieces containing not only ceramic powder but also metal hydroxide and bromine-based flame retarding agent exhibit good flame retardance of rank HB. In particular, the test piece containing metal hydroxide, bromine-based flame retarding agent and an increased proportion of ceramic powder boasts very excellent flame retardance of rank V0.

Table 12 Fire retardancy of test specimen

		Ceramic powder	Ceramic powder + metal hydroxide	Ceramic powder + metal hydroxide + bromine-based fire retardant
Ceramic powder content, weight parts	0	×	HB	HB
	100	HB	HB	HB
	200	HB	HB	V1
	300	HB	HB	V0

(Definitions of flammability)

HB (slow-burning): combustion velocity 40 mm/min or lower (not self-extinguishing)

V1 (flame-retardant): combustion time 30 sec. or shorter (self-extinguishing)

V0 (flame-retardant): combustion time 10 sec. or shorter (self-extinguishing)

## 7. Conclusion

NTN's newly developed rubber antenna material comprises rubber as a base material, and is capable of arbitrary setup of relative dielectric constant (in a range of 4 to 20) by adequately adjusting the content of highly dielectric ceramic powder contained in it. Being flexible, this novel material excels in shock resistance, does not develop cracks even when dropped, and can be readily attached to a curved surface. Additionally, when designed to be more flame-retardant, this material can have a flame retardance rank of V0. Furthermore, the material can be formed into a large-sized sheet (150 mm × 150 mm to 230 mm × 230 mm) that is not available with a ceramic-only or resin-only material.

To sum up, NTN's newly developed rubber antenna material has unique advantages many conventional materials do not offer. Thus this new material may be used in applications with which conventional ceramic or resin antennas cannot cope.

## References

- 1) J.W. Schulz, J.S. Colton, and C.K. Berkowitz: 45th International SAMPE Symposium, (2000) 1863-1873
- 2) Nakashima, Ohira: The Society of Rubber Industry, Japan 2004 Annual Conference Research Report Abstracts, 43 (2004)
- 3) Nakashima, Ohira, Sakai: The Society of Rubber Industry, Japan 2006 Annual Conference Research Report Abstracts, 70 (2006)
- 4) Egami, Ohira: The Society of Rubber Industry, Japan 2008 Annual Conference Research Report Abstracts, 119 (2008)
- 5) Ohira: Development of "rubber antenna material" that can have its relative dielectric constant set at will, Jido Ninshiki Monthly, Vol.1, 54-57 (2007)

## Photo of author



Kouya OOHIRA

Elemental Technological  
R&D Center

## Development of Sensing System for Cerebral Aneurysm Treatment



Yoshitaka NAGANO\*  
Hideo FUJIMOTO\*\*

In recent years, endovascular coil embolization has become a standard treatment option for people with cerebral aneurysms. Since coil embolization requires an advanced coil insertion technique, an analysis of the technique and the development of a surgical system for assistance and training are desirable. We have developed a novel optical force sensor for the coil delivery wire. This paper presents the sensor and the results of an evaluation of the sensor by using a silicone dummy aneurysm.

### 1. Foreword

Minimally invasive therapy has become increasingly attractive in modern medicine, particularly in the field of surgical applications. "Minimally invasive therapy" is a therapeutic method that minimizes the damage and pain to the patient when receiving a surgical operation. A typical example of such a surgical method is catheter surgery, in which a thin tube known as "catheter" is inserted into an appropriate human blood vessel and through which a variety of instruments and/or medicines can be delivered to an affected area to help treat the possible ailment. In particular, a surgical operation executed by inserting a catheter into a problem blood vessel is known as endovascular therapy or surgery. For this operation, the surgeon involved must have a higher level of skill in manual technique to be able to prevent endovascular damage.

As the age of society increases, the number of patients with subarachnoid hemorrhages (SAH) has been increasing. In this context, endovascular therapy has been applied to prevent rupture of a cerebral aneurysm, which is the major cause of SAH. As schematically illustrated in Fig. 1, a cerebral aneurysm occurs when a weak portion of vascular wall inflates like a balloon due to a factor such as blood pressure. The vascular wall of a cerebral aneurysm is vulnerable because it is thin, and it can rupture easily. In a typical endovascular therapy for cerebral aneurysms, a plurality of platinum coils are packed into the cerebral aneurysm in order to intentionally develop a thrombus

in the aneurysm and prevent it from rupturing. This technique is known as coil embolization<sup>1)-3)</sup>. In this surgical operation, a catheter is inserted into the cerebral aneurysm in question and through this catheter, platinum coils are delivered into the rupture-prone aneurysm: therefore, the coil insertion force needs to be finely controlled.

To help support the brain surgeon during the coil embolization operation for cerebral aneurysms, a three-dimensional cerebral artery model has been developed to assist in pre-operation simulation and surgical training<sup>4)</sup>. However, no instrument is currently available which is dedicated to support coil embolization for cerebral aneurysms. If a coil insertion force input sensor used during this operation can be developed, an excessive coil insertion force will be

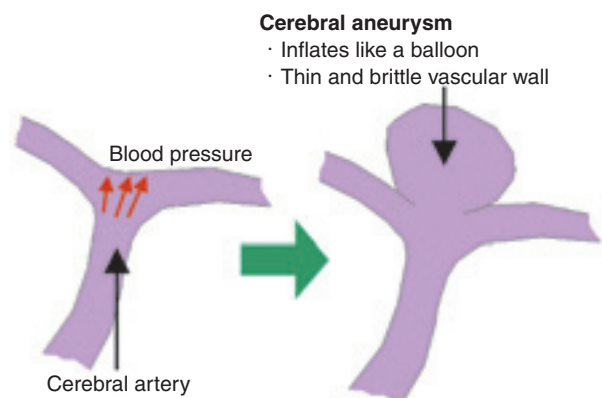


Fig. 1 Cerebral aneurysm

**Cerebral aneurysm**  
· Inflates like a balloon  
· Thin and brittle vascular wall

\*Mechatronics Research Dept. New Product Development R&D Center

\*\*Professor, Nagoya Institute of Technology

avoided and rupturing of cerebral aneurysm will be eliminated.

In addressing this challenge, NTN has undertaken research in cooperation with Professor Hideo Fujimoto, Graduate School of Engineering, Nagoya Institute of Technology to develop a unique sensor that allows the operating surgeon to sense a delicate force (insertion force with the coil) at their fingertip while manipulating the coil<sup>5)-7)</sup>.

This paper reports the result of a coil insertion test in which the NTN-developed sensor was inserted into the dummy cerebral aneurysm made of a silicone resin.

## 2. Coil embolization technique for cerebral aneurysms

As shown in **Fig. 2**, in a coil embolization operation for cerebral aneurysm, a surgeon will insert the coil into the artery at the femoral region via a surgical instrument known as the Y-connector. **Fig. 3** schematically illustrates the steps (1) through (5) for inserting coils into the cerebral aneurysm. The details of these steps are as described below.

- (1) The surgeon directs the catheter into the cerebral aneurysm.
- (2) The surgeon inserts the delivery wire whose end point has the platinum coil into the catheter. Once

reaching the cerebral aneurysm, the platinum coil restores its three-dimensional spiral structure (shape memory feature).

- (3) The surgeon determines the state of cerebral aneurysm and coil based on an X-ray image, and manipulates the delivery wire to insert the coil into the aneurysm. Once the entire coil has been inserted into the aneurysm, the coil is cut off from the delivery wire.
- (4) Steps (2) and (3) are repeated to pack a plurality of coils into the aneurysm at a high density.
- (5) The cerebral aneurysm packed with a plurality of coils turns into thrombus to prevent the aneurysm from rupturing.

## 3. Detecting principle and structure of the sensor

The diameter of the catheter used for endovascular coil embolization of cerebral aneurysms measures approximately 1 mm, and that of delivery wire is as small as 0.3 mm. Consequently, it is very difficult to directly mount a sensor piece to these thin members. Therefore, in the development of our new sensor system, we have attempted to maintain compatibility with conventional surgical instruments.

**Fig. 4** shows the appearance of the newly developed sensor. This sensor is unique in that it is

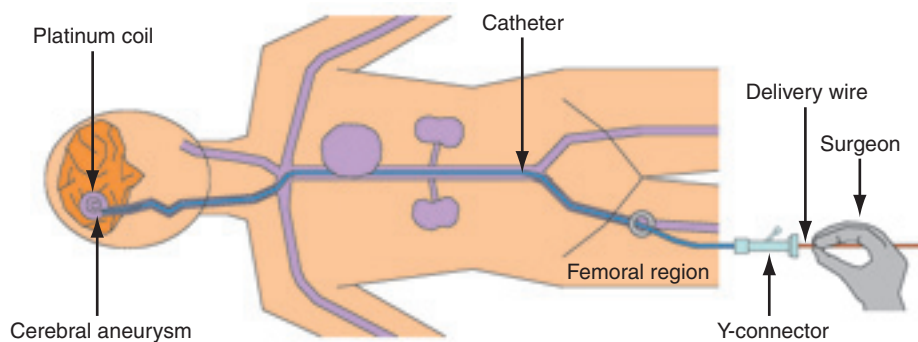


**Fig. 2** Endovascular coil embolization of cerebral aneurysm

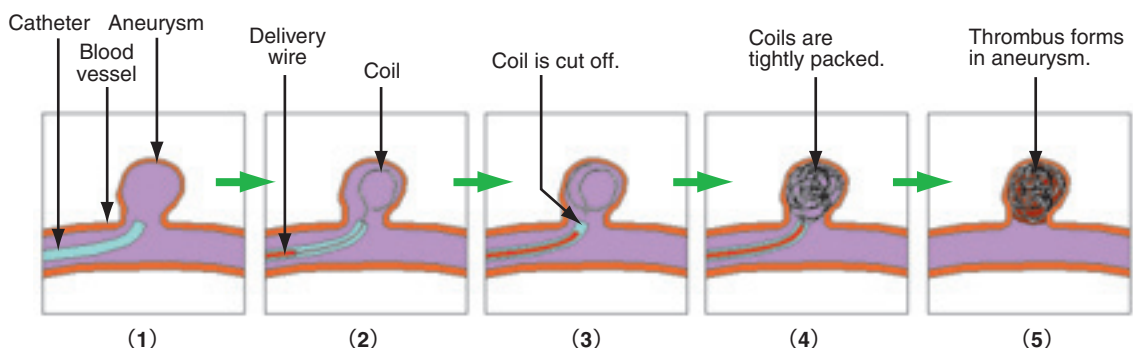


**Fig. 3** Treatment by embolization coil

configured around the Y-connector that has been conventionally used in surgical operations of cerebral arteries. The Y-connector used for inserting the delivery wire into the catheter comprises a junction of two insertion ports for inserting the delivery wire and introducing physiological salt solution. While holding the Y-connector with the left hand, the surgeon inserts and manipulates the coil with right hand.

Our insertion force sensor has been built into the middle portion of the Y-connector.

Fig. 5 shows the internal structure of the Y-connector. As illustrated in this diagram, an opening is situated at the middle of the Y-connector, and the wire flexes at this opening according to the insertion force acting on it. The newly developed sensor optically detects the resultant deflection amount to estimate the insertion force acting on the wire.

As with any medical equipment, the member directly delivered into a human body must be maintained at sterilized state. With our newly developed sensing

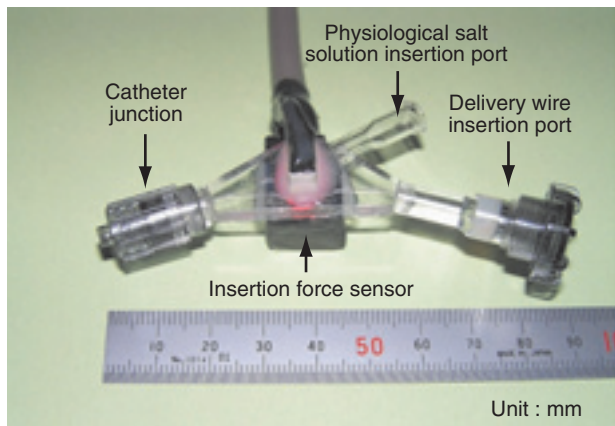


Fig. 4 Y-connector with built-in force sensor

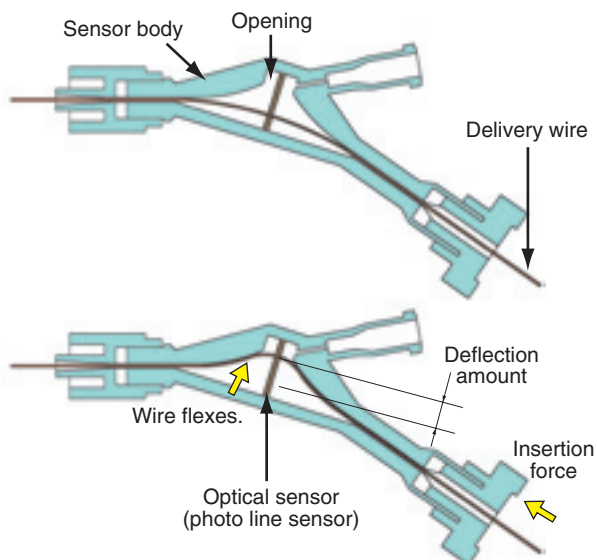


Fig. 5 Structure of the Y-connector with built-in force sensor

technique, the deflection amount of the wire is optically measured on a non-contact basis, and no is problem with sterilization requirements.

Fig. 6 schematically illustrates the optical configuration of the newly developed sensor. The sensing optical system comprises an LED, a lens array and a photo line sensor, wherein the sensor body is made of a transparent resin to enable transmission of LED light. Each optical part is embedded in the resin and is watertight, thereby the sensor can be rinsed with water.

Fig. 7 schematically illustrates the principle of wire position detection for measuring the deflection amount of the wire. This diagram shows a cross-sectional plan of the sensor body taken along the wire deflection direction. The light from the LED passes through the sensor body, and then the light path is altered by a lens array consisting of SELFOC lens and directed to the photo line sensor. The wire within the sensor body blocks a portion of the LED light, thereby the wire

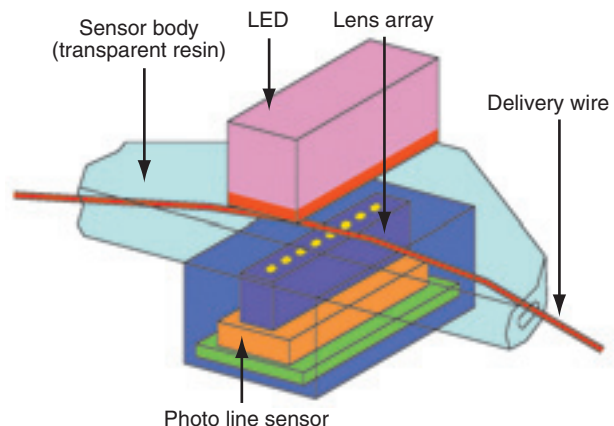


Fig. 6 Optical system of the force sensor

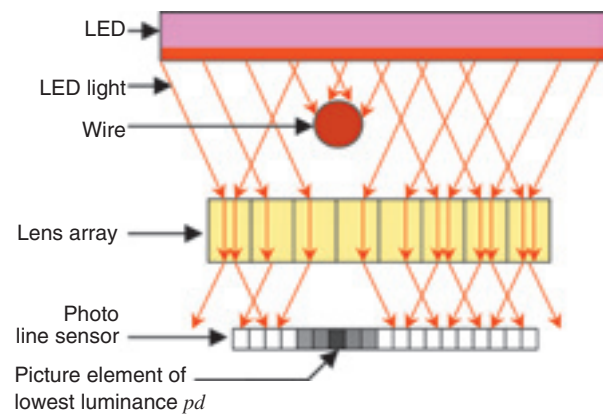


Fig. 7 Conception diagram of wire position detection

location is represented as the identification pd of the picture element exhibiting the lowest luminance within the photo line sensor. The photo line sensor consists of 128 picture elements and features resolution of 400 dpi (approximately 63  $\mu\text{m}$ ). Weighting has been attempted based on the locations and luminance of the picture element pd and nearby picture elements, thereby the deflection amount of the wire has been measured at precisions greater than the resolution of the photo line sensor.

## 4. Performance evaluation

### 4.1 Detection accuracy of insertion force

Using a delivery wire for coil embolization, the relation between the insertion force and deflection amount of the wire has been measured, and Fig. 8 graphically plots the result. Based on this result, the sensor output has been calibrated.

Fig. 9 presents the relation between the wire

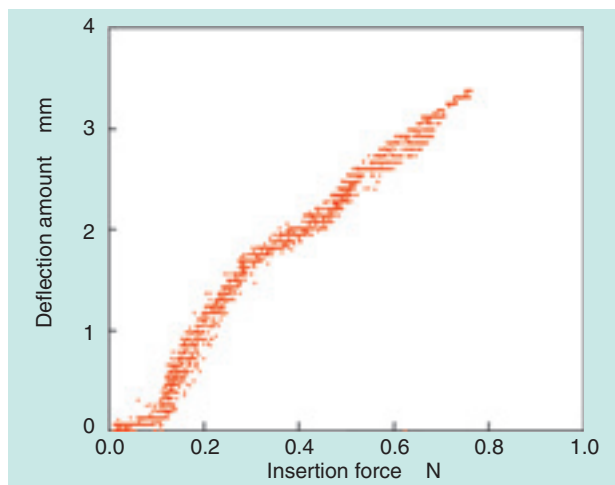


Fig. 8 Input force and bending value

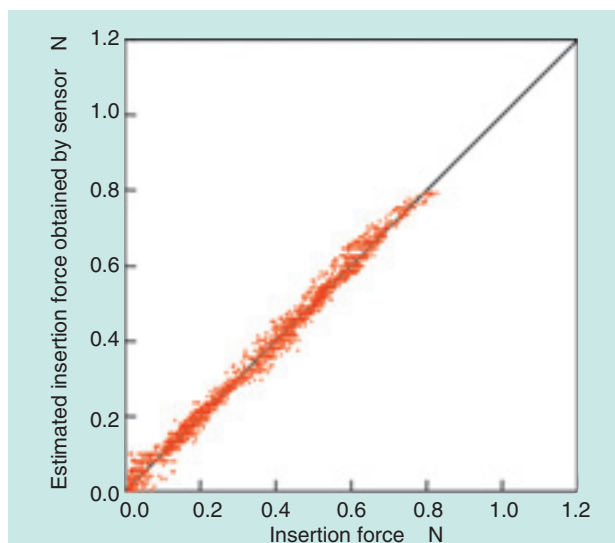


Fig. 9 Calibrated sensor output

insertion force estimated from the sensor output and the actual wire insertion force. It has been learned that the maximum detection error falls in a range of  $\pm 0.05$

### 4.2 Evaluation using dummy cerebral aneurysm

Using the test system shown in Fig. 10, a coil embolization test has been executed with a dummy cerebral aneurysm. The dummy cerebral aneurysm was fabricated with a transparent silicone resin so that the effect of coil embolization can be visually monitored, wherein the diameter of dummy aneurysm measured 4 mm and that of cerebral artery measured 3 mm. While progress of coil embolization was viewed with the monitor display connected to the CCD camera, the delivery wire insertion force was measured with the newly developed sensor.

Fig. 11 provides a view of the dummy cerebral aneurysm filled with a plurality of compacted coils.

Fig. 12 shows the resultant measurements for delivery wire insertion force. This diagram illustrates intermittent variation in insertion force occurring as time elapsed. This variation occurred because the

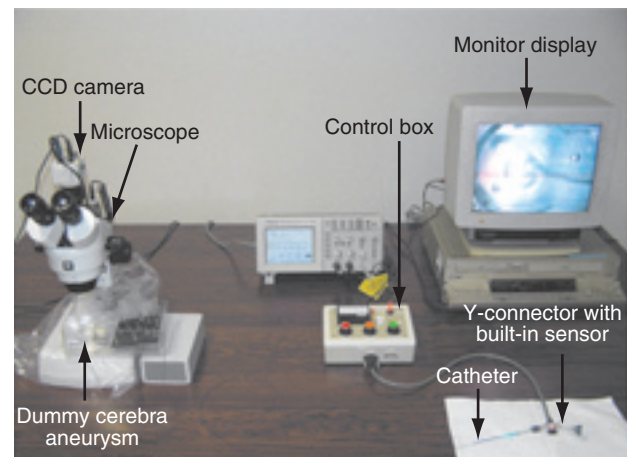


Fig. 10 Photograph of experimental system for coil embolization

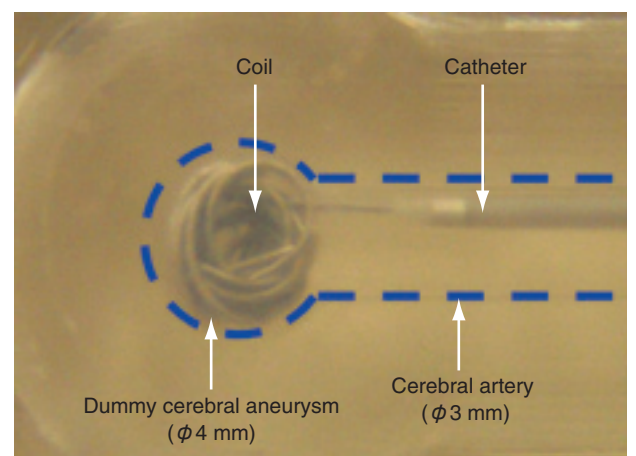


Fig. 11 Photograph of coil embolization

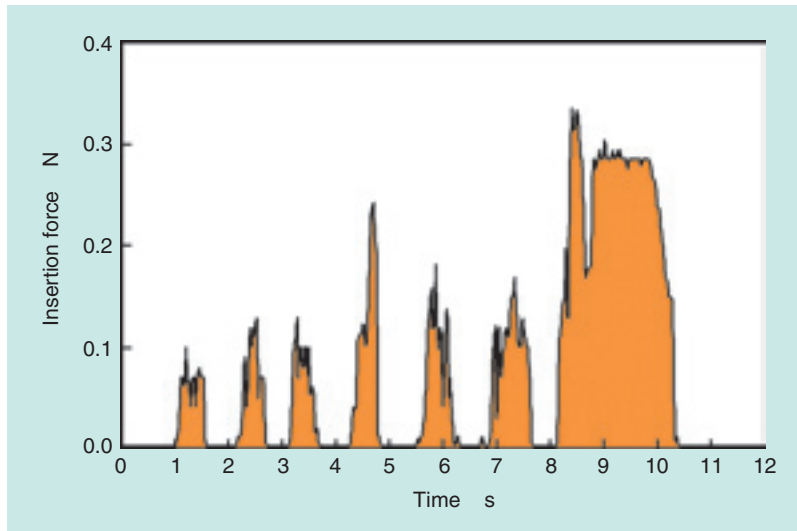


Fig. 12 Measurement result of insertion force

wire was pinched with fingers and progressively inserted in order to simulate an actual coil embolization operation. It has been learned that as the dummy cerebral aneurysm was progressively filled with coils, the insertion force gradually increased. At the final phase of coil insertion operation, an insertion force of approximately 0.3 N was measured.

## 5. Conclusion

We have developed a novel sensor that can measure coil insertion force exerted by a surgeon in a coil embolization operation for cerebral aneurysms. So that conventional catheter, coil and delivery wire can be used without any modification, we have incorporated an insertion force sensor into a Y-connector to be able to maintain compatibility with conventional coil embolization techniques.

We will accumulate additional test data and evaluate the accumulated data to help realize more advanced coil embolization practices for cerebral aneurysms.

## References

- 1) H. Kikuchi: "State of the Art Medicine Series 29 Neurosurgery—Recent Neurosurgery Treatment Developments," PET Journal (2004)
- 2) S. Miyachi: "Treatment Inside Cerebrovascular Vessels," Gendai Igaku 52 (1), (2004) 73-84
- 3) A. Hyodo, S. Nemoto: "Cerebral Aneurysm Surgery Inside the Artery Using GDC," Igaku Shoin, (1999)

- 4) S. Ikeda, F. Arai, T. Fukuda, K. Irie and M. Negoro: "Three Dimensional Photoelastic Stress Analysis on Patient-Tailored Anatomical Model of Cerebral Artery," Proc. 2004 Int. Symp. on Micro-Nanomechanics and Human Science, 145-150 (2004)
- 5) Y. Nagano, A. Sano, M. Sakaguchi, H. Fujimoto, "Development of a super fine and long linear sensor for physiological applications," 44(3), Transactions of the Society of Instrument and Control Engineers, (2008) 278-284
- 6) Y. Nagano, A. Sano, M. Sakaguchi, H. Fujimoto, S. Miyachi, T. Oshima, N. Matsubara, O. Hososhima, J. Yoshida: "Development of Sensing System for Cerebral Aneurysm Treatment," 16th Japan Society of Computer Aided Surgery Conference, (2007) 61-62
- 7) O. Hososhima, S. Miyachi, T. Oshima, T. Izumi, N. Matsubara, A. Tsurumi, J. Yoshida, Y. Nagano, M. Sakaguchi, H. Fujimoto: "Development of a coil insertion force measurement device using optical sensors," 1 (2), 23rd Annual Meeting of the Japanese Society for Neuroendovascular Therapy, (2007) 156 (Bronze medal poster in the doctors division)

## Photos of authors



Yoshitaka NAGANO

Mechatronics Research Dept.  
New Product Development  
R&D Center

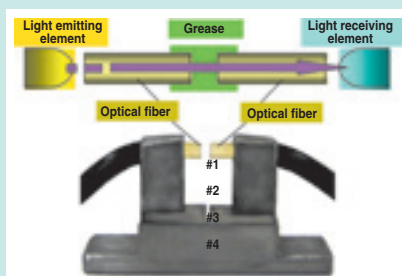


Hideo FUJIMOTO

Professor,  
Nagoya Institute of  
Technology

## Development of a Method for Monitoring Lubricant Deterioration

Kentaro NISHIKAWA\*  
Tomomi ISHIKAWA\*



The monitoring of debris and wear particles in lubricating oil and grease is desired for early prediction of the failure of machinery components. The state of lubrication can be estimated by monitoring the amount and size of the particles in the lubricating material. This paper describes the configuration and principle of the detection, and shows experimental results.

### 1. Introduction

Because it is the goal of all bearings to satisfy a higher degree of reliability, a technique is much needed to be able to sense the state of the internal condition of bearings while in operation. If detection of the degree of wear of each bearing member is possible, failure prediction for the bearing in question will be also possible. As a result, the maintainability and reliability of the associated machine will be much improved.

For oil-lubricated bearings, a device capable of sensing the state inside a bearing has been commercially used wherein wear particles (ferromagnetic material) occurring from the bearing in question are captured by a permanent magnet piece arranged in the oil circulating line and the captured magnetic particles are monitored with a magnetic sensor or electric-resistance detection sensor<sup>1)</sup>. Recently, bearings have been increasingly used in high-speed applications, typically on machine tool main spindles, and, in this context, hybrid bearings having ceramic rolling elements have been increasingly adopted. However, because ceramic material is non-magnetic and non-conductive, a measuring system capable of detecting metal wear particles cannot be used for analyzing ceramic wear debris. There have been reports about measuring an amount of ceramic wear debris, and the examples of the reported measuring technique include a dielectric factor method based on a fact that the dielectric factor measured with ceramic debris is several times as high as that with lubricating oil; and a method using an

electrostatic sensor<sup>2)</sup> that detects electrostatic buildup on ceramic debris immediately after their peel-off from a mother material. However, these techniques have problems to be solved in terms of detection accuracy and reliability.

Incidentally, large-sized bearings prelubricated with grease are usually maintained at regular intervals based on data about run hours elapsed. For example, grease is sampled from bearings for railway rolling stocks, thereby its acid number, consistency, oil separation ratio, constituents, water content and other factors of the grease are determined<sup>3)</sup>.

Quantification of amount of worn metal in bearing poses the most important challenge in lubrication management<sup>4)</sup>. However, there has been no report about a system that enables full-time monitoring of amount of metal in bearing.

This paper describes NTN's newly developed lubrication-related technologies: they are a technology for detecting ceramic powder in lubricating oil and another technology for sensing state of grease in bearing.

### 2. Ceramic debris detection sensor<sup>5)</sup>

#### 2.1 Detection principle and overview of sensing apparatus

Fig. 1 schematically illustrates our newly developed sensing apparatus. Two electrode plates are arranged in an opposing relation within a lubricating oil system, wherein one electrode plate is forced to the other by linear motion of an electromagnetic solenoid. If foreign matters are present in the lubricating oil, a portion of

\*Mechatronics Research Dept. New Product Development R&D Center

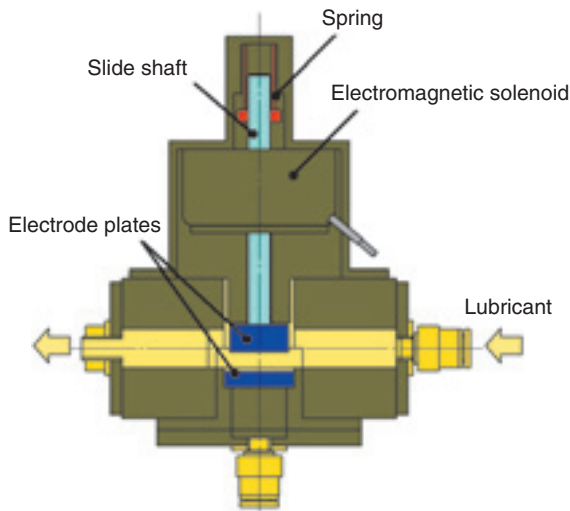


Fig. 1 Sensing apparatus for ceramic debris

these foreign matters is forced into the space between both electrode plates, and the distance between the electrode plates will fluctuate. The distance between electrode plates is determined by measuring capacitance across electrode plates, thereby the maximum size of foreign matters passing between both electrode plates is estimated. Our sensing apparatus is unique in that the surface of the electrodes is coated with insulation, so that capacitance measurement is possible without occurrence of short-circuit, even when conductive foreign matters such as metal debris are pinched between the electrodes.

The electrodes used on the prototype apparatus were flat disks measuring 15 mm in diameter. The surface area of the electrodes is sufficiently large relative to the sizes of foreign matters, and even when foreign matters are pinched between the electrodes, the capacitance is governed only by the distance between the electrodes.

Consequently, the maximum size of foreign matters pinched between the electrodes can be estimated by measuring the capacitance across the electrodes.

A spring installed to the slide shaft on the electromagnetic solenoid applies a preload between both electrodes, and when the electromagnetic solenoid is powered up, the distance between both electrodes is adjusted to 5 mm at maximum. In addition, one electrode is made of aluminum, and its surface is electrically insulated by anodizing.

**2.2 Method for evaluation test**

Fig. 2 schematically illustrates the lubricating oil circulation system used for the evaluation test of our sensor.

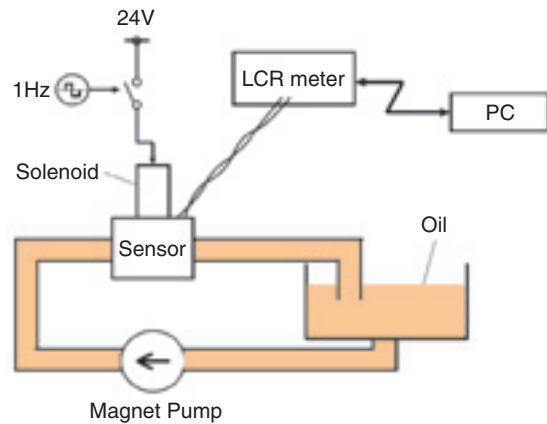


Fig. 2 Test equipment

In the test, oil (Nissan Motor Oil Strong Save X 0W-20, 1500 cc) was circulated at a flow rate of 5 L/min with a magnet pump, and ceramic powder was mixed into the circulating oil.

The electromagnetic solenoid inserted into the circulating system was turned ON/OFF once a second, allowing the capacitance to be measured with an LCR meter. By statistically treating the obtained capacitance measurements, the sizes and quantity of captured ceramic particles were estimated.

**2.3 Result of evaluation test for ceramic debris detection sensor**

Fig. 3 provides a graphical plotting of time-dependent change in the particle sizes of captured ceramic debris.

In this test, 1300 seconds or 3000 seconds after the start of measuring operation, 0.01 g of silicon nitride featuring mean particle size of 30 μm was mixed into the oil. In a time span between 4100 seconds and 5400 seconds after the start of test, an oil filter that captures particles larger than 20 μm was inserted in the piping to remove the ceramic particles from the oil. Then, the filter was taken out, and alumina powder

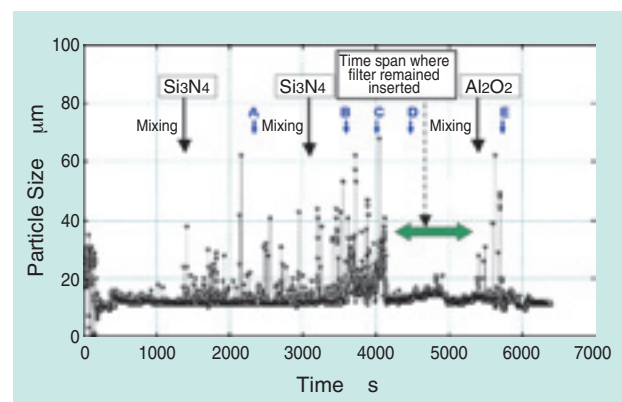


Fig. 3 Experimental result

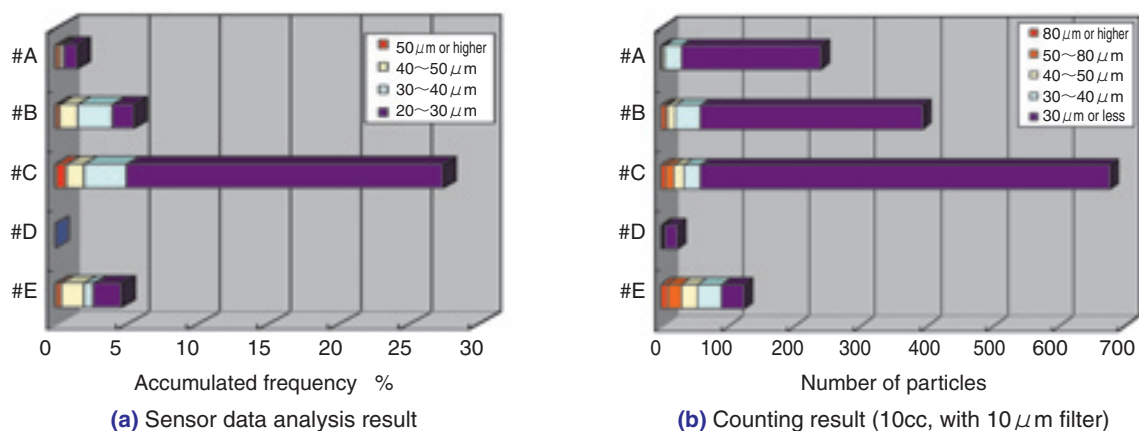


Fig. 4 Analysis result of detected data and counting result of sampling oil

measuring 75  $\mu\text{m}$  in mean particle size was mixed into the oil.

From Fig. 3, it should be understood that after ceramic powder is mixed, a number of occasions for capturing foreign matters increases and that virtually no foreign matters are detected during a time span where the filter remains inserted in the oil line.

Note also that even when the electrodes are in close vicinity, the distance between them does not decrease to zero: in other words, the minimum detectable particle size is limited by the thickness of oil film (approximately 10  $\mu\text{m}$  in Fig. 3) formed between the electrodes. This is because the pressure for forcing the electrodes together (preload) is as low as 0.5 N. It will be possible to detect much smaller particles by adopting a greater preload or providing a mechanism to eliminate the oil film between the electrodes.

Fig. 4 (a) provides the particle size measurements obtained from 5-minutes measurements (number of measurements: 300 = once/s  $\times$  300 sec.) in the time span between time points A through E in Fig. 3.

Also, 10-cc samples A through E taken at the timings A through E were each allowed to pass a 10  $\mu\text{m}$ -mesh filter, thereby the residual debris on filter samples were counted and classified, and Fig. 4 (b) provides the actual counts grouped by particle sizes. The trend in size distribution obtained from detection result with the sensor shown in Fig. 4 coincides fairly well with the size distribution of the particles captured with the filter shown in Fig. 4. Thus we have learned that the result of detection by sensor reflects the reality. It has been proved that even in a measuring operation with a very low sampling rate, that is, once a second, severity of contamination with foreign matters can be determined by subjecting a plurality of measurement results to a statistical process.

### 3. Grease state detection sensor<sup>6)</sup>

#### 3.1 Detection principle

Our newly developed sensor optically detects the amount of wear particles in grease occurring from a worn bearing. As shown in Fig 5, the sensor comprises a light emitting element, a light receiving element and a length of optical fiber. The light from the light emitting element is directed to the grease, and based on the intensity of light reaching the light receiving element, the quantity of wear debris in the grease from the bearing is determined. By inserting a length of a flexible optical fiber between the light-emitting element and the light-receiving element, we have attempted to improve freedom of layout with these elements.

Fig. 6 is a graphical plotting of the relation between the quantity of fine iron oxide powder ( $\text{Fe}_2\text{O}_3$ , red) of mean particle size 1.5  $\mu\text{m}$  mixed into grease and the light transmittance of the grease. The light transmittance has been defined as a ratio of the output from light receiving element when no foreign matters are mixed in the grease to the output from light receiving element when iron oxide is mixed in the grease. The logarithmic values of iron oxygen content are linearly proportional to those of light transmittance.

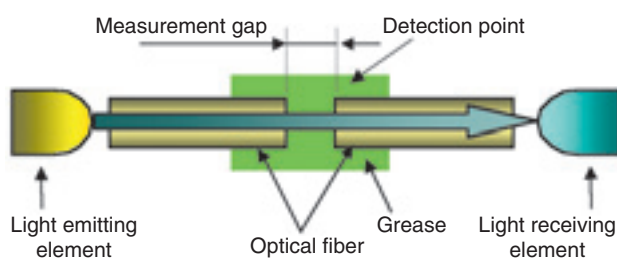


Fig. 5 Principle of optical sensor

Grease samples were taken from a plurality of bearings used in two applications, and Fig. 7 graphically plots the relation between the iron contents in greases and light transmittances. It should be understood that the logarithmic values of iron content in grease are linearly proportion to those of light transmittance as in the case of Fig. 6 and that the proportional constant between two sets of logarithmic values can vary depending on where the bearing is used. This seems to be because the size and color of wear debris can vary; therefore, an application-specific calibration curve needs to be developed so that the resultant measurements can be correctly calibrated.

**3.2 Configuration for test sensor unit**

Fig. 8 shows a cross-sectional view of a bearing with a built-in sensor unit. The grease in the bearing is released from the raceway surface and is trapped between the rolling element end faces and the cage, and then flows outward to the circumferential direction as the bearing runs<sup>7)</sup>.

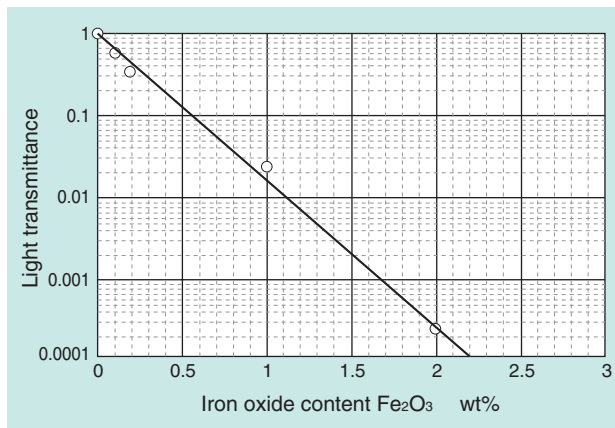


Fig. 6 Optical transparency of test grease

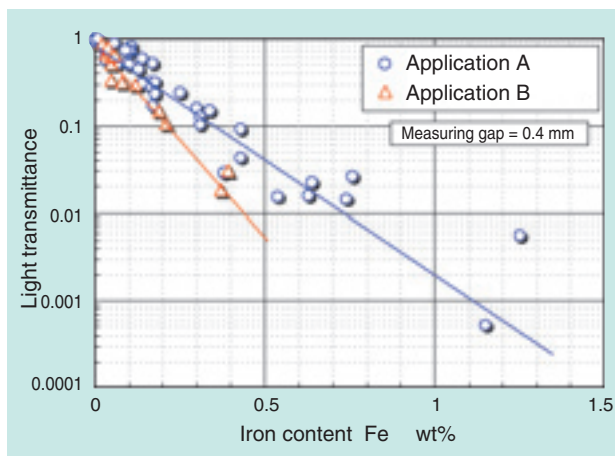


Fig. 7 Optical transparency of used grease

We have attempted to detect grease being released from the rolling surface by situating the sensor detection point in the vicinity of the raceway surface on the inner ring outer circumference.

Fig. 9 schematically illustrates the construction of our prototype sensor unit that is intended for incorporation into the test bearing. The detection point alone is projected in this sensor unit, and the other portion is enclosed in a sensor cover.

**3.3 Evaluation test**

A contaminated grease was prepared by mixing fine iron oxide powder ( $Fe_2O_3$ , red) of mean particle size  $1.5 \mu m$ . The running test was performed while this contaminated grease was injected between the rolling elements, and the test results are plotted in Figs. 10 and 11. Fig. 10 graphically plots the estimated amount of iron oxide detected by our sensor system for 10 hours after the start of bearing operation test and Fig. 11 provides a plotting of similar data for 500 hours. In advance, we prepared grease containing 5 wt% iron oxide. At 3.5 hours ( $T_2$  timing) and 100 hours ( $T_5$

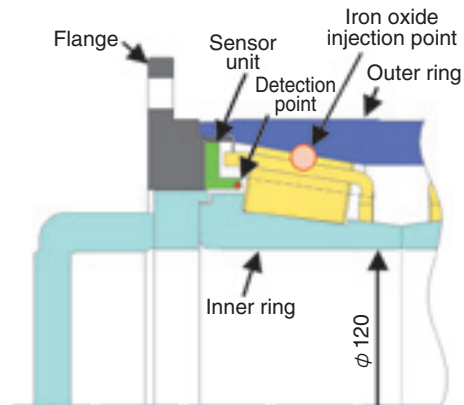
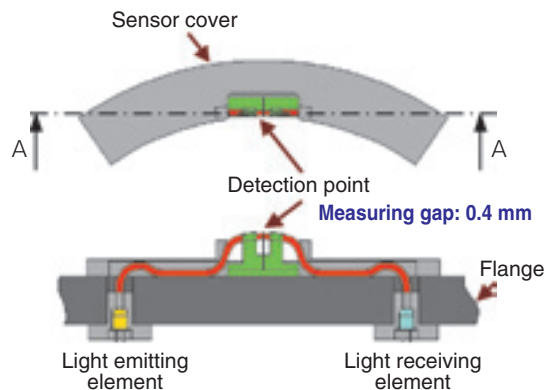


Fig. 8 Test bearing with sensor unit



View along A-A

Fig. 9 Sensor unit

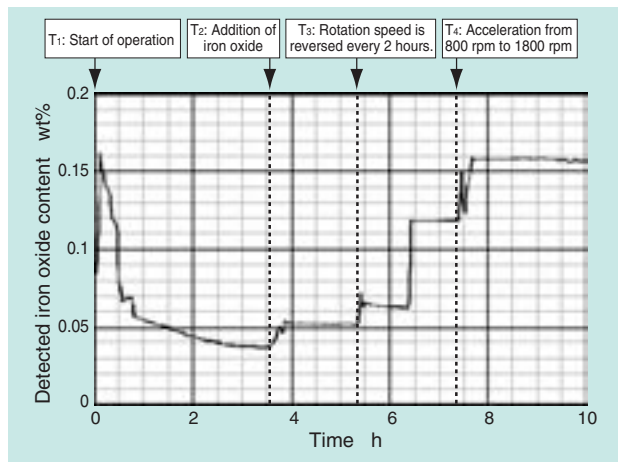


Fig. 10 Experimental result (T<sub>1</sub>~T<sub>4</sub>)

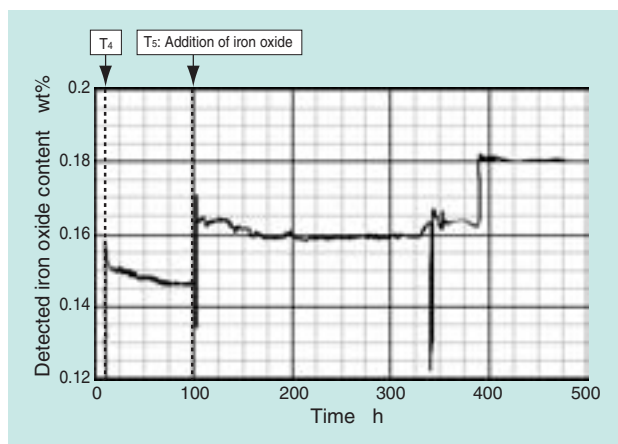
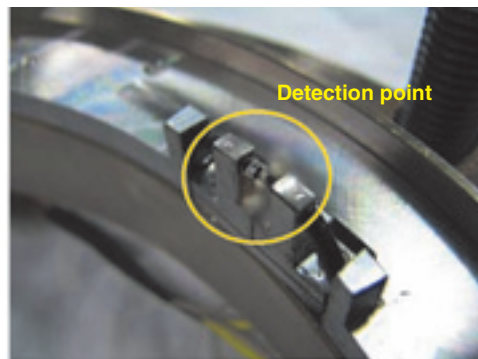


Fig. 11 Experimental Result (T<sub>1</sub>~T<sub>5</sub>)

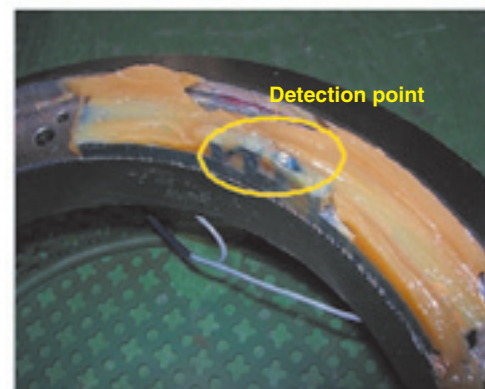
timing) after the start of bearing operation, 1 g of the contaminated grease at a time was added into the bearing. At the T<sub>3</sub> timing onwards, the direction of rotation was reversed once every 2 hours. The bearing speed in the time span T<sub>1</sub> through T<sub>4</sub> was 800 rpm, and in each section after T<sub>4</sub> was 1800 rpm.

From the test result, it is apparent that until 1 hour has elapsed after the start of bearing operation, the sensor output level gradually decreases and stabilizes at around 0.04 wt%. Immediately after iron oxide powder has been added, the iron oxide content increases. The change in sensor output level is observed when the grease flow greatly varies because rotation direction on bearing is reversed.

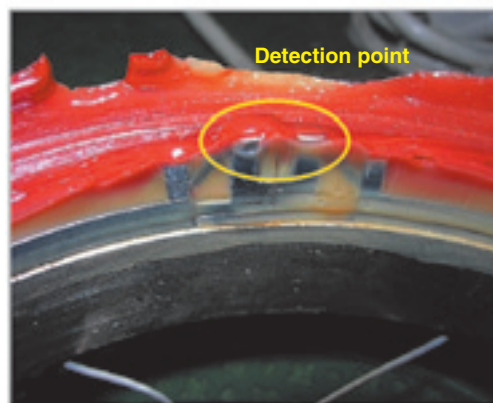
Fig. 12 shows various states of grease deposition around the detection point of the sensor unit during the test. As the test has progressed, the color of grease has changed, indicating that the iron oxide concentration in the grease around the detection point has apparently increased. In the situation immediately after the start of bearing rotation as shown in Fig. 12



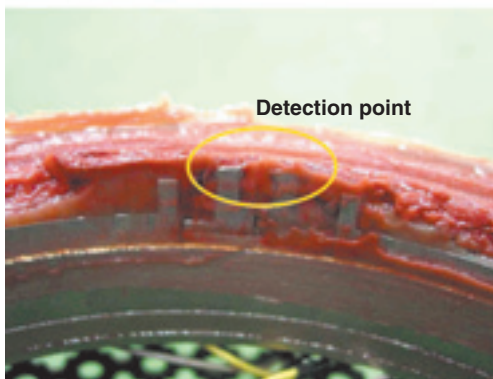
(a) Before Examination



(b) Condition of the attached grease to detection point



(c) Condition of the attached grease to detection point after 100 hours



(d) After examination

Fig. 12 State of grease around detector

(b) (a state before the timing  $T_2$  in Fig. 10 in which iron oxide powder was added, the grease has not yet been thoroughly stirred and grease deposition is not uniform around the detection point. At the time point 100 hours after the start of bearing operation as shown in Fig. 12 (c) (a state before the timing  $T_5$  in Fig. 11 in which the iron oxide powder was added), a fresh grease layer appearing reddish in color owing to contained iron oxide has been formed on the existing layer of previously released grease. Thus, it should be understood that the grease injected at the earlier phase of the test remains around the sensor cover. Furthermore, when 500 hours have elapsed after the start of bearing operation as shown in Fig. 12 (d), the grease has been more thoroughly stirred compared with the state in Fig. 12 (c). However, even at this state, the grease has not yet been homogenized. We have obtained an iron oxide content through conversion from the sensor output taken on the detection point having undergone 500 hours of test. Thereby, we have learned that the resultant iron oxide content level is twice as high compared with an iron oxide content in grease that simulates uniformly distributed iron oxide powder.

#### 4. Conclusion

We have developed a unique sensor product that can measure the size and quantity of wear debris and foreign matters in a lubricant. This sensing technology can be used to detect the state of mechanical components. This newly developed technology can be summarized as follows:

- (1) We have developed a unique technology according to which ceramic debris in lubricating oil are mechanically pinched and their sizes are measured. Furthermore, we have established a technique that can help estimate the amount of ceramic powder mixed into a lubricating oil through statistical processing of obtained sensing data.
- (2) We have established a technique that can help calculate the amount of foreign matters mixed into lubricating grease by an optical sensing technique for measuring the resultant light transmittance. Also, we have incorporated our newly developed sensor into a bearing, and we have verified that this arrangement can help estimate the amount of wear in the bearing.

#### References

- 1) S. Itomi, H. Ito: Sensor Units for Construction Machines, Construction Machinery and Equipment, (2008) 9
- 2) S. Morris, H.E.G. Powrie et al., Electrostatic charge monitoring of unlubricated sliding wear of a bearing steel, *Wear*, 255, (2003) 430-443
- 3) Railway Technical Research Institute, Organization of application methods for grease management standards, Rolling stock diagnostic technologies research group, Oil analysis subcommittee materials, 6 (2004)
- 4) Y. Suzuki: Deterioration of grease in use and methods of determining it, *Lubrication*, Vol.15, No.7 (1970) 439-453
- 5) T. Takahashi, T. Ishikawa: Detection of ceramic fragments in lubrication oil using a direct drive actuator, Japan Society of Mechanical Engineers, D&D 2007 Lecture No.735, 2007
- 6) K. Nishikawa, T. Takahashi, 2008 Spring Tribology Conference Proceedings, Tokyo 2008-5, (2008) 133-134
- 7) Y. Suzuki, S. Sugiyama, Deterioration of rolling stock axle grease, *Lubrication*, Vol.19, No.4 (1974) P341-346

#### Photos of authors



Kentaro NISHIKAWA

Mechatronics Research Dept.  
New Product Development  
R&D Center



Tomomi ISHIKAWA

Mechatronics Research Dept.  
New Product Development  
R&D Center

# Heat Transfer Analysis of Machine Tool Main Spindle



oshimitsu HIRASAWA\*  
Yukimitsu YAMAMOTO\*

CAE analysis is very useful for shortening development time and reducing the need for development trials. To use CAE effectively, the analysis results must be accurate. This report describes the use of the Finite Element Method to estimate the temperature distribution of machine tool main spindle bearings and the test machine during steady state heat transfer.

## 1. Introduction

Higher running speed has been increasingly needed for main spindles of machine tools such as machining centers in order to help achieve improved machining efficiency. When a main spindle runs at higher speeds, heat is generated in the bearings that support it, causing the difference in temperature between the inner ring and outer ring or the inner ring spacer and outer ring spacer to be greater than expected. If such a situation occurs, an ideal preload setup will not be maintained. To address this problem, the effects of spacer width and cooling efficiency on high-speed machine tool main spindles need to be more diligently studied. Previously, an appropriate preload setup reflecting these considerations has been determined on the basis of trial and error or past experience. If an appropriate preload setup can be simulated with higher accuracy through CAE analysis, bearing development work will be dramatically accelerated and the number of test runs necessary can be significantly reduced. In this paper, we will present our study of finite element method based steady state thermal analysis for estimating the temperature distribution of the machine tool main spindle bearings in our test machine including a comparison of these results to measured temperature data.

## 2. Overview of steady state thermal analysis

### 2.1 Steady state thermal analysis defined

Steady state thermal analysis can be defined as

"analysis technique for determining the temperature distribution on an object in a situation where the quantity of heat generated on the object is in equilibration with the quantity of heat dissipated from the object (the object is in steady state)".

For example, when a bearing is run under a combination of given load and speed, the temperature of the bearing will increase for a certain duration after the start of test. As time elapses, the rate of temperature rise decreases and finally levels off at a particular temperature (see Fig. 1). This state is defined as steady state: where the quantity of heat generated by the bearing is equal to the quantity of heat dissipated from the bearing. Steady state thermal analysis is an analysis practice for determining the temperature distribution of an object in steady state.

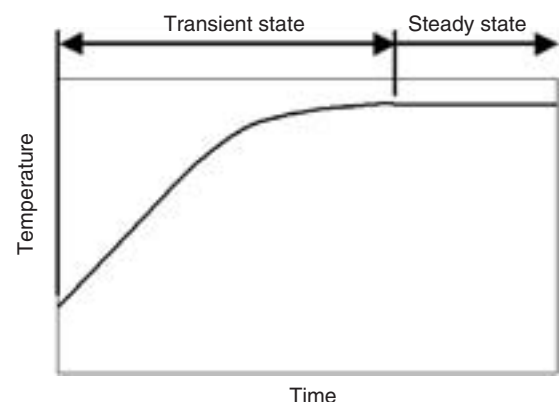


Fig. 1 Transient state and steady state

\*Product Design Dept. Industrial Sales headquarters

## 2.2 Comparison of stress analysis with steady state thermal analysis

**Table 1** compares features of CAE and finite element analysis used for stress analysis with those used for steady state thermal analysis.

In CAE, an input is a factor that alters the state of an object. The input in stress analysis is a load or forced displacement, while that in steady state thermal analysis the input is heat generation (more strictly, quantity of heat generated per unit time) or a fixed temperature.

A boundary condition for stress analysis is a constraint that inhibits the motion of an object. Boundary conditions considered for steady state thermal analysis include heat generation, heat insulation, heat transfer coefficient and fixed temperature. The most important boundary condition in steady state thermal analysis is heat transfer coefficient, which will be described in detail later.

The material physical properties required for stress analysis include Young's modulus and Poisson's ratio, while the physical property used for steady state thermal analysis is thermal conductivity, which is a measure of the ability to transmit heat within the material. Note that thermal conductivity is different in concept from the above-mentioned heat transfer coefficient though both appear somewhat similar.

The output obtained as a result of stress analysis is a stress distribution while the output obtained as a result of steady state thermal analysis is the temperature distribution of an object.

**Table 1** Comparison between stress analysis and heat transfer analysis

	Stress analysis	Steady thermal analysis
Input	Load, forced displacement	Heat generation, fixed temperature
Boundary conditions	Constraint	Heat generation, heat insulation, heat transfer coefficient, fixed temperature
Physical property values	Young's modulus, Poisson's ratio	Heat conductivity
Output	Stress distribution	Temperature distribution

## 2.3 Challenges to be addressed for steady thermal analysis

Unlike stress analysis, steady state thermal analysis requires that "certain boundary conditions need to be set for the entire surface of an object". As mentioned earlier, for steady state thermal analysis, there are four boundary conditions, that is, heat generation, heat insulation, heat transfer coefficient and fixed

temperature, the definitions of which are given in **Table 2**.

When considering the actual physical phenomena of heat transfer, most cases involve emission and absorption of heat on the surface of an object; therefore, a heat transfer coefficient needs to be set for the surfaces of the objects being analyzed. The specific value for the heat transfer coefficient can be difficult to determine. It is not a material physical property, and can vary depending on various factors such as the shape and size of the object as well as the physical properties, flow velocities, and temperatures of external fluid (air, oil, etc.). How to estimate heat transfer coefficients is an important but challenging point in steady state thermal analysis.

**Table 2** Boundary condition of heat transfer analysis

Heat generation	Condition where a particular quantity of heat per unit time is being generated at the surface of an object; or where the surface is absorbing a particular quantity of externally generated heat per unit time. This condition is used to establish the heat source.
Heat insulation	Condition where no heat is generated or absorbed on the surface of an object. This condition is used when the temperature at the surface of an object and the temperature of the surroundings are the same. It is also used where in a physically symmetrical system the temperatures are the same on each side of the plane of symmetry.
Heat transfer coefficient	Condition where heat is transferred through the surface of an object. The heat transfers from a zone of high temperature to a zone of low temperature, and the quantity of heat transferred is determined by the temperature difference between the surface of the object and the exterior of the object and the heat transfer coefficient.
Fixed temperature	Condition where the temperature on the surface of an object is fixed regardless of whether or not heat generation/absorption takes place on that surface. This condition is applied to a surface where the object being analyzed is in contact with an object having very high heat capacity relative to the object being analyzed.

## 2.4 Method for estimating heat transfer coefficient

As mentioned above, the heat transfer coefficient for an object is difficult to determine. One possible method for estimating the heat transfer coefficient is calculation based on a theory from heat transfer engineering.

A typical sequence of heat transfer coefficient calculation based on this heat transfer engineering theory is presented in **Figs. 2** and **Table 3**, and Expressions ① through ⑦<sup>1)</sup>. This sequence describes calculation of the heat transfer coefficient of the side face of the rotating inner ring of a bearing.

In the practice of heat transfer engineering, attention is first placed on the presence of flowing fluid (in this case, air) over the surface of an object. Fluid flow caused by forced movement of fluid is called "forced convection" while flow caused only by

temperature variation of the fluid in the vicinity of the surface of an object is called “natural convection”.

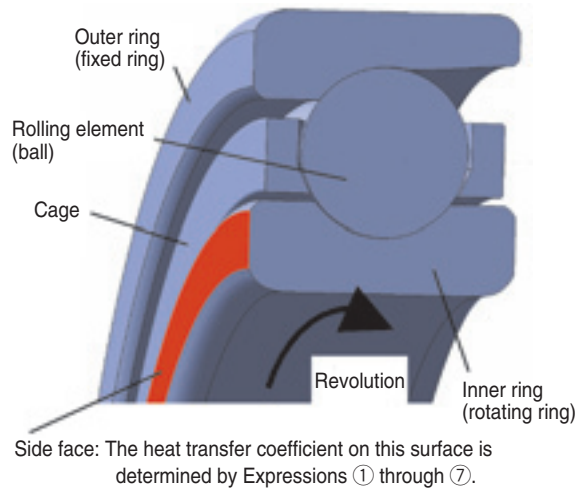


**Fig. 2** Cross section of bearing

**Table 3** Values for heat transfer coefficient calculation

Symbol	Description	Unit
$\rho$	Density of air	kg/m <sup>3</sup>
$cp$	Constant pressure specific heat of air	J / (kg · °C)
$\mu$	Viscosity coefficient of air	kg / (m · s)
$\lambda$	Thermal conductivity of air	W / (m · °C)
$\omega$	Rotational speed of rotating ring	rad / s
$r$	Radius of side face	m

**Expressions describing heat transfer for side face of rotating inner ring**

Dynamic viscosity of air

$$\nu = \frac{\mu}{\rho} \quad (\text{m}^2/\text{s}) \dots\dots\dots\text{①}$$

Thermal conductivity of air

$$\kappa = \frac{\lambda}{\rho \cdot cp} \quad (\text{m}^2/\text{s}) \dots\dots\dots\text{②}$$

Prandtl number

$$Pr = \frac{\nu}{\kappa} \dots\dots\dots\text{③}$$

Rotating Reynolds number

$$Re_{\omega} = \frac{\omega r^2}{\nu} \dots\dots\dots\text{④}$$

Case where  $Re_{\omega} \leq 3 \times 10^5$  (laminar flow):

$$\text{Nusselt number } Nu_r = 0.399 Re_{\omega}^{0.5} Pr^{0.43} \dots\dots\dots\text{⑤}$$

Case where  $Re_{\omega} > 3 \times 10^5$  (turbulent flow):

$$\text{Nusselt number } Nu_r = 0.0238 Re_{\omega}^{0.8} Pr^{0.6} \dots\dots\dots\text{⑥}$$

Heat transfer coefficient

$$H = \frac{Nu_r \cdot \lambda}{2r} \quad (\text{W}/(\text{m}^2 \cdot \text{°C})) \dots\dots\text{⑦}$$

Next, attention is placed on the velocity (more strictly, Reynolds number) of the convection system under consideration. If the velocity is smaller than a threshold value per heat transfer engineering, the fluid flows in a smooth orderly fashion (laminar flow); if the velocity is greater than the threshold value, the fluid flow develops irregular vortices (turbulent flow).

If we can establish demarcation between these two flow modes, we will be able to calculate the heat transfer coefficient on the surface of a given object based on the physical properties of air and the object’s physical parameters including its dimensions.

Let us apply this theory to the rotating ring of a given bearing. The surfaces on the rotating ring are moving relative to the surrounding air. This situation is analytically the same as a system where the component is at a standstill while the air surrounding it is in motion. Thus, this can be regarded as a system in a state of “forced convection” with air. Likewise, the air flow occurring over a fixed ring can be assumed to be in a state of “natural convection”. For components under natural convection, we need to consider the orientation of the bearing (horizontal or vertical) because heated air in natural convection flows vertically upward.

In addition, whether the flow is “laminar flow” or “turbulent flow” is decided based on considerations including the rotational velocity of the rotating ring.

In Expressions ① through ⑦, we have only presented a calculation process for the side face of the rotating ring. Using a similar procedure, we can perform these calculations for the inner and outer diameter of the rotating ring and for the surfaces of the fixed ring.

Incidentally, consideration of heat radiation from the surface of an object is necessary, although this practice is not explained in this paper.

This method for estimating the heat transfer coefficient is very refined; however, when this value is actually used for steady state thermal analysis, and the resulting temperature distribution is compared with actual measured results, acceptable levels of error are not always attained. The reasons for this may include error caused by incorrect assumptions made when calculating the heat transfer coefficient (for example, when considering natural convection, the surface temperature on an object must be assumed and this assumed value should be close to the actual value) or an error related to the environment where actual measurement is taken (for example, in heat transfer engineering calculations, the size of the laboratory room is assumed to be infinite; however, effects from the floor, ceiling and walls are unavoidable in an actual test).

Therefore, in order to further improve the precision of steady state thermal analysis, we will perform analysis for a system for which the temperature distribution has already been measured. More specifically, actual temperature measurements on various areas of the system are prepared in advance, analysis is performed using a heat transfer coefficient that was obtained based on the theory of heat transfer engineering, and the temperature distribution obtained from actual measurements is compared with that obtained from theoretical analysis. If the temperature distribution of the actual measurements does not match that of the theoretical analysis, then it will be necessary to vary the heat transfer coefficient such that the analysis results more closely match the measurement results in order to improve the accuracy of the analysis. This process is referred to as "tuning".

### 2.5 Significance of steady state thermal analysis

To perform steady state thermal analysis on a new bearing application, it is necessary to obtain actual temperature measurements (in other words, we must perform a series of test runs), and the man-hours required for testing a new bearing product will not be decreased. It should be noted that steady state thermal analysis can be conveniently utilized downstream of this stage of testing. Once "tuning" has been performed to better define a heat transfer coefficient for a given bearing application, further analysis including changes to the system such as material changes or changes in the quantity of heat generated may be performed with greater accuracy, and without requiring additional tuning. Thus, the advantage of steady state thermal analysis may be summarized as follows: though tuning of heat transfer coefficients to better match test results must be performed first, once this has been completed, analysis can be performed at high precision without performing additional testing even if new conditions are adopted.

## 3. Application of steady state thermal analysis to spindle test

### 3.1 Objective of application to spindle test

At NTN, the design specification of a spindle bearing is studied in the following manner:

- ① According to the required rigidity, accuracy and boundary dimensions, an appropriate bearing part number is selected.
- ② Relative to an initial preload setting, the operating preload is estimated.

The factors required for the estimation of ② are the temperature gradient across the inner ring and outer

ring caused by heat generation in the bearing, and variation in preload due to variation in the spacer width. Using conventional methods, these factors have been determined based on accumulated test data, performance data and experience provided by the customer, or measurements obtained from development testing. We have attempted to estimate these factors using steady state thermal analysis in order to improve efficiency in performing simulation for prototype bearings.

### 3.2 Test rig configuration

Figures 3-1 and 3-2 illustrate the configuration of a test rig used for the testing required to perform tuning for steady state thermal analysis. The main spindle is attached to the motor via a coupling. The positional relation between two angular contact ball bearings in a back-to-back arrangement can be adjusted by varying the spacer width. Cooling oil flows through a spiral groove formed circumferentially on the outer diameter of the housing to absorb heat from the bearings. The bearing lubrication system is air-oil lubrication.



Fig. 3-1 Test machine

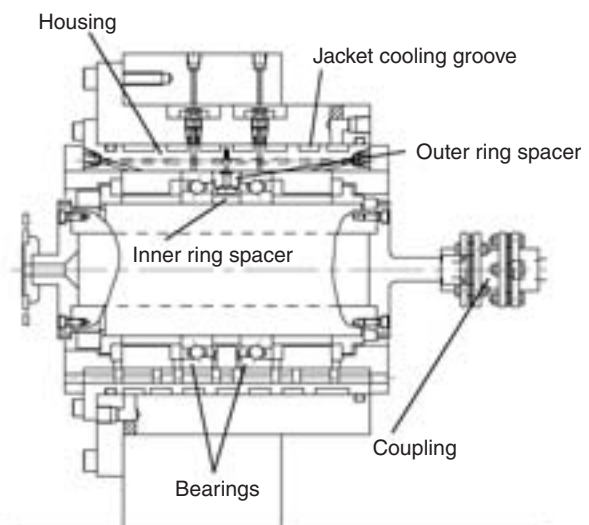
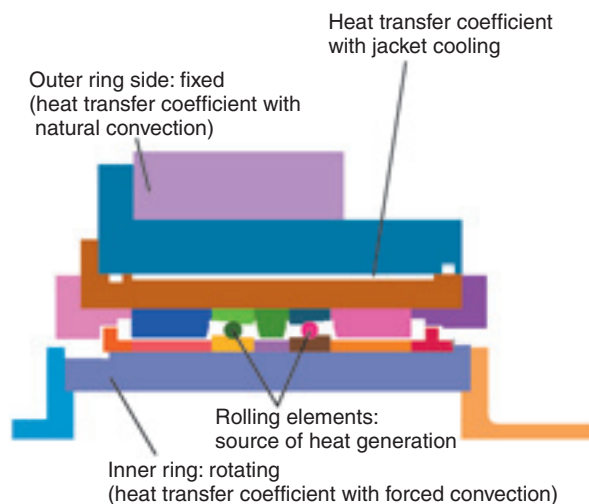


Fig. 3-2 Cross section of test machine

The parameters measured in this test are torque, surface temperatures at various locations, the cooling oil inlet and outlet temperatures, and the room temperature.

### 3.3 Analysis model

**Fig. 4** illustrates a CAE finite element analysis model that represents our test configuration. The results of temperature measurements obtained from this test showed no significant temperature difference at locations in the circumferential direction; therefore, we have developed a 2D axisymmetric model that simulates the bearings and peripheral components. The heat source in this test was defined as the rolling elements (balls), and the quantity of heat generated was determined based on actual torque measurements performed on the spindle. The surfaces of the test rig were divided into finite elements, and based on the size and location of each element and the principals of heat transfer engineering, the heat transfer coefficient for each element was determined. The heat transfer coefficient



**Fig. 4** Analysis model

of the air in the bearings was determined assuming that the air rotates at a velocity equal to that of the rolling elements and cage, and that its temperature corresponds to an average of the inner ring temperature and outer ring temperature. The heat transfer coefficient of the cooling jacket groove was determined by calculating the quantity of heat removed by the cooling oil flowing through the test rig and then using tuning to determine the heat transfer coefficient that matched this amount of heat removal.

### 3.4 Analysis result

**Figure 5-1** presents analysis results prior to tuning, **Fig. 5-2** presents post-tuning analysis results, and **Fig. 5-3** and Table 4 offer comparison of analysis results with actual test measurements. When the pre-tuning analysis temperature values are compared with actual measurements, the average temperature difference of all measuring points is 5.4°C while the maximum temperature difference is 10.7°C. During the actual test, the average temperature of the test rig increased from room temperature (28.7°C for the purpose of present analysis) to 36.0°C; thus, the error in average temperature increase between the actual data and the analysis data, is  $5.4 / (36.0 - 28.7) = 74\%$ . On the other hand, comparing post-tuning analysis temperatures with actual measured temperatures, the average temperature difference is 0.8°C, the maximum temperature difference is 1.4°C, and the error in average temperature increase between actual data and analysis data is  $0.8 / (36.0 - 28.7) = 11\%$ . This indicates that the accuracy of the analysis has been much improved by tuning. Because the error is very small, we believe the analysis data correlates to the actual measurement data very well.

Additionally, though not summarized in **Table 4**, the average temperature of the inner ring is approximately 50°C and that of the outer ring is approximately 39°C. Thus, the temperature difference between the inner ring and outer ring is approximately 11°C. With this



**Fig. 5-1** Analysis result of pre-tuning



**Fig. 5-2** Analysis result of post-tuning

**Table 4** Comparison between test data and analysis data

Measuring point	Actual measurement <a>	Analysis value (pre-tuning) <b>	Analysis value (post-tuning) <c>	<b>-<a>	<c>-<a>
A	28.4	32.8	27.4	4.4	-1.0
B	28.5	32.0	27.2	3.5	-1.3
C	27.7	31.3	27.0	3.6	-0.7
D	27.5	32.2	27.4	4.7	-0.1
E	29.6	34.5	28.4	4.9	-1.2
F	39.9	42.3	39.1	2.4	-0.8
G	40.3	44.2	40.0	3.9	-0.3
H	50.3	55.8	50.2	5.5	-0.1
I	50.7	55.8	50.0	5.1	-0.7
J	36.0	46.7	37.4	10.7	1.4
K	36.6	46.8	37.4	10.2	0.8
Average	36.0	41.3	35.6		
Error in increase of average temperature				5.4	0.8

※Error in increase of average temperature =  $\frac{\sum_{A}^K | \text{Actual measurement} - \text{Analysis value} |}{11}$

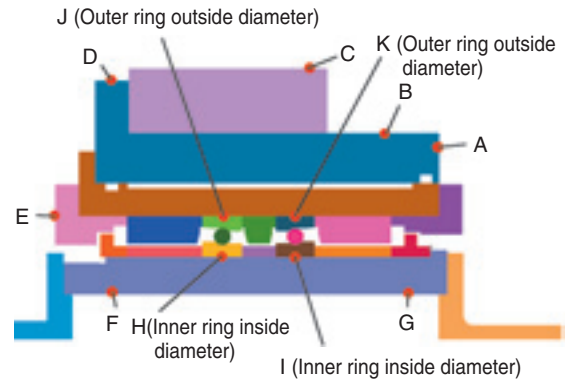


**Fig. 5-3** Compared points between test data and analysis data

information it is now possible to estimate the reduction in radial clearance (increase in preload) within a bearing based on the bearing diameter and the linear expansion coefficient of the bearing material. Likewise, if we obtain the data about the inner ring spacer temperature and shaft temperature and the outer ring spacer temperature, then we will be able to estimate the increase in the set axial clearance (decrease in preload) based on the linear expansion coefficients of materials of various assembly components.

Furthermore, by adopting these post-tuning boundary conditions, it is now possible to perform an analysis operation with changes in initial preload, bearing speed, spacer width, etc. **Fig. 6** and **Table 5** provide a comparison between actual test measurements and analysis values for the same system but with wider spacers (no tuning under this set of conditions). It is apparent that the actual values match the analysis values fairly well.



**Fig. 6** Analysis result with wide spacer

**Table 5** Comparison between test data and analysis data with wide spacer

Measuring point	Actual measurement	Analysis value	Actual measurement - Analysis value
A	27.3	27.3	0.0
B	27.3	26.9	-0.4
C	26.5	26.6	0.1
D	26.6	27.2	0.6
E	29.2	28.7	-0.5
F	35.8	34.5	-1.3
G	35.4	35.2	-0.2
H	38.1	38.3	0.2
I	38.4	38.0	-0.4
J	31.8	31.3	-0.5
K	30.8	31.2	0.4
Average	31.6	31.4	
Error in increase of average temperature			0.4

## 4. Conclusion

To be able to estimate temperature distributions on a machine tool main spindle bearing and a test rig, we have committed to steady state thermal analysis through finite element method. We have established a technique that combines a theory of heat transfer engineering with a parameter tuning technique. As a result, we are now able to set up an appropriate initial preload more efficiently for a given machine tool main spindle bearing.

We will apply this unique technique to other industrial fields and gain experience from performing analysis work in various applications to further improve efficiency in bearing design.

## References

- 1) Y. Katto: Introduction to Heat Transfer, Yokendo, (1964) P165

## Photos of authors

---



Yoshimitsu HIRASAWA

Product Design Dept.  
Industrial Sales  
headquarters



Yukimitsu YAMAMOTO

Product Design Dept.  
Industrial Sales  
headquarters

# Development of High-Speed Cylindrical Roller Bearings for Machine Tools

Masatsugu MORI\*  
Takuji KOBAYASHI\*



A newly designed cylindrical roller bearing has been developed so that the cylindrical roller bearing can operate as fast as the high-speed angular contact ball bearings used for machine tool main spindles under the condition of air-oil lubrication. The cage riding structure improves lubrication of the cage-guiding surface at high-speed operation by guiding the cage bore on the air-oil nozzle outside surfaces. The inner ring made of ceramic prevents excessive bearing preloading in the radial direction due to thermal and centrifugal

expansion in order to enable high-speed rotation. The ceramic inner ring is compressed radially by ring spacers that also work as ribs to reduce the hoop stress generated in the inner ring. The prototyped bearing with an inner diameter of 70 mm successfully operates at a speed of 3.25 million  $d_{mN}$ , which compares with air-oil lubricated, ultrahigh-speed, angular contact ball bearings for machine tool spindles.

## 1. Introduction

Any machine tool main spindle usually needs to be capable of higher speed and rigidity in order to improve machining efficiency and machining accuracy. Efficiency and accuracy in machining are principally governed by performance of the bearing arrangement supporting the machine tool main spindle. A variety of rolling bearing arrangements for supporting machine tool main spindles are available<sup>1)</sup>, and combinations comprising angular contact ball bearings and cylindrical roller bearings are often used. Angular contact ball bearings boast high-speed capability (this capability may depend on the contact angle) and can carry a load in both radial and axial directions. In contrast, a cylindrical roller bearing, which carries a load in the radial direction in a linear contact system, excels in rigidity; however, this bearing type is inferior to angular contact ball bearings in the areas of running torque and component precision. In terms of  $d_{mN}$  value (bearing pitch diameter mm  $\times$  bearing speed min<sup>-1</sup>) which is an index representing high-speed running performance of a given rolling bearing, the performance of angular

contact ball bearings is about 30% better compared with that of cylindrical roller bearings.

Usually, a bearing arrangement for high-speed machine tool main spindle comprise four rows of angular contact ball bearing on the front side (greater shaft diameter) and one to two rows of angular contact ball bearings or a single cylindrical roller bearing on the rear side (smaller shaft diameter). In higher-speed applications with definite position preload systems (these systems boast higher rigidity) there is increased demand for cylindrical roller bearings on the smaller diameter rear side (this side is free side). Furthermore, there have been increasing cases of hybrid machine tools whose milling main spindles have, on their front side, not only angular contact ball bearings but also cylindrical roller bearings in order to enhance rigidity of the main spindles.

Therefore, a new cylindrical roller bearing for machine tool main spindle needs to be developed, and this cylindrical roller bearing needs to feature high-speed performance coming close to that of angular contact ball bearings.

Previously there have been many numerical analysis-based studies in the area of cylindrical roller

\*Elemental Technological R&D Center

bearings that are run at higher speed. Examples of these studies include an investigation of cage to roller sliding based on 2D static analysis incorporating knowledge about elastohydrodynamic lubrication <sup>2)</sup>; static analysis that also reflects thermal analysis <sup>3)</sup>; and 2D dynamic modeling and analysis efforts<sup>4-7)</sup>. Also, there has been an experimental study to observe the actual behavior of the rollers and cage of high-speed cylindrical roller bearings.<sup>8)</sup> However, we did not know any previous example of research that has achieved super high-speed operation with  $d_{m\Omega} = 3$  million or over with air-oil lubrication while limiting the inner ring temperature to 70°C or lower which is said to be an upper limit of inner ring temperature for bearings in commercial applications.

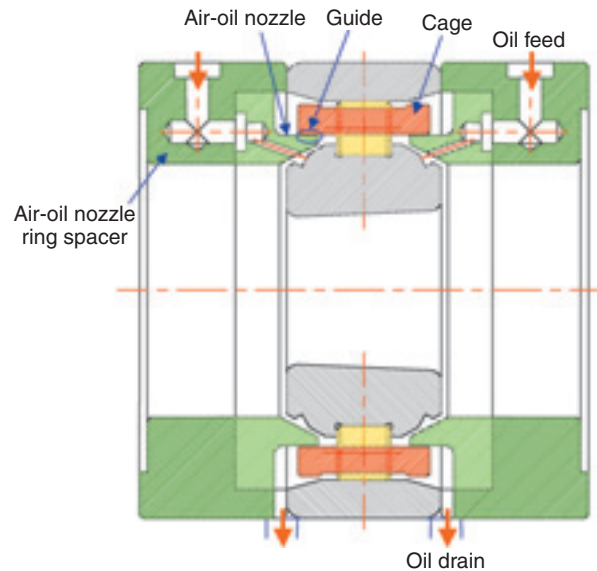
We have prototyped and tested a high-speed cylindrical roller bearing that is lubricated with an air-oil lubrication system, and achieved an unprecedentedly high speed of  $d_{m\Omega} = 3.25$  million. This report presents this achievement. This speed is comparable with air-oil lubricated super high-speed angular contact ball bearing for machine tool main spindle <sup>9)</sup>.

## 2. Researches of elemental technologies for higher bearing speed

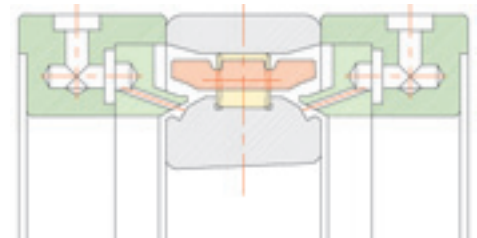
### 2.1 Cage

Currently, an increasingly used material for the cage on high-speed bearings is PEEK (PolyEtherEtherKetone) which is a light-weight resin material boasting excellent rigidity, heat resistance and hydrolysis resistance. As to cage guiding types, a raceway ring guiding system is preferable to a roller guiding system because of better stability with cage motion in a high-speed bearing operation situation. Further, an outer ring land riding system is more advantageous than an inner ring land riding system because of improved centrifugal force-induced behavior of lubricating oil. However, with a bearing having an outer ring land riding system, there is a possibility of direct contact between guide surfaces, since the roller axial gap can get excessively small because that the linear expansion coefficient of a PEEK-made cage is twice as large as the steel outer ring and additionally the roller axial gap can be affected by centrifugal force. Assuming the outer ring guide surface can be regarded as an oil-lubricated small-width dynamic pressure journal bearing, and in the case of a bearing whose bore diameter falls in a range of 50 to 100 mm, we will wish to set the roller axial gap of this bearing group to 0.1 to 0.2 mm. Nevertheless, there are above-mentioned issues, and it is difficult to attain an optimal gap design.

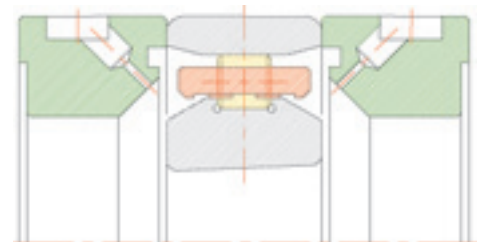
To address this problem, we have invented a novel cage guiding type shown in Fig. 1 (a), based on the high-speed cylindrical roller bearing shown in Fig. 1 (b) that is suitable for air-oil lubrication, wherein air-oil mixture ejected from the air-oil nozzle hits the rotating inner ring ramp and is then directed into the bearing



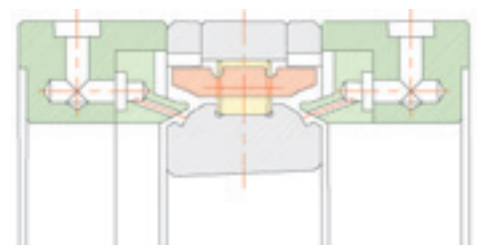
(a) Nozzle outside-surface riding



(b) Roller riding



(c) Inner ring land riding



(d) Outer ring land riding

Fig. 1 Cage guiding types

interior along the ramp. Due to the centrifugal force and surface tension acting on the oil, the oil finally splashes to the outer circumferential direction at the top ridge of the ramp, contributing to lubrication. Compared with a conventional arrangement in which air-oil jet is directed to the gap between the inner ring and cage, our new arrangement is effective in improving quietness and reducing air-oil consumption. The construction shown in Fig. 1 (a) maintains these advantages as well as adopts a novel arrangement where the outside surface of the air-oil nozzle guides the bore surface of the cage.

Generally, the slip sliding areas of a rolling bearing are supplied with a sufficient amount of oil and a minimum necessary quantity of oil is fed to the rolling contact areas of the bearing in order to reduce rolling viscous resistance; this arrangement is important to reduce torque loss and heat generation within the bearing to help the bearing to run at a higher speed. The guide way needs to be supplied with plenty of oil to constitute a sliding bearing; with our bearing construction, a portion of oil splashed at the upper edge of the inner ring ramp moves by centrifugal force from the bearing interior through the roller axial gap to the bearing end side together with the air ejected from the nozzle, thereby the oil is smoothly supplied and drained (see Fig. 1 (a)). In other words, the guide way is always lubricated with fresh oil of relatively low temperature, and hot oil does not remain trapped. Because the torque loss power is in proportion to the cube of guide section radius<sup>10)</sup>, our arrangement is more advantageous than an outer ring land riding system. Furthermore, with our arrangement, the roller axial gap between the steel nozzle and the PEEK-made cage does not decrease to zero even during high-speed bearing operation and the nozzle and cage do not come into contact with each other.

We have actually compared high-speed operating performance of our prototype bearing having the construction shown in Fig. 1 (a) (hereinafter referred to as "nozzle outside-surface riding type") with that of bearings of other guiding types. The construction in Fig. 1 (b) shows a roller riding type, Fig. 1 (c) an inner ring land riding type and Fig. 1 (d) an outer ring land riding type. Because of the reasons previously mentioned, the roller axial gap of the outer ring land riding type is greater than that of other guiding types. Fig. 2 schematically illustrates the construction of our spindle test rig in which a single-row test bearing and two rows of back-to-back angular contact ball bearings (5S-BNT008) support the rotating shaft that is driven with a built-in motor (an arrangement identical to that of a high-speed machine tool main spindle). A jacket cooling arrangement was provided, and the

temperature on the inner ring was measured with a telemeter. Table 1 summarizes the basic specifications for the test bearings and operation conditions. The tests and experiments presented below within this paper have been performed with bearings equivalent to cylindrical roller bearing N1014, and the spindle test rig features the construction shown in Fig. 2.

The results of high-speed operation test are presented in Fig. 3. High-speed operation quality of each bearing sample is evaluated based on the running speed of its inner ring at a time point when the inner ring temperature has reached 60°C. Fig. 3 illustrates that high-speed operating quality can be ranked in the following order (from worst to best): roller riding type, inner ring land riding type, outer ring land riding type and nozzle outside-surface riding type. In Fig. 3, the difference in the maximum inner ring speed reached is relatively small between the outer ring land riding type and nozzle outside-surface

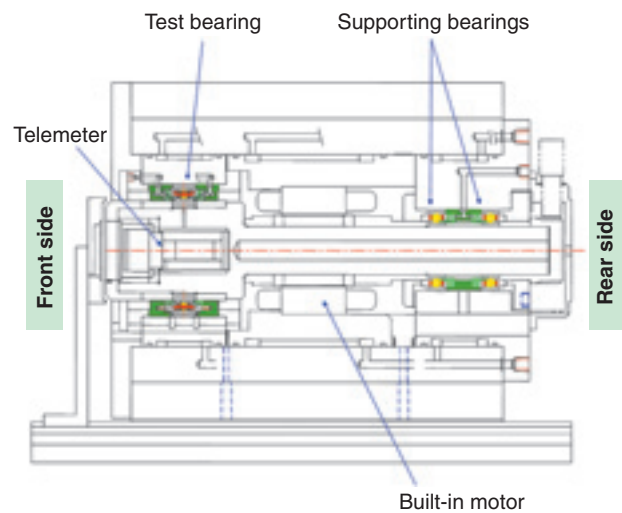
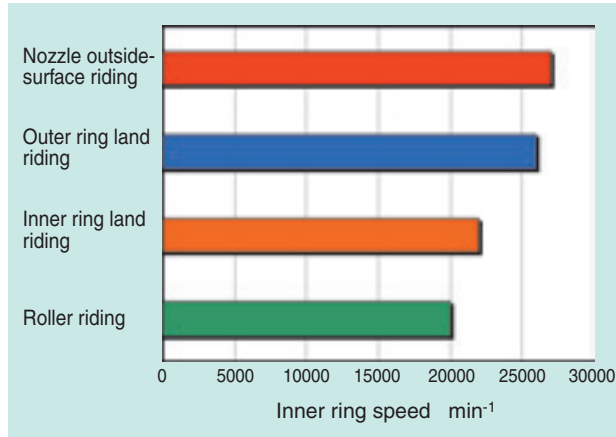


Fig. 2 Section view of spindle test rig

Table 1 Bearing specifications and test conditions in high-speed operation test with various cage guiding types

Bearing	Description	Equivalent to N1014HSL
	Size	ID $\phi 70 \times$ OD $\phi 110 \times$ W20
	Pitch diameter	93 mm
	Raceway ring	SUJ2
	Rollers	$\phi 7 \times 7$ , Si <sub>3</sub> N <sub>4</sub> , 22 rollers
Cage	PEEK + CF30 %	
Test conditions	Initial radial clearance	0~2 $\mu$ m
	Bearing lubrication	Air-oil lubrication system ISO VG32 Oil feed from both ends of bearing 0.01cm <sup>3</sup> /10 min $\times 2$
	Jacket cooling oil temperature	Room temperature $\pm 1^\circ\text{C}$



**Fig. 3** High-speed operation test results with various cage guiding types

riding type: however, considering the possibility of contact between the guide ways and ease of draining of lubricating oil, the nozzle outside-surface riding type is more advantageous in higher speed applications.

## 2.2 Inner ring

Machine tool main spindles require cooling in order to inhibit thermal deflection. Normally refrigerant is circulated in a jacket (usually located on the static side) in order to cool rolling bearings and a built-in motors on machine tools. If such an arrangement is employed, the bearing inner ring will be hotter compared with the outer ring owing partly to heat generation from the motor and effects from the heat radiation structure; consequently, in the case of a cylindrical roller bearing, its preload in the radial direction will be greater. Also the effect of centrifugal force-induced expansion of the inner ring cannot be ignored for high-speed operation; as a result, preload can further increase, and operation may become impossible due to excessive heat generation. In other words, inhibition of excessive preload can greatly contribute to higher speed operation with a bearing.

Therefore, let us think of a bearing having a steel outer ring and a ceramic inner ring, the ceramic material features the linear expansion coefficient approximately 30% and density approximately 40% compared with a steel material. Use of a ceramic material for rolling bearing elements has long been proposed<sup>11)</sup>, and a fairly large number of ceramic rolling elements have already been used. However, when an inner ring is made of ceramic material great pressure may be applied the inner ring bore due to thermal and centrifugal expansion of the mating shaft outer surface. This cause the hoop stress which is the vertical stress component along the circumferential direction on the inner ring to be excessive, and, as a

result, the inner ring can fracture.

On our newly developed high-speed cylindrical roller bearing, we have employed a novel technique: ring spacers are press-fitted onto both ends of a ceramic inner ring raceway ring to apply in advance a radial compressive stress to the inner ring so that tensile hoop stress during high-speed operation is mitigated. This can be comparable with a case where a shrink-fit cylinder can withstand a higher internal pressure compared with an independent cylinder of same size. **Fig. 4** schematically illustrates the construction of our new development: ring spacers are press-fitted over both shoulders of the ceramic inner ring; the fitting mode between the inner ring and the shaft is interference fit and that between the ring spacers and the shaft is clearance fit. The ring spacers not only exert radial compressive stress to the inner ring but also function as ribs. Because thermal expansion and physical density of ceramic are smaller compared with steel, the initial fitting allowance of the inner ring relative to the shaft can be smaller.

When a ceramic inner ring having a bore diameter of about 50 to 100 mm is run at high speed with  $d_{m\dot{n}} = 2$  million or higher, the recommended fitting allowance of the inner ring to the shaft should be about 5  $\mu\text{m}$  or less. In the case of a ceramic inner ring, the necessary fitting allowance to the shaft will be in a range of 20 to 30  $\mu\text{m}$  to cope with heat-induced and centrifugal force-induced expansion during high-speed operation. In other words, use of a ceramic inner ring will help simplify press-fitting work during the spindle assembly process. With most steel inner rings in ordinary cylindrical roller bearings, their bore is tapered as shown in **Fig. 1**, and the inner ring is press-fitted onto the shaft, thereby utilizing the resultant elastic deformation, the fitting of inner ring to the shaft is adjusted by measuring the initial radial gap. This fitting technique is not valid for a ceramic inner ring because the Young's modulus of a typical ceramic material is approximately 1.5 times as high as that of a typical steel material. As shown in **Fig. 4**, the bore of the inner ring in our bearing design is a

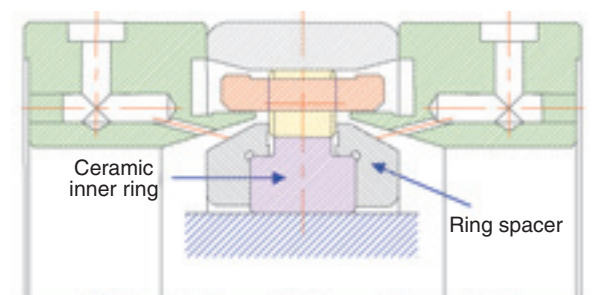


**Fig. 4** Ceramic inner ring and its ring spacers

straight hole: thereby the initial radial gap is determined by adjusting the bore diameter of the inner ring and the outside diameter of the shaft through machining. Also, featuring a higher Young's modulus, ceramic materials are favored as they satisfy higher rigidity required for machine tool bearings.

Now, let us schematically illustrate how much difference can take place on the expansion owing to heat generation and centrifugal force between ceramic ( $\text{Si}_3\text{N}_4$ ) inner rings and steel inner rings. Suppose the inner ring (ceramic or steel) on the cylindrical roller bearing equivalent to N1014 in Fig. 1 is conformably fitted over the rotating shaft, thereby the deflection on inner ring outside diameter (expansion) and maximum hoop stress occurring on the bore surface of ceramic inner ring have been calculated, and the calculated values are plotted in Fig. 5, where the inner ring speed is set at targeted  $35,000 \text{ min}^{-1}$  (equivalent to  $d_{mN} = 3.25$  million) and is plotted as a function of the temperatures of inner ring and shaft. The maximum permissible temperatures for the inner ring and shaft in practical applications seem to fall in a range of 60 to 70°C. Now, let us assume that this temperature is 60°C: then the deflection in the outside surface of ceramic inner ring is about 27 μm smaller than that will steel inner ring: use of a ceramic inner ring appears to be positively effective in inhibiting excessively large preload working onto the inner ring.

The resultant calculated hoop stress is about 160 MPa: we have actually prepared a system illustrated in Fig. 6 and thermally applied a hoop stress onto the ceramic ring that simulates an inner ring to experimentally determine whether or not the ceramic ring could withstand fracture. We have adjusted the initial (room temperature 20°C) fitting allowance to 5, 10 and 19 μm and heated the ceramic ring and shaft

to 150°C in a constant temperature chamber. The ordinates in Fig. 7 represent calculated maximum hoop stress values relative to the respective temperatures. As a result, no fracture was observed at least up to a temperature of 150°C. From Fig. 7, it should be understood that the hoop stress at 150°C exceeds 350 MPa while the maximum hoop stress of 160 MPa in Fig. 5, where actual operation is simulated, is about a half of the value in Fig. 7. In an application in Fig. 4 where the ring spacer exerts a radial compressive stress to the inner ring, the maximum hoop stress shifts to a much safer side. Remember, however, to be aware of the "dimension effect" when intending to employ a greater bearing size.

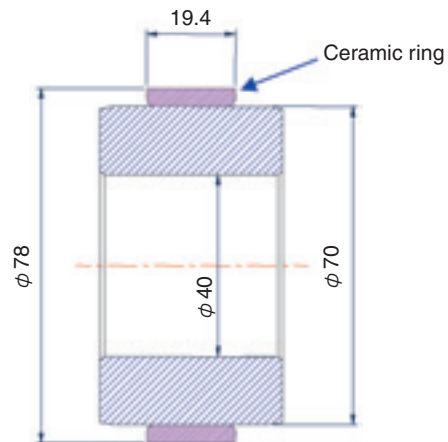


Fig. 6 Imitated ceramic inner ring and its fitting to shaft for hoop stress resistance test

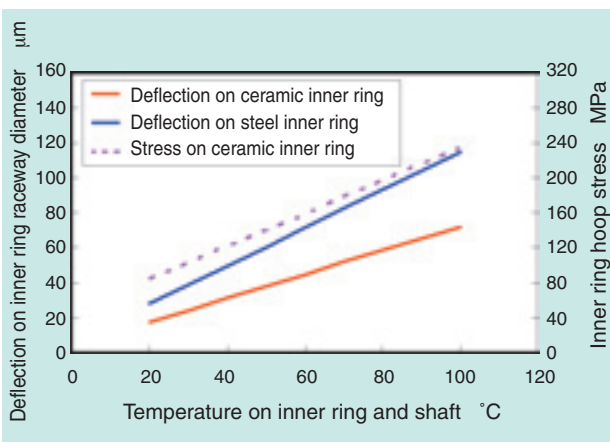


Fig. 5 Calculated radial deflection and maximum hoop stress of inner ring due to heat and centrifugal force  
Object bearing: Ref. Fig. 1, Rotational speed:  $35000 \text{ min}^{-1}$

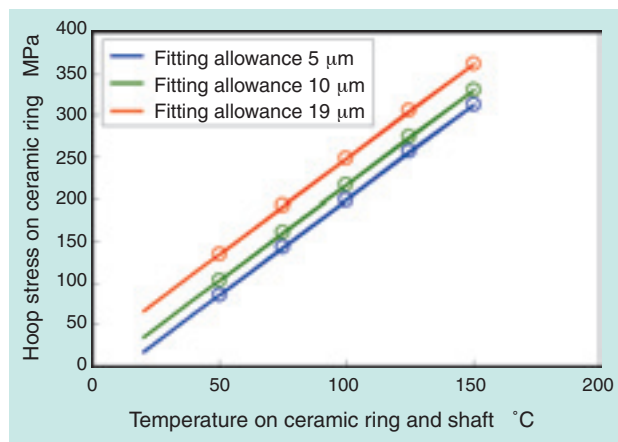


Fig. 7 Calculated maximum hoop stress of ceramic ring associated with Fig. 6

### 2.3 Rib

When attempting to realize high speed operating with a cylindrical roller bearing, it will be necessary to consider interference between the roller side planes and ribs. Therefore, we have experimentally investigated interrelation between the roller-to-inner ring rib axial gap and lubricity or that between rib angle and lubricity as shown in Fig. 8.

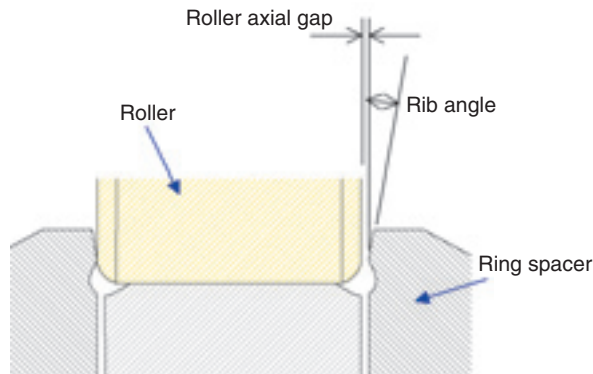


Fig. 8 Exaggerated view of roller axial gap and rib angle in Fig. 4

We have evaluated lubricity on the ribs by measuring the temperatures on the inner ring and outer ring while the inner ring was running at 25000 min<sup>-1</sup>. In particular, this bearing is not carrying an axial load, and the test conditions are basically identical to those summarized in Table 1. Fig. 9 plots the evaluation results with “roller axial gap ratio” meaning the ratio of this bearing’s roller axial gap to that of the standard bearing design and “rib angle ratio” standing for the ratio this bearing’s rib angle to that of the standard bearing design.

Fig. 9 (a) shows the relation between roller axial gap ratio and temperatures on the inner ring and outer ring where the ring angle ratio is taken as 1.0. There is no apparent interrelation between roller axial gap and temperature. Fig. 9 (b) illustrates the relation between rib angle ratio and temperatures on the inner ring and outer ring, wherein the roller axial gap ratio was varied in five levels in a range of 0.4 to 2.32. Even when the rib angle is altered, there is no apparent change in the temperature on the inner ring and outer ring. Additionally, when the roller axial gap ratio is altered by approximately 2.0, the resultant variation in temperature on the inner ring and outer ring is approximately 2 to 3°C.

To sum up, it is apparent that the effect of roller axial gap and ribs is small. This is because the area of each actual roller, from the chamfer to the flat side plane, is machined into a smooth shape, causing the edge load to be mitigated; at the same time, fluid film lubrication effect takes place at this area, helping prevent occurrence of solid contact that can lead to surface damage. In other words, regardless of the geometrical conditions of roller axial gap and ribs, the fluid film lubrication effect appears to be dominant.

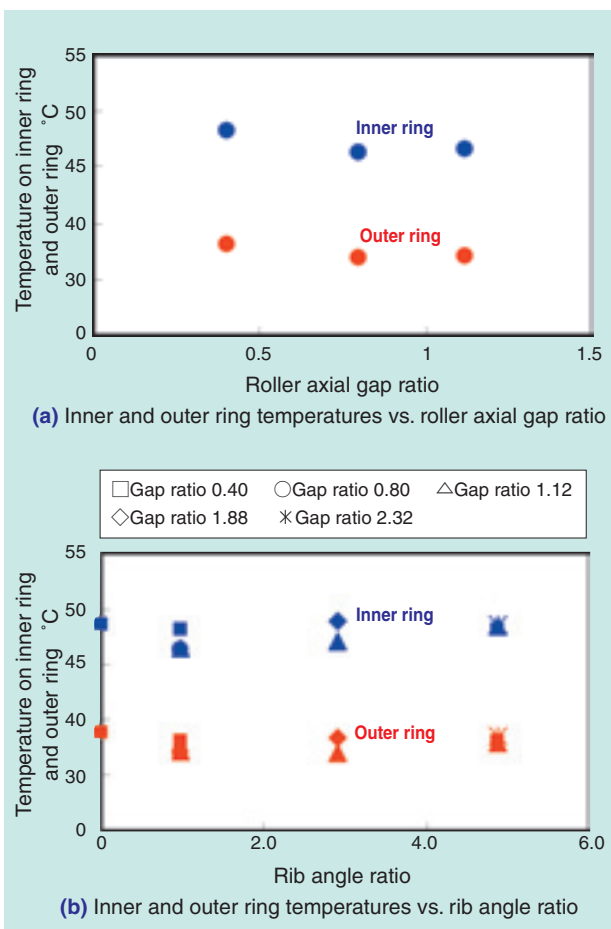


Fig. 9 Inner and outer ring temperatures vs. roller axial gap and rib angle

### 3. Performance verification for our newly developed bearing

Remaining aware of the elemental technology for higher speed operation described in Section 2, we have developed a prototype bearing shown in Fig. 10. As shown in Fig. 4, this bearing comprises a nozzle outside-surface riding type cage and a ceramic inner ring with a ring spacer, wherein the cage is made of PEEK and the rollers are made of steel or ceramic. Table 2 summarizes the specifications for our newly developed bearing and a benchmark bearing having the structure shown in Fig. 1 (a); as well as the test conditions applied. The benchmark bearing comprises a roller riding type PEEK cage and steel inner ring and rollers.

Fig. 11 provides the results of measurements for temperatures taken on the inner ring and outer ring



Fig. 10 Prototype of developed bearing

Table 2 Specifications of developed and benchmark bearings and test conditions

Newly developed bearing	Description	Equivalent to N1014HSL
	Size	ID $\phi 70 \times$ OD $\phi 110 \times$ W20
Benchmark bearing	Pitch diameter	93 mm
	Inner ring	Si <sub>3</sub> N <sub>4</sub> (spacer ring: SUJ29)
	Outer ring	SUJ2
	Rollers	$\phi 7 \times 7$ , SUJ2 or Si <sub>3</sub> N <sub>4</sub> , 22 rollers
	Cage	PEEK + CF30%, nozzle outside-surface riding type
Test conditions	Description	Equivalent to N1014HSL
	Size	ID $\phi 70 \times$ OD $\phi 110 \times$ W20
	Pitch diameter	93 mm
	Inner ring and outer ring	SUJ2
Test conditions	Rollers	$\phi 7 \times 7$ , SUJ2 or Si <sub>3</sub> N <sub>4</sub> , 22 rollers
	Cage	PEEK + CF30%, roller riding type
	Initial radial gap	0~3 $\mu$ m
	Bearing lubrication	Air-oil lubrication system ISO VG32 Oil feed from both sides of bearing 0.01 cm <sup>3</sup> /5min $\times 2$
Jacket cooling oil temperature	Room temperature $\pm 1$ °C	

relative to inner ring rotating speeds. Fig. 11 (a) provides the resultant temperature measurements on the inner ring and outer ring of our newly developed bearings with steel rollers and a benchmark bearing with steel rollers. The temperature on the inner ring and outer ring of the benchmark bearing samples began to increase rapidly at a bearing speed of about 22000 min<sup>-1</sup> and further operation was interrupted. In contrast, our newly developed bearing did not exhibit rapid temperature increase even when operated at a speed of 35000 min<sup>-1</sup> which is equivalent to  $d_{mN} = 3.25$  million and operation at higher speed seemed possible: nevertheless, since the temperature on the inner ring exceeded 70°C (a temporary threshold), the test run was then aborted. Fig. 11 (b) shows the result obtained from our newly developed bearing having ceramic rollers in place of steel rollers. In this case too, temperature increased gently: however, because the temperature on the inner ring exceeded 70°C at a speed of 35000 min<sup>-1</sup> operation was interrupted.

When the result in Fig. 11 (a) is compared with that in Fig. 11 (b), it should be understood that temperature gradient is somewhat gentler with our

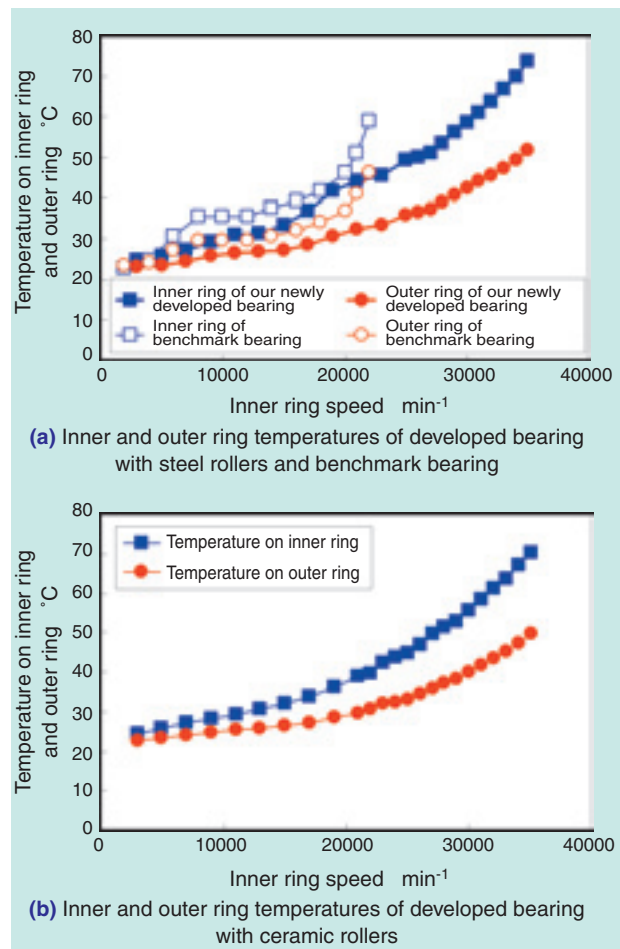


Fig. 11 Inner and outer ring temperatures vs. rotational speed

newly developed bearing having ceramic rollers compared with our bearing having steel rollers, and that the temperature on the inner ring and outer ring on the former bearing type at  $35000 \text{ min}^{-1}$  is 2 to  $3^{\circ}\text{C}$  lower compared with that of the latter bearing type. This trend appears to stem from the effect of ceramic rollers: better high speed performance is in principle derived from nozzle riding cage and ceramic inner ring having side spacer.

We have investigated various interior areas of our bearings after testing and have not found any damage on the raceway surfaces on the inner ring and outer ring, rolling surfaces on rollers, pockets and guide way on cage, and roller end planes and ribs.

As mentioned above, it has been learned that our newly developed bearing under air-oil lubrication condition is capable of  $d_{m11} = 3.25$  million which is comparable with performance of air-oil lubricated super high-speed angular contact ball bearing.

#### 4. Conclusion

To improve high-speed performance of air-oil lubricated cylindrical roller bearings for machine tool main spindles to a level equivalent to that of angular contact ball bearings, we have developed unique cylindrical roller bearings having a novel construction. With our newly developed bearings equivalent to N1014, we have succeeded in operating the bearing at  $d_{m11} = 3.25$  million by adopting air-oil nozzle outside-surface riding type resin cage and ceramic inner ring having rib side spacer. We believe that realization of this high-speed performance is mainly due to improved lubricity on cage guide way and inhibition of excessive radial preload.

NTN will remain committed to technological improvement of machine tools that support competitiveness of manufacturing through further sophistication in bearing technology and tribology technology.

#### References

- 1) NTN Catalogue Precision Rolling Bearings, CAT. No.2260-II/J (2008) 22-23
- 2) Poplawski, J.V.: "Slip and Cage Forces in a High-Speed Roller Bearing," ASME J. of Lubrication Technology, 94, 2, (1972) 143-152
- 3) Rumberger, J.H. Filetti, E.G. and Gubernick, D., "Gas Turbine Engine Mainshaft Roller Bearing-System Analysis," ASME J. of Lubrication Technology, 95, 4, (1973) 401-416
- 4) Conry, T.F.: "Transient Dynamic Analysis of High-Speed Lightly Loaded Cylindrical Roller Bearings, I-Analysis," NASA Contractor Report 3334, (1981)
- 5) Conry, T. F.: "Transient Dynamic Analysis of High-Speed Lightly Loaded Cylindrical Roller Bearings, II-Computer Program and Results", NASA Contractor Report 3335, (1981)
- 6) Chang, L.: "Analysis of High-Speed Cylindrical Roller Bearings Using a Full Elastohydrodynamic Lubrication Model, Part 1: Formulation," STLE Tribology Trans., 33, 2 (1990) 274-284
- 7) Chang, L.: "Analysis of High-Speed Cylindrical Roller Bearings Using a Full Elastohydrodynamic Lubrication Model, Part 2: Results," STLE Tribology Trans., 33, 2 (1990) 285-291
- 8) Markho, P.H., Smith, B.V. and Lalor, M.J.: "An Advanced Apparatus for the Study of Roller and Cage Slip in High-Speed Roller Bearings," ASME J. of Lubrication Technology, 103, 1, (1981) 46-54
- 9) NTN Catalogue Precision Rolling Bearings, CAT. No.2260-II/J (2008) 160-161
- 10) N. Soda, Bearing, Vol.3, Iwanami, 35 (1968)
- 11) K. Rokkaku, K. Nishida, Ceramic roller bearings, Japan Society for Precision Engineering, Vol.54, No.7, (1988) 1240-1244

Photo of authors



Masatsugu MORI  
Elemental Technological  
R&D Center



Takuji KOBAYASHI  
Elemental Technological  
R&D Center

# Angular Contact Ball Bearings that Require a Minimum Quantity of Grease Supply for Lubrication

Sun-Woo LEE\*  
Tadaaki MAEDA\*\*



A new grease lubrication system named **Minimum Quantity of Grease Supply (MQGS)** lubrication was developed. MQGS lubrication angular contact ball bearings have minimum quantity reservoir mechanisms for grease lubrication installed in spacers in the outer ring. It was developed so that high speed and long life can coexist in machine tool applications, and it has succeeded in practical use with a high-speed drive of  $d_{mN} 1.9 \times 10^4$  in a fixed-position. The outline of development is introduced in this text.

## 1. Foreword

Higher speed is needed for main spindle systems on machining centers and hybrid machine tools in order to improve machining efficiency and surface quality of finished work pieces. To cope with this trend, NTN has been developing new technologies, examples of which include "ULTAGE Series precision bearings for machine tools" <sup>1)</sup> that boast advanced functionality. Two varieties include "ecological air-oil lubricated bearings for machine tools" <sup>2)</sup> dedicated to air-oil lubrication arrangement and "jet-lubricated MQCJ having inner race cooling arrangement and optimal minimum lubrication mechanism for rolling surface" <sup>3)</sup> which is a novel jet lubrication system. Incidentally, an excellent lubrication system has been more strongly needed that is suitable for improving work environment and mitigating environmental impacts. At the same time, there has been a strong need for high-speed bearing operation and longer bearing life with a grease lubrication system that can help reduce occurrence of oil mist and decrease the quantity of energy consumed by the outside device.

To satisfy these needs, we have previously developed improved grease-lubricated bearing systems that include the "BNS Type sealed angular contact ball bearing ( $d_{mN} 1.4 \times 10^4$ )" and the faster

"BNFS Type sealed super high-speed angular contact ball bearing ( $d_{mN} 1.7 \times 10^4$ )" <sup>4)</sup>.

We have recently realized higher speed of  $d_{mN} 1.9 \times 10^4$  and longer life by combining "new grease lubrication system for machine tool main spindle" <sup>5)</sup> that is a maintenance-free grease lubrication system, a sample of which was exhibited in JIMTOF 2006 in the paper titled "BNFS Type" <sup>4)</sup> featuring optimized internal design; and new grease "SE-1". This paper describes the advantages of our new grease lubricated angular contact ball bearings and illustrates results of evaluation tests performed on them.

This new grease lubrication system has come to be known as "**MQGS lubrication**" after its acronym (**M**inimum **Q**uantity base oil of **G**rease **S**upply).

## 2. Features of MQGS lubrication mechanism

### 2.1 Optimized minimum quantity lubrication mechanism and longer life

To be able to achieve higher speed and longer life with grease lubrication, it is necessary not only to ensure lubricating performance in high-speed operation, but also to allow the quantity of grease filled in the bearing to supply oil for a prolonged duration with the lubrication mechanism.

\*Application Engineering Dept. Industrial Sales headquarters

\*\*Product Design Dept. Industrial Sales headquarters

Our newly developed MQGS lubrication mechanism features a unique construction where the base oil within a quantity of grease in a grease-prefilled spacer is supplied to the raceway surface of the bearing during operation. Fig. 1 schematically illustrates a typical construction of our MQGS lubrication angular contact ball bearing that comprises a bearing, outer race-fixed spacer and a grease-prefilled spacer.

Additionally, a restrictive lubrication gap is provided on the outer circumference, in the vicinity of contact points between the rolling elements and outer race raceway surface. It has been already learned that when the restrictive lubrication gap falls within a range of 0.05 to 0.1 mm, the base oil delivered from the grease is smoothly supplied to the raceway surface of the bearing<sup>5)</sup>. Therefore, we have adopted a unique configuration in which the grease-prefilled spacer has a step on its leading edge so that a restrictive lubrication gap of 0.05 to 0.1 mm is reliably maintained. The restrictive lubrication gap is connected to the grease chamber in the grease-prefilled spacer to allow a necessary quantity (minimum amount) of lubricating oil to be supplied to the running bearing, thereby realizing a longer bearing life of  $d_{m11} 1.90 \times 10^4$  ( $d_{11} = 1.50 \times 10^4$ ).

**2.2 Realization of maintenance-free feature**

Needs for grease-lubricated machine tool main spindle bearings have been ever mounting as end users want higher bearing speed in order to reduce machining time as well as mitigate environmental impacts related to the bearing. Incidentally, there has been a conventional approach where a necessary quantity of grease is force-fed from a device outside the bearing; however, with this arrangement, supply lines and auxiliary equipment need to be incorporated, and energy sources for driving these additions are needed; in other words, this arrangement does not have benefits such as maintenance-free feature and decreased system cost.

With our MQGS lubrication mechanism, a grease-prefilled spacer is situated at the bearing front face and a minimum amount of lubricating oil is supplied to the raceway surface of the bearing owing to temperature variation on the running bearing, thereby an outside lubrication oil supply device is eliminated and the bearing can operate without additional maintenance work.

**3. Lubrication life with MQGS lubrication**

**3.1 Quantity of base oil delivered and run time**

To determine the interrelation between the quantity of base oil delivered from grease and the bearing run time, we have performed base oil delivery confirmation testing with MQGS lubrication at speed of  $d_{m11} 1.90 \times 10^4$  that is the development target for a definite position preloaded bearing system. Next, we have calculated the quantity of base oil delivered by comparing the difference in weight of the grease-prefilled spacer before and after the test. Table 1 summarizes the test conditions applied, and Fig. 2 schematically illustrates the construction of the test spindle. The test bearings used are angular contact ball bearings with a bore diameter of 100 mm, installed in a back-to-back duplex configuration (DB set) and then subjected to the test. Table 2 summarizes the bearing specifications, and Fig. 3 illustrates a cross-sectional view of the test bearing. The heat cycle patterns for the operation test have been such that the temperature differences on the outer race of the running bearing were 3°C (41°C ⇔ 38°C) and 15°C (41°C ⇔ 26°C). The temperature difference of 3°C simulates a temperature difference deriving from control of the jacket cooling temperature during continuous bearing operation, and the temperature difference of 15°C represents the difference in bearing temperature between the running condition and when the bearing is at a standstill.

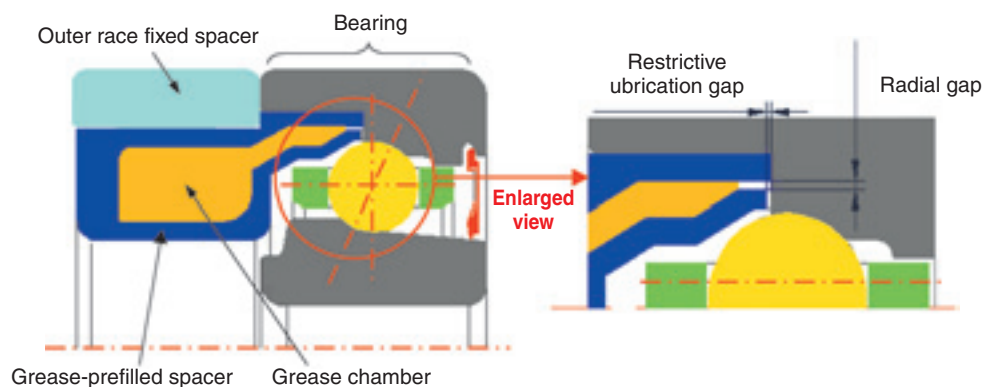


Fig. 1 Schematic construction of MQGS lubrication

Fig. 4 (a), (b) shows the heat cycle patterns applied, and Fig. 5 illustrates the interrelation between the quantity of base oil delivered and the run time. The absolute value of the quantity of base oil delivered under a temperature difference of 3°C differs from that under a temperature difference of 15°C, demonstrating that the quantity of base oil delivered tends to be greater with a greater temperature

Table 1 MQGS grease life test conditions

Item		Content
Operating conditions	Definite position preloading	Shaft attitude and number of test spindle Horizontal (1 unit)
		Preload Post-assembly gap 0 μm
		Bearing speed 15000min <sup>-1</sup> ( <i>d</i> <sub>mn</sub> 1.90×10 <sup>4</sup> )
	Jacket cooling temperature	Room temperature ±1°C

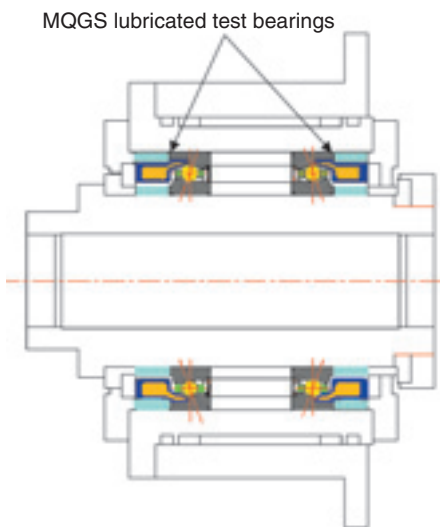


Fig. 2 Schematic construction of test spindle

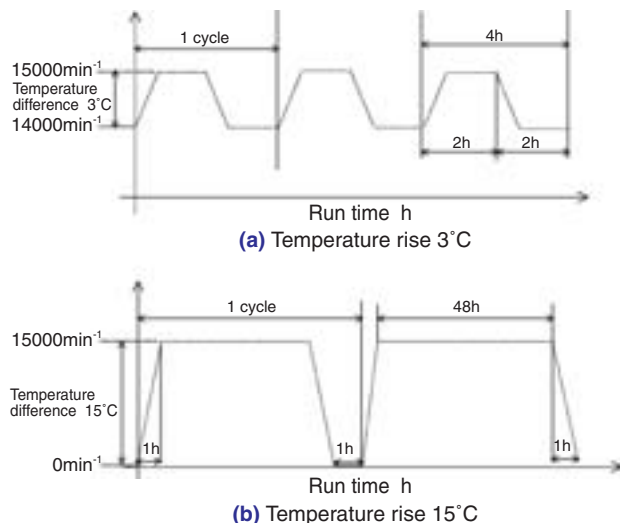


Fig. 4 Heat cycle pattern

difference and a longer run time.

Incidentally, when grease lubrication is adopted for machine tool main spindle bearings, durability life of 20,000 hours or longer is typically required.

To satisfy this requirement, 47 g of grease has been filled into the grease-prefilled spacer (It is known from base oil separation test that approximately 60% of the amount of grease is separated. From this fact, we

Table 2 Bearing specifications for test

Test bearing	φ 100× φ 150×24 mm
Contact angle	20°
Rolling element material	Si <sub>3</sub> N <sub>4</sub>
Cage material	Laminated phenol resin
Grease filled in bearing	SE-1, 8 g filled
Grease filled in grease-prefilled spacer	SE-1, 47 g filled
Restrictive lubrication gap	0.07 mm

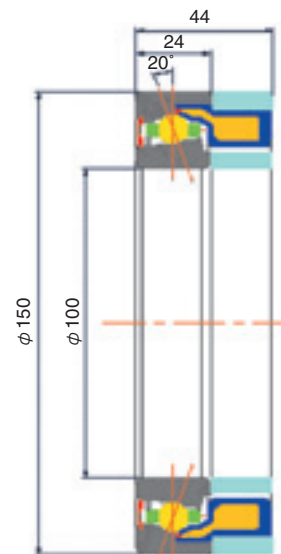


Fig. 3 Section view of test bearing

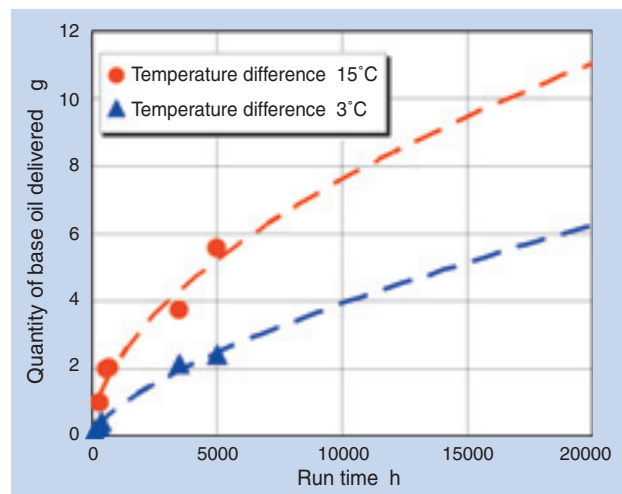


Fig. 5 Driving time and amount of base oil delivery

have selected 47 g as a standard amount for a bearing whose bore diameter measures 100 mm so that the grease-prefilled spacer can continue to deliver base oil for 50,000 hours even at a temperature difference as great as 15°C).

Thus, we believe that by adopting the MQGS lubrication mechanism, we can satisfy application durability requirements. To determine lubrication life, we are now continuing life test with bearing samples, one sample group is being tested at a temperature difference of 3°C while the other sample group is being tested at a temperature difference of 15°C.

### 3.2 Bearing size and quantity of base oil delivered

To determine bearing size-specific base oil delivery quality, we performed a test using bearing size-specific spacer models suitable for bearing bore

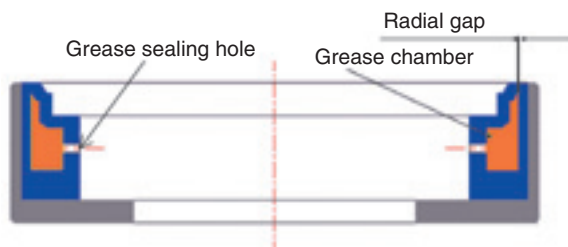


Fig. 6 Sketch of model test rig for base oil delivery

Table 3 Test conditions of model test rig for base oil delivery

Item	Contents
Spacer	Spacers compatible with bearing bore diameters of $\phi$ 100 mm, $\phi$ 70 mm and $\phi$ 50 mm
Grease	SE-1, 47 g filled
Test equipment	Constant temperature chamber
Temperature change	3°C (38°C/2h $\leftrightarrow$ 41°C/2h)
Test duration	200 h

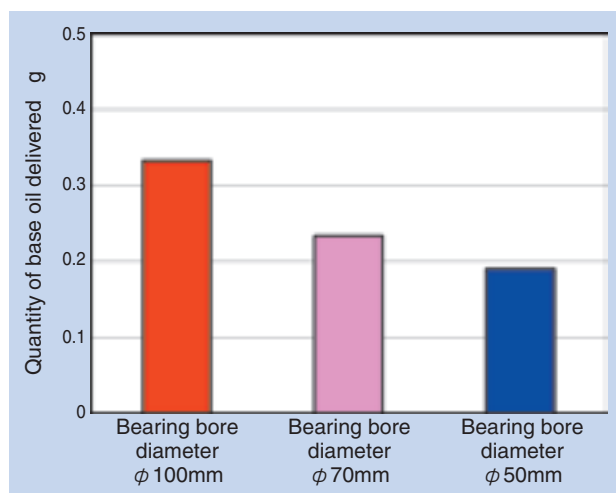


Fig. 7 Bore diameter and amount of base oil delivery

diameters of 100 mm, 70 mm and 50 mm. Fig. 6 schematically illustrates the base oil delivery model test rig used, and Table 3 summarize5s the test conditions applied.

The radial gap at the leading edge where the base oil is delivered was adjusted to 0.07 mm, and the grease-prefilled spacer was filled with 47 g of grease, thereby allowing determination of the interrelation between bearing size and quantity of base oil delivered. Based on the outer race temperature of a running bearing, one heat cycle consisted of 4 hours at 41°C followed by 4 hours at 38°C (temperature difference of 3°C) and this cycle was repeated. 200 hours later, the quantity of base oil delivered was measured, and the result is plotted in Fig. 7.

It is apparent that the absolute value of the quantity of base oil delivered differs between bearing bore diameters of 100 mm, 70 mm and 50 mm, and further that the quantity of base oil delivered is greater with a larger bearing bore diameter, nearly in proportion to the bearing size. From this result, we can determine the optimal quantity of grease to be filled in the grease-prefilled spacer for a given bearing size. For example, a bearing with bore diameter 50 mm has a size 50% as large as that of a bearing having bore diameter 100 mm, and the quantity of grease in the grease-prefilled spacer of the former should be 23.5 g (47 g  $\times$  0.5).

## 4. High-speed operation test

Using our newly developed MQGS lubrication angular contact ball bearings, we have performed an operation test simulating bearing operation on an actual machine tool main spindle. The type of bearing used is an angular contact ball bearing with a bore diameter measuring 100 mm. The bearing specifications, test spindle construction and bearing cross-sectional view are identical to those presented in Table 2, Fig. 2 and Fig. 3 respectively,

### 4.1 Test results

To investigate operation characteristics of the minimum amount lubrication bearing, we have measured temperature increase on the MQGS lubrication angular contact ball bearings in a definite position preloaded arrangement, and then we have compared the resultant temperature increase with that of an "HSE Type high-speed angular contact ball bearing" <sup>6)</sup>. Table 4 summarizes the test conditions applied Fig. 8 (a) schematically illustrates the HSE Type, and Fig. 8 (b) graphically plots the comparative results of HSE and MQGS. We have run the bearings in a definite position preloaded arrangement and

**Table 4** High speed test conditions

Item		Contents	
MQGS type	Grease-prefilled spacer data	Minimum amount lubrication gap	0.07mm
		Prefilled grease	SE-1
		Quantity of prefilled grease	47g
	Bearing preload	Definite position preloading	Post-assembly gap 0 μm
	Jacket cooling temperature	Room temperature ±1°C	
HSE type	Lubricating oil	ISO VG 32	
	Oil feed rate	0.03 mL/shot (oil shot intervals; 5 min.)	
	Air flow rate	40NL/min	
	Bearing preload	Definite position preloading	Post-assembly gap 0 μm
	Jacket cooling temperature	Room temperature ±1°C	

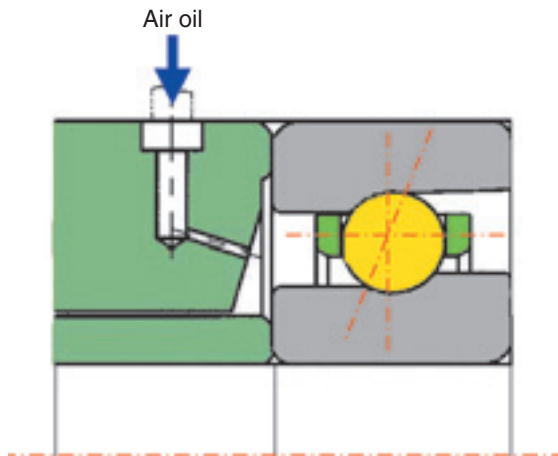


**Fig. 8 (a)** Section view of HSE type

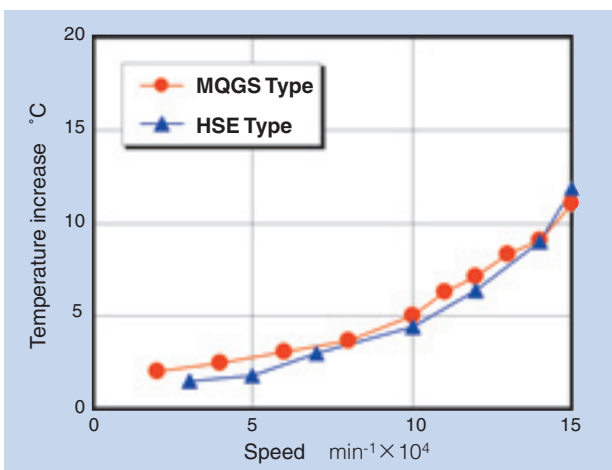


**Fig. 8 (b)** Temperature rise between MQGS and HSE type

verified that our bearing with MQGS is stable at various speeds up to  $d_{mN} 1.90 \times 10^4$  without posing any problem. The temperature increase with our bearing at  $d_{mN} 1.90 \times 10^4$ , which is the development target for MQGS, is virtually at the same level compared with HSE. Thus, we have proven that angular contact ball bearings lubricated with MQGS can run at a high-speed range which was previously possible only with an air-oil lubrication system.

**4.2 Life test**

We have subjected the MQGS lubrication angular contact ball bearings to life testing which has been executed in the definite position preloading mode and definite pressure preloading mode as shown in **Table 5**. As illustrated in **Fig. 9**, the heat cycle temperature difference for the definite position preloaded mode has been set to 3°C and one heat cycle in the run pattern consists of 14,000 min<sup>-1</sup>/2 hrs. and 15,000 min<sup>-1</sup>/48 hrs. To be able to evaluate the effect of main spindle attitude, the test has been performed with the two main spindle attitude modes—vertical attitude mode and horizontal attitude mode.

In case of the definite pressure preloaded system, the heat cycle temperature was set to 15°C and one heat cycle within the run pattern consists, as shown in

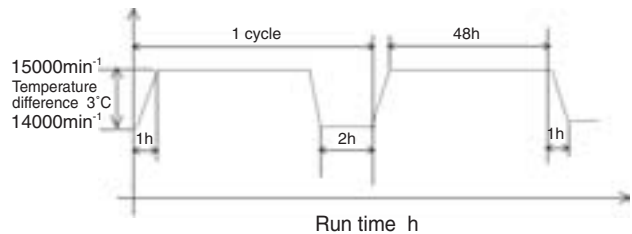


**Fig. 9** Heat cycle pattern

**Table 5** Life test conditions

Item		Contents		
Grease-prefilled spacer data	Minimum amount lubrication gap	0.07mm		
	Prefilled grease	SE-1		
	Quantity of prefilled grease	47g		
Operating conditions	Definite position preloading	Spindle attitude and number of tests	Vertical (one spindle), horizontal (two spindles)	
		Preload	Post-assembly gap 0 μm	
		Speed	15000 min <sup>-1</sup> ( $d_{mN} 1.90 \times 10^4$ )	
	Definite pressure preloading*	Spindle attitude and number of tests	Horizontal (one spindle)	
		Preload	2.2 kN	
		Speed	15000 min <sup>-1</sup> ( $d_{mN} 0.90 \times 10^4$ )	
Jacket cooling temperature		Room temperature ±1°C		

\*: Life test has been in progress since JIMTOF 2004.

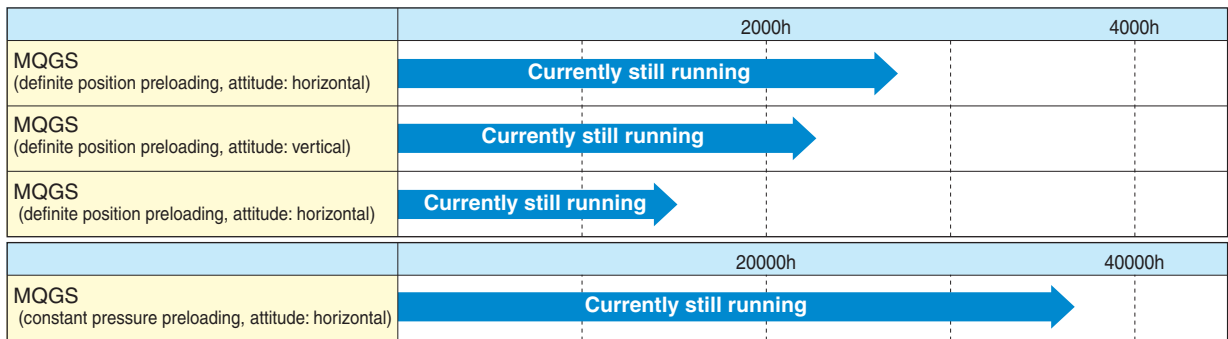


Fig. 10 Life test results

Fig. 4 (b), of 15,000 min<sup>-1</sup>/48 hrs. and stopping to zero speed in 1 hr., thereby this cycle has been periodically repeated.

Fig. 10 summarizes the test results. Currently, the life tests are still in progress. However, we believe that we can achieve problem-free high-speed operation of  $d_{m1} 1.90 \times 10^4$  (possibly the world's highest level with a definite position preloaded system) and longer bearing life.

### 5. Conclusion

We believe that by adoption of our MQGS lubrication angular contact ball bearings, machine tool main spindles can run at higher speeds not possible with conventional grease-lubricated bearings, and that we can positively contribute to higher performance, lower energy consumption and mitigated environmental impacts on machine tools that incorporate NTN bearings.

### References

- 1) H. Takiuchi and F. Kosugi: "ULTAGE" Series Precision Bearings for Machine Tools, NTN Technical Review No.72 (2004) 26-29
- 2) Y. Akamatsu and M. Mori: Development of Eco-friendly Oil Jet Lubricated Angular Contact Ball Bearings for Machine Tools, NTN Technical Review No.72 (2004) 6-10
- 3) M. Koyama: Minimum Quantity and Cooling Jet Lubricated Angular Contact Ball Bearings for Machine Tools, NTN Technical Review No.74 (2006) 22-25
- 4) F. Kosugi:  $d_{m1} 170 \times 10^4$  Sealed High-Speed Angular Contact Bearing "New BNS Type," NTN Technical Review No.74 (2006) 22-25
- 5) Sun-Woo Lee and M. Mori: Development of a New Grease Lubrication System Machine Tool Main Spindles, NTN Technical Review No.74 (2006) 8-15
- 6) NTN Catalogue Precision Rolling Bearings, CAT. No.2260/J. 74

Photo of authors



Sun-Woo Lee

Application Engineering Dept.  
Industrial Sales  
headquarters



Tadaaki MAEDA

Product Design Dept.  
Industrial Sales  
headquarters

# Minimum Quantity and Cooling Jet Lubrication Single-row Cylindrical Roller Bearings

Futoshi KOSUGI\*  
Susumu NOJIMA\*\*



NTN has developed an angular contact ball bearing with minimum quantity and cooling jet (MQCJ) lubrication. A new jet lubrication method with an inner ring cooling system and an optimally minimized quantity lubrication mechanism for the raceway were adopted. A new product that has applied MQCJ lubrication to a single row cylindrical roller bearings was developed. We introduce this single row cylindrical roller bearing with the new jet (MQCJ) lubrication method.

## 1. Introduction

Compared with conventional jet lubrication systems, our MQCJ lubrication system boasts much decreased power loss. In the 23rd Japan International Machine Tool Fair held in 2006 (JIMTOF 2006), an actual example of a MQCJ lubrication angular contact ball bearing was installed on a machining center main spindle and its performance was demonstrated in machining operation. Recently, we have adopted the MQCJ lubrication system to cylindrical roller bearings, thereby realizing super high-speed operation with maximum  $d_{mN}$  of 3.35 million (practical  $d_{mN}$  of 3 million) with oil lubrication. By utilizing MQCJ lubrication, a cylindrical roller bearing can be incorporated into the rear side (free side) of a main spindle, helping simplify the main spindle structure.

This paper hereunder presents the features of the "Minimum Quantity and Cooling Jet (MQCJ) lubrication single-row cylindrical roller bearings" and the result of evaluation testing for these bearings.

## 2. Features of MQCJ lubrication

### 2.1 System overview

To our Minimum Quantity and Cooling Jet (MQCJ) lubrication single-row cylindrical roller bearings, a lubrication system identical to that for MQCJ

lubrication angular contact ball bearings can be applied. **Fig. 1** schematically illustrates such a lubrication system <sup>1), 2)</sup>.

With this lubrication mechanism, one common oil supply device supplies oil to the bearing section and the jacket cooling section, and the used oil is recovered with a scavenge pump. Since the jacket cooling oil also functions as the bearing lubricating oil, auxiliary equipment to the bearing system is simplified.

### 2.2 Specifications of MQCJ lubrication cylindrical roller bearings

The MQCJ lubrication system is a jet lubrication system that is capable of cooling the inner race and has a minimum quantity lubrication mechanism for the rolling surface. On our MQCJ lubrication angular contact ball bearings (**Fig. 2**), a jet of lubricating oil is directed to the inner race scoop and lubricating oil adheres to the inside surface of scoop, and is then transferred to the conical surface outside of the inner race by centrifugal force and surface tension, with the result that only a small quantity of lubricating oil is fed into the bearing.

Since the lubrication space defined by the conical surface and the outer race spacer limits the quantity of lubricating oil fed into the bearing, a larger portion of lubricating oil takes part in cooling of the inner race and only a small portion of lubricating oil flows through

\*Application Engineering Dept. Industrial Sales headquarters

\*\*Product Design Dept. Industrial Sales headquarters

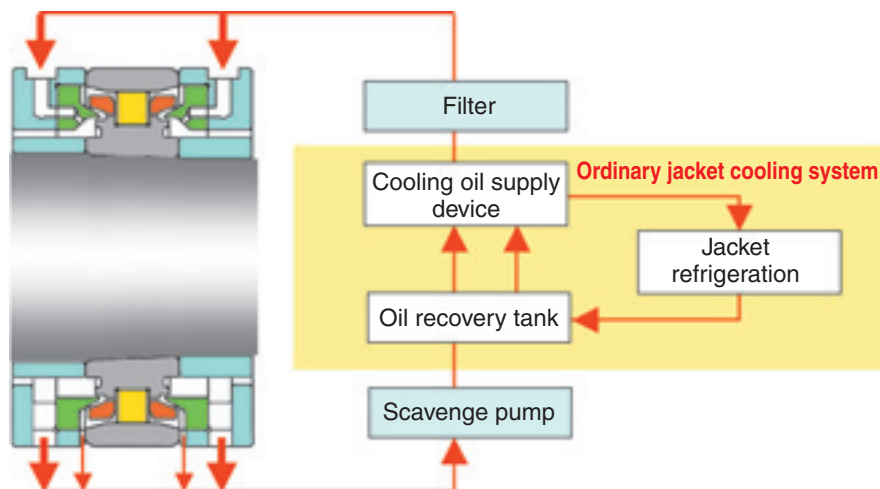


Fig. 1 MQCJ lubrication system

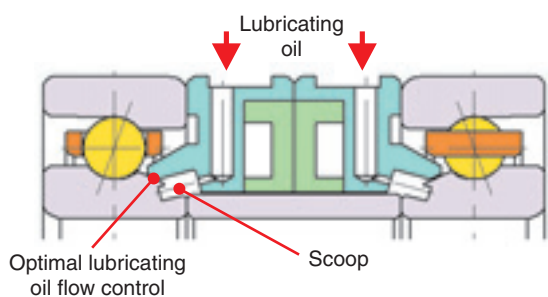


Fig. 2 MQCJ lubrication angular contact ball bearing

the bearing, thereby resultant power loss will be reduced<sup>2)</sup>.

Incidentally, our cylindrical roller bearings are basically intended for use on the rear side: therefore, we should remember that when a main spindle is running, the shaft elongates to the rear side (free side) owing to heat generated.

Lubrication space may be defined by the inner race conical surface and the outer race spacer (as in cases with angular contact ball bearings). However, depending on the installation orientation of the nozzle

spacer, the lubrication space can vary while the bearing runs: as a result, the lubrication space can get narrower (Fig. 3) or wider (Fig. 4) owing to elongation on the shaft.

Because variation in the size of lubrication space can affect the quantity of oil passing through the space, we have invented a horizontal space design (Fig. 5) to prevent variation in the size of lubrication space owing to elongation of the shaft. By adopting the horizontal space design, we can avoid adverse effects from variation in the size of lubrication space that results from bidirectional shaft elongation.

Though based on ULTAGE Series single-row cylindrical roller bearings (roller guided cage), our MQCJ lubrication single-row cylindrical roller bearings adopt an inner race guided cage to stabilize rotation of the cage in order to run at a higher speed range. With a conventional design, lubricating oil was supplied from one side only; as a result, lubrication on the roller end faces and inner race ribs on the side opposite to oil supply can be unstable. In contrast, with our new bearings, lubricating oil is supplied from both sides: as a result, all the areas between the roller end faces and

Gap between inner race and spacer will shrink.

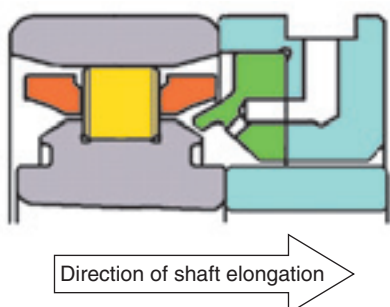


Fig. 3 change of lubrication space ①

Gap between inner race and spacer will expand.

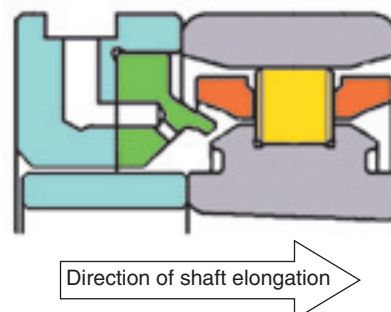


Fig. 4 change of lubrication space ②

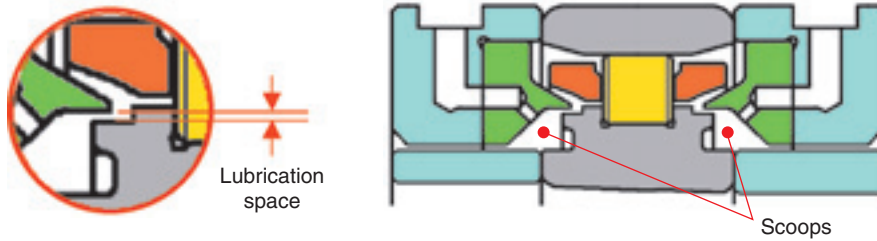


Fig. 5 MQCJ lubrication cylindrical roller bearings

inner race ribs are smoothly lubricated and the inner race is more effectively cooled, thereby increase of preload is inhibited and stable high-speed operation is ensured.

2.3 Test data

Table 1 summarizes the test conditions applied, and Fig. 6 schematically illustrates the test spindle used.

The test bearing was based on the N1011HSR (bore diameter 55 mm) belonging to the ULTAGE Series high-speed cylindrical roller bearing family. This bearing size was based on the assumption that the front main spindle bearings were comprised of dia. 70 mm MQCJ lubrication angular contact ball bearings in definite position preloading configuration. The test spindle used was a vertical test rig driven by a built-in motor.

The support bearing unit consisted of a pair of angular contact ball bearings in DB configuration and was air-oil lubricated. Figs. 7 and 8 plot the test results based on samples with a single-sided lubrication nozzle, and Figs. 9 and 10 are plotted based on a double-sided lubrication nozzle configuration. On both single-sided and double-sided lubrication nozzle configurations, temperature increase is small and power loss is low (including power loss at rear bearing) with MQCJ lubrication compared with conventional jet lubrication. This is due to the effectiveness of the MQCJ lubrication system that positively cools the bearing (inner race) and supplies a

minimum quantity of lubricating oil into the bearing.

Compared with the single-sided lubrication nozzle configuration, the double-sided lubrication nozzle configuration is capable of much higher bearing speed (maximum  $d_{mn}$  3.35 million).

Incidentally, in tests with air-oil lubrication and a single-sided lubrication nozzle configuration, lubricating oil (VG32) was fed at a rate of 0.02 mL/10 min, thereby it has been learned that both temperature increase and power loss are more significant with MQCJ lubrication. This is because the quantity of oil fed into both bearings is greater with MQCJ lubrication, and the effect of stirring resistance in the bearings is greater.

Fig. 11 graphically plots the results of passing oil flow measurements on bearings with conventional jet lubrication and MQCJ lubrication, Fig. 12 illustrates measurement positions for passing flow and non-passing flow relative to quantity of lubricating oil supplied. With conventional jet lubrication scheme, the horizontally situated lubrication nozzle aims at a location between the cage and bearing ring, with approximately 50% of lubricating oil passing through the bearing. On the other hand, with MQCJ lubrication, lubricating oil is injected to the scoops on the inner race and the horizontal gap is regulated by the spacer and stepped inner race, thereby the quantity of passing lubricating oil at higher bearing speed is as low as approximately 10%.

Results for air-oil lubrication with a double-sided

Table 1 Test conditions

Item	Content
Test bearing	N1011HSR basis ( $\phi 55 \text{ mm} \times \phi 90 \text{ mm} \times 18 \text{ mm}$ )
Support bearing	5S-2LA-HSL007DB (air-oil lubrication)
Main spindle attitude	Vertical
Target assembly gap	0 $\mu\text{m}$
Spacer nozzle	Nozzle diameter $\phi 1 \text{ mm}$ , two positions (180-degrees spacing)
Oil flow rate	1~5L/min
Lubricating oil	VG1.5 (VG32)
Temperature of lubricating oil supplied	23~24°C (setting: 20°C)
Jacket cooling	Yes (5 L/min)

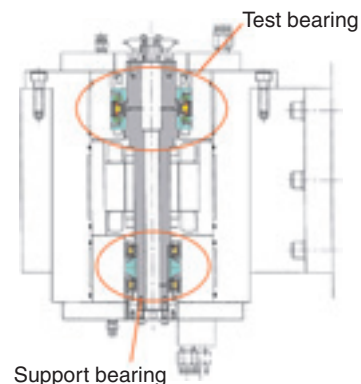


Fig. 6 Schematic construction of test spindle

nozzle configuration are shown in Figs. 9 and 10 ; wherein like in the case of MQCJ lubrication, the test was performed while lubricating oil (VG 1.5) was fed into the bearing at a rate of 0.5 mL/min (maximum feed rate for air-oil lubrication unit).

The oil feed rate with air-oil lubrication is significantly low compared with MQCJ lubrication: however, temperature increase at lower speed range is very high with air-oil lubrication. This seems to result from stirring of lubricating oil. Note, additionally, that there is temperature drop at the middle-speed range.

This appears to be because that the rollers and cage generate an air curtain, and, as a result, a proportion of lubricating oil not fed into the bearing increases and the centrifugal force helps increase the quantity of lubricating oil released from inside the bearing, thereby the stirring resistance decreases.

Note also that the temperature at lower speed range is low with MQCJ lubrication and jet lubrication, each involving greater oil feed rate compared with air-oil lubrication. This appears to be because a large quantity of oil cooled by MQCJ lubrication or jet

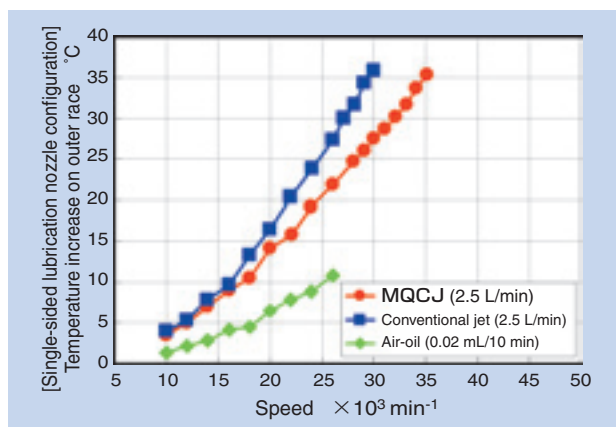


Fig. 7 Outer race temperature

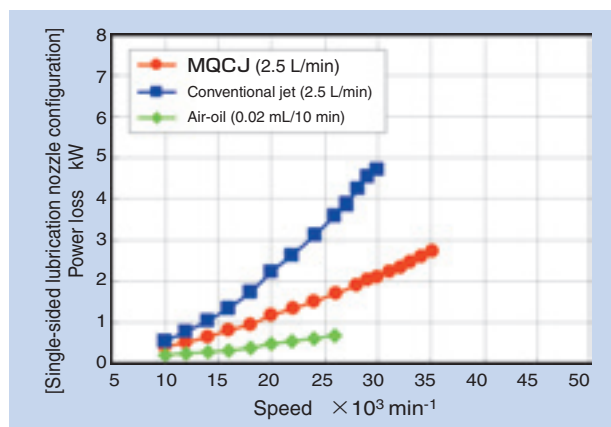


Fig. 8 Power loss

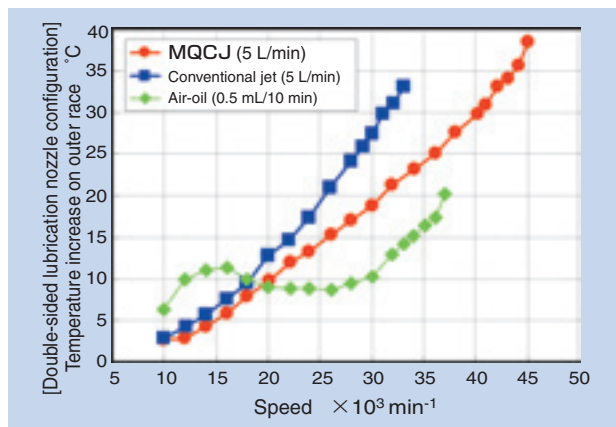


Fig. 9 Outer race temperature

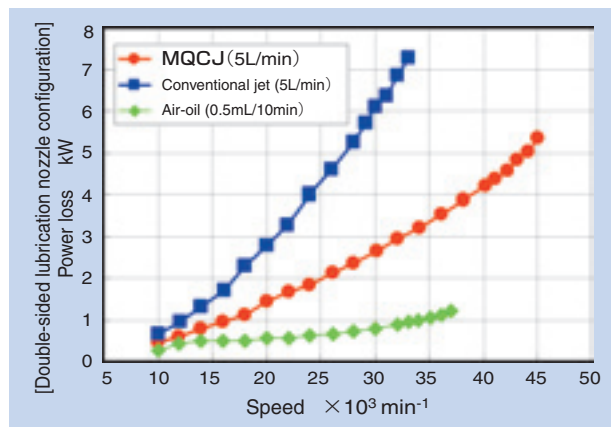


Fig. 10 Power loss

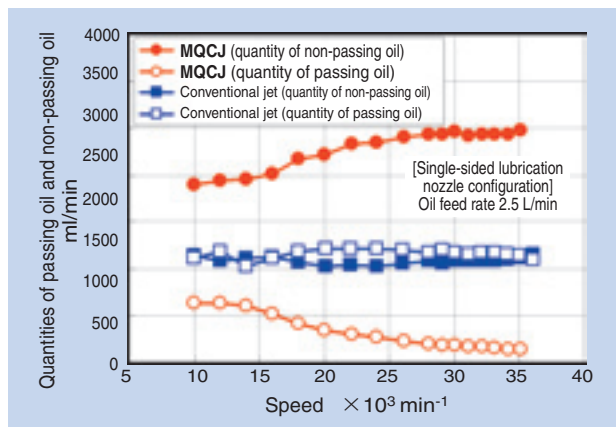


Fig. 11 Amount of oil that passes in bearing

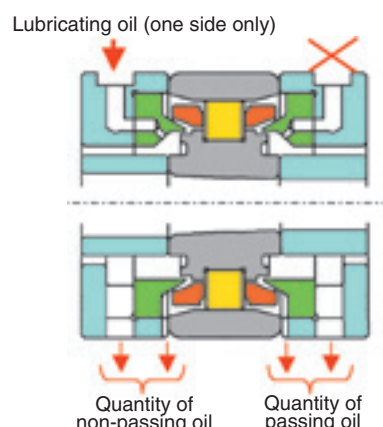


Fig. 12 Measurement position

lubrication removes heat energy that is greater than heat derived from stirring of the oil.

The graphical plotting in Fig. 13 illustrates the effect of varied oil feed rate on temperature rise at the outer race for a double-sided lubrication nozzle with MQCJ lubrication. When the feed rate of lubricating oil is increased, the temperature increase on the outer race is mitigated: the cooling effect of the lubricating oil is greater with higher bearing speed.

Also, the graphical plotting in Fig. 14 allows us to determine variation in the power loss. It should be understood that when the feed rate of lubricating oil is increased, the power loss increases. (In both Figs. 13 and 14, values obtained from air-oil lubrication are superposed and circled in red for comparison.)

From these findings, it is apparent that with MQCJ lubrication, the relation between oil feed rate and power loss conflicts with the relation between oil feed rate and bearing cooling effect. Therefore, we need to define lubrication conditions that best suit the intended bearing operating conditions.

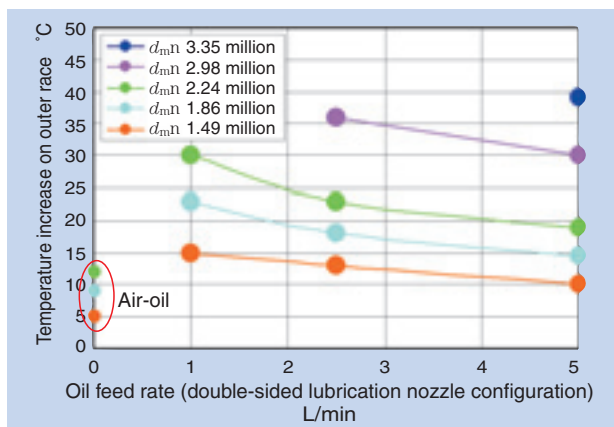


Fig. 13 Outer race temperature

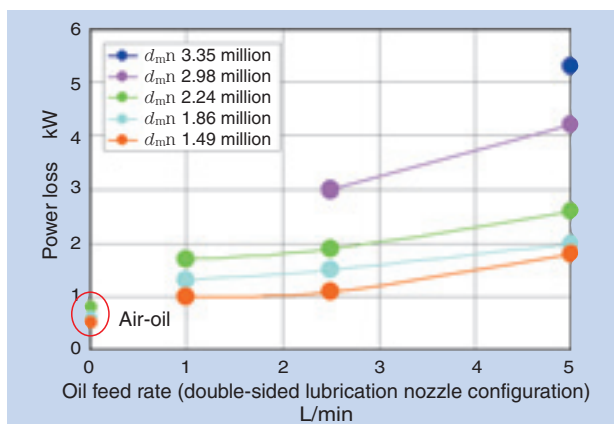


Fig. 14 Power loss

### 3. Conclusion

Our MQCJ lubrication single-row cylindrical roller bearings can be used as a rear-side bearing on machine tool main spindles whose front-side bearing comprises a MQCJ lubrication angular contact ball bearing in definite position preloading mode.

NTN has already developed an angular contact bearing arrangement that achieves high-speed operation of 40,000 min<sup>-1</sup> with MQCJ lubrication, using bearings with bore diameter of 70 mm -which are arranged in DB set configuration and are provided with definite position preload. Since our newly developed bearings are intended for use on the rear-side of this bearing arrangement, the maximum speed of our new bearing design is as high as 40,000 min<sup>-1</sup>; thus our new bearing design is capable of commercial high-speed operation of  $d_{m\Omega}$  3 million.

Note that our MQCJ lubrication system is essentially a jet-lubricated system, and that main spindle construction involving an MQCJ lubrication system requires a much enhanced labyrinthine structure in addition to the system configuration described previously in the system overview section. Notwithstanding, we believe that our new development helps increase possible options for selecting bearing and lubrication arrangement for bearings that support super high-speed machine tool main spindles. We hope that NTN's new lubrication system helps assist in realizing further sophistication of machine tool main spindles.

### References

- 1) Y. Akamatsu and M. Mori: Development of Eco-friendly Oil Jet Lubricated Angular Contact Ball Bearings for Machine Tools, NTN Technical Review No.72 (2004) 6
- 2) M. Koyama: Minimum Quantity and Cooling Jet Lubricated Angular Contact Ball Bearings for Machine Tools, NTN Technical Review No.74 (2006) 22

### 執筆者近影



Futoshi KOSUGI

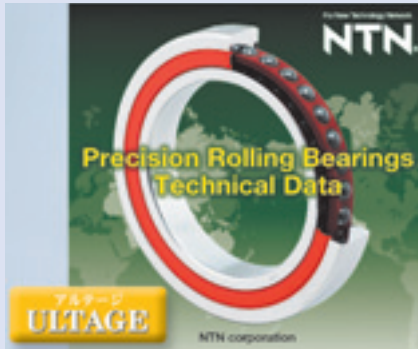
Application Engineering Dept.  
Industrial Sales  
headquarters



Susumu NOJIMA

Product Design Dept.  
Industrial Sales  
headquarters

## Introduction of 3D Electronic Catalog for Precision Machine Tool Bearings



Takehiko UMEMOTO\*

Machine tool makers use 3D CAD data in CAE to reduce development time and conduct advanced analysis, which may include thermal analysis and/or structural analysis for high precision applications.

This document introduces 3D CAD data (i.e. electronic catalog) for precision bearings and shows examples of 3D CAD analysis .

### 1. Introduction

Having been developed as precision bearings for machine tools, NTN ULTAGE Series bearing products are used in various areas on main spindles and feed systems of machine tools. Their high precision and advanced functionality have been highly appreciated by machine tool manufacturers. The term “ULTAGE” was created from a combination of “ULTIMATE” (meaning last in progression) and “STAGE”. This name is meant to convey NTN’s goal that this series of products are unsurpassed in a range of applications. In order to meet this target, the ULTAGE Series bearing products are being produced in a wide range of sizes.

Recently, NTN developed a 3D Electronic Catalog of ULTAGE Series Bearing Products for Machine Tools (3D CAD Data) and has started providing it to machine tool manufacturers (reported in the Nikkei Sangyo Shimbun on p. 15 of the April 22, 2008 issue).

3D CAD helps customers clearly understand bearing design features. This allows design, manufacturing and sales to easily communicate and collaborate during the development phase. For this reason, 3D CAD systems are being adopted by an increasing number of manufacturers.

Additionally, 3D CAD data can be used to provide information for thermal analysis, stress analysis, structural analysis and other types of analysis. 3D CAD data also allows designers to analyze various areas on main spindles and associated structures,

thereby resulting in a decrease in the expected number of prototype bearings required.

This paper presents the configuration of NTN’s 3D electronic catalog that was recently released, and provides example applications for using the 3D data.

### 2. 3D Electronic catalog interface

The 3D electronic catalog is provided to users in the form of a CD-ROM that includes: ① 2D and 3D CAD data, ② a user’s guide for the CAD data, ③ a precision rolling bearings catalog (in PDF format), ④ access to “mt-tecnos” (a web site dedicated to precision bearings technology for machine tools), ⑤ a user’s guide for “mt-tecnos” and ⑥ access to NTN’s home page. Fig. 1 below shows the starting screen that appears on the computer screen after installation of the CD-ROM.

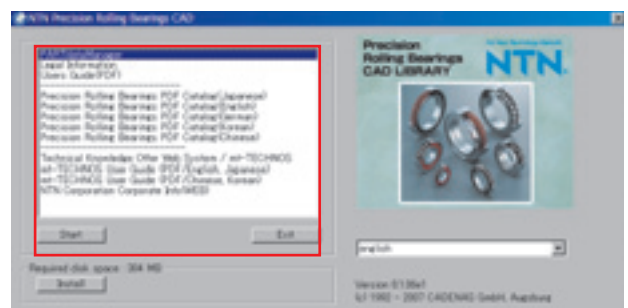


Fig. 1 Activation screen for CD-ROM

\*Product Design Dept. Industrial Sales headquarters

For detailed information about these features, refer to user's guides ② and ⑤ on the CD-ROM.

**(1) Structure of 3D CAD data**

The "3D Electronic Catalog for Precision Machine Tool Bearing Products" contains data for angular contact ball bearings and cylindrical roller bearings used on main spindles and feed systems of machine tools. The CD-ROM has 3D CAD data for a total of 1329 bearing base sizes that include 1039 angular contact ball bearings (including those with ceramic balls), 212 cylindrical roller bearings and 78 ball screw support bearings.

**Table 1** summarizes all bearing series stored on the CD-ROM.

The CAD data is displayed on the computer screen in the file structure format shown in **Fig. 2**.

**Table 1** Bearing series stored on CD-ROM

Angular contact ball bearings: 1039 base sizes	
Standard	7805C~7834C, 7900U~7934U 7000U~7040U, 7200C~7226C
High-speed	HSE910~HSE934, HSE010~034
Axial load carrying	HTA920U~HTA964U HTA010U~HTA064U
For grinding machines	BNT900~BNT913, BNT000~BNT014 BNT200~BNT216
Sealed standard	7900~7910LLB 7000~7010LLB
Sealed high-speed	BNS910~BNS920LLB BNS009~BNS020LLB
Ball screw support bearings: 78 base sizes	
Ball screw support bearings	BST17x47~BST60x120 7000HT~7002HT, 7203HT~7208HT
Cylindrical roller bearings: 212 base sizes	
Standard double-row	NN3005~NN3036
Standard single-row	N1006~N1032
High-speed double-row	NN3005HS~NN3026HS
High-speed single-row	N1011HSRT6~N1020HSRT6

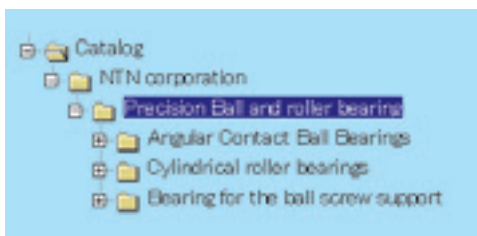


**Fig. 2** CAD data file structure

**Figs 3, 4 and 5** show examples of screens displaying different levels of the CAD data file structure.

By clicking on the icon for a particular bearing series, the user can access the corresponding 3D CAD data.

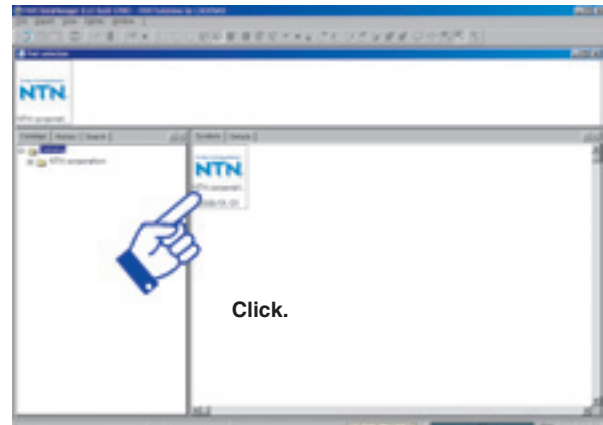


**Fig. 3** Top screen

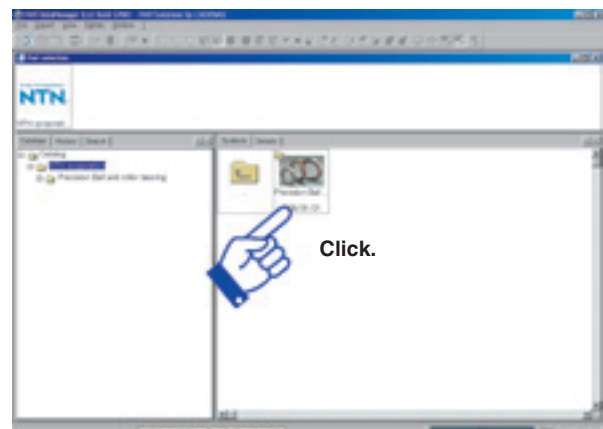


**Fig. 4** Precision bearing screen

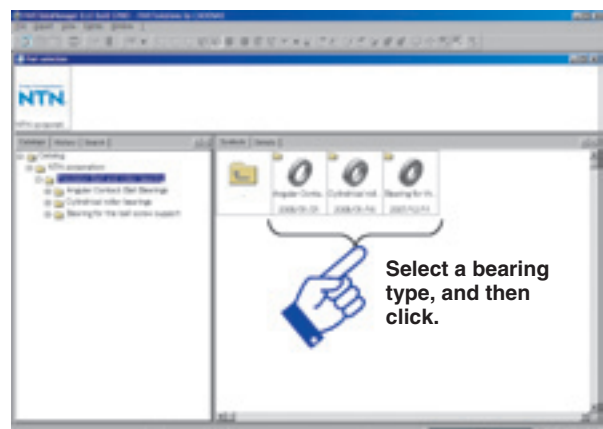


**Fig. 5** Precision bearings icons

**(2) Accessing 3D CAD data**

After selecting the appropriate bearing icon, corresponding bearing part numbers can be selected to access their 3D CAD data. An example of this process is illustrated in Fig. 6 through Fig. 10.

For example, suppose data is required for the standard angular contact ball bearing base sizes 7015US (ID  $\phi$  75 mm  $\times$  OD  $\phi$  115 mm  $\times$  W 20 mm).

After clicking on the appropriate icons, the monitor will eventually display the bearing data as shown in Fig. 9.

Once a bearing base sizes is selected, then the screen will show:

- ① Bearing boundary dimensions (section A)
- ② 3D CAD data (section B)
- ③ Bearing bill of materials (section C)

The 3D CAD data shown in item ② is saved to the CD-ROM so it can be downloaded to the user's computer. The different formats available on the 3D Electronic Catalog are listed in Fig. 10.

The available file formats (SAT, STEP, IGES, DXF, etc.) are used to import the data in to various CAD systems (Solidworks, Inventor, OneSpaceModeling, Solid Edge, etc.).

When saving these files, the user will obtain the CAD data complete with constraint conditions, i.e. the relationships between parts and assemblies are maintained. The user should be sure to select the file format that works best with the CAD software currently being used.

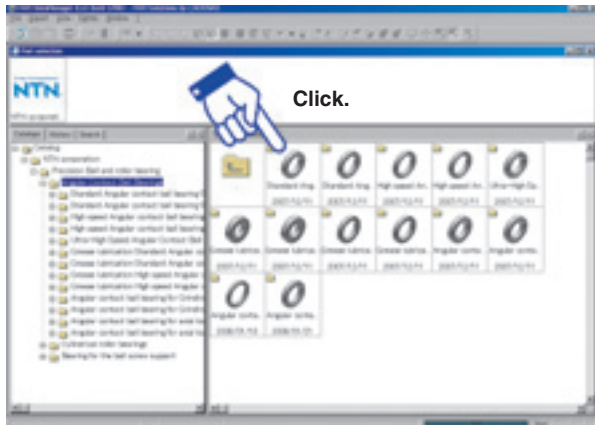


Fig. 6 Angular contact ball bearing icon

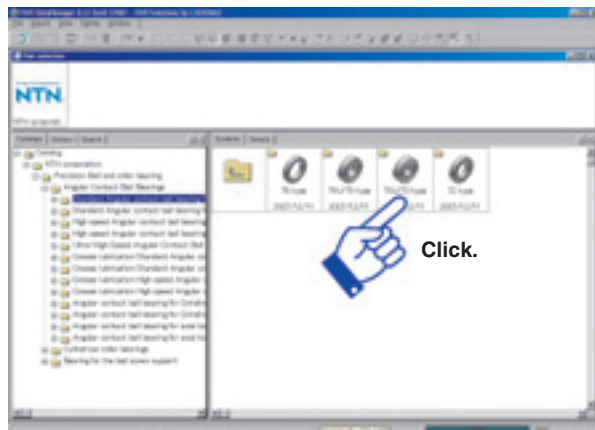


Fig. 7 Standard angular contact ball bearing icon

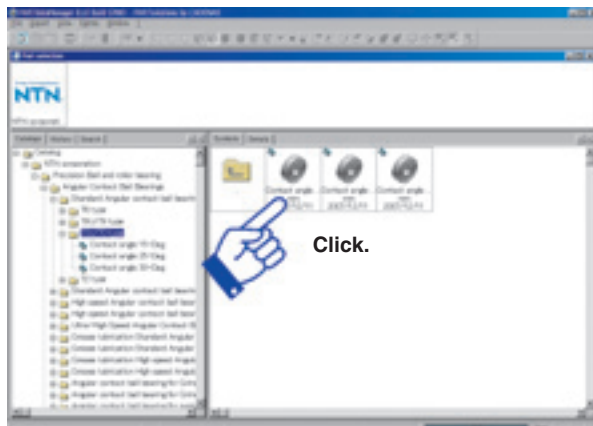


Fig. 8 70U/70 series icon

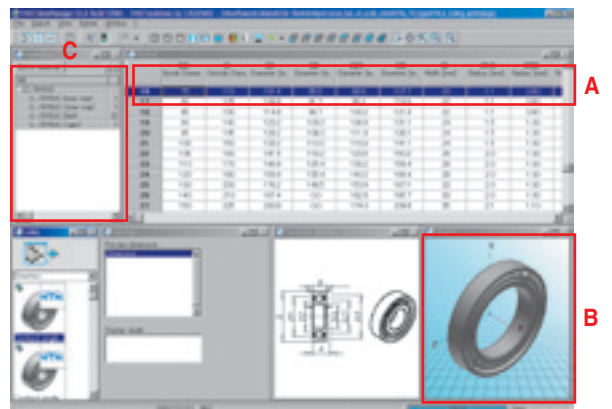
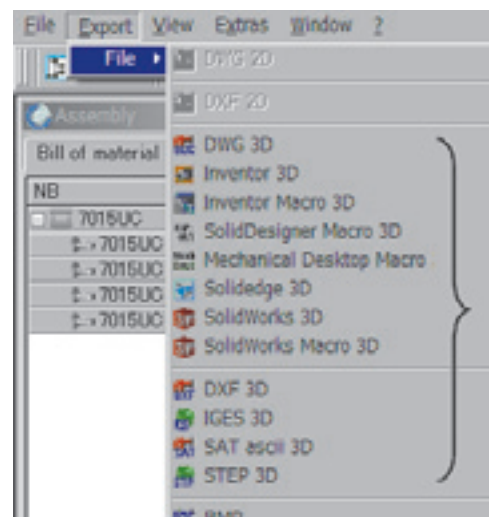


Fig. 9 Example of standard angular contact ball bearing p/n 7015UC



Copied 3D CAD data

Fig. 10 CAD data formats available

Also, for information about the software in a specific language, NTN Engineering should be contacted for technical assistance.

### 3. Typical applications

A 3D CAD image helps everyone easily visualize and understand the bearing design. Thus, 3D CAD imaging is expected to reduce the design time for a new product as well as the workload for the whole development process through commercialization of the product (see items ① ~ ④ below);

- ① Design Confirmation
- ② Application to Analysis
- ③ Reduction in Prototype Cost
- ④ Data Management

It is getting more common to check for possible interference and perform other various analysis to optimize the design prior to prototype fabrication. As a result, both time and cost have been reduced for prototypes and testing.

Examples of activities NTN is undertaking associated with items ① and ② are described below.

#### (1) Design Confirmation

One major objective of 3D CAD is to assist the designer in detecting potential interference between adjacent components in order to prevent a deficient design.

By reviewing the 3D CAD data provided on the CD-ROM, the dimensional issues described below can be checked when the bearing is being specified for an application:

- ① Verification of appropriate shoulder height for bearing inner and outer ring when compared to the dimensions of the shaft and spacer.
- ② Confirmation that the oil nozzle on the spacer lines up with the oil feed/drain piping in the housing.
- ③ Ensure proper bearing position with respect to the lubricating oil jet ejected by the nozzle.

**Fig. 11** shows a typical 2D arrangement of an angular contact ball bearing and a bearing spacer with an oil feed nozzle. A 3D model allows the user to view the bearing from various angles and confirm the proper position of the nozzle tip with respect to the oil hole/drain hole (see **Fig.12**).

#### (2) Application to Analysis

Higher precision bearings are being made to endure with applications running at higher speeds. Also, to reduce the number of sample test runs, thermal analysis, stress analysis and structural analysis are now being performed during the design phase.

By performing stress analysis and thermal analysis

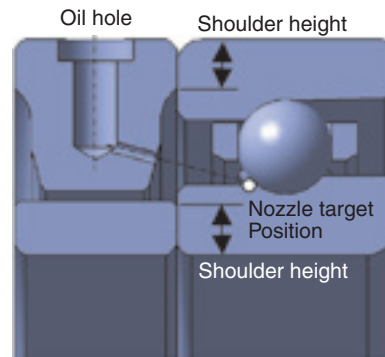


**Fig. 11** Angular contact ball bearing with spacer

#### Design Confirmation

- ① Confirmation that the oil nozzle on the spacer lines up with the oil feed/drain piping in the housing
- ② Ensure proper location of spacer positioning pins
- ③ Verification of oil feed/drain piping in the housing
- ④ Detection of interference between the bearing, spacer and adjacent components
- ⑤ Determination of bearing and spacer width surface contact length

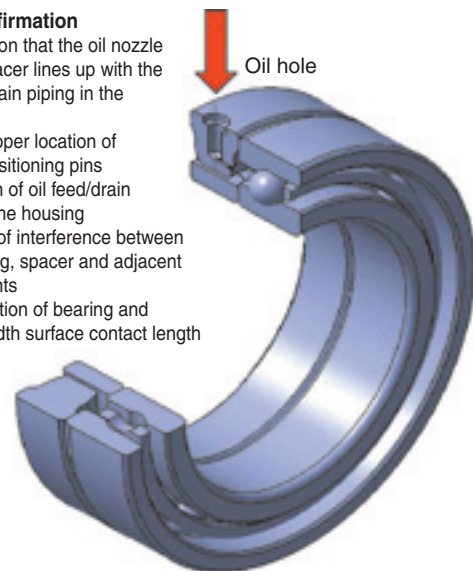


**Fig. 12** 3D validation

by loading graphic data into analysis software<sup>NOTE)</sup>, it is possible to predict potential issues and develop countermeasures to increase bearing life.

**NOTE): Analysis software is not included on this electronic catalog CD-ROM.**

#### Example of Mode Analysis

An example of the simplest analysis using 3D graphic data for a bearing is calculation of its natural frequencies.

**Fig. 13** illustrates deep groove ball bearing part number 6208 (ID  $\phi$  40  $\times$  OD  $\phi$  80  $\times$  W 18 mm). **Table 3** summarizes the natural frequencies of this bearing.

**Table 3** shows the fundamental frequencies for the inner and outer rings from the first harmonic through the fifth harmonic. When reviewing the calculated values only, it is extremely difficult to imagine the mode diagram for a particular harmonic. In contrast, with a 3D image for a given harmonic, it dramatically helps visualization of the mode image.

For example, 6208 mode diagrams for the first

harmonic to third harmonic of the inner ring are shown in **Table 4**. By reviewing these diagrams, it is clear that the pattern of the first harmonic is a simple oval shape; the pattern of the second harmonic is wavy in

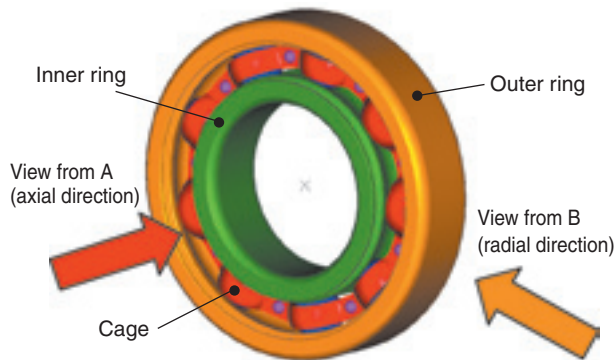


**Fig. 13** 6208 Deep groove ball bearing

**Table 2** Inner ring and outer ring properties

Young' modulus	Poisson's ratio	Specific gravity
208000MPa	0.3	7.8

**Table 3** Fundamental frequencies

Harmonic	Inner ring	Outer ring
1	6727	2526
2	9140	4475
3	18205	7042
4	23313	12994
5	33011	13217

**Table 4** Inner ring mode chart

Harmonic	View from A (axial direction)	View from B (radial direction)
1		
2		
3		

the axial direction; and the pattern of the third harmonic exhibits a basic triangular shape.

**Structural Analysis Example**

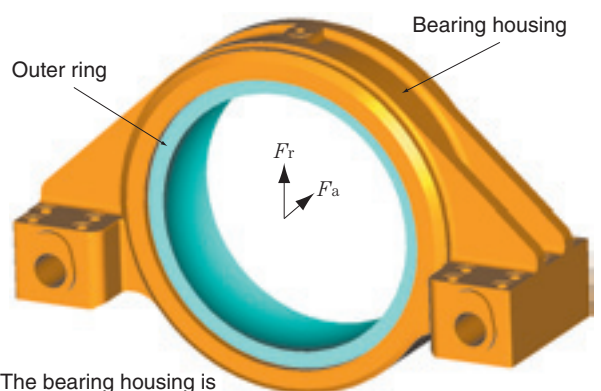
Structural 3D analysis is often used to investigate the stress and displacement that occur when an external load and rotation-induced centrifugal force are applied to a bearing. An example of this analysis is described below, referencing the structure shown in **Fig. 14**. This structure is comprised of a rhomboidal bearing housing with a self-aligning roller bearing installed into its bore. For simplicity, the diagram shows the bearing outer ring only (light blue portion).

An axial load  $F_a$  is applied to the bearing and bearing housing via the main spindle, and a radial load  $F_r$  is applied to the upper portion of the housing. As a result, the load is transferred to the bearing housing via the main spindle, inner ring, rolling elements and outer ring.

The stress analysis of this bearing and housing assembly is described below.

First of all, it should be mentioned that for the loads acting on the outer ring and housing, the loading of each rolling element (spherical rollers: 30 rollers/row  $\times$  2 rows) was calculated in advance. Using these calculated loads, structural analysis for the outer ring was performed.

(When planning to perform a detailed investigation as shown in this example, **NTN** should be contacted for the calculation results on rolling element loading and the spring constant of the rolling elements.)



The bearing housing is bolted down to a baseplate.

**Fig. 14** Analysis example

**Fig. 15** illustrates the stress distribution of the bearing housing.

The red portions of this diagram indicate the highest stresses. By optimizing the shape and wall thickness of the housing flange sections, the calculated stress levels of these portions is reduced.

**Fig. 16** shows a view of the housing from underneath: this diagram reveals the stress caused by individual rollers (see arrows) on the housing bore surface.

**Figs. 17** and **18** exhibit the amount of deformation of the bearing and housing.

The amount of bearing and housing deformation does not pose a problem. However, the stress distribution does need to be studied carefully for an extreme case. When a sleeve is mounted to the inner ring, it can be deformed and displaced by the applied load and centrifugal force, causing it to come in contact with the housing bore surface.

### ■ Thermal Analysis Example

Finally, an example of thermal analysis is presented below.

When the temperature distribution on and around a shaft is relatively constant, 2D thermal analysis is often used.

For the following example, 2D thermal analysis was performed on an NTN high-speed test rig, and the analysis result was been compared with the test data from an NTN bearing.

(For more detail, refer to the “Heat Transfer Analysis of Machine Tool Main Spindle” section in this Technical Review Manual.)

The horizontal bearing test rig shown in **Fig. 19** features the internal construction show **Fig. 20**.

The test rig features a simple structure: both ends of the main spindle have an angular contact ball bearing, a spacer is situated in the middle of the rig and the bearing housing is surrounded by a cooling jacket.

In order to obtain an array of bearing test data, this

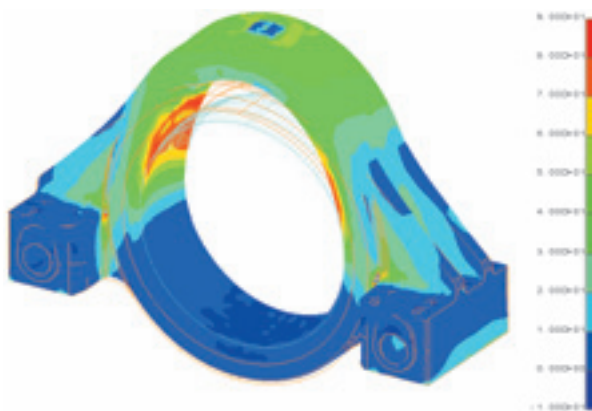


**Fig. 15** Housing stress distribution

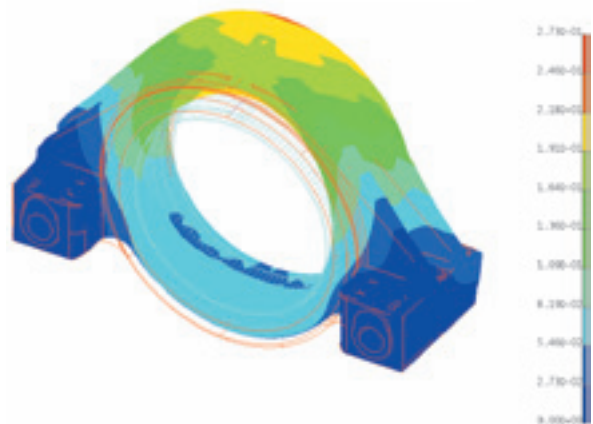


**Fig. 17** Deformation of housing from overhead

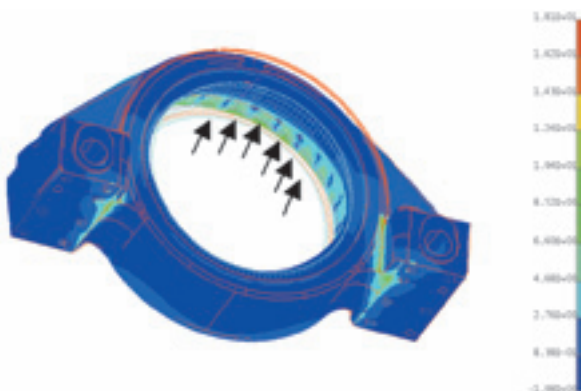


**Fig. 16** Housing stress distribution

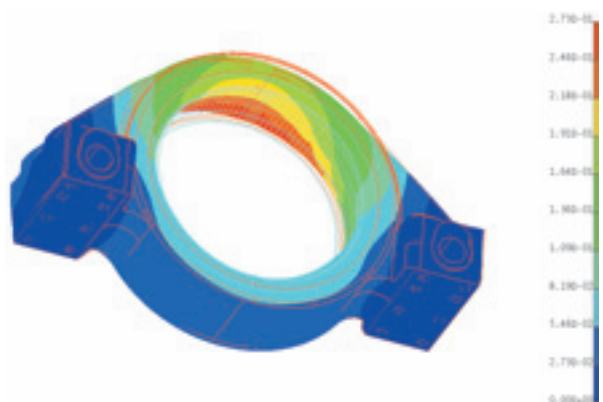


**Fig. 18** Deformation of housing from underneath

rig is capable of testing a range of bearing and spacer dimensions and can vary its operating conditions (eg. running speed, lubrication conditions and jacket cooling capacity).

**Fig. 21** shows an example of thermal analysis.

When a bearing is running at a high speed, thermal analysis demonstrates how the heat is transmitted and how the resultant heat gradient appears.

During an early stage of this test, the results of the test rig thermal analysis were compared with the actual test data (temperature data from 14 test points shown in **Fig. 20**). In certain cases, the difference between these two results exceeded 5°C.

To minimize this difference, a tuning technique can be utilized to reduce the average error. After this tuning technique is applied, the average difference between the thermal analysis and actual test data falls in a range of  $\pm 1^\circ\text{C}$ . (Tuning for a case in **Fig. 21** is primarily intended for thermal conductivity.)

The acquisition of basic data using a test rig as shown in **Fig. 19** involves a lot of equipment set-up time, and the corresponding data acquisition also requires many man-hours.

Currently, it is difficult to achieve perfectly accurate temperature estimation by thermal analysis only (i.e. without performing an actual test). Nevertheless, NTN will further accumulate theoretical data and improve its thermal analysis technique to achieve better approximation of the estimated temperature and develop improved techniques with other test rigs.

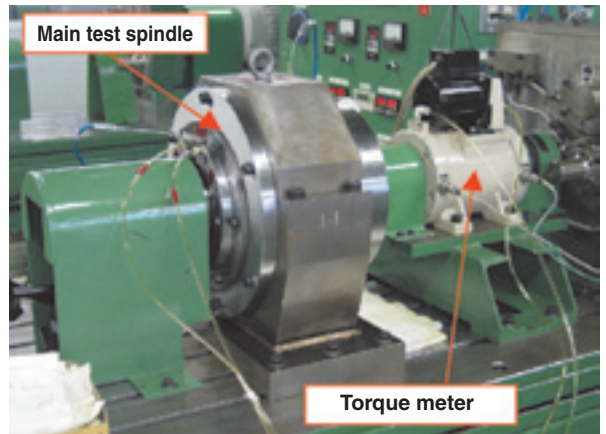


**Fig. 19** Test equipment

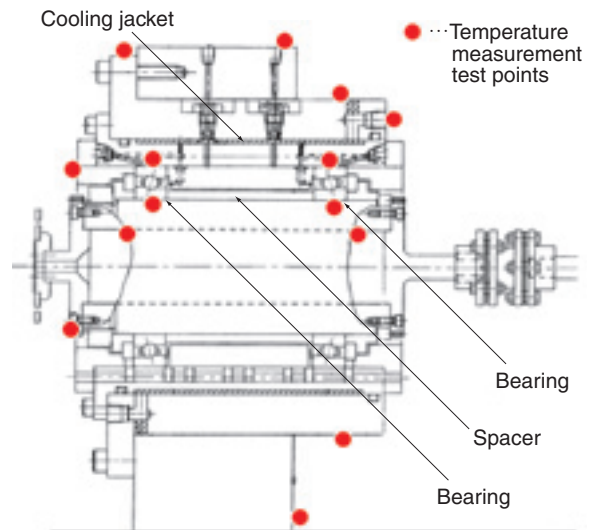


**Fig. 20** Test equipment layout

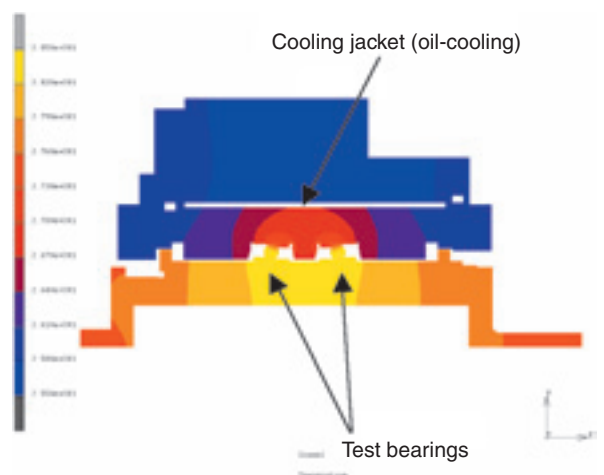


**Fig. 21** Thermal analysis (estimated temperature distribution)

## 4. Conclusion

One of recent trends of machine tool manufacturers is the increased use of 3D CAD-based design and development. For this reason, there have been increasing requests for 3D CAD data for bearings used in machine tool applications (including main spindles, feed axis and table axis).

In response to numerous inquiries from machine tool manufacturers, NTN has started supplying 3D CAD data (in the form of an electronic catalog) for the most popular precision bearings from the ULTAGE Series. Included in this new electronic catalog are angular contact ball bearings and cylindrical roller bearings (a total of 1329 bearing base part numbers).

By using 3D CAD data, all customer personnel can more easily interpret the information listed on bearing drawings. Thus, every detail of the bearing design can be confirmed and be clearly understood. Furthermore, by importing the 3D CAD data into stress analysis and thermal analysis, the application can be analyzed even further to ensure that the bearing design is optimized.

This report presented some examples of NTN's analysis techniques. Incidentally, machine tool manufacturers have been utilizing various analysis methods to facilitate higher precision requirements, more severe application conditions and a shorter development period for new machine tool bearings. Consequently, NTN believes that machine tool manufacturers will ultimately develop new machines that make use of these advanced analysis techniques.

NTN hopes that its new 3D CAD Data Electronic Catalog will help develop the machine tools of the future.

Photo of author

---



Takehiko UMEMOTO

Product Design Dept.  
Industrial Sales  
headquarters

## ULTAGE Series

### Large, Long-lasting Double-row Cylindrical Roller Bearings for the Main Spindles of Large Turning Machines

Naota YAMAMOTO\*



NTN has responded to the need for improved efficiency, reliability, quality and environmental responsibility for machine tools by developing the ULTAGE Series of super-high-speed precision bearings. NTN has developed a new long-life double-row cylindrical roller bearing for large turning machines as one part of the ULTAGE Series product line. Long life is accomplished by optimization of the internal design and adoption of a lightweight, high-strength modified PPS resin cage.

Furthermore, grease reservoirs inside the cage pockets extend the lubrication life to more than 5 times that of the current bearing (including high strength brass cage). This paper outlines the development process.

## 1. Introduction

Double-row cylindrical roller bearings are widely used on machine tool main spindles that must satisfy requirements for high rigidity and high accuracy, and typical examples of such machine tools are turning centers and machining centers. As machine tools are increasingly sophisticated and cutting operation has to be performed more efficiently, their main spindles need to have longer life. Recently, in particular, demands for large machine tools have been mounting; consequently, the needs for higher speed, advanced sophistication and longer life have been ever increasing for use as main spindle bearings on large turning centers.

Our recently developed NN30xxHSRT7 Series large size double-row cylindrical roller bearings are intended for use as main spindle bearings on large turning centers.

## 2. Features

### (1) Adoption of special PPS resin cage

NTN has already been marketing highly rigid PEEK resin cages for bearings up to medium sizes. The primary applications for medium sized bearings in the market are turning centers and machining centers.

Machining centers in particular are often operated in the super high-speed range; therefore, their main spindle bearings use PEEK cages which have excellent rigidity. Large sized bearings in contrast, being mainly used in turning centers often employ cages made of a special PPS resin that is readily injection-molded and boasts lower material cost.

### (2) Optimized internal design

#### ① Grease reservoirs in cage bars

In many cases, large size bearings for machine tools are grease-lubricated; to help extend grease life in the bearing, we have incorporated two types of grease reservoirs into the cage bars (see **Figs. 1** and **2**).

Grease reservoirs in the outside surface of the cage supply grease to the crowned area of each roller, while the grease reservoirs in the bore side not only retain grease, but also help prevent the leading edges of each cage bar from coming into contact with the rollers during high-speed operation of the bearing.

#### ② Thicker cage ring and increased inner ring center rib width

A cage ring of increased wall thickness has been adopted to increase rigidity of the cage, mitigating deformation of the cage bars during high-speed bearing operation.

\*Product Design Dept. Industrial Sales headquarters

In addition, adoption of a wider rib on the inner ring helps increase the space between rows in the middle of the bearing and an increased quantity of grease can be retained, leading to extended grease life (see **Figs. 1** and **2**).

**Fig. 3** shows an example of result of FEM analysis of the cage design, and **Fig. 4** graphically plots the amount of radial displacement based on FEM analysis results at  $d_{m\Omega} 75 \times 10^4$ . With the old design in these diagrams, the ratio of ring thickness to roller length

falls in a range of approximately 20% to 30%, and rigidity of the cage is low in high-speed operation, resulting in a high degree of cage deformation. In contrast, with our new bearing design, the ratio of ring thickness to roller length falls in a range of approximately 30% to 40%, thereby rigidity of the cage is increased in high-speed operation and resultant deformation of the cage is small.

The amount of deformation of our new cage design is approximately half that of the old design; thus, it

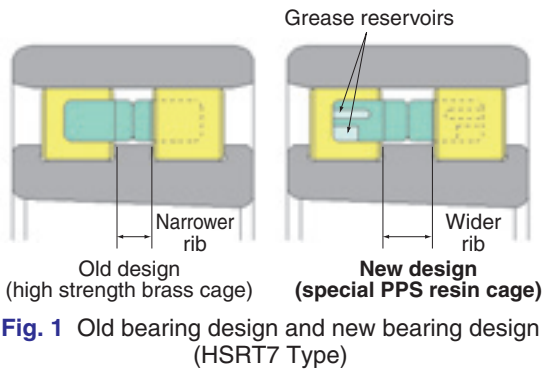


**Fig. 1** Old bearing design and new bearing design (HSRT7 Type)

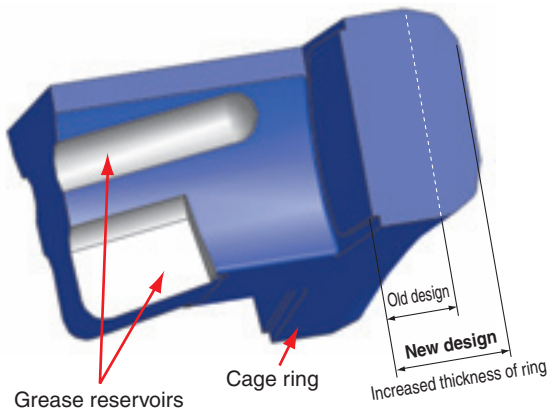


**Fig. 2** Drawing of the cage

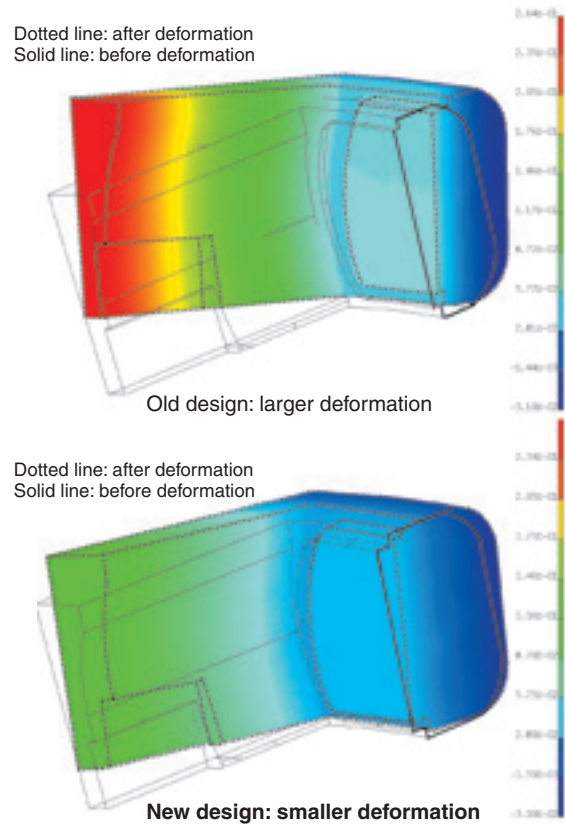


**Fig. 3** FEM analysis of deformation (NN3028K,  $d_{m\Omega} 75 \times 10^4$ )

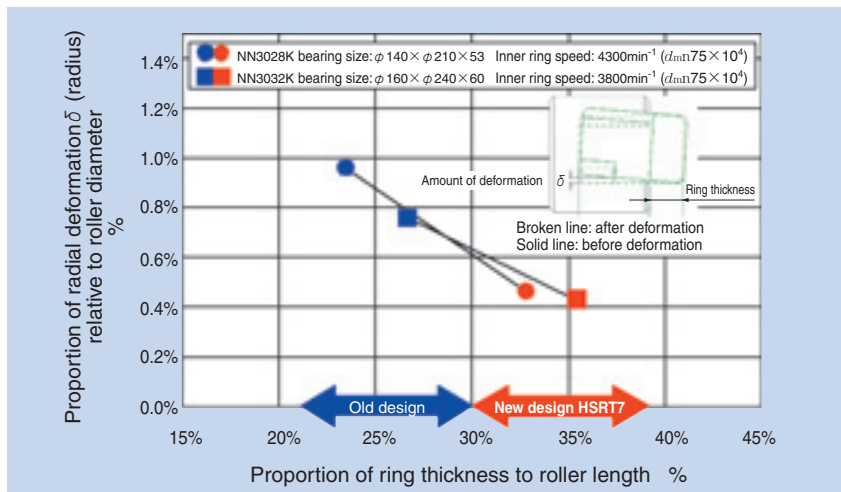


**Fig. 4** Relation between width of ring and deformation (FEM analysis of deformation)

should be understood that our new design can more positively limit heat generation resulting from contact between rollers and cage in high-speed operation.

### 3. Results of grease lubrication test

#### (1) Performance test

Fig. 5 graphically plots the results of temperature increase at the bearing outer ring. Temperature increase at the outer ring of our new bearing design is less apparent compared with that of the benchmark bearing having a high strength brass cage. With our new design, the bearing speed that corresponds with temperature increase of approximately 20°C on the outer ring is 6,500 min<sup>-1</sup> ( $d_{m\Omega} = 114 \times 10^4$ ); with the old design having high strength brass cage, the speed corresponding with a similar temperature increase is 4,500 min<sup>-1</sup> ( $d_{m\Omega} = 79 \times 10^4$ ). In other words, the maximum permissible running speed of our new design is 45% greater compared with the old design.

#### (2) 2,000 hours continuous endurance test

Two sizes of our new design (bore diameters  $\phi$  140 mm and  $\phi$  160 mm) have been subjected to a 2,000 hour endurance test, with samples of each sizes successfully completing the test (test conditions applied are as follows: running speed  $d_{m\Omega} = 75 \times 10^4$ ,

post-assembly radial internal gap: -5  $\mu$ m, grease: urea-based grease, jacket cooling: synchronized with room temperature).

The appearance inside the cage after completing the test is positively acceptable; grease remains in the grease reservoirs in the cage bars and the bearing samples of our new design are judged capable of further continuous operation (Photo 1).

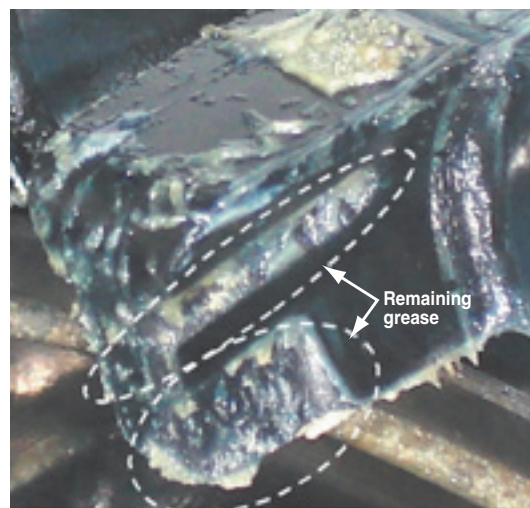


Photo. 1 Condition of grease in the reservoirs after 2000 (h) of endurance test

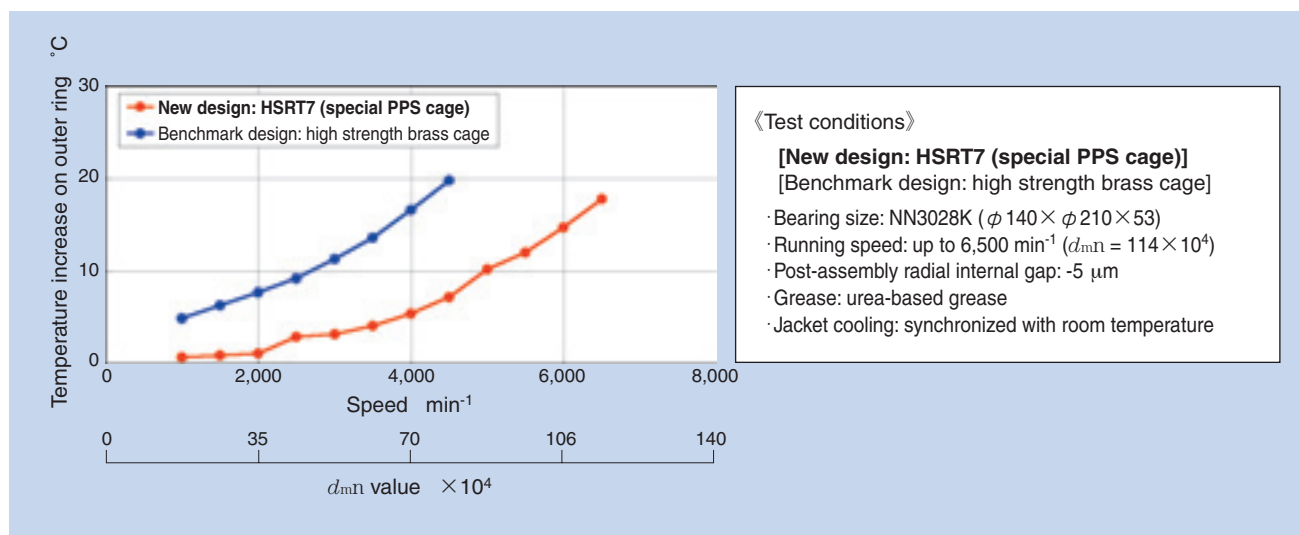


Fig. 5 Temperature raise test results at grease lubrication

**(3) Rapid acceleration/deceleration test**

Fig. 6 presents rapid acceleration/deceleration test conditions. One cycle consists of a rapid acceleration phase, constant speed operation phase, rapid deceleration phase and standstill phase. This cycle, simulating actual operation pattern of the bearing, was repeated one hundred thousand times in order to verify 100-thousand cycle endurance of the cage. After completion of the rapid acceleration/deceleration test, the bearing performance test was conducted again to verify that temperature increase behavior of the samples exhibited no problems and that the bearing and cage of our new design having undergone repeated tests are free from any problems (Photo 2).



**Photo. 2** Condition of cage after 2000 (h) of rapid acceleration and slowdown test

**4. Conclusion**

Our newly developed ULTAGE Series double-row cylindrical roller bearing NN30xxHSRT7 products, which are grease-lubricated, have achieved longer life in continuous endurance test at  $d_{mN} 75 \times 10^4$ . NTN believes that this new development will positively fulfill the market needs for much faster main spindles in large turning center applications.

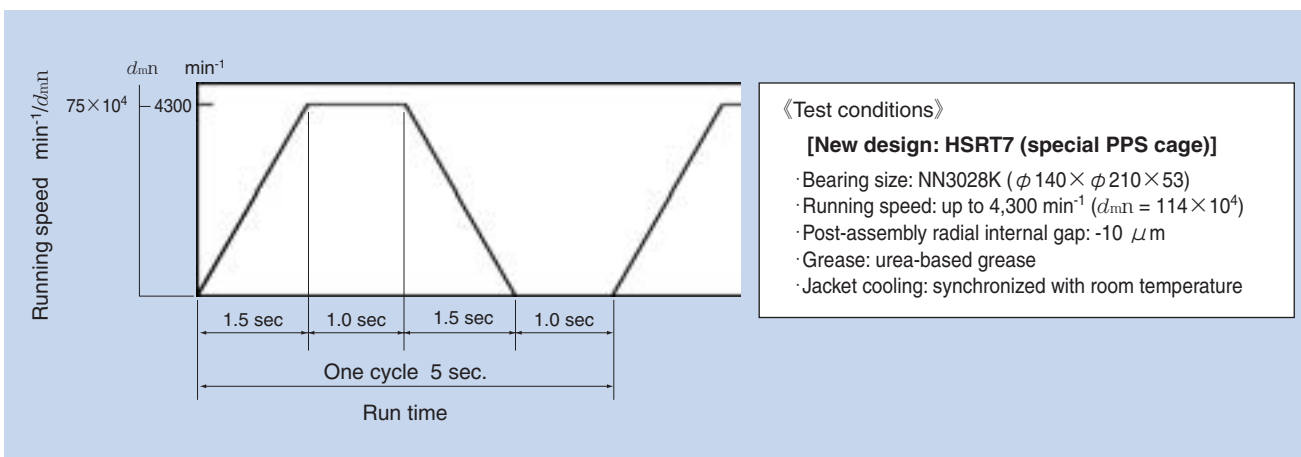


**Fig. 6** Rapid acceleration and slowdown test condition at grease lubrication

Photo of author



Naota YAMAMOTO

Product Design Dept.  
Industrial Sales  
headquarters

## Technical Trends in Wind Turbine Bearings

Souich YAGI\*  
Nobuyuki NINOYU\*\*



The ecologically friendly wind power industry, which emits no carbon dioxide and utilizes the renewable power of wind, is growing remarkably. The industry is in a new stage of size increases to the turbine and performance enhancements as large wind farms begin to be placed offshore.

Because they help reduce friction and power losses in the drivetrain bearings are an important component in wind turbines. This paper will cover the evolving technology and special features found in bearings destined for wind turbines.

### 1. Introduction

For many years NTN has been supplying bearings to the wind turbine industry. This paper will describe the features, drawbacks and technical trends for these bearings. Specifically this paper will focus on the bearings found on the main shaft, in the gearbox, in the generator and in the yaw drive.

### 2. Increases in wind turbine size

The wind turbine industry offers a variety of turbines configurations with both horizontal and vertical shaft alignments as well as models that do not include a gearbox. In general though the vast majority of industrial scale wind turbines (generally speaking machines that generate more than 500 kW of power) use a three bladed rotor on horizontal shaft connected to a gearbox that drives a generator. **Fig. 1** illustrates the nacelle from a typical wind turbine. Inside the nacelle are the mainshaft support bearings, gearbox, induction generator and the yaw drive system. With this mechanism, the energy in the wind used to turn the rotor. This rotation is passed through a gearbox that increases the shaft speed and then passed into a generator where the electricity is produced.

With any given wind turbine, the amount of electrical power generated is proportional to the square of the

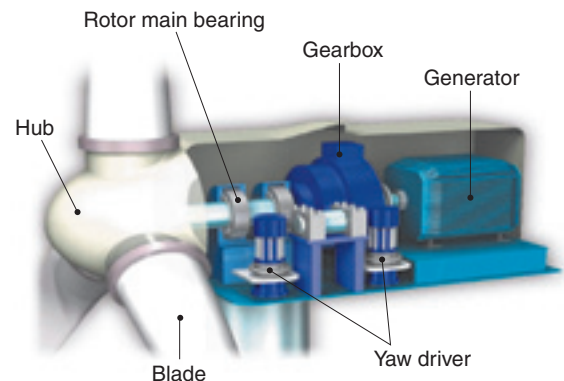


**Fig. 1** Nacelle

blade length. Accordingly large wind turbines feature increasing blade lengths. This increase in length was possible due to improvements in blade materials which allow the blades to remain a one-piece component.

**Fig. 2**<sup>1)</sup> graphically presents the trend in maximum output and rotor diameter for wind turbines from 1991 to 2007.

The largest wind turbine currently in existence is a 5 MW unit featuring a rotor diameter of 126 m.

According to statistic data by BTM Consult ApS, a Danish consulting firm, the average rated output of the wind turbines installed around the world stood at 1.28 MW in 2005, 1.42 MW in 2006 and 1.49 MW in 2007.

\*Industrial Engineering Dept.

\*\*Application Engineering Dept. Industrial Sales headquarters

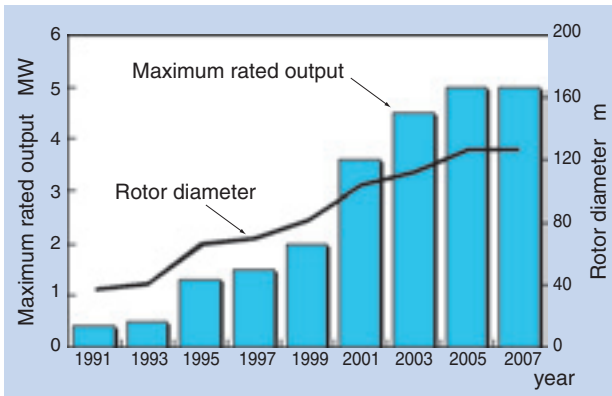


Fig. 2 Upsizing of wind turbines<sup>1)</sup>

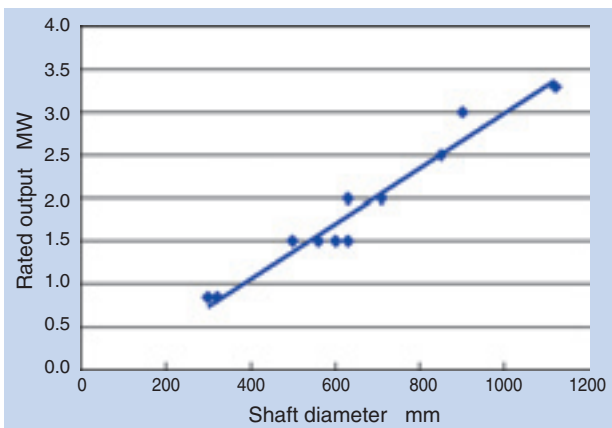


Fig. 3 Wind turbine capacity and bearing size

As larger wind turbines have been adopted, larger sized main bearings are needed to support the larger rotors. Fig. 3 graphically plots the relation between rated output of a wind turbine and main bearing size.

### 3. Main shaft bearing

#### 3.1 Selection of the main shaft bearing

In a wind turbine the weight and rotation of the rotor blades applies a load to the main shaft bearing. The wind turbine manufacturer considers the normal operating conditions for the wind turbine and assumes certain equipment failure modes when calculating the loads applied to the main shaft bearing and presents the results to the bearing manufacturer. Note that a special program has been developed for this process according to the guidelines set up by the International Electrotechnical Commission (IEC)<sup>2)</sup> and Germanischer Lloyd (GL)<sup>3)</sup>.

International standards, including ISO, IEC and GL, have settled on a minimum acceptable calculated life for the main shaft bearings of 175,000 (20 years). Additionally a safety factor of at least 2.0 is required (safety factor = static load rating/static equivalent load).

Bearing life is calculated using the following equation.

$$L_{nmh} = a_{ISO} \times \frac{10^6}{60n} \left( \frac{C}{P} \right)^p$$

$a_{ISO}$ : life correction coefficient

$n$ : rotating speed ( $\text{min}^{-1}$ )

$C$ : basic load rating [N]

$P$ : dynamic equivalent load [N]

$p$ :  $p = 3$  for ball bearing,  $p = 10/3$  for roller bearing

ISO 281, the international standard for calculating the life of bearings, was revised in 2007. The revision introduced a coefficient,  $a_{ISO}$ , which accounts for various factors that influence bearing life including fatigue limit load, lubrication conditions and contamination in the lubricating oil. Based on this new coefficient, NTN is performing bearing life calculations with a special program that considers the displacement of the shaft, rigidity of the housing, bearing internal clearance and fatigue limit load of the shaft system. This process results in a more reliable calculation for the main shaft bearings.

The load working on a wind turbine can randomly fluctuate depending on local wind conditions. To allow analysis of the wind turbine system the loads are broken down into a Load Duration Distribution (LDD). The LDD takes the loads that the turbine encounters and divides them into a number of segments (usually between 100 and 300). The amount of time spent at each load segment is also determined. Each segment is referred to as a "Bin". The bearing life is then calculated for each Bin, after which a statistical process is used to determine the overall bearing life.

Fig. 4 illustrates the results of a deformation analysis performed on the housing and bearing outer

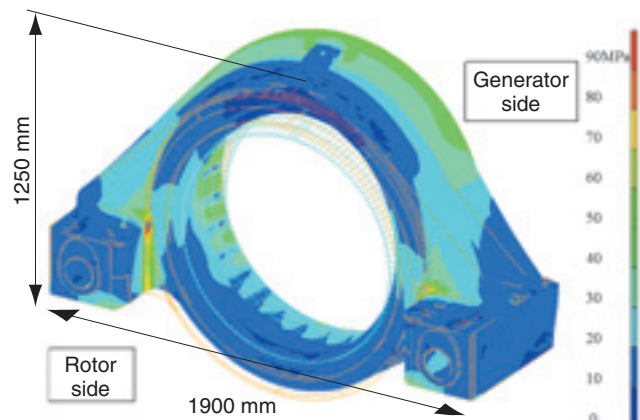


Fig. 4 Analysis example of main bearing

ring for a main shaft using a self-aligning roller bearing. By investigating the effects that deformation in the housing has on radial clearance, the load distribution of the rolling elements and consequently bearing life the design of the bearing can be optimized. Furthermore, NTN has expanded the scope of analysis to include the base where the housing and gearbox are installed in order to develop a more reliable design specification.

### 3.2 Main shaft configurations and associated problems

Various main shaft configurations are available for wind turbines. **Table 1** summarizes three typical main shaft configurations.

#### <Type A>

This is the most common configuration and uses two bearings. The main shaft uses a self-aligning roller bearing while the inside of the gearbox uses a full complement cylindrical roller bearing. To prevent the bearing mounted in the gearbox from receiving axial load from wind, the axial play in the self-aligning roller bearing needs to be smaller than that of the gearbox bearing. Furthermore, the effect that temperature has on bearing internal clearance and bearing-shaft fit needs to be limited in order to improve reliability.

NTN is supplying a unique self-aligning roller bearing for the blade side bearing where the internal clearance has been reduced to a special smaller clearance range.

NTN design practice aims to maintain the internal clearance on a bearing at an appropriate level while

limiting the axial play in order to improve reliability. At the same time, the NTN self-aligning roller bearing is a design that tolerates high dynamic and static mounting errors. These errors come from such factors as dynamic deflections of the nacelle frame and shaft due to the wind load as well as vibration caused by mounting misalignment between the main shaft and gearbox.

#### <Type B>

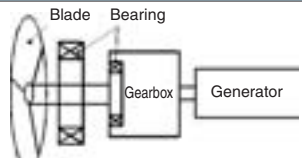
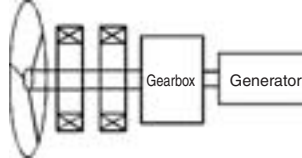
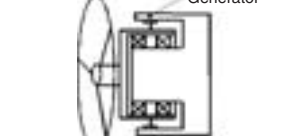
This configuration mounts two bearings on the mainshaft. This configuration is more common with the higher loads seen in larger (2 MW+) wind turbines. When a double-row tapered roller bearing is used as the blade-side bearing, the bearing is preloaded to limit the axial play in the shaft as well as fretting within the bearing. However the design cannot tolerate the high mounting errors that the self-aligning roller bearing can, requiring a higher degree of mounting accuracy.

#### <Type C>

This configuration is used in direct drive wind turbines that eliminate the gearbox. A generator is mounted on the outer surface of the bearing and the outer ring is rotated (compared to the inner ring in Types A and B) directly driving the generator. The rotor is supported with two bearings. When this bearing configuration is grease-lubricated, a special lubricating scheme is adopted and a special cage is used to allow grease to readily enter the bearing.

When tapered roller bearings are used, temperature differences between the inner ring and outer ring can affect the internal clearance of the bearing. This could

**Table 1** Construction of the main shaft

	Drivetrain layout	Blade-side bearing	Generator-side bearing	Features
Type A		SRB	CRB FCCRB (NFV type)	<ul style="list-style-type: none"> <li>Induction generator with gearbox</li> <li>Generator-side bearing also functions as input bearing for gearbox.</li> </ul>
Type B		SRB TRB DTRB	SRB TRB CRB	<ul style="list-style-type: none"> <li>Induction generator type with gearbox</li> <li>Two bearings support main shaft.</li> </ul>
Type C		TRB DTRB	TRB CRB	<ul style="list-style-type: none"> <li>Synchronous generator without gearbox</li> <li>Rotating outer ring</li> </ul>

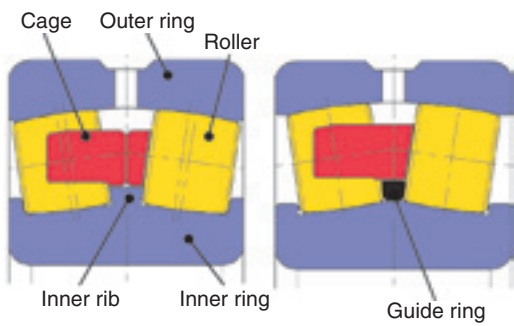
SRB: Self-aligning Roller Bearing    CRB: Cylindrical Roller Bearing    FCCRB: Full Complement Cylindrical Roller Bearing  
 TRB: Single-row Tapered Roller Bearing    DTRB: Double-row Tapered Roller Bearing

either result in excessive preload, which can shorten bearing life or excessive internal clearance which can trigger fretting inside the bearing. To avoid these problems, careful considerations need to be made including a heat transmission analysis for the bearing housing and peripheral members.

### 3.3 Features of self-aligning roller bearings for the main shaft

Currently many wind turbines use a self-aligning roller bearing for supporting the main shaft. The NTN self-aligning roller bearing (Fig. 5: Asymmetrical roller design) has a fixed rib at the center of the inner ring to reliably guide the rollers, even in fluctuating wind conditions. Competing self-aligning roller bearing designs (Fig. 5: Symmetrical roller design) use a central floating guide ring.

Fig. 6 illustrates the results of a torque analysis on a self-aligning roller bearing commonly found in 1.5 MW turbines (NTN part number 240/600B, boundary dimensions:  $\phi 600 \times \phi 870 \times 272$  mm). The bearing operated under wind velocities of 8 m/s and 16 m/s.



Asymmetrical roller design (NTN Design) Symmetrical roller design

Fig. 5 Spherical roller bearing

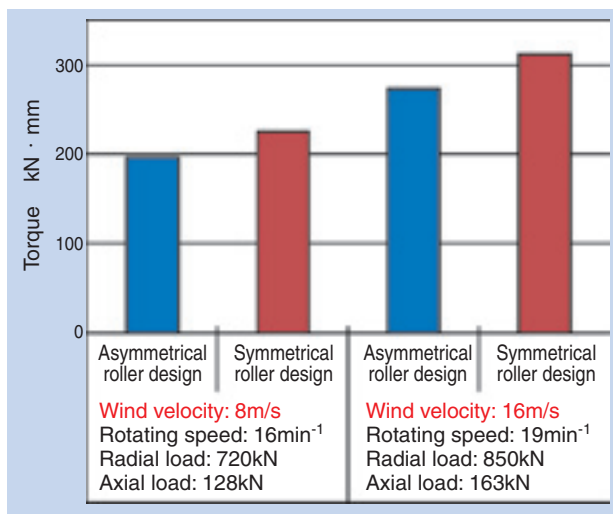


Fig. 6 Torque of the bearing and wind velocity

When compared to a bearing that uses symmetrical rollers, the NTN design exhibits lower torque for both wind velocity conditions. As a result of this analysis, it has been verified that the NTN design offers a stable guiding arrangement for the rollers by limiting tilt and skew in the rollers (factors that would increase torque). With the lower torque in the NTN design comes lower heat generation when compared with the symmetrical roller design. Because a main bearing on a wind turbine has to carry an axial load from the rotor, the NTN design is capable of stable operation with lower torque and limited heat generation.

## 4. Gearbox

The gearbox increases the shaft speed of the rotor (10-30 min<sup>-1</sup>) to a higher speed for the induction generator (usually, 1200-1800 min<sup>-1</sup>) by using a series of gears.

A gearbox is a critical component in many wind turbine designs, and standardization for this component has long been attempted. The current guideline for gearboxes was formulated by the American Gear Manufacturers Association (AGMA)<sup>4)</sup> Recently the need for the development of an international standard for gearboxes has been mounting. Therefore, a joint working group consisting of the IEC and ISO has been developing a new standard.

Fig. 7 illustrates the layout of a typical gearbox. Rotation from the rotor (input shaft in the figure) drives the carrier of the planetary gears, which then drives the low-speed shaft then the intermediate shaft and finally the high-speed shaft. At each step the rotational speed is increased resulting in a higher output speed. Table 2 summarizes the bearing types used in various locations of the gearbox.

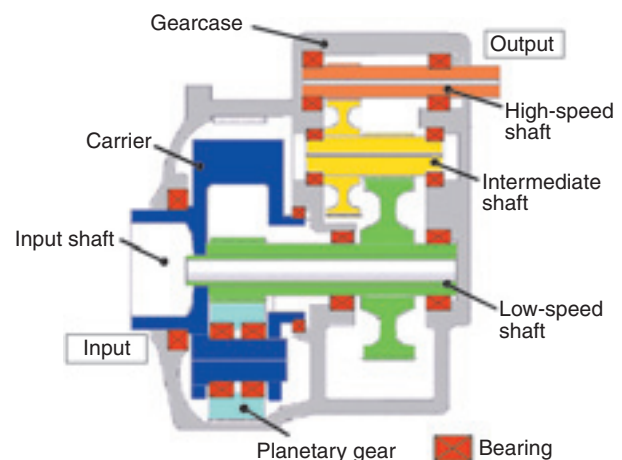
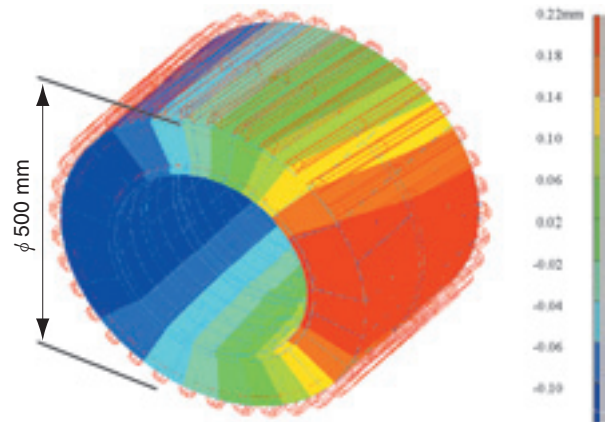


Fig. 7 Construction of the gearbox

**Table 2** Bearing type for gearbox <sup>4)</sup>

Area	Bearing type	
High-speed shaft	Fixed-side	SRB, CRB, TRB, BB, 4PCBB
	Free-side	SRB, CRB, BB
Intermediate shaft	Fixed-side	SRB, CRB, TRB, 4PCBB
	Free-side	SRB, CRB
Low-speed shaft	Fixed-side	SRB, TRB
	Free-side	SRB, CRB, FCCRB
Planetary gear	SRB, CRB, FCCRB, TRB	
Carrier	FCCRB, SRB, TRB	

SRB: Self-aligning Roller Bearing CRB: Cylindrical Roller Bearing  
 FCCRB: Full Complement Cylindrical Roller Bearing TRB: Tapered Roller Bearing  
 BB: Deep Groove Ball Bearing 4PCVBB: Four Point Contact Ball Bearing



**Fig. 8** Analysis example of planet gear

Recently, the input torque on gearboxes has been increasing as a result of larger wind turbine designs. To keep pace the size of the carrier and planetary bearings have also been increasing. In an effort to reduce weight in the gearbox the outer ring on certain planetary designs has been eliminated with the gear bore surface being used as the outer raceway surface. Other designs are using two stage planetary gearing to reduce weight.

**4.1 Gearbox bearing selection**

**Table 3** summarizes the design criteria that go into selecting gearbox bearings. The two design criteria are contact stress and required life. The actual design criteria vary depending upon the location within the gearbox.

To support planetary gearing it is common to use two rows of bearings, usually cylindrical roller bearings, in the planet gears. To select the proper bearings it is necessary to consider deformation in the planetary gearing as a result of the loads transmitted between the sun gear and ring gear.

To illustrate this process the analysis performed on a planet gear from a 1.5 MW turbine is presented. The planet gear used two double row cylindrical roller bearings (4 rows total). The analysis examined the deformation in the gears and bearings as well as how well the load is distributed in each row.

**Fig. 8** illustrates the deformation on the planet gear and bearing under maximum torque conditions. **Fig. 9** shows the load distribution in each row after accounting for the deformation found in **Fig. 8**.

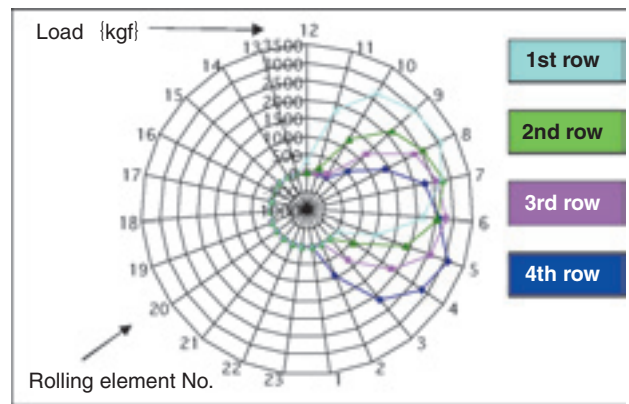


**Fig. 9** Load distribution of each 4-row

**Table 3** Maximum contact stress and required life <sup>4)</sup>

Position	Max. contact stress (MPa)	Required life $L_{10}$ (hours)
High-speed shaft	1300	30,000
Intermediate shaft	1650	40,000
Low-speed shaft	1650	80,000
Planetary gear	1450	100,000
Carrier	Not specified	100,000

**4.2 Common problems in gearbox bearings**

Because wind turbine gearboxes are located high in the nacelle the main gearbox requirements are high reliability, light weight and small size. The bearings on the planetary shaft, medium-speed shaft and high-speed shaft all see a complex series of loads consisting of both high axial and radial loads. Compared with a bearing for a low-speed shaft, these bearings have to feature not only greater load carrying capacity but also smooth high-speed operation.

To address these issues, NTN has developed a new bearing product, the separator style cage <sup>5)</sup> (**Fig. 10**). The bearing uses small separators for the cage and these separators hold the rollers in the bearing. The small separator allows for larger and/or more rollers, similar to a full complement bearing. The increased roller size and quantity allow the bearing to achieved a rated life more than 1.5 times greater than a conventional bearing with a standard cage (the envelope dimensions remain the same for both bearings). Additionally since there is a cage the rollers do not come in contact with each other. The lack of roller to roller contact means that the new bearing

avoids a major drawback of a full complement bearing—limitations in high-speed performance—and achieves maximum allowable speeds comparable to that of a standard caged bearing. Fig. 11 provides a comparison of the new NTN design with a standard caged bearing and a full complement bearing.



Fig. 10 High load capacity cylindrical roller bearings

striped pattern develops (Fig. 12) on the raceway and rolling surfaces. This can create severe vibration and the bearing will fail to function properly.

To address this issue NTN has developed an insulated bearing (Fig. 13). The outer diameter and both side faces of the outer ring undergo a thermal spray treatment, which applies a special ceramic coating. The resulting bearing will have a resistance of 100 MΩ or greater and a dielectric breakdown voltage of 2 kV or higher. Fig. 14 shows a cross-sectional view of the insulated bearing.

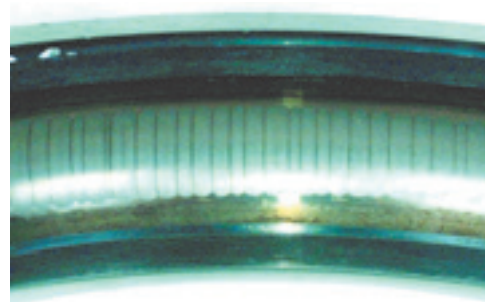
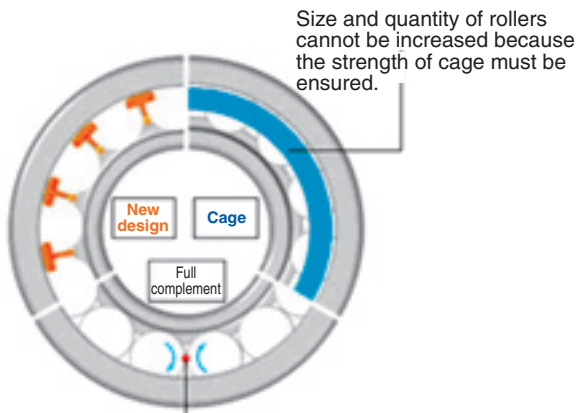


Fig. 12 Example of electrical pitting



Rollers rotating in reverse directions come into contact with each other, leading to greater frictional resistance.

Fig. 11 Comparison of structure

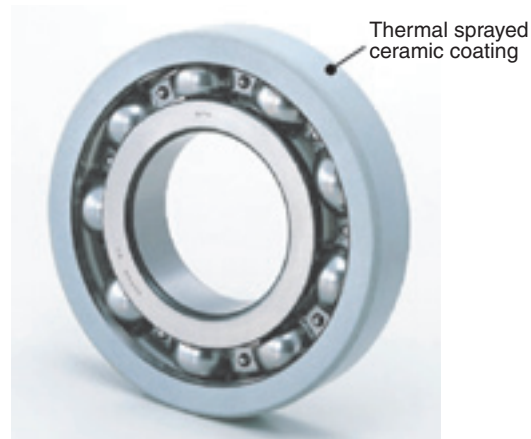


Fig. 13 Insulated bearing

## 5. Generator bearings

A grease filled, deep groove ball bearing is usually used to support the shaft in a generator. For a 1.5 MW size generator, the shaft diameter can exceed 150 mm.

Electrical pitting is a serious concern for any bearing used in a generator. Electrical pitting is damage that occurs on the raceway and rolling surfaces of the bearing due to the passage of electric current through the bearing. The current will create a spark at the point of contact between the rolling elements and raceway surface. When electrical pitting progresses, a

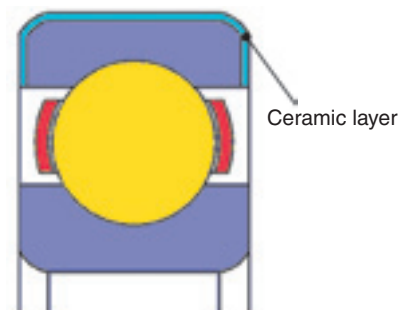
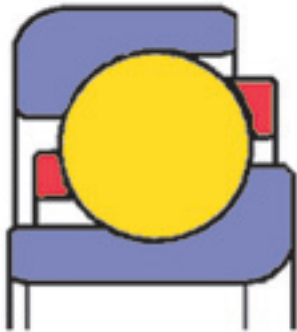


Fig. 14 Schematic of insulated bearing

## 6. Yaw drive bearing

In order to produce power the nacelle needs to always point into the wind. In order for the nacelle to rotate it rests upon a four-point contact ball bearing and a sliding bearing. These bearings carry the weight of the nacelle and rotor as well as any loads created by the wind. To power the nacelle's rotation a yaw drive is used. The yaw drive consists of an electric motor and a gearbox to reduce the motor's rotational speed. The gearbox in a yaw drive must be compact and capable of transmitting great torque. The bearings in the gearbox need to feature a low-profile design and higher rigidity to handle the moment loads applied from the pinion.

The angular contact ball bearing used for the main shaft in the yaw drive features a special design: the inner and outer rings have raceway surfaces with deeper grooves so that the bearing can support a greater axial load. **Fig. 15** shows a cross-sectional view of this special angular contact ball bearing. Note this design is capable of handling higher axial loads when compared to a standard angular contact ball bearings.



**Fig. 15** Schematic of angular contact ball bearing

## 7. Latest trends in wind power technology

### <Lighter weight>

A lighter nacelle design allows for a thinner wall thickness in the tower while still ensuring necessary design strength. This reduces costs for construction, installation and transportation of the wind turbine components. To aid in this effort the following industry efforts are profiled.

- 1) Improvements to main shaft design such as elimination of main shaft itself, adoption of a hollow main shaft, and lightweight design for the housing, among others
- 2) Incorporation of two-stage planetary gearing and helical gearing into the gearbox allowing for a

compact, lightweight design. This approach is very important for wind turbines of 2 MW or greater.

The demands for higher performance and smaller size have seen the development of a novel power train layout. The new hybrid wind turbine design combines a synchronous generator and a gearbox consisting of a single-stage planetary gear to achieve both higher performance and lighter weight.

Another wind turbine design employs a system of multiple generators to improve generator efficiency in low wind conditions. In this design the output from the generator is adjusted by operating only the needed generators. The main bearing in such a system is a large size tapered roller bearings.

### <Longer life>

For both main shaft and gearbox bearings maximization of load capacity is a key consideration for long bearing life. For generator bearings control of electrical pitting is important in realizing longer bearing life.

Offshore sites have recently attracted attention as locations for wind turbines. Compared to sites on land offshore sites boast better wind characteristics. In Japan, a nation not possessing a continental shelf, expectation is mounting for development of floating offshore wind turbines. Bearings used on a floating offshore wind turbine are subjected not only to wind loads but also to loads caused by oscillation of the floating structure. Therefore, these bearings must have a larger basic load rating when compared with bearing used on current land-based wind turbines.

Wind turbines are being designed to lower the amount of load that gets applied to the bearings to promote longer life. New wind turbine designs have been commercialized that cope with variations in torque when the wind turbine is braked or extreme wind conditions occur (such as those from a typhoon). The new designs may have a novel mechanism that switches from upwind mode to downwind mode to minimize the effects of wind load. A downwind style turbine may also be used.

To achieve longer bearing life, operating conditions also need to be considered. In addition to fatigue life other problems can occur to the main shaft bearings such as lightning-induced damage or seawater ingress from a faulty seal section. Improved bearing maintenance technique need to be implemented while at the same time the bearing design must allow for easy component replacement.

We believe that as the scale of wind farms has expanded it will become increasingly necessary to acquire the current operating condition of individual wind turbines. This will be achieved through the use of

automatic monitoring and fault detection systems. This will allow for the prompt detection of problems and immediate repairs.

## 8. Conclusion

The power output from wind turbines has been increasing year by year. The demands for highly reliable wind turbine products with longer life are increasing. Additionally the turbines must be able to withstand severe natural environments such as those found on offshore wind farms.

In the technical field of bearings the needs are mounting for not only standard designs but also special designs dedicated to wind turbines.

Through development and stable supply of its' products, **NTN** wishes to contribute to the development of wind power generation technology and to the prevention of global warming.

## References

- 1) 2007 2nd wind power generation system technology course materials: Japan Wind Energy Association
- 2) IEC 614000-1: Wind Turbines—Part 1: Design requirements, edition 3 (2005)
- 3) Germanischer Lloyd: Guideline for the Certification of Wind Turbines Edition 2003
- 4) ANSI/AGMA/AWEA 6006-A03: Standard for Design and Specification of Gearboxes for Wind Turbines
- 5) T. Ozu: High Load Capacity Cylindrical Roller Bearings, NTN Technical Review No.74 (2006)

## Photo of authors



Souichi YAGI

Industrial Engineering Dept.



Nobuyuki NINOYU

Application Engineering Dept.  
Industrial Sales  
headquarters

## NTN Sensor Units for Construction Machinery



Shoji ITOMI\*  
Hiroyoshi ITO\*

Recent construction machines use a lot of electronic controls and it is expected that in the near future an even greater variety of controls with more advanced technology will be used in construction machines.

NTN currently supplies a wide variety of sensor units for construction machine applications that support operation accuracy, efficiency and ease of maintenance.

This report introduces four types of sensor units that NTN has developed.

### Foreword

NTN has been developing various sensor units based on its processing technologies and experiences in precision bearings. These sensor units have been commercialized and are used in the areas summarized in **Table 1**. These provide higher precision, better efficiency and improved maintainability for construction machines.

This paper provides information about the following four types of sensor units.

**Table 1** NTN sensor units

NTN sensor	Subject being detected
Angle sensor unit	Detection of operating angle of boom and arm of hydraulic shovel and wheel loader arm, etc.
Rotation sensor-integrated bearing	Detection of rotation speed of driving hydraulic motor and electric motor
High-resolution rotation sensor-integrated bearing	Detection of high-performance rotation speed of driving hydraulic motor and electric motor
Magnetically operating iron particle sensor unit	Detection of quantity of iron particles in engine oil, transmission oil and axle oil

### 1. Angle sensor unit

An angle sensor unit for construction machines detects the operating angle of a joint of a boom, arm, etc. and monitors the position of bucket: then based on the detected joint angle, bucket position is controlled so that accurate excavation work is attained.

In 1993, NTN developed and commercialized an angle sensor unit for construction machines that provides the following advantages:

- 1. Excellent vibration and shock resistance performance**
- 2. Appropriate signal precision**
- 3. Excellent environment resistance (immunity against temperature change, water resistance, dust resistance)**
- 4. Excellent durability**

#### 1.1 Structure and features

**Table 2** summarizes product specifications of angle sensor units for construction machines.

The conventional product in **Table 2** was available before 1993, and is comprised of a shaft supported by a needle roller bearing. The shaft is coupled to the rotation shaft of a market-available potentiometer.

The disadvantages of this product may be summarized as follows:

\*Application Engineering Dept. Industrial Sales headquarters

- ① A needle roller bearing supports the shaft: this design cannot support an axial load.
- ② The rotation shaft of market-available potentiometer is supported by a simple sliding bearing: consequently, owing to the initial clearance on the sliding bearing and increase in the clearance resulting from wear, an excessively large load is applied to the brushes. When this sensor is installed to a construction machine and is subjected to severe vibration and/or shock, its brushes are repeatedly deformed and can eventually fracture.
- ③ Two shafts are coupled with a coupling: consequently, backlash occurs between the two shafts, and delay in response of potentiometer output for operating angle is unavoidable.

The "current product" in **Table 2** means a product NTN is currently mass-producing (**Photo 1**).

The brushes of the potentiometer are directly mounted to the shaft to eliminate backlash. In addition, the shaft is supported by a preloaded ball bearing to eliminate the axial clearance on the bearing. This provides a structure of higher bearing rigidity, thereby minimizing shaft displacement resulting from load, vibration and shock. As a result, sensor response to operating angle is improved, variation in brush pressure becomes smaller, positively preventing brush fracture and deterioration in precision of output signal.

The housing of the angle sensor unit consists of a casting to ensure mechanical strength, while the sensor shaft is provided with an oil seal to prevent ingress of water and dust. An O-ring is inserted between the plate at the bottom of unit and the housing to prevent ingress of water.

The new design in **Table 2** is a non-contact angle sensor unit developed by NTN in 2007 (**Photo 2**).

On this sensor unit, a combination of a magnetic sensor and a magnet detects a rotation angle. In place of brushes, the magnet is directly mounted to the shaft; and like with the current sensor unit, two preloaded ball bearings support the shaft in order to maintain rigidity of the shaft.

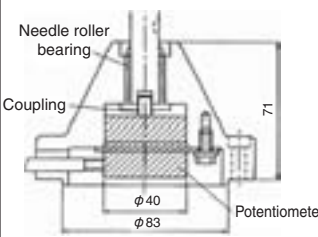
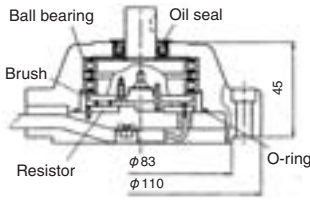
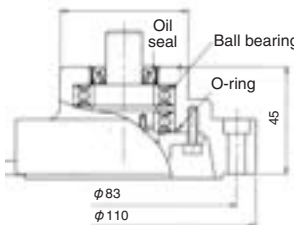


**Photo 1** NTN angle sensor unit (Analog type)



**Photo 2** NTN angle sensor unit (Digital type)

**Table 2** Specifications of angle sensor units

	Conventional sensor unit	Current sensor unit (NTN)	New design
Structure			
Sensor type	Potentiometer (contact)	Potentiometer (contact)	Magnetic sensor (non-contact)
Output signal	Analog	Analog	Analog or digital
Max. allowable load on shaft	Axial load is not carried.	$F_r : 1 \text{ kN}, F_a : 1 \text{ kN}$	$F_r : 1 \text{ kN}, F_a : 1 \text{ kN}$
Signal accuracy* (individual linearity)	2% max.	0.5% max.	0.5%以下

\* : Linearity of output signal relative to shaft rotation angle

The advantages of this new design are as follows:

- ① The sensor works on a non-contact basis. Consequently, loss in life and detection precision owing to worn brushes and substrate does not occur even during long operation, and problem occurring from fractured brush(es) is positively avoided.
- ② Either analog or digital (PWM or serial protocol) output signal can be used.
- ③ Rotation angle of up to 360° can be detected.

NTN is going to incorporate this non-contact angle sensor unit as a next generation angle sensor unit into many construction machines including hydraulic shovel and wheel loader.

### 1.2 Typical application

When installed to a hydraulic shovel to monitor the current bucket position, the new angle sensor helps the hydraulic shovel achieve safe and accurate excavation work (Fig. 1).

Delicate work such as excavation on slope, which was previously dependent on the skill of operator, can be executed by a less experienced operator through control of the bucket position.

Furthermore, use of digital sensor output signal helps limit the error in bucket position caused by noise interference, leading to more accurate excavation work.

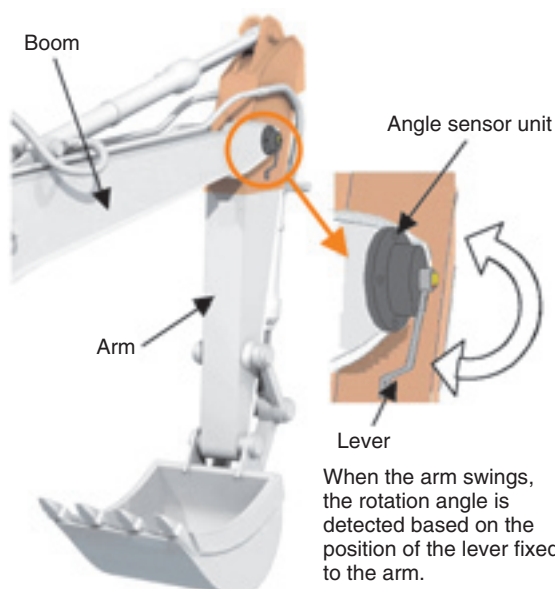


Fig. 1 The example of attachment of an angle sensor

## 2. Rotation sensor-integrated bearings

Rotation sensors are used for rotation speed control of AC/DC servo motors and hydraulic motors.

Previously, conventional sensors including magnetic gear speed sensor have been often used for driving AC/DC servo motors on battery forklift trucks. Recently, rotation sensor-integrated bearings, each being a unitized product comprising a deep groove ball bearing and a rotation sensor, have been more commonly adopted.

In the field of construction machinery, there have been needs for satisfying requirements of emission control and improved fuel economy. In an attempt to satisfy these needs, a development effort is in progress for a hybrid system that consists of an electric motor and a diesel engine. In this context, the demand for electric motors for construction machinery will increase, and the needs for rotation sensor-integrated bearings for this purpose will also increase.

### 2.1 Structure and features

Our rotation sensor-integrated bearing features a unique structure (see Fig. 2 and Photo 3). The inner ring side of a deep groove bearing is permanently fixed to a magnetic pulser ring (multi-pole permanent magnet) having alternately arranged N poles and S poles along its circumference. The outer ring is fixed to a magnetic sensor such as a Hall's IC\*.

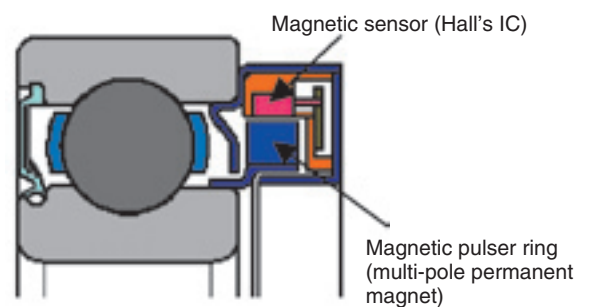


Fig. 2 Sectional view of integrated sensor bearing



Photo 3 Cut model of integrated sensor bearing

When the magnetic pulser ring rotates together with the inner ring and passes the vicinity of the magnetic sensor fixed to the bearing outer ring, the magnetic sensor detects variation in the magnetic field on the magnetic pulser ring (for example, change from N pole to S pole) and outputs a pulsed electric signal corresponding to the current bearing speed (repetition of High voltage and Low voltage levels) (see Fig. 3). By arithmetically processing this cycle, the bearing rotation speed can be determined.

The number of High and Low voltage signals repeated per rotation of the magnetic pulser ring coincides with the number of magnetic poles (N poles and S poles) on the magnetic pulser ring. As a result, with a larger number of the magnetic poles, the number of High and Low voltage signal pulses per rotation is greater, contributing to more accurate rotation speed control.

To be able to judge rotation direction of the shaft, two magnetic sensors used, one for phase A output and the other one for phase B output. These sensors are fixed such that the phase of electric signal output from one sensor is deviated by 90 degrees from that of the other sensor (see Fig. 3). By detecting the rising timings with pulses of these electric signals, it is possible to judge the rotation direction of the shaft.

Integration of a rotation sensor with a bearing provides the following advantages compared with conventional rotation sensors:

- ① **Sensor gap adjustment and alignment adjustment are not needed. The unit can be readily assembled into equipment.**
- ② **A bearing and a rotation sensor are unitized. Thus, axial space can be reduced.**
- ③ **The unit incorporating a magnetic sensor is immune to outside disturbances including dew condensation.**

Hall's IC\*: Hall's sensor having a built-in output transistor.

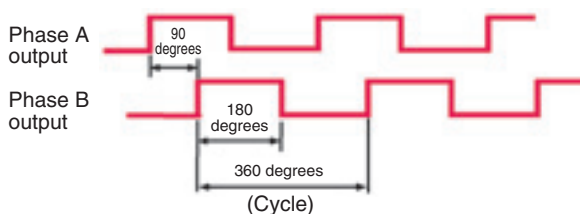


Fig. 3 Output signal of sensor

## 2.2 Typical application

A typical example of an application of an our rotation sensor-integrated bearing is the travel motor on a battery forklift truck is presented below. Fig. 4 schematically presents the control system for the travel servo motor, and Fig. 5 schematically illustrates a cross-sectional view of the servo motor complete with our rotation sensor-integrated bearing.

Let us describe the control scheme for the servo motor. The operator depresses the accel pedal, an electric signal corresponding to the amount of actuation with the accel pedal is transmitted to the motor controller, and then the motor controller sends an electric signal representing a command for controlling the rotation speed to the servo motor: at the same time, the rotation sensor mounted to the servo motor always correctly detects the rotation speed of the motor shaft with good response speed and sends a relevant electric signal to the motor controller: the motor controller compares the electric signal from the accel pedal with that from the rotation sensor, and controls the speed of servo motor.

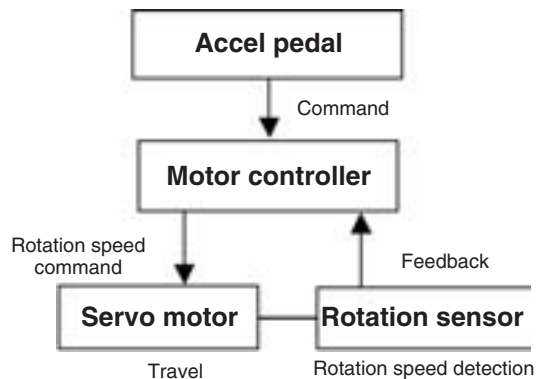


Fig. 4 Servo system of servo motor

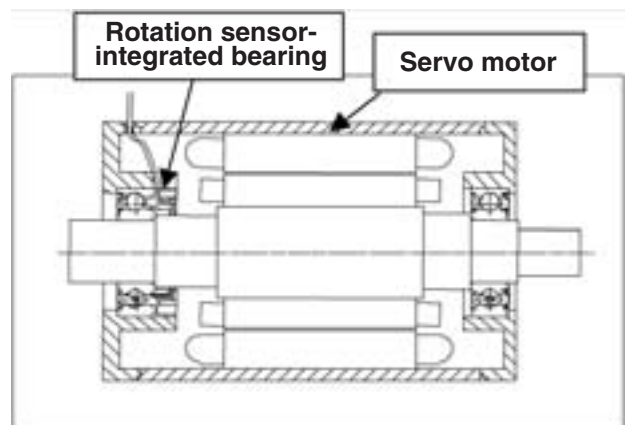


Fig. 5 Sectional view of servo motor

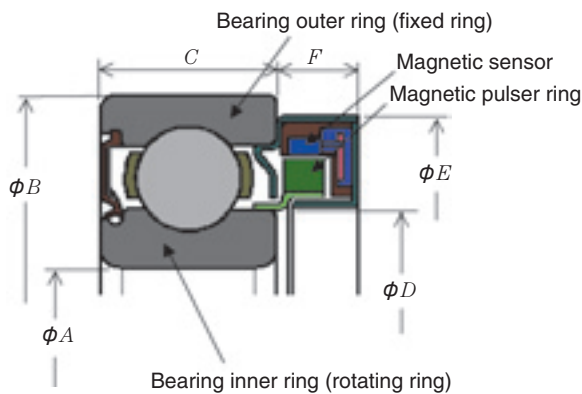
### 2.3 Series of NTN rotation sensor-integrated bearing products

**Table 3** summarizes the specifications of standard types of NTN rotation sensor-integrated bearing.

Other than the standard type, a magnetic field immune type is less prone to malfunction even if built into an electric motor, which generates a strong magnetic field, such as a high-torque motor and a high-temperature type that can be used at a higher temperature for example 150°C.

**Table 3** Specification of standard type of integrated sensor bearing

		Bearing number				
		6202	6204	6206	6208	6209
Number of output pulses		32	48	64	80	80
Bearing	$\phi A$	15	20	30	40	45
	$\phi B$	35	47	62	80	85
	$C$	11	14	16	18	19
Sensor	$\phi D$	18	29.5	40.6	53	57.3
	$\phi E$	32	46.6	58	75	77
	$F$	7.5				



### 3. High-resolution rotation sensor-integrated bearings

SNR, one of NTN group companies, has developed a unique magnetic sensor. Using this sensor, we have developed a "high-resolution rotation sensor-integrated bearing" whose rotation detection maximum resolution is 40 times higher than conventional sensors.

This sensor element comprises an IC on which several sensors are arranged, wherein the electric signal output from each magnetic sensor is appropriately processed in order to achieve higher resolution.

NTN's experiences in sensor mounting technology and conventional sensors produced a new sensor element with reduced dimensions.

**Fig. 6** illustrates a cross-sectional view of deep groove ball bearing 6202 (ID  $\phi$  15 mm, OD  $\phi$  35 mm). The bore diameter and outside diameter of our new sensor are same as those of conventional deep groove ball bearing 6202: however, the new sensor is capable of 1280 pulses per rotation. This is 40 times as many compared with the conventional sensor (32 pulses per rotation) (see **Fig. 7**).

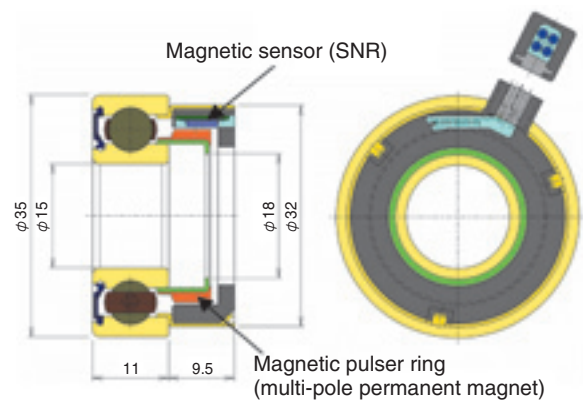


**Fig. 6** Sectional view of integrated high resolution sensor bearing



**Photo 4** External view of integrated high resolution sensor bearing

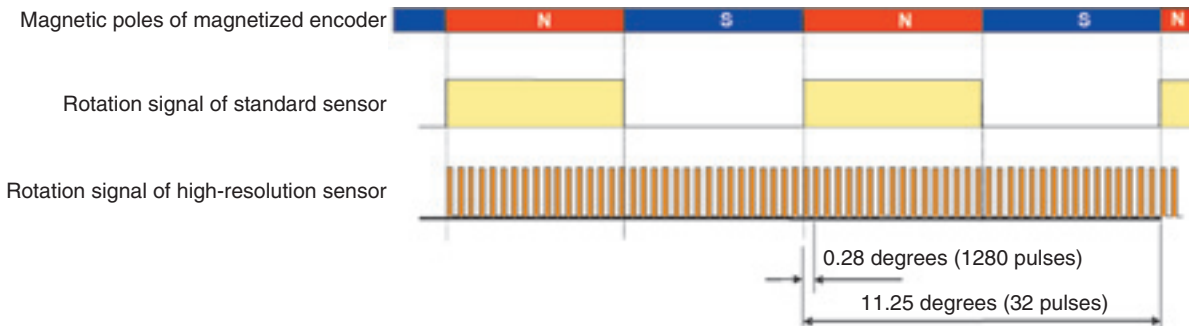


**Fig. 7** Comparison of rotational signal of standard sensor and high resolution sensor

The NTN high-resolution rotation sensor-integrated bearing has the following advantages:

- ① More precise rotation speed control is possible, compared with the conventional rotation sensor-integrated bearing.
- ② Our high-resolution sensor is a magnetic sensor. Thus, it boasts resolution as high as that obtained with an optical rotation sensor: as it is not adversely affected in a severe environment where mist or dust is present (an optical rotation sensor may not be used in such an environment).

#### 4. Magnetically operating iron particle sensor unit

NTN has developed a magnetically operating iron particle sensor unit that can detect quantity of ion wear particles in six levels (**Photo 5**). The iron wear particles occur from operation of transmissions and axles on construction machines. Certain machines used in construction sites or mines are operated 24 hours a day: therefore, use of this sensor unit may allow these machines to be maintained as necessary and improve their operation efficiency.

##### 4.1 Structure and features

**Fig. 8** schematically illustrates the structure of the new NTN magnetically operating iron particle sensor unit.

This unit is essentially comprised of a central electrode having an internal magnet and six rod electrodes arranged around the central electrode: when iron powder deposits between these electrodes, and if the electric resistance across electrodes drops below a particular level, the sensor unit outputs a signal. The level of output signal will vary in six settings depending on the quantity of iron particles deposited on the electrodes. In other words, this sensor unit attracts iron particles from the transmission oil and outputs a signal whose level is proportional to the quantity of attracted iron particles,

thereby the sensor unit detects the quantity of iron particles in the transmission oil.

**Fig. 9** illustrates an example of output pattern and associated quantities of deposited iron particles.

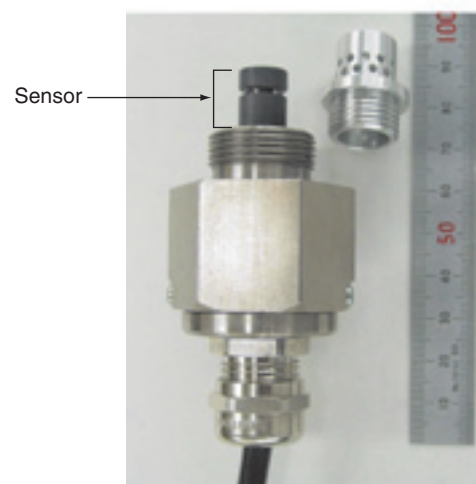
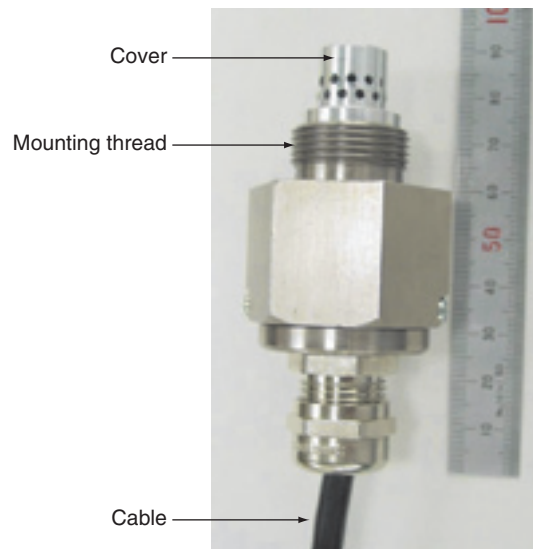


**Photo 5** Iron particle sensor (fixed type)

### 4.2 Typical application

NTN has so far developed two types of magnetically operating iron particle sensor unit: a fixed type (Photo 5), in which the sensor section is fixed to a vessel such as an oil pan, and a coupler type (Photo 6), in which the mount is independent of the sensor section and the sensor section can be coupled and uncoupled without causing oil leakage.

The coupler type allows the user to determine the quantity of iron particles deposition on the sensor section either based on sensor signal or through visual check. Also, the user can visually determine the size of wear particles. Fig. 10 illustrates a scheme for mounting the coupler type.

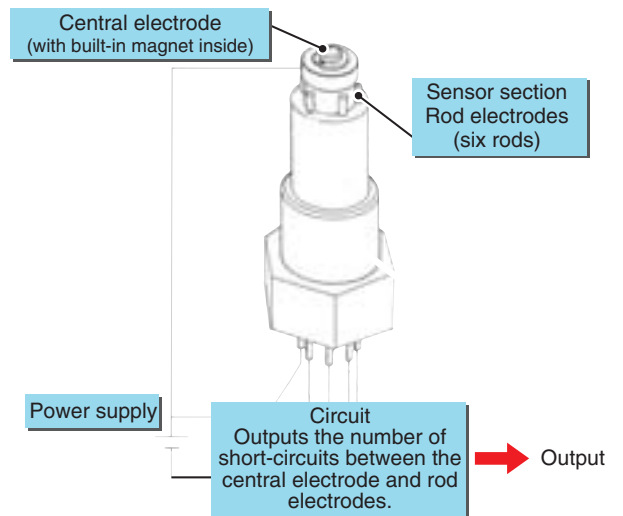


Fig. 8 Structure

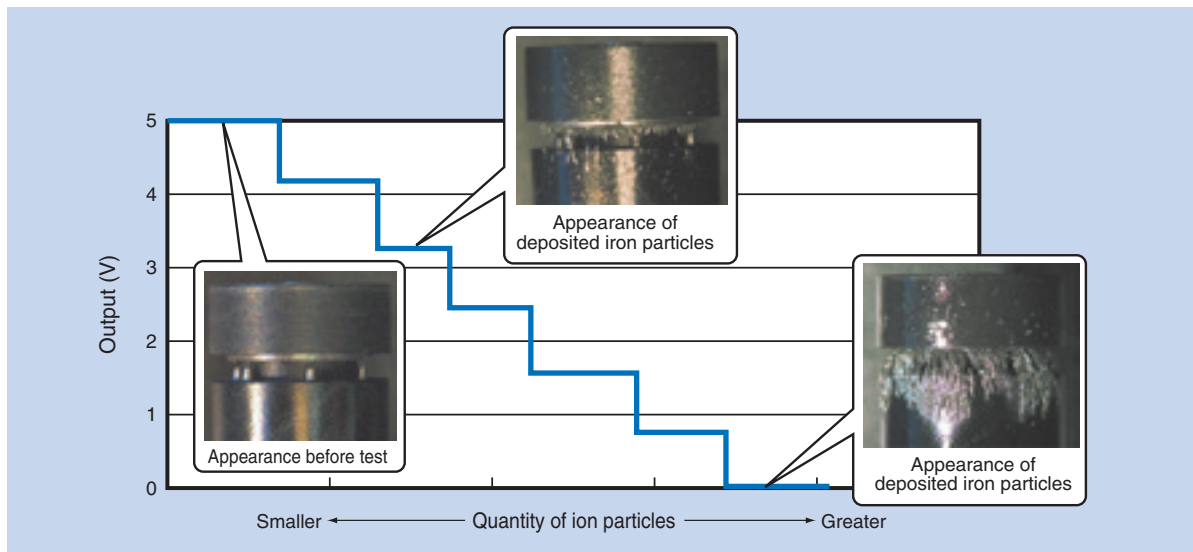


Fig. 9 Output signal and condition of iron particle

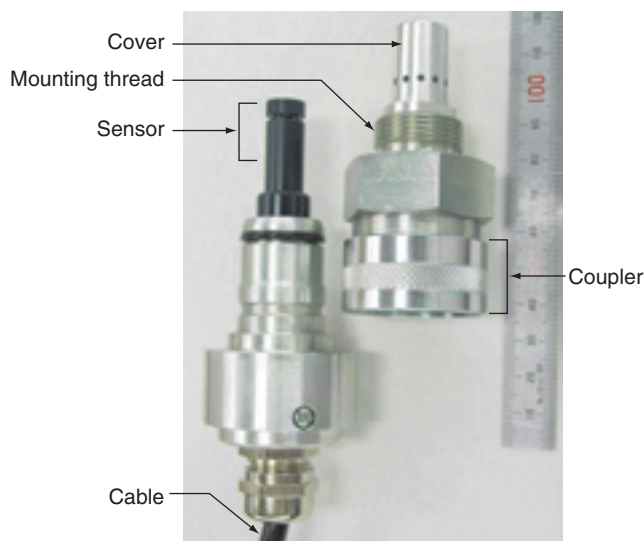


Photo 6 Coupler type

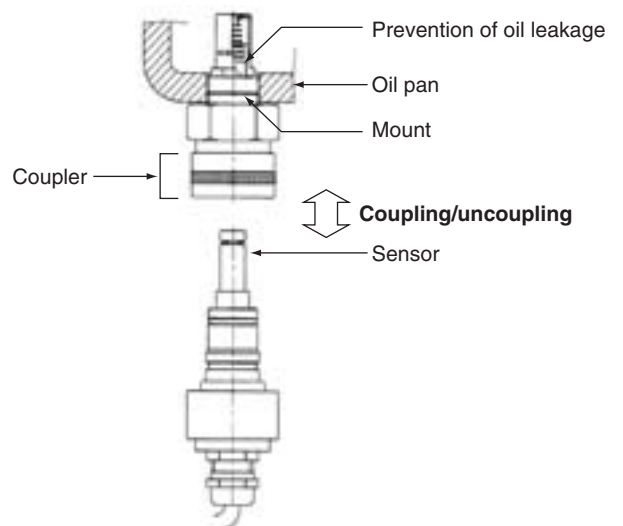


Fig. 10 Schematic view of coupler type

## 5. Conclusion

This paper has offered information about four types of NTN's unique sensor units.

We believe that construction machines will increasingly employ electrical control schemes to help achieve more accurate work, higher efficiency and much improved maintainability. To help fulfill these goals, NTN remains committed to improve performance of conventional sensor units and develop new and improved sensor units.

### Photo of authors

---



Shoji ITOMI

Application Engineering Dept.  
Industrial Sales  
headquarters



Hiroyoshi ITO

Application Engineering Dept.  
Industrial Sales  
headquarters

## Duplexing Gear Unit for Office Equipment

Tsutomu MAIWA\*



Duplex printing is widely used in current copy machines and printers as a measure to protect the environment. Those copy machines and printers generally use reversal mechanisms to reverse paper by using forward and reverse rotation of the paper feed roller.

NTN has developed a “Duplexing Gear Unit for Office Equipment” without using an electric motor for forward and reverse rotation. This new unit only uses one-way rotation, which is created by another drive system.

This report introduces the structure and function of this product.

### 1. Foreword

Duplex printing-photocopying machine and printer models are increasingly marketed for their ability to help reduce paper consumption as well as contribute to environmental conservation. For duplex printing, a reversal mechanism is necessary for reversing the paper stock. With a typical reversal mechanism, a paper stock having undergone printing on its front side is switched back by reversing the running direction of the drive motor to the paper feed roller and then printing is resumed on the back side of paper stock.

NTN has developed a unique Duplexing Gear Unit for office equipment that would replace a motor dedicated to the reversal mechanism and a drive motor component such as a fusing section used to mechanically switch the direction of rotation reducing energy consumption and cost.

The Duplexing Gear Unit is available in two types, each having unique input scheme. They are two-input one-output type (hereinafter “two-input duplexing gear unit”) and one-input one-output type (hereinafter “one-input duplexing gear unit”) (Table 1).

### 2. Explanation of two-input duplexing gear unit

#### 2.1 Description of operation

##### 1) First input gear forward rotation mode

When the first input gear is turned in the forward direction, the spring clutch locks the first input gear, causing the output gear engaged with the spring clutch to turn in the forward direction. During this course, the second reverse input gear turns in the forward direction together with the output gear (Fig. 1).

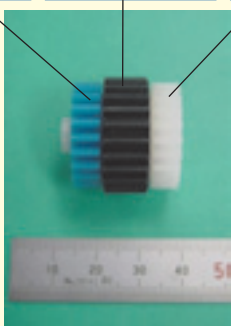
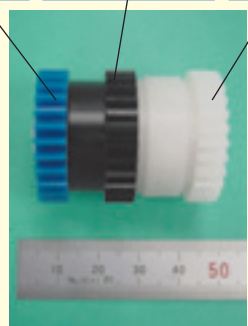
##### 2) Second input gear reverse rotation mode

When the second input gear is turned in the reverse direction, it comes into contact with the unlock hook of the spring clutch, causing the diameter of spring clutch to reduce. As a result, the spring clutch is unlocked; thereby interrupting drive power transmission from the first input gear to the output gear.

When the second input gear is further turned, it comes into contact with the output gear while reducing the diameter of the spring clutch and unlocking the spring clutch, causing the output gear to turn in the reverse direction (Fig. 2).

\*Application Engineering Dept. Industrial Sales headquarters

**Table 1** Summary of direction change unit

	Two-input Duplexing Gear Unit (two-input one-output type)	One-input Duplexing Gear Unit (one-input one-output type)
Appearance		
Dimensions	Gear OD $\Phi 26 \times$ overall length 28 mm	Gear OD $\Phi 30 \times$ overall length 44 mm
Features	<p>This type consists of three gears—first input gear, output gear and second input gear. When the first input gear turns in the forward direction, the output gear turns in the direction same as that of the first input gear [forward rotation]. Next, when the second input gear turns in the reverse direction, the output gear can turn in the direction same as that of the second input gear, regardless of the rotation direction of the first input gear [reverse rotation].</p>	<p>This type consists of three gears—(first) input gear, output gear and control gear. When the control gear is allowed to freely rotate and the input gear is turned in the forward direction, the control gear turns in the direction same as that of the output gear [forward rotation]. Incidentally, when the control gear is braked to stop its rotation (locked state), the output gear turns in the reverse direction [reverse rotation]. Note that the control gear is braked with a solenoid or electromagnetic clutch.</p>

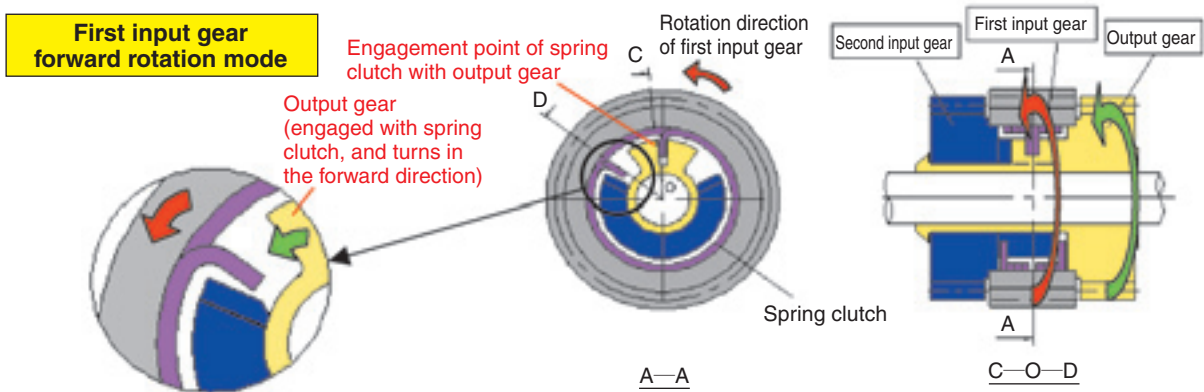


**Fig. 1** Forward rotation of two input type direction change unit

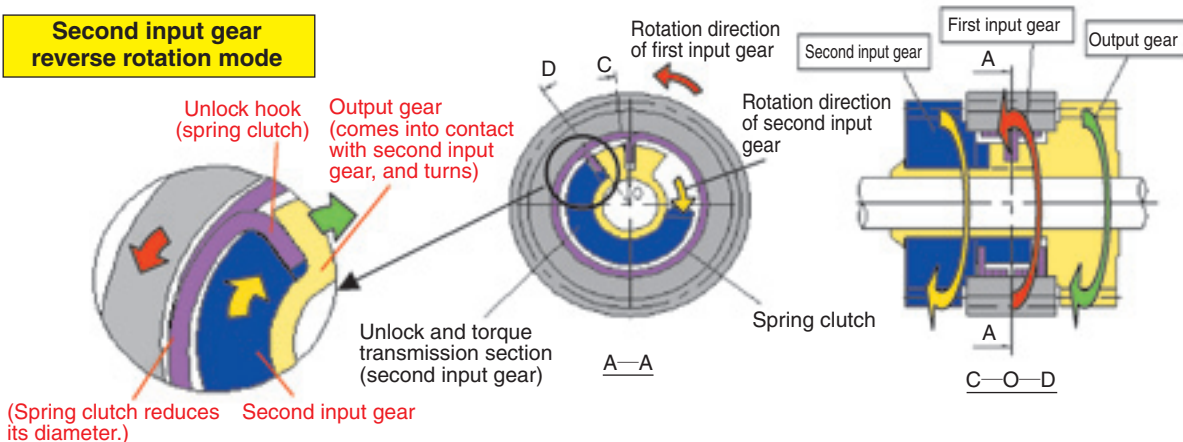


**Fig. 2** Reverse rotation of two input type direction change unit

### 3. Explanation of one-input duplexing gear unit

#### 3.1 Description of operation

##### 1) Input gear forward rotation mode (control gear in free state)

When the input gear is turned in the forward direction, the spring clutch locks the input gear, causing the intermediate shaft engaged with the spring clutch to turn in the forward direction and the output gear to turn in the forward direction as well. Note, however, that the braking means for the control gear is in the OFF state (free state) (Fig. 3).

##### 2) Input gear forward rotation mode (control gear in locked state)

When the control gear is braked (locked state) by a braking pawl (\*1), the unlock hook on the spring clutch comes into contact with the control gear, reducing the diameter of spring clutch: consequently, the spring clutch is unlocked blocking the transmission of drive power from the input gear to the output gear.

When the input gear is further turned while the control gear remains in the braked state, the intermediate shaft stops rotation. As a result, the bevel gears rotate, causing the output gear to rotate in the reverse direction (Fig. 4).

**NOTE: Braking pawl (\*1) is not included in the Duplexing Gear Unit proper. An actual braking pawl requires use of a solenoid or electromagnetic clutch.**

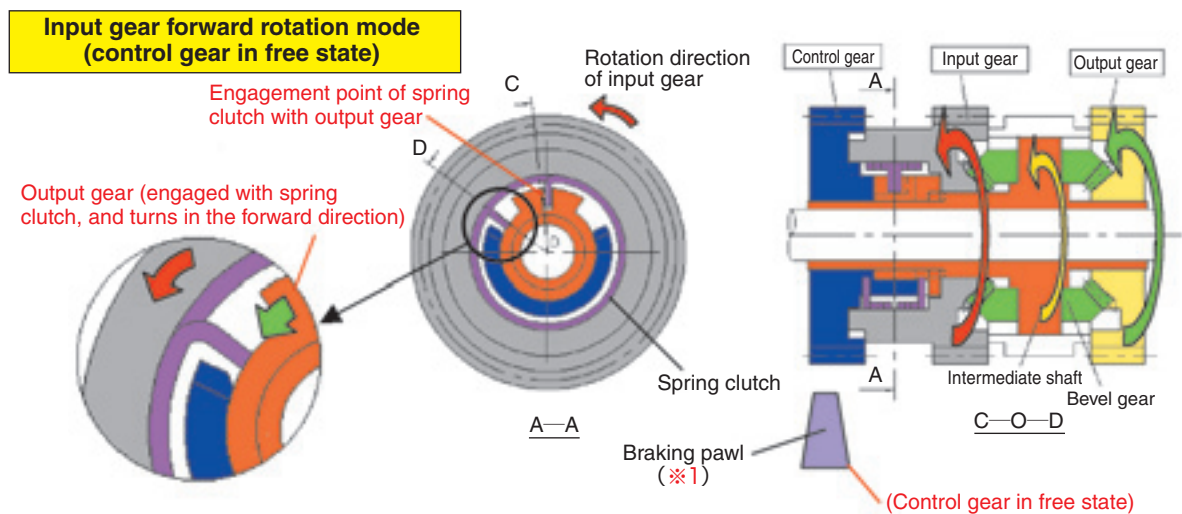


Fig. 3 Forward rotation of one input type direction change unit

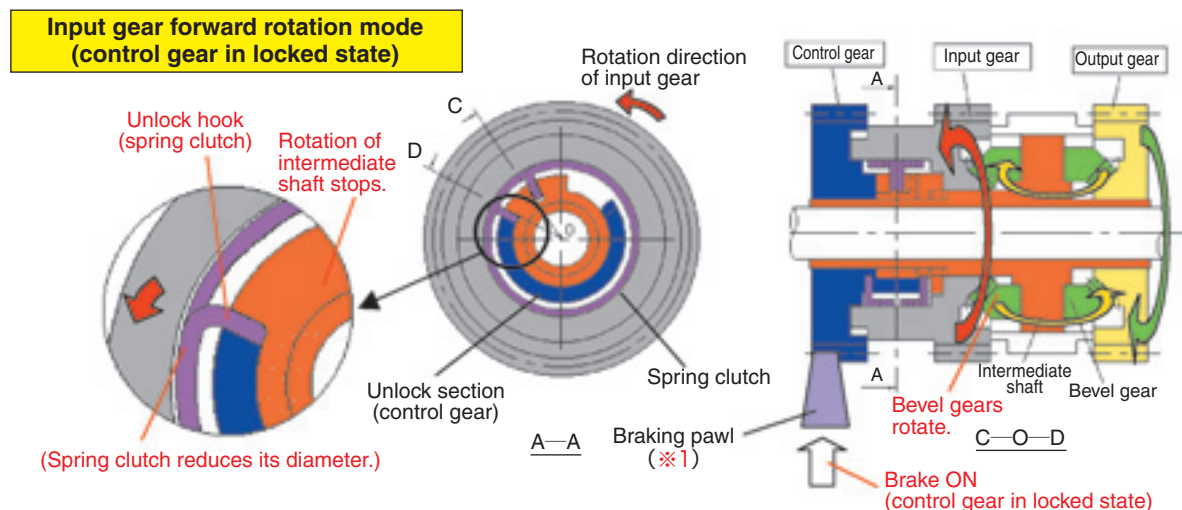


Fig. 4 Reverse rotation of one input type direction change unit

## 4. Endurance test

Endurance of each Duplexing Gear Unit has been checked under NTN endurance test conditions (Table 2).

**Table 2** Test condition of Endurance test (Test condition of NTN)

	Condition 1 (two-input)	Condition 2 (one-input)
Rotating speed	300min <sup>-1</sup>	300min <sup>-1</sup>
Ambient temperature	100°C	Ordinary temperature
Load torque	0.1N·m	0.1N·m
One cycle	3 sec. FWD⇒BWD 3 sec.	3 sec. FWD⇒BWD 3 sec.

Endurance test rigs for Duplexing Gear Unit are shown in Figs. 5 and 6 (Fig. 5 for two-input type, and Fig. 6 for one-input type).

The endurance test rig for two-input Duplexing Gear Unit in Fig. 5 uses two motors—the first input gear driving motor and the second input gear driving motor. Reverse rotation cycles are provided by disengagement and engagement with an electromagnetic clutch.

The endurance test rig for one-input Duplexing Gear Unit in Fig. 6 uses only one motor—the input gear driving motor. The brake for control gear is applied and released by an electromagnetic brake.

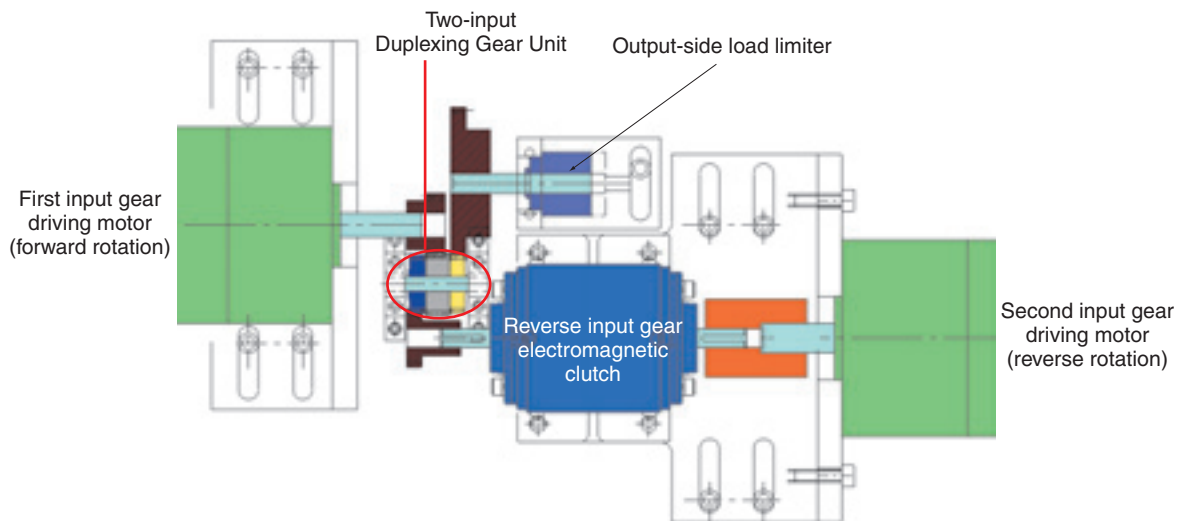


**Fig. 5** Endurance test machine of two input type direction change unit

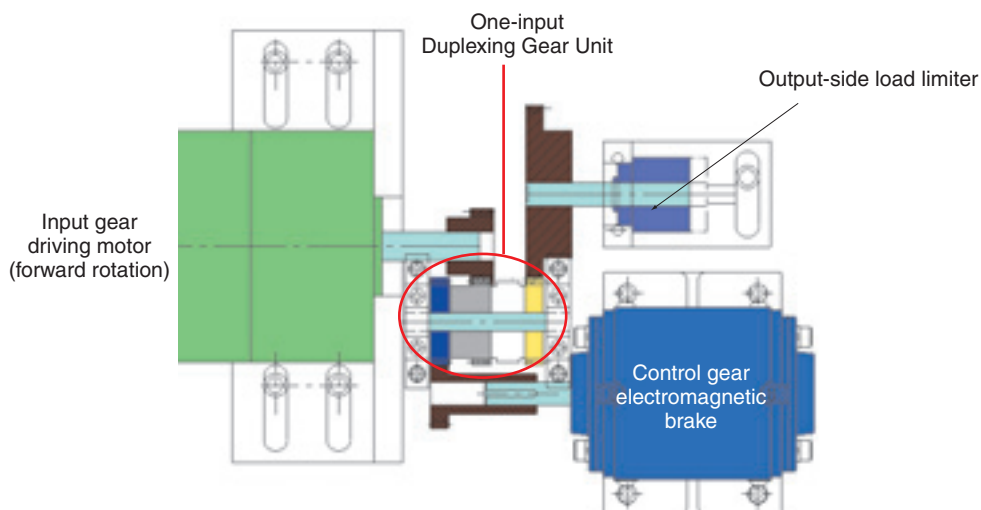


**Fig. 6** Endurance test machine of one input type direction change unit

#### 4.1 Test result

**Table 3** summarizes the results of endurance test. NTN studied the operation appearance quality of samples that underwent 300 thousands cycles (endurance requirement for ordinary printers), and learned that all the gears are free from any damage or fracture and function normally.

#### 5. Conclusion

Society will increasingly become eco-conscience oriented. In this context, duplex printing function will be increasingly adopted even for less expensive photo copying machines and printers as this function can help reduce paper consumption. Consequently, there will be growing needs for cost reduction with the costs of components used for producing this function.

The Duplexing Gear Unit for office equipment NTN has recently developed is a unique product intended to serve for ecological conservation and value addition, and is characterized in that an electric motor dedicated to duplex printing is eliminated, paper feed direction can be mechanically switched over between forward direction and reverse direction, thereby duplex printing mechanism is available at a lower cost. NTN will further reduce cost, improve performance and propose new applications; thereby NTN will contribute to improve the environment and value.

**Table 3** Test results

		Two-input	One-input
Appearance after test	Exterior state	Gearing has certain degree of fouling, but each gear poses no problem. 	Gearing has certain degree of fouling, but each gear poses no problem. 
	Spring clutch	Light contact has occurred on the outer circumference: no deformation at all.	Light contact has occurred on the outer circumference: no deformation at all.
Operation quality		No problem with both forward rotation and reverse rotation	No problem with both forward rotation and reverse rotation

Photo of author



Tsutomu MAIWA

Application Engineering Dept.  
Industrial Sales  
headquarters

# Large Gantry Table for the 10th Generation LCD Substrates

Katsuyoshi SUZUKI\*  
Naoshi SUZUKI\*



NTN has deeply cultivated precision positioning technology and applied it to various types of positioning systems. One of their major fields of application is LCD manufacturing equipment, and NTN provides large, long-stroke XY tables suitable for various types of equipment, including NTN LCD repair systems.

This paper describes problems arising from the growing size of XY tables and gives an outline of a prototype gantry-type XY table that meets the upcoming super-sized (about 3-m<sup>2</sup> G10) glass substrates.

## 1. Foreword

The demands for flat panel displays, typically flat-screen television sets, have been increasing at a rapid pace. To address this trend, flat panel manufacturers have been making investments for production of displays that are capable of providing images of higher definition and quality, by adoption of larger sized glass substrate in order to improve production efficiency and enhance value of display products. In this context, longer stroke and higher precision are needed for XY tables that constitute the core of equipment for manufacturing and inspecting LCD substrate.

NTN has been improving and enhancing its XY table products through lighter, larger more rigid designs, and has been incorporating its improved XY tables into LCD repair equipment, color filter repair equipment and plasma display repair equipment. Building upon this accumulated experience, NTN has also been actively developing large-sized tables. We have recently developed a large XY table to be able to handle the generation 10 LCD mother glass substrate (the world's largest size). This paper hereunder describes the engineering challenges, and the results of the technical evaluation for this product.

## 2. History of upsizing of LCD glass substrate

As the applications of LCD expand from personal computers to television sets, the need for larger screens continues to increase rapidly. To cope with this trend, facilities and technologies for producing LCD panels have been improving. Consequently, the size of LCD mother glass substrate has been dramatically increasing.

**Table 1** summarizes history of upsizing of LCD glass substrate sizes. The generation 10 mother glass, whose production has started recently, measures about 3,000 mm in one side. The stroke of an XY table, on which such large LCD mother glass substrate is subjected to processing such as laser cut, must also exceed 3,000 mm, and the size of the table needs to be accordingly as large.

**Table 1** LCD mother glass size

Generation 2	270×360mm	(1987)
Generation 3	360×465mm	(1994)
Generation 4	550×650mm	(1997)
Generation 5	680×880mm	(2000)
Generation 6	1100×1250mm	(2002)
Generation 7	1500×1800mm	(2004)
Generation 8	1870×2200mm	(2005)
Generation 9	2160×2460mm	(2006)
Generation 10	2850×3050mm	(2009)

\*Actual year of realization may differ with a given LCD panel manufacturer.

### 3. Restrictions about upsizing of table

So far, in response to the need for handling larger glass substrate, LCD panel manufacturers have been achieving compact table structure by optimizing the shape of the base on an XY table, and improving layout for the linear guide, linear motor, and cable chain. This achievement helps reduce the necessary floor area of the XY table in a clean room and contributes to prevention of occurrence of problems in manufacture and transportation of XY table. In the case of the tables capable of handling generation 10 LCD glass substrate, the minimum table width exceeds 3,500 mm. Consequently, the following two problems have to be addressed:

#### 1) Problem arising from allowable work piece size for machine tool

A relatively high number of machine tools can machine work pieces whose width measures less than 3,000 mm. In contrast, a smaller number of machine tools are capable of processing work pieces with width over 3,000 mm, and machine tool users may fail to satisfy the customer's request for lead time.

#### 2) Problem about maximum allowable dimensions for transportation

With respect to transportation, a larger XY table poses a problem. A relevant law or regulation in Japan (Law of Road Transport Vehicles etc.) stipulates that land transportation with an ordinary vehicle is not permitted if the cargo width exceeds 3,500 mm. A transportation agent may acquire special road occupation permission from a relevant authority and transport the large XY table on a public road during night time. If the machine is fabricated in a sea-side plant, it can be transported on a maritime vessel. Considering these additional requirements, an XY table capable of handling work pieces exceeding 3,500 mm in width poses a large challenge in fulfilling requirements for shorter lead time, and timely fabrication and delivery.

### 4. Considerations about split structure

The above-mentioned problems can be solved by adopting a split-structured design for the base of XY table. Because dimensions of individual units are smaller, and the scope of available machine tools is greater, engineering considerations about the shape and precision of work piece can be less demanding. At the same time, considerations about limitations with transportation are not necessary.

In developing a block structure, certain requirements need to be satisfied. The structure must feature a design that excels in restoration of accuracy after

transportation as separate units, and the machine must be able to be quickly reassembled and adjusted at the site where the machine is installed. More specifically, the block structure must clear the following issues:

#### ① Accuracy of parts mounting surfaces and joint faces

The mounting surfaces on the base for mounting the linear guide, linear scale, linear motor, etc. are important factors that determine the characteristics of XY table. Therefore, higher levels of precision in flatness, straightness, etc. must be satisfied.

When a plurality of bases are assembled into one entity, accuracy of table operation can be jeopardized or the effective life of the linear guide can become shorter if the joints have a problem such as height difference or bend. To avoid this problem, machining precision for each mounting surface needs to be improved, and at the same time, incorporation of an adjusting mechanism will be necessary.

#### ② Easy disassembly, reassembly and adjustment

To help simplify disassembly before shipment, and reassembly and adjustment after delivery at site, the XY table has to consist of a minimum number of components. The XY table needs to be designed such that the functional units mounted can be removed in the form of single block. Additionally the XY table must allow handling with accessible equipment, such as hydraulic jack, through adoption of light-weight, highly rigid members.

#### ③ Accuracy measurement at site

After joining and reassembly of the base, it is necessary to confirm restoration of accuracy of the base. Note, however, the utilities including electric power supply and compressed air may not yet be available at site. Therefore, a simple accuracy confirmation method has to be established in advance.

### 5. Specifications of super-large table

**Table 2** summarizes the specifications of the NTN gantry table that is capable of generation 10 (G10) LCD glass substrate, and **Fig. 1** shows appearance of the gantry table.

The Y-axis base can be split into two pieces at its near-middle location, with the line of separation being parallel with the X-axis gantry beam. Therefore, the location of the base joint coincides with the location of the linear guide joint (**Fig. 2**).

Because of availability and reasonable cost, cast structures have been adopted for the base and beam, each a major member of the XY table.

Compared with stone material, steel material boasts

higher rigidity and this feature helps achieve a lighter structure in spite of somewhat inferior vibration damping quality. Steel material also features higher degree of freedom in a shape-forming process. In designing the base and beam, NTN has attempted to realize simplicity and restoration of accuracy in

**Table 2** Specification of table for G10 LCD glass substrate

Table specifications	X-axis	Y-axis
Stroke	3,200mm	3,650mm
Max. velocity	1,500mm/s	1,500mm/s
Max. deceleration/acceleration	0.3G	0.3G
Resolution	0.1 μm/pulse	0.1 μm/pulse
Positioning accuracy	30 μm	30 μm
Repeated positioning accuracy	±0.5 μm	±0.5 μm
Horizontal straightness	40 μm	40 μm
Vertical straightness	20 μm	20 μm
Linear motor	Coreless	Cored
Linear scale	Permanently glued	Removable
Gantry constitution	Upper axis beam	Lower axis base
Splitting	None	Two pieces
Material	Steel (can structure)	
External dimensions	W3,900×D5,200×H2,500 mm	
Total mass	15,000 kg	

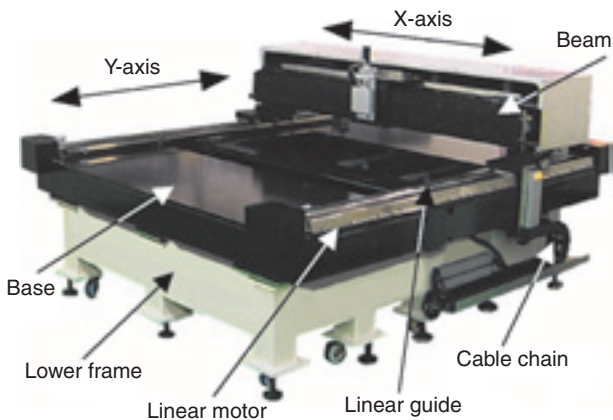


**Fig. 1** Appearance of the super-sized table

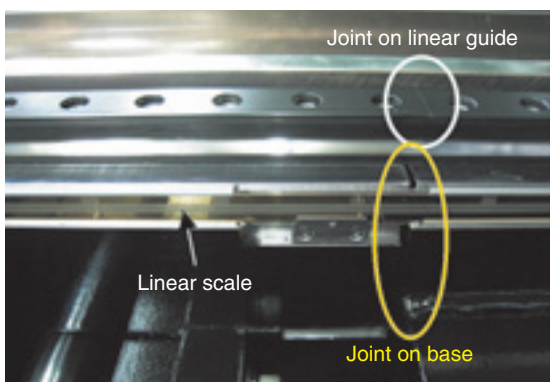


**Fig. 2** Division part of the Y-axis base

disassembly and reassembly work while addressing technical challenges associated with disassembly and reassembly procedure.

High performance linear motors have been incorporated into the drive system of the gantry table to cope with the longer stroke and higher speed with the larger XY table. A high thrust cored linear motor (**Fig. 3**) has been adopted for the Y-axis to be able to drive the heavy gantry beam with sufficient acceleration, and a coreless linear motor (**Fig. 4**) featuring smaller space and constant speed has been adopted for the X-axis.

Upsizing of the LCD glass substrate is intended for improved productivity. A longer process time in proportion with the glass substrate size cannot be justified. Therefore, the table must be faster. The table speed has been increased to 1,500 mm/s by improving thrust for the linear motor and incorporating a lighter table design. Additionally, these enhancements have realized acceleration/deceleration rates of 0.3 G with the table (ability to accelerate to 1,500 mm/s in approximately 0.5 sec.).

To ensure easy disassembly and reassembly of the table, a detachable linear scale that boasts good workability and reliable restoration for mounting accuracy has been selected.

The drivers to be used in conjunction with the linear motors are types featuring high-speed response, helping achieve improved resolution for scale signals: this feature leads to improved controllability that helps inhibit speed variation.



**Fig. 3** Linear Servomotor with iron core



**Fig. 4** Coreless Linear Servomotor

## 6. Evaluation test

A sample temporarily assembled (state before disassembly) and another sample in disassembled state were transported on a truck for about 10 km. Then, the samples were reassembled and adjusted. Next, these samples were compared with each other in terms of resultant positioning accuracy, repeated positioning accuracy, and horizontal/vertical straightness in order to confirm effect of reassembly on original accuracy.

As summarized in **Table 3**, we have been able to confirm restoration of accuracy to the specified levels after the Y-axis base was disassembled and reassembled. It has also been verified that disassembly/reassembly is completed in the expected time span.

**Fig. 5** plots the difference in actual measurement of positioning accuracy with Y-axis between before and after disassembly of the Y-axis base. Similarly, **Fig. 6** plots the difference in terms of horizontal straightness.

Before the evaluation test, the impact of vibration and installation site factors (such as floor structure) on the performance of the NTN gantry table were unknown. In

**Table 3** Result of evaluation test (Y-axis)

Evaluation criteria	Variation after reassembly
Positioning accuracy	5.0 μm max.
Repeated positioning accuracy	0.1 μm max.
Horizontal straightness	7.0 μm max.
Vertical straightness	0.1 μm max.

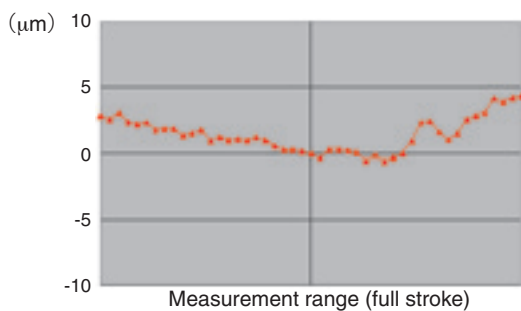


**Fig. 5** Difference of positioning accuracy (Y-axis) before and after disassembly and transportation

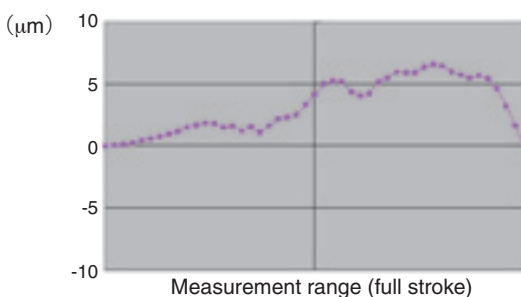


**Fig. 6** Difference of horizontal straightness (Y-axis) before and after disassembly and transportation

the present evaluation, our gantry table has not exhibited any adverse effects on various accuracy criteria including static accuracy, positioning accuracy, and straightness. In order to fully develop XY table performance, a vibration damping mechanism will be needed which can inhibit transmission of floor vibration to the XY table and promptly dampen residual vibration occurring from transportation of a heavy object. Various vibration damping units and combinations are available, including vibration damping rubber material, vibration damping damper, passive vibration isolation table, and active vibration isolation table. To support a greater table mass, it is necessary to select vibration isolating parts that are resilient, boasting larger load carrying capacity and higher performance. As an XY table manufacturer, NTN will address difficult challenges as to optimum selection and proposal of an XY table type that best suits the intended application and performance requirement, while satisfying the cost-performance need.

## 7. Conclusion

Performance of a large XY table directly governs the performance of LCD manufacturing equipment. In the context of upsizing and achieving higher precision with LCD glass substrate, the requirements have been increasingly complex for the XY table used in LCD manufacturing equipment, and such complex requirements include shape, functions, controllability, and performance.

Based on its accumulated technologies and experiences, NTN will address the challenges at higher levels for development, including higher precision, higher speed, and enhanced performance. NTN as an XY table manufacturer, will further remain committed to improve productivity and quality of flat panel displays.

## References

- 1) Electronic Journal supplement 2007, LCD fab/equipment /facilities, Electronic Journal, 2007 LCD Equipment Data Book

## Photo of authors



Katsuyoshi SUZUKI

Product Engineering Department  
Precision Equipment Division



Naoshi SUZUKI

Product Engineering Department  
Precision Equipment Division

# Development of a Linear Changer with a Built-in Pasting Unit for a Flat Panel Defect Repair System

Akihiro YAMANAKA\*  
Akira MATSUSHIMA\*



The NTN color filter repair system fixes defects in color filters, which are the primary components of liquid crystal displays.

The most important feature of this system is the function of pasting ink to a colorless spot, commonly referred to as a "white defect", on the color filter.

The pasting unit carries out the ink pasting process using a pasting needle. The system moves the pasting needle to touch the defect in the color filter and pastes a slight amount of ink from the tip of the pasting needle to the defect. The pasting needle system can stably carry out the pasting process because there is no possibility of clogging as in a dispenser system. It has received favorable comments from many customers.

This paper explains the outline of the pasting mechanism and the linear changer with built-in pasting units.

## 1. Foreword

In the past several years, flat panel displays (FPD) such as liquid crystal displays (LCD) and plasma displays (PDP) have been widely used for home television sets, and their screen size has been ever increasing.

Since 1990, NTN has been developing and marketing pattern repair systems that repair defects occurring in production processes for these FPD products. When used to repair defects and reduce defective substrates being scrapped, the NTN repair systems have been contributing to mitigation of environmental impacts and reduction in FPD production cost. In recent years, a repair process has been widely recognized as mandatory in FPD manufacturing while larger, more finely defined screens are increasingly demanded.

To help improve production efficiency for LCD, the size of LCD mother glass substrate has been rapidly increasing, and production of the generation 10 size (2850×3050 mm, t = 0.7 mm) is going to start very soon.

Using the NTN ink pasting unit used for repairing color filter (CF) for LCD as an example, this report describes our newly developed linear changer with built-in pasting unit.

## 2. Possible defects on color filter (CF) of LCD and repair method

As illustrated in Fig. 1, an LCD comprises a TFT substrate and a CF substrate which are glued together. Both substrates are separated with pillars called photo spacers. The space between both substrates is filled with liquid crystal and a back light is situated on the back face of LCD.

A color filter (CF) is a component that adds color information to light that is turned ON/OFF by the liquid crystal. The CF consists of a glass substrate on which

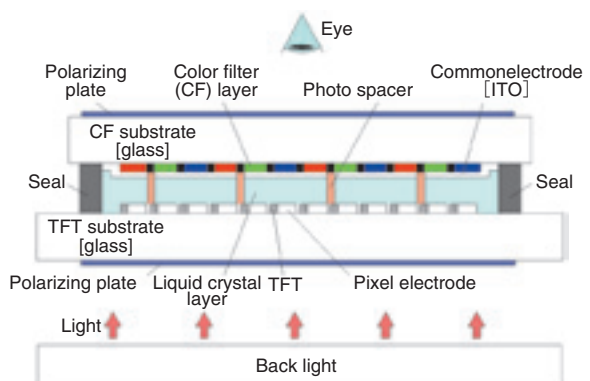


Fig. 1 LCD structure figure

\*Product Engineering Department Precision Equipment Division

R (red), G (green) and B (blue) pixels are arranged in a stripe or matrix pattern. Light passing the CF is provided with color information corresponding to the pixels involved. As a result of this addition of color information by the CF, the LCD exhibits a color image.

A color filter (CF) repair system, repairs a defect occurring in a color filter (CF) during CF panel production process.

A white defect is defined as a defect of a pixel which has lost its color, and can be repaired with a pasting unit by applying ink whose color is same as that of the defective pixel.

A black defect is defined as a defect of a pixel to which another color has been mixed or dust or contaminant has been discarded. This type of defect can be repaired first by removing a defective area with a laser to convert the black defect into a white defect, and then applying ink of the same color as that of the original pixel to the white defect.

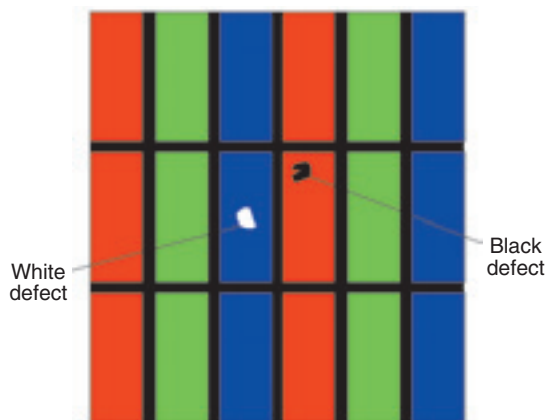


Fig. 2 The defect of CF panel

### 3. History of pasting units

A color filter (CF) repair system, shown schematically in Fig. 3, has a pasting unit mounted beside an observation optical system that can be shifted to an arbitrary location on a color filter substrate that is to be repaired.

During a defect repairing process, the observation optical system is shifted to the location of the defect, the defect is observed, and then repaired by applying ink to the defect with the pasting unit.

#### 3.1 Initial model pasting unit

To apply ink to a white defect on a color filter (CF), NTN has adopted a system using a the pasting

needle. The tip of the pasting needle has a unique shape so that ink can be very stably applied to a very small area about  $30\ \mu\text{m}$  to  $300\ \mu\text{m}$  in diameter. Consequently, this system is highly appreciated by the users. Unlike an ink pasting operation with a dispenser where ink is dispensed through a fine hole, the pasting operation with a pasting needle has an advantage because the pasting needle is free from clogging and can handle paste of a wider scope of viscosity.

The ink pasting unit NTN initially developed is schematically illustrated in Fig. 4.

NTN's initial ink pasting unit was comprised of an actuator that moves the pasting needle up/down, a rotary table that carries ink cassettes (four ink cassettes for repairing color filter, that is, R (red), G (green), B (blue) and Bk (black)), the rinsing mechanism that is mounted on the rotary table in order to rinse the pasting needle, and the air purge mechanism that dries the rinse liquid deposited on the tip of pasting needle.

In the ink pasting operation, ink is allowed to adhere to the tip of the pasting needle, and then the tip of the pasting needle is brought into contact with a white defect to transfer ink on the needle tip to the defect.

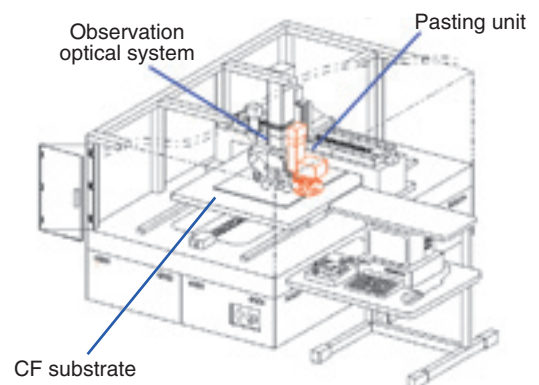


Fig. 3 Color filter repair system

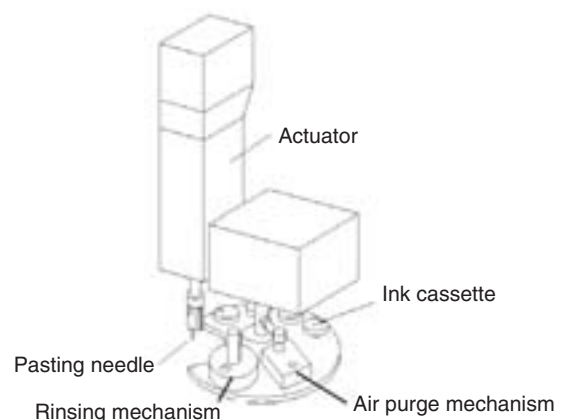


Fig. 4 Initial model pasting unit

The pasting needle is mounted to the end of an actuator drive shaft for driving the pasting needle via a vertically movable slide mechanism, wherein constant contact pressure is maintained between the tip of the pasting needle and the substrate during the ink pasting process.

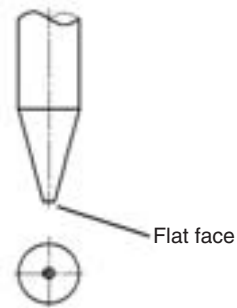


Fig. 5 Needle tip shape

The end of the pasting needle is tapered as shown in Fig. 5, and the needle tip is machined to have a flat face that is square to the axis of the needle.

When ink is allowed to adhere to the tip of the pasting needle, the ink is drawn up along the pasting needle by surface tension. By transferring ink on the flat face of the needle tip to a defect, very delicate ink application is stably executed. The dimension of the flat face on the needle tip can be varied to adjust the pasting size. Consequently, pasting with a diameter size of 30 μm to 300 μm is possible as previously mentioned.

The initial model of the pasting unit was equipped with only one or two pasting needles. Therefore, when ink color had to be changed, the pasting needles needed to be rinsed in order to avoid mixing colors. The pasting needles were rinsed with the rinsing mechanism and air purge mechanism shown in Fig. 4.

The rinsing mechanism rinses a pasting needle by stirring rinsing liquid in the rinsing vessel with a propeller mounted to the motor shaft. Then, the air purge mechanism blows air around the pasting needle to dry any rinsing liquid remaining at the tip of needle to complete the rinsing process.

### 3.2 Improved pasting unit

As larger screen LCD television sets have been increasingly marketed, pixel sizes have become increasingly larger, and larger defects are occurring more frequently. To shorten repair tact time for such larger defects, NTN has developed the improved pasting unit shown in Fig. 6.

The improved pasting unit features the following major improvements.

#### (1) Adoption of drive mechanism dedicated to pasting

On the initial model pasting unit, the optical system for observing defects was offset from the location of pasting needle as shown in Fig. 7. Therefore, in order for pasting to be possible, the pasting needle had to be shifted to the observation location by moving the table on the defect repair system.

In the improved pasting unit, a drive mechanism dedicated to pasting has been developed to shorten the time needed for travelling the offset distance, wherein the pasting needle is deployed into the observation location beneath the objective lens to apply ink to a defect. By adoption of this arrangement, the pasting needle can be quickly deployed to the pasting position.

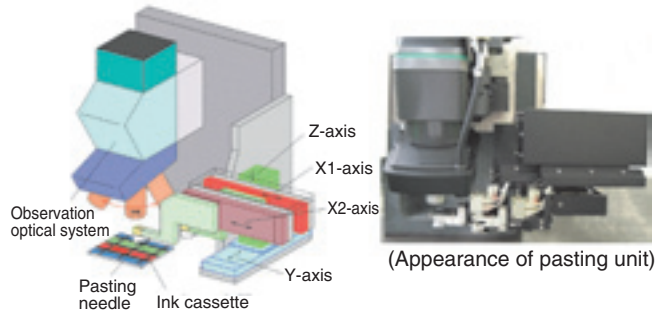


Fig. 6 Improved pasting unit

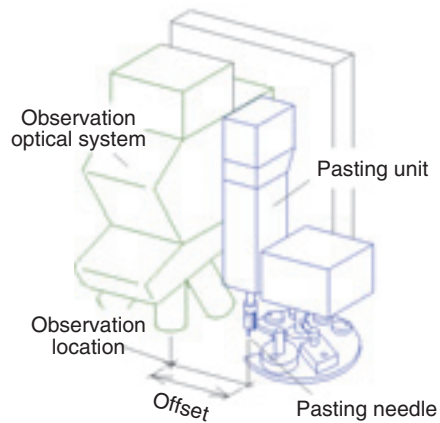


Fig. 7 Arrangement of observation optical system and Initial model pasting unit

#### (2) Adoption of pasting needles each dedicated to specific repair ink

As previously mentioned, the initial model pasting unit had only one or two pasting needles. Because of this, the pasting needle needed to be rinsed before a different color ink could be used. To eliminate this rinsing process to shorten the pasting tact time, the improved pasting unit has four color-specific pasting needles—R (red), G (green), B (blue) and Bk (black). Thanks to this arrangement, the repair tact time has been much reduced.

**(3) Integrated support structure comprising pasting needle and ink cassette**

Because the improved pasting unit has four pasting needles as mentioned above, the arrangement for ink cassettes has been reconsidered. Therefore as shown in Fig. 8, an ink cassette of a particular color is assigned to a pasting needle dedicated to that color and individual units each consisting of a pasting needle and ink cassette are independently supported.

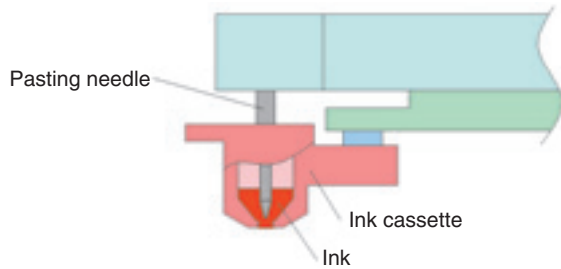


**Fig. 8** United support construction of the Needle and Ink cassette

Each ink cassette has holes on its top and bottom so that a pasting needle can penetrate it. The pasting needle is inserted downward through the upper hole. The tip of the pasting needle always remains immersed in ink in the ink cassette so that ink on the tip of the needle does not dry. In an ink pasting process, the tip of the pasting needle protrudes through the lower hole of the ink cassette, and comes into contact with a defect to apply ink to the defect. As mentioned previously, the pasting needle during this process remains secured to the drive shaft of the pasting needle driving actuator via the vertically movable slide mechanism, thereby maintaining contact pressure between the pasting needle and the substrate.

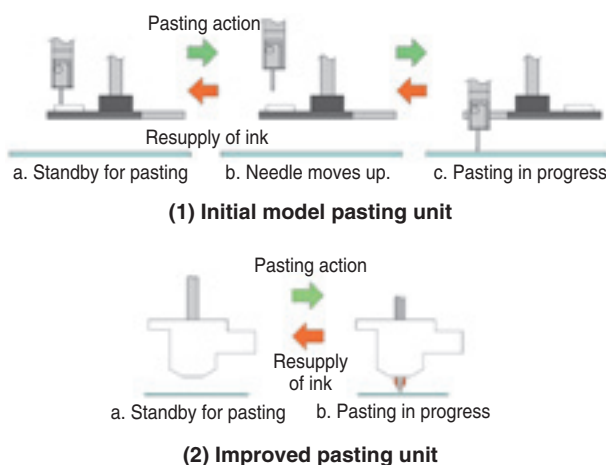


**Fig. 9** Ink pasting process comparison

As a result of adopting a support construction that unites the pasting needle and the ink cassette, repair ink is fed to the pasting needle by simply stroking the pasting needle into and out of the ink cassette. As illustrated in Fig. 9, and compared with the initial model pasting unit, the improved pasting unit is capable of completing repairing for repeated repairing ink applications with a plurality of defects.

Thanks to the above-mentioned improvements, the improved pasting unit has reduced the repair tact time by 70% compared to the initial model pasting unit.

**4. Linear changer with built-in pasting unit**

As described above, NTN has been improving its pasting unit. To further reduce repair tact time and improve positioning accuracy for pasting, NTN has recently developed a linear changer with a built-in pasting unit.

**4.1 Linear changer**

(new objective lens switch-over mechanism)

On the improved pasting unit, the pasting needle is inserted into the observation location beneath the objective lens, and then pasting action is performed. However, this system has a drawback—because of limitation in the work distance with the objective lens used for observation (distance between the subject being observed and the objective lens), the pasting needle can be inserted into the observation location only when an objective lens of a lower magnification power is used. Consequently, if ink is to be applied to a defect that is observed with a high magnification power objective lens, a low magnification objective lens needs to be deployed and only when pasting is executed. Therefore, time needed for switching-over of objective lenses poses a challenge in reduction of repair tact time.

Previously, the revolver unit shown in Fig. 10 was used to switch over between objective lenses. This unit holds several objective lenses and indexes these



**Fig. 10** Revolver unit

lenses to move a necessary lens to the observation location. To reduce the lens switch-over tact time, the lenses need to be turned at a higher speed. Therefore, NTN has been improving this unit to reduce lens switch-over time. However, since this mechanism mechanically stops each objective lens at an observation location, if the revolver is turned at a higher speed, it is difficult to stop an intended objective lens exactly at an observation location. In other words, further reduction in lens switch-over time with this system appears to be nearly impossible.

To address this problem, NTN has developed a directly acting (linear system) objective lens switch-over unit (linear changer).

This unit has several objective lenses, each objective lens assigned to a laser of unique frequency for cutting a defect. Depending on the intended application, the unit may be equipped with a laser capable of emitting a variety of frequencies. Accordingly, the linear changer has been designed to hold a maximum of ten objective lenses.

If ten objective lenses are arranged in one line and one lens is selected from this line, the length of the linear changer will be excessively large, and the linear changer will not be easily built into the pasting system. To avoid this problem, a configuration of five lenses in two rows has been adopted. With a two-row layout, the objective lenses need to be shifted in two directions (X and Y directions). When a laser beam is allowed to enter a given objective lens, there is limitation in the distance between the lens barrel and the objective lens pupil plane owing to the relationship with the imaging lens. That is, if the thickness of the linear changer is large, the distance between the objective lens pupil plane (lens plane at the upper portion of objective lens) and lens barrel is greater and the laser power density on the objective lens pupil plane is greater, which will damage the objective lens. To avoid this situation, NTN has invented an improved XY feed mechanism that allows the distance between the objective lens and lens barrel to fall within an appropriate range.

A linear motor and a linear encoder (resolution of 0.1  $\mu\text{m}$ ) have been adopted as a means for actuating the XY feed mechanism in order to realize higher speed for actuation and improved positioning accuracy.

#### 4.2 Pasting unit built into linear changer

In conjunction with the development of the linear changer, NTN has reconsidered the arrangement of the ink pasting unit. The integrated support structure comprising the pasting needle and ink cassette, adopted for the improved pasting unit, is very compact.

Starting with the improved pasting unit, NTN attempted to design a more compact pasting unit. Consequently, NTN has succeeded in developing a very compact pasting unit that can be built into the linear changer.

Remember that on the improved pasting unit, the pasting needle is inserted in the visual field being observed. However, on the linear changer that incorporates the pasting unit, the pasting needle does not interfere with the objective lens, and the linear changer can hold a greater number of pasting needles compared with the improved pasting unit.

On the pasting unit that is built into the linear changer, the space occupied by one objective lens can accommodate two pasting needles in place of one objective lens, thereby enabling the pasting units to hold a maximum of eight pasting needles in place of objective lenses.

Recently in the flat panel manufacturing industry, screens of different sizes are obtained from single mother substrate. In this case, it may be necessary to simultaneously repair pixels of different sizes. To cope with such a situation, the new pasting unit can simultaneously mount a variety of pasting needles of different sizes for differently sized pixels. Also, in the recent LCD industry, development of a novel color filter has been disclosed. This color filter is capable of five colors, including yellow and cyan in addition to RGB colors already available with conventional color filters, in order to improve image quality attained with LCD. NTN's new pasting unit is capable of repairing such multi-color color filter.

#### 4.3 Features of linear changer with built-in pasting unit

The newly developed linear changer with a built-in pasting unit is schematically illustrated in **Fig. 11**.

##### (1) Improved positioning accuracy for pasting

The improved pasting unit described in Sec. 3.2 has improved positioning accuracy by eliminating the necessity for offset compensation, which was previously accomplished by turning the table in the pasting unit. However, when a variety of defects are present in the visual field being observed, the table yet needs to be turned accordingly. This is because, on the improved pasting unit, when the pasting needle is inserted in the visual field being observed and the needle applies ink to a defect, the needle can interfere with a nearby objective lens, and at the same time, not attain a sufficient travel distance for a pasting needle in the visual field being observed. Since travel of the table is unavoidable, a longer repair tact time is accordingly necessary if a variety of pixels in the

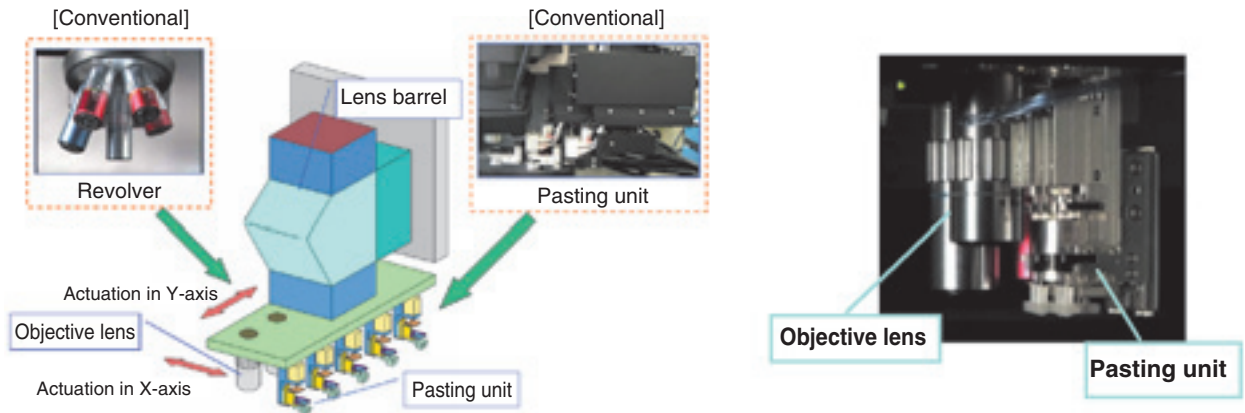


Fig. 11 Linear Changer with built-in pasting unit

visual field being observed have to be repaired.

Remember that the revolver type objective lens switch-over system mechanically positions the intended objective lens. As a result, positioning accuracy for objective lens will somewhat deteriorate as the objective lens switch-over system is repeatedly actuated.

On NTN's newly developed linear changer with built-in pasting unit, travel of the objective lens and pasting needle to the intended observation location is achieved with the XY feed mechanism on the pasting unit alone, thereby enabling execution of highly accurate ink pasting at high speed.

**(2) Reduction in repair tact time**

Unlike the improved pasting unit, the NTN linear changer with built-in pasting unit is free from interference between a pasting needle and an objective lens, and can immediately start pasting regardless of the magnification power of the objective lens currently used for observation. Also, the linear changer boasts increased objective lens switch-over speed and greater pasting needle shift speed.

Through the above-mentioned improvements, the linear changer with built-in pasting unit has achieved reduction of approximately 20% in repair tact time compared with the improved pasting unit.

**5. Conclusion**

This report has described the NTN linear changer with built-in pasting unit. NTN has been committed to not only development of this product but also to improvement in repair quality and reduction in repair tact time through improvement of the pasting needle for the pasting unit. Also, NTN has been helping realize labor saving through development of automatic defect repair software.

As up sizing of mother glass substrates used for LCD

production continues (generation 10 glass substrate will be processed soon), reduction in tact time and saving in labor saving on a given flat panel production equipment are critical considerations for improving productivity. NTN wishes to develop novel equipment that helps improve productivity for plat panels.

**References**

- 1) Yamanaka, Monthly Display, Dec. 2004
- 2) Yamanaka, New material developments and manufacturing processes in color filters compilation, Jul. 2006 issue
- 3) Yamanaka, Monthly Display, Dec. 2006
- 4) Saruta: NTN Technical Review No.72 (2004)
- 5) Yamanaka and Matsushima: NTN Technical Review No.72 (2004)

Photo of authors



Akihiro YAMANAKA  
Product Engineering Department  
Precision Equipment Division



Akira MATSUSHITA  
Product Engineering Department  
Precision Equipment Division

2007 Engineering Award, The Japan Society for Precision Engineering

# Development and Practical Application of MQCJ-Lubricated Angular Contact Ball Bearings for Machine Tool Main Spindles

Masatsugu MORI, Yoshinobu AKAMATSU, Mineo KOYAMA, Futoshi KOSUGI, and Hiroshi TAKIUCHI

## 1. Features of MQCJ-lubricated angular contact ball bearings <sup>1)</sup>

Our newly developed angular contact ball bearings incorporate newly developed MQCJ lubrication mechanism and boast not only bearing cooling capability of jet lubrication but also low power loss feature of air-oil lubrication.

The MQCJ lubrication system can inhibit overheating of a bearing even under high-speed running conditions and contribute to super high-speed operation with constant pressure preloading, increased preload (higher rigidity) by definite position preloading, and mitigation of environmental impacts.

## 2. Structure of MQCJ-lubricated angular contact ball bearings

Fig. 1 schematically illustrates the structure of an MQCJ-lubricated angular contact ball bearing set and the associated lubricant flow path. Lubricant fed through the oil hole on the outer ring spacer is squeezed by the nozzle, and a high-speed jet of lubricant hits the scoop formed around the entire circumference of the inner ring side plane to thoroughly cool down the inner ring. A large portion of the lubricant received by the scoop is allowed to drain away; the remaining portion of lubricant adheres to the ramp on the inner ring, and moves toward the bearing interior along the ramp due to centrifugal force and surface tension and lubricates the bearing.

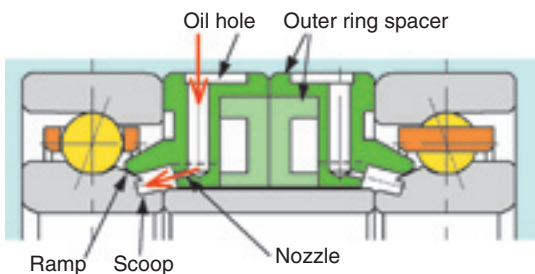


Fig. 1 Structure and lubricant flow

## 3. Test results <sup>2)</sup>

The temperature difference across the inner ring and outer ring as well as power loss were analyzed for an angular contact ball bearing configured with constant pressure preloading and a bore diameter measuring 70 mm. The bearing was lubricated with MQCJ lubrication, jet lubrication and air-oil lubrication. Then, the analysis results obtained from these lubrication systems have been compared with each other.

Fig. 2 graphically plots temperature differences across the inner ring and outer ring and power losses obtained from these lubrication systems. From these charts, it should be understood that the bearing cooling performance of MQCJ lubrication is equivalent to that of jet lubrication, and fairly excels that of air-oil lubrication; and that power loss with MQCJ lubrication is equivalent to that with air-oil lubrication and is much smaller than that with jet lubrication.

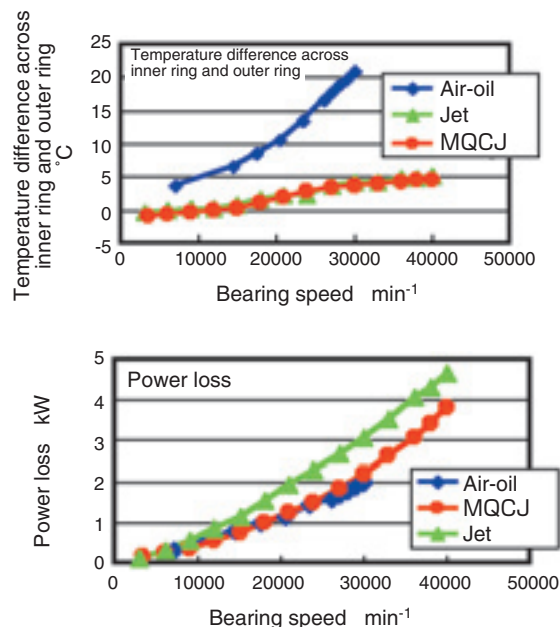


Fig. 2 Temperature difference between inner and outer rings and comparison of power loss among lubrication types

## 4. Conclusion

The newly developed MQCJ-lubricated angular contact ball bearings satisfy requirements for high-speed performance, higher rigidity and low environmental impact quality, which are the requirements recent machine tool main spindle bearings must satisfy, and will help machine tools reach a higher level of engineering excellence.

## References

- 1) M. Koyama: Minimum Quantity and Cooling Jet Lubricated Angular Contact Ball Bearings for Machine Tools, NTN Technical Review No.74 (2006) 22-25
- 2) Mori, Akamatsu, Koyama, Kosugi, Takiuchi and Furubayashi: Development and Practical Realization of Minimum Quantity and Cooling Jet Lubricated Angular Contact Ball Bearings for Machine Tools, Journal of JSPE, Vol.74 No.6 (2008) 539-542

Photo of authors(Leader)

---



Masatsugu MORI

Elemental Technological  
R&D Center

## V-series Hub Joint

A hub joint is integrated with a constant-velocity joint to achieve a **compact, light-weight** hub joint design!



### Features

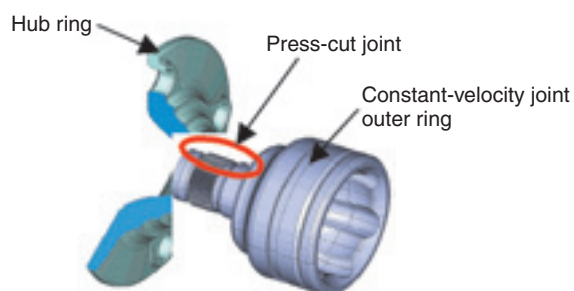
- (1) **Weight:** 12% weight reduction (compared to conventional design)
- (2) **High performance:** No play between hub bearing and constant velocity joint. Prevents stick-sliding noise.
- (3) **Simpler assembly work:** Number of work hours at the user's site is decreased as a hub joint is integrated with a constant-velocity joint.

### Applications

- Hub bearing and driveshaft for automotive applications resistance.

### Construction [means for realization]

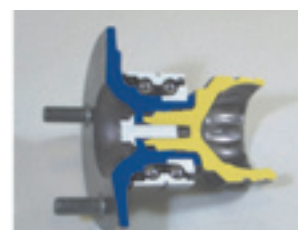
- Adoption of novel joining technique—Press-cut joining



- Two arrangements are available—Consolidated type (hub bearing is consolidated with constant-velocity joint) and separable type (hub bearing can be separated from and joined again to constant-velocity joint).



[Consolidated hub joint]



[Separable hub joint]

## V-series Angular Unit

Need for **light-weight design** and **decreased material use** are simultaneously achieved while necessary mechanical strength is realized!!



### Features (comparison to conventional design)

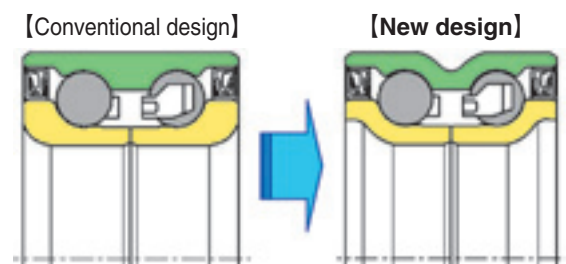
- (1) Weight: 12% lighter
- (2) Amount of material used: 30% reduction
- (3) Simplicity of assembling: Can be assembled with peripheral components in an unmodified conventional process

### Applications

- Automotive hub bearing

### Construction

- Light-weight shape: Precision metal-forming technique is applied to the inner ring and outer ring.



## Hub Bearing w/ Built-in Load Sensor

The sensor is effective even at a **vehicle speed of 0 km/h**. It detects a cornering force working on a running vehicle on a **real-time** basis in order to help assist control in side skidding of the vehicle!



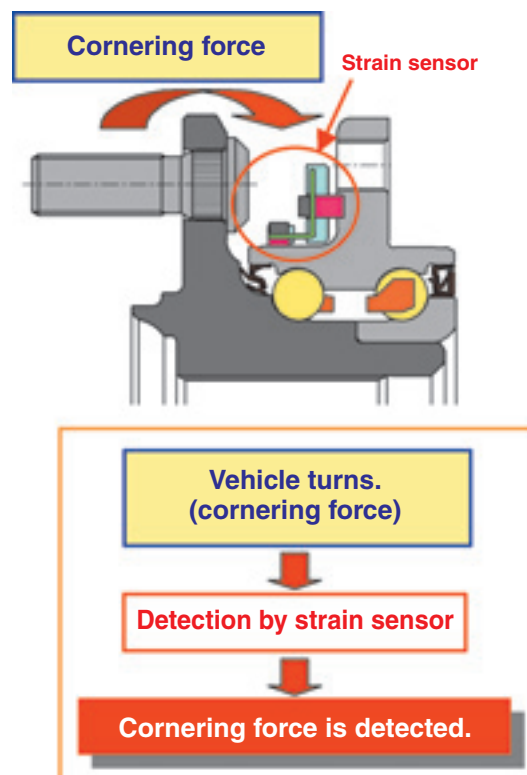
### Features

- (1) Sensor installed on each wheel detects the cornering force; the magnitude of detected cornering force is important in controlling the skidding behavior of the vehicle in question.
- (2) Improved response in detecting cornering force
- (3) Even when a particular wheel is locked (zero wheel velocity), a cornering force working on it can be detected.
- (4) Load detection range: -4 kN to 10 kN
- (5) Detection accuracy:  $\pm 3\%$ FS (full scale)  
Acceleration equivalent to that on a car in 0.6G turn

### Applications

- Hub bearings for passenger cars

### Construction



## High-Efficiency Compact Constant-Velocity Joint (ELJ)

**Compact, light-weight, highly efficient** drive shaft constant-velocity joint



### Features (comparison with conventional design)

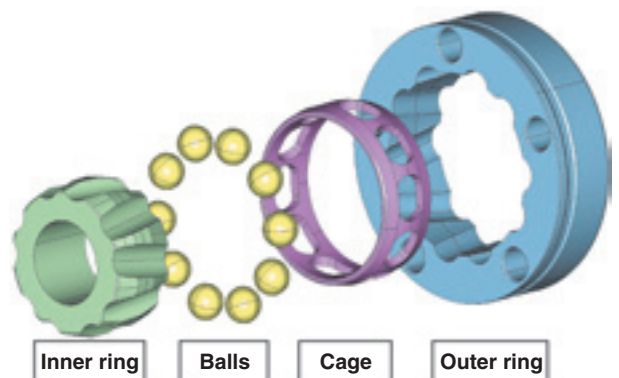
- (1) Compact, light-weight
  - Outer ring outside diameter: 4% size reduction
  - Weight: 18% reduction
- (2) Higher efficiency
  - Torque loss rate: 50% reduction
- (3) Lower slide resistance
  - Slide resistance: 50% reduction

### Applications

- Automotive driveshaft

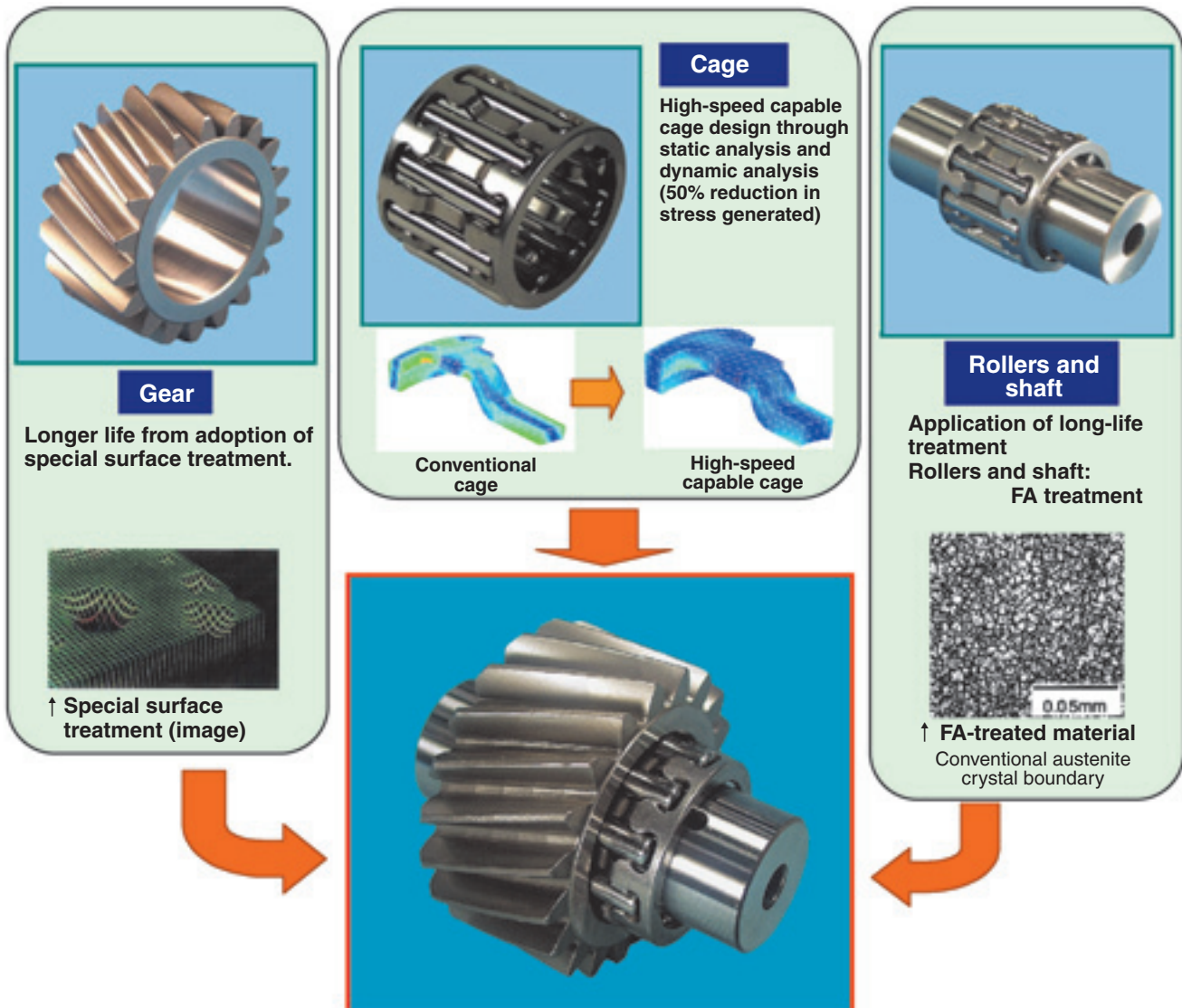
### Construction

- Cross groove type constant-velocity joint with ten balls (conventionally, six)



## Planetary Gear Unit for Automotive Transmission

Realization of both **higher speed** and **compact size!!**



### Features

- (1) High-speed capability:  
Capable of 25,000 rpm (47% increase over conventional design)
- (2) Compact design:  
20% size reduction in gear width (when conventional gear unit life is maintained)

### Applications

- Automotive transmissions (AT, CVT, hybrid system)

# Oilless Chain Tensioner

**Oil supply from the engine is not needed!**



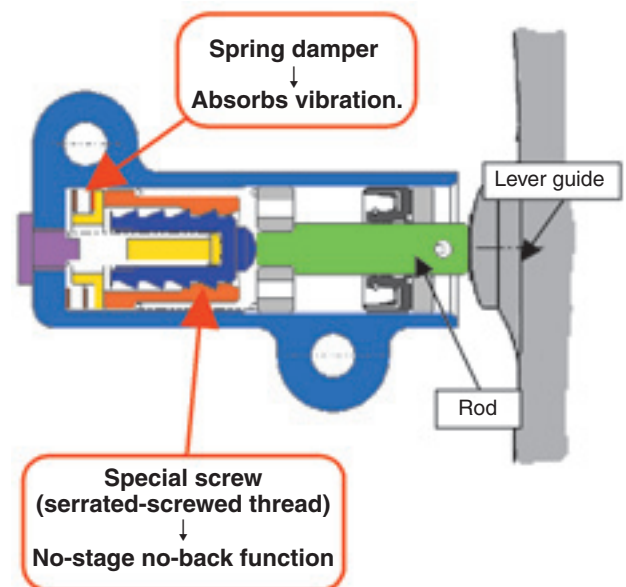
## Features

- (1) Oil supply from the engine is not needed.
- (2) Provision of oil piping in the engine is not needed.
- (3) Efficiency of a chain tension adjustment function is equivalent with that of a conventional hydraulic chain tensioner.
- (4) Complete with no-stage no-back function

### <No-stage no-back function>

Conventionally, when the engine is shut off while the chain remains tensioned, then the rod may remain in the pushed-in position: then if, in this situation, the engine is restarted and the chain gets loosened, noise will occur at the mesh points with the camshaft and crankshaft. In contrast, the rod in our new product can be retained (no-back) at an arbitrary (no-stage) projected position; noise occurrence is prevented.

## Construction

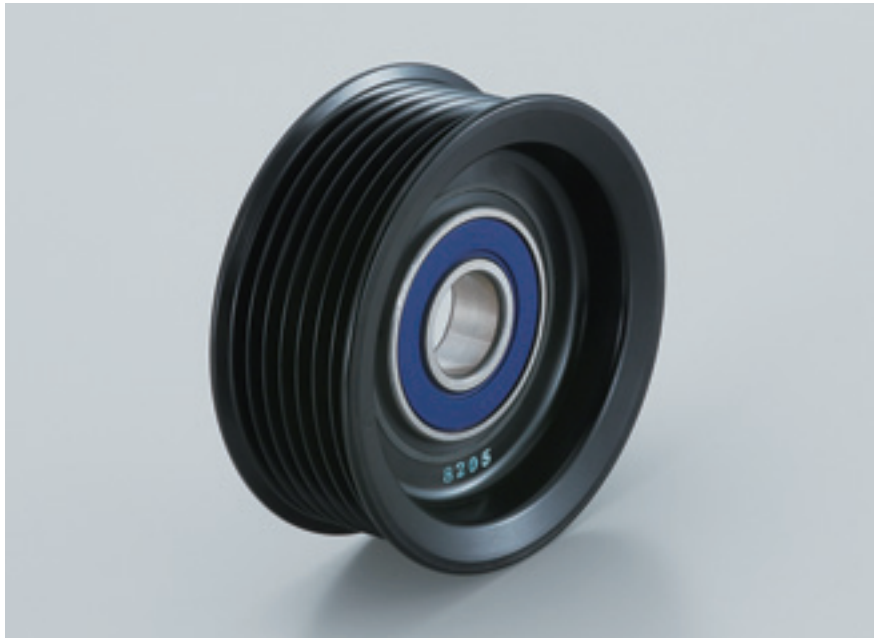


## Applications

- Auto-tensioner for timing chain on four- and two-wheeled vehicles

## High-Temperature Resin Pulley Unit for Automotive Auxiliaries

**Light weight**—its life is equivalent to or better than that with conventional iron pulley unit!



### Features

**(1) Weight: 65% reduction**

[Compared to conventional iron pulley unit]

**(2) Bearing life: At least twice as long**

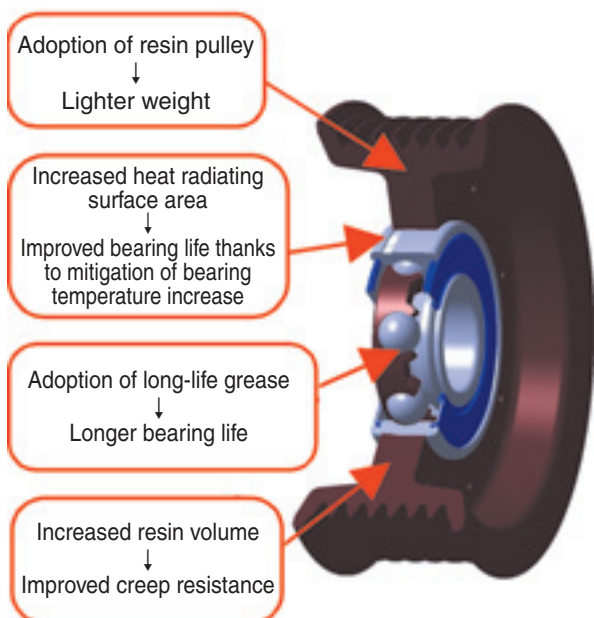
**(3) Creep resistance: At least twice as strong**

[Compared to conventional resin pulley unit]

### Applications

- Idler pulley for belt on automotive auxiliary

### Construction [means for realization]



## Super-High Load Carrying Cylindrical Roller Bearing

The number and length of rollers have been maximized to help realize a bearing design featuring a much **smaller size** and **lighter weight!**



### Features

[Comparison to bearing of same bearing life and rigidity]

- (1) **Lighter weight: 58% weight reduction**
- (2) **Compacter size: 17% reduction in outside diameter and 25% reduction in width**

[Comparison to bearing of same size]

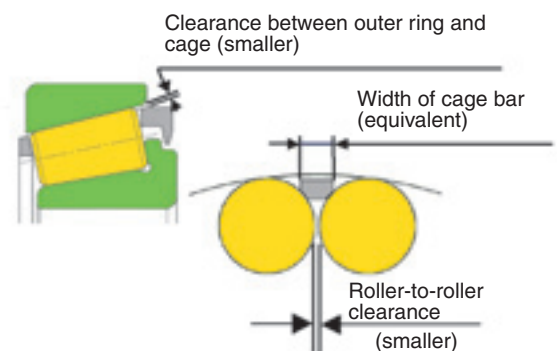
- (3) **Higher rigidity: 16% increase in rigidity**
- (4) **Longer life: five times as long (in clean oil-lubrication environment)**

### Applications

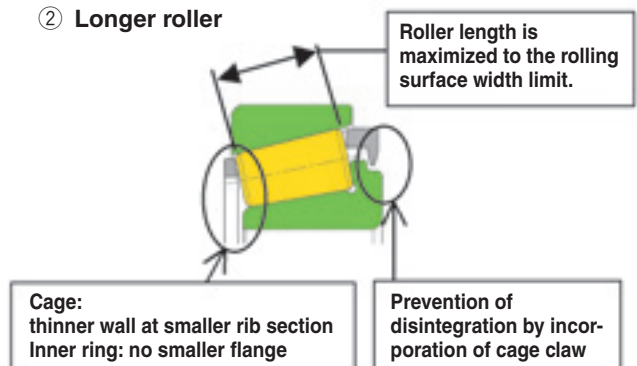
- **Differential gearing in automotive transmission**

### Construction [means for realization]

#### ① Increased number of rollers



#### ② Longer roller



## Low-Friction Capable Needle Roller Bearing for Automotive Engine

Approximately 3% improvement in **fuel economy** (10.15 mode)  
 Helps promote introduction of **compact, lighter** oil pump and starter!!



### Features

- (1) Reduction in friction  
 Reduction in bearing running torque:  
 approx. 50% reduction
- (2) Compacter starter may be adopted.  
 Reduction in bearing start torque:  
 approx. 90% reduction
- (3) Compacter oil pump may be adopted.  
 Necessary quantity of lubricating oil can  
 be decreased to 1/10.



- (1) Improved fuel economy for cars  
 ⇒Improvement of approx. 3% in  
 10.15 mode (desk study)
- (2) A total package can be adopted in  
 VAVE applications.

### Construction [means for realization]

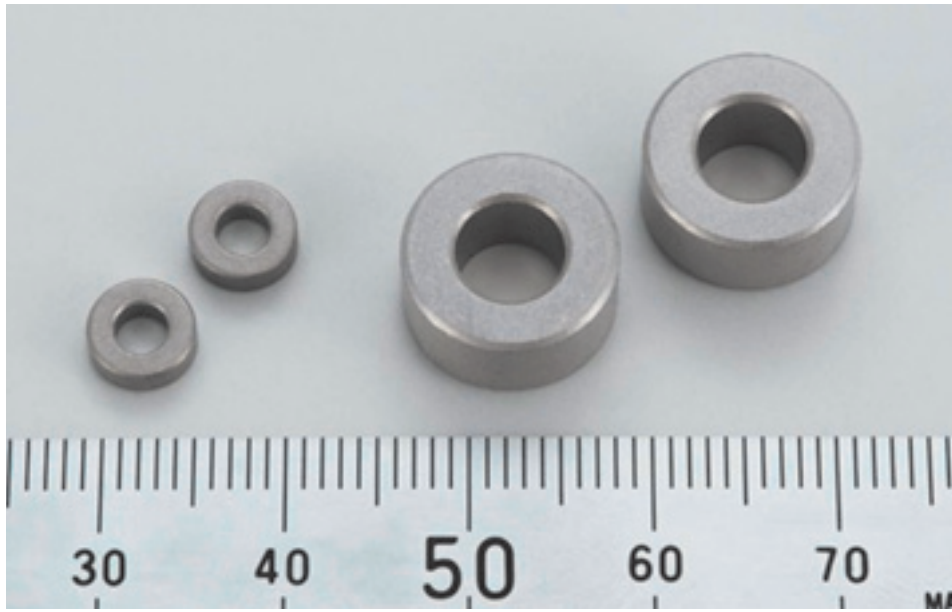
- **Crankshaft support**
  - Thanks to newly developed split outer ring design, the bearing can have a much lower profile: outer ring wall can be as thin as 2 mm.
  - Cage design is optimized for application to engine, boasting improved seizure resistance and enhanced mechanical strength.
- **Camshaft support**
  - Outer ring is formed by pressing process, and the bearing can have a much lower profile: outer ring wall can be as thin as 0.6 mm.
  - Shape of the outer ring is optimized through utilization of FEM analysis, and the outer ring boasts enhanced mechanical strength.

### Applications

- **Automotive engine**  
 (for supporting crankshaft and camshaft)

## MnS-Blended Stainless Steel Sintered Oil-impregnated Bearing

NTN has developed and commercialized a low-friction bearing that excels in **corrosion resistance**, **seizure resistance** and **wear resistance**!!



### Features

- (1) **Corrosion resistance**  
Uses stainless steel as base metal.
- (2) **Seizure resistance and wear resistance**  
Blended MnS (manganese sulfide) helps form a sulfur-based lubricant film, achieving excellent seizure resistance and wear resistance.

### Applications

- IT (information technology) equipment, automotive fuel pump, medical equipment, food machinery, etc.

This product has been developed in cooperation with Nagoya Municipal Industrial Research Institute.

### Construction [means for realization]

#### Challenges of conventional technology to be addressed

- (1) Graphite (C) and molybdenum disulfide ( $\text{MoS}_2$ ), etc. are blended into stainless steel base metal.  
⇒ Chemical compound is formed as result of sintering, and this compound is harder than the base metal, attacking the mating shaft.
- (2) Lead (Pb), which is highly sliding material, is added as lubricant.  
⇒ Use of lead is regulated or banned because it is hazardous to human health.



#### Newly developed technology that has solved previous challenges

- ※ Appropriate amount of manganese sulfide is added to stainless steel base metal.
- ⇒ Sulfur deriving from manganese sulfide helps form a highly lubricating film boasting excellent extreme pressure performance.

The newly developed bearing product boasts excellent **corrosion resistance**, **seizure resistance** and **wear resistance**.